Universiteit Leiden
The Netherlands

Cellular development of the human cochlea and the regenerative potential of hair follicle bulge stem cells

Locher, heiko

Citation
Locher, H. (2015, December 8). *Cellular development of the human cochlea and the regenerative potential of hair follicle bulge stem cells*. Retrieved from https://hdl.handle.net/1887/36534

Version:	Corrected Publisher's Version
License:	Licence agreement concerning inclusion of doctoral thesis in the Institutional Repository of the University of Leiden
Downloaded from:	https://hdl.handle.net/1887/36534

Note: To cite this publication please use the final published version (if applicable).

Cover Page



Universiteit Leiden



The handle http://hdl.handle.net/1887/36534 holds various files of this Leiden University dissertation

Author: Locher, Heiko
Title: Cellular development of the human cochlea and the regenerative potential of hair follicle bulge stem cells
Issue Date: 2015-12-08

Cellular Development of the Human Cochlea

and the Regenerative Potential of Hair Follicle Bulge Stem Cells



Author: H. Locher
Cover design: H. Locher *(drawings from G.L. Streeter, 1906)*
Layout: H. Locher
Printing: Mostert & Van Onderen, Leiden

Cellular Development of the Human Cochlea

and the Regenerative Potential of Hair Follicle Bulge Stem Cells

PROEFSCHRIFT

ter verkrijging van
de graad van Doctor aan de Universiteit Leiden,
op gezag van Rector Magnificus prof.mr. C.J.J.M. Stolker,
volgens besluit van het College voor Promoties
te verdedigen op dinsdag 8 december 2015
klokke 15.00 uur

door

HEIKO LOCHER

geboren te Amsterdam in 1982

Promotor

Prof.dr.ir. J.H.M. Frijns

Copromotores

Dr. M.A. Huisman

Dr. S.M. Chuva de Sousa Lopes

Promotiecommissie

Prof.dr. G.J. Fleuren

Prof.dr. C.L. Mummery

Prof.dr. J.G.G. Borst (Erasmus MC)

Dr. J.K.L. Klis (UMC Utrecht)

Voor Jennifer
en Jasmijn
zonder wiens liefde
dit proefschrift al twee jaar eerder af was geweest

"Lieve hart, mijn boek is af, mijn boek is af!"
Multatuli, 1859

CONTENTS

Chapter 1	Introduction	11
Chapter 2	Neurosensory Development and Cell Fate Determination in the Human Cochlea *Neural Development, 2013*	23
Chapter 3	Distribution and Development of Peripheral Glial Cells in the Human Fetal Cochlea *PLOS ONE, 2014*	43
Chapter 4	Development of the Stria Vascularis and Potassium Regulation in the Human Fetal Cochlea: Insights into Hereditary Sensorineural Hearing Loss *Developmental Neurobiology, 2015*	113
Chapter 5	TUBB3: Neuronal Marker or Melanocyte Mimic? *Cell Transplantation, 2014*	141
Chapter 6	Class III β-tubulin, a Novel Biomarker in the Human Melanocyte Lineage. *Differentiation, 2013*	147
Chapter 7	Hair Follicle Bulge Cultures Yield Class III β-tubulin-positive Melanoglial Cells. *Histochemistry and Cell Biology, 2015*	169
Chapter 8	Discussion	181
Appendix	Summary	200
	Samenvatting	202
	Abbreviations	205
	List of Publications	206
	About the Author	207


cochlea
cochlea

1

INTRODUCTION

Hearing: Anatomy and physiology

Of all the human senses, hearing is the most astounding achievement of evolution. Sound, be it spoken language or originating from another source, reaches the tympanic membrane by travelling through the external auditory meatus (ear canal) (Figure 1). The sound waves are propagated by the tympanic membrane (eardrum) that passes its vibrations on to the ossicles, the three smallest bones of the human body: the malleus (hammer), incus (anvil) and stapes (stirrup). The footplate of the stapes, which is inserted into the oval window, serves as a piston so that the mechanical energy is transferred into the cochlea, which houses the sensory receptors of hearing.

The cochlea (from the Greek κοχλιασ (kokhlias) meaning snail) is a bony structure that coils around its own axis. In humans it has approximately 2.5 turns[footnote1]. It contains three fluid-filled compartments of which the outer two, the scala vestibuli and scala tympani, are connected in the helicotrema at the apex of the cochlea. The middle compartment, the

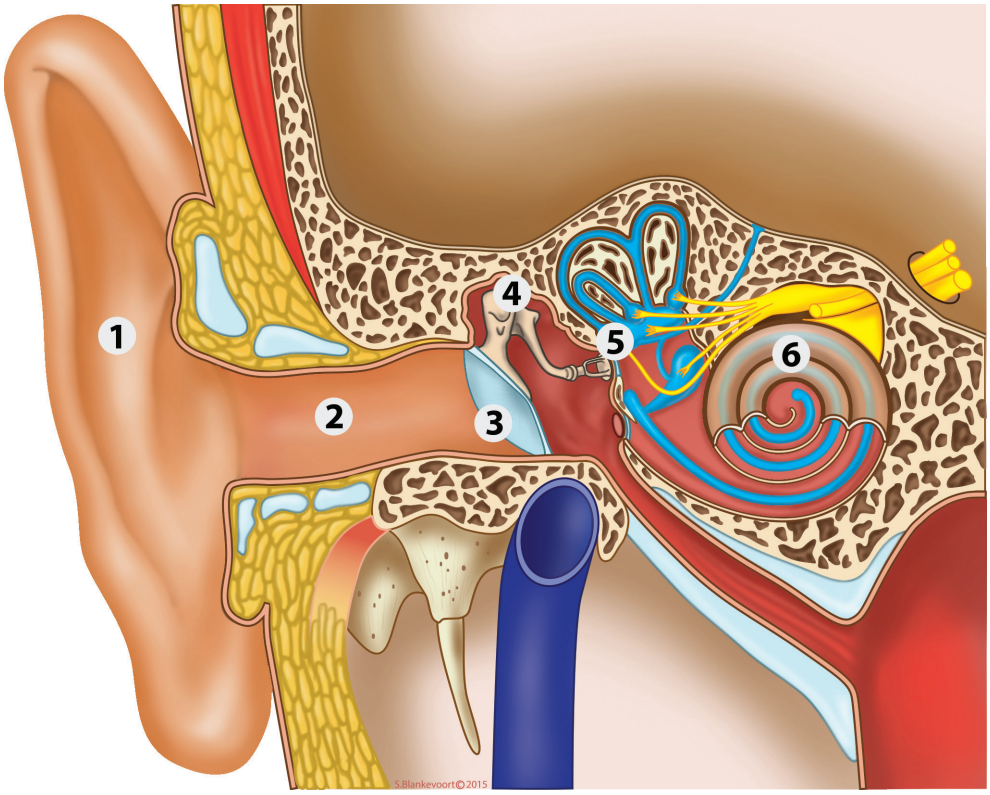


Figure 1. Schematic illustration of the outer, middle and inner ear.
1: auricle (pinna), 2: external auditory meatus (ear canal), 3: tympanic membrane (eardrum), 4: the three auditory ossicles (malleus or hammer, incus or anvil, and stapes or stirrup), 5: oval window with the footplate of the stapes, 6: cochlea. *Picture courtesy of S.B. Blankevoort and R.G.E. Noteboom.*

cochlear duct (or scala media), contains the structure that houses the sensory receptors of hearing: the organ of Corti (Figures 2 and 3).

Vibration of the stapes creates a traveling wave in the fluid (perilymph) of the scala vestibuli and scala tympani. This results in displacement of the floor (basilar membrane) of the cochlear duct, onto which the organ of Corti is located. The location of maximum displacement depends on the sound frequency: high frequencies are detected in the basal turn, whereas lower frequencies are detected in the more apically located turns. The organ of Corti contains the hair cells: in humans, it consists of one row of inner hair cells (~3,500 cells) and three rows of outer hair cells (~12,000 cells) [1]. If the displacement of the basilar membrane is large enough, mechanosensitive transduction channels in the stereocilia of the hair cells are opened. The fluid of the cochlear duct (endolymph) is rich in potassium, which is secreted by the stria vascularis, and opening of the transduction channels causes an influx of potassium ions leading to depolarization of the hair cells. Here, the mechanical energy is converted into an electrochemical signal as the hair cell activates the connecting nerve endings (synapses) of the spiral ganglion neurons by releasing neurotransmitters. Inner hair cells are the principal sensory receptors of hearing, whereas outer hair cells are thought to affect cochlear sensitivity. Multiple type-I spiral ganglion neurons (90-95% of the total population) make synaptic contacts with a single inner hair cell, while a single type-II spiral ganglion neuron contacts multiple outer hair cells. Spiral ganglion neurons are the afferent transmitters of information: upon neurotransmitter release by the hair cells, spiral ganglion

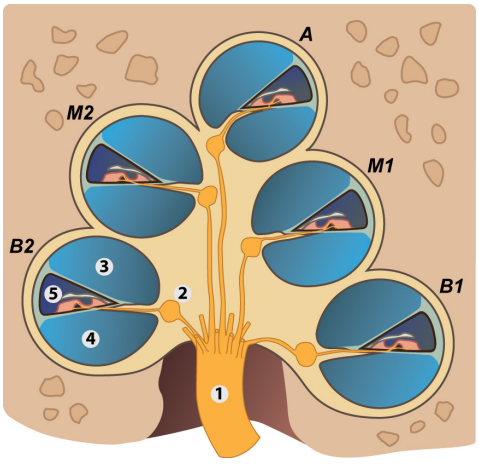


Figure 2. Schematic representation of a midmodiolar transection of the adult human cochlea.
1: cochlear nerve, 2: spiral ganglion, 3: scala vestibuli, 4: scala tympani, 5: cochlear duct / scala media. B1: lower basal turn, B2: upper basal turn, M1: lower middle turn, M2: upper middle turn, A: apex. *Picture courtesy of S.B. Blankevoort.*

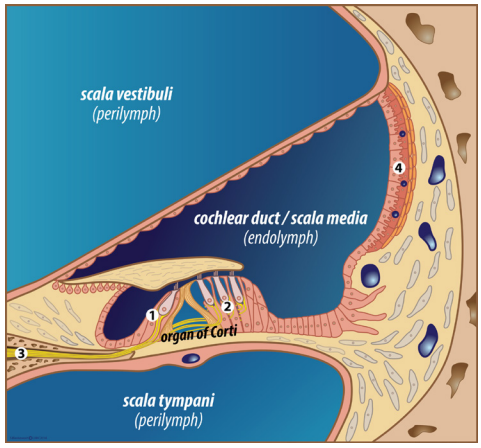


Figure 3. Schematic illustration of the cochlear duct and surrounding structures.
1: inner hair cell, 2: outer hair cells, 3: nerve fibers innervating the hair cells, 4: stria vascularis. *Picture courtesy of S.B. Blankevoort.*

neurons depolarize and generate action potentials that travel along the cochlear nerve (i.e., the cochlear branch of the 8th cranial nerve) to the brainstem. Efferent connections to hair cells are provided by neurons originating in the brainstem itself.

Hearing: Development

The human cochlea reaches its final size and shape in the fetal stages of development. Early during gestation in the growing embryo, a specific area of thickened surface ectoderm called the otic placode arises, which is destined to develop into the inner ear (Figure 4). The otic placode invaginates to form the otic vesicle (or otocyst) during the 6th week of gestation[footnote2] [2]. In the subsequent weeks, the otic vesicle polarizes and transforms into the membranous labyrinth, a continuum of fluid filled canals and chambers of both the vestibular organ

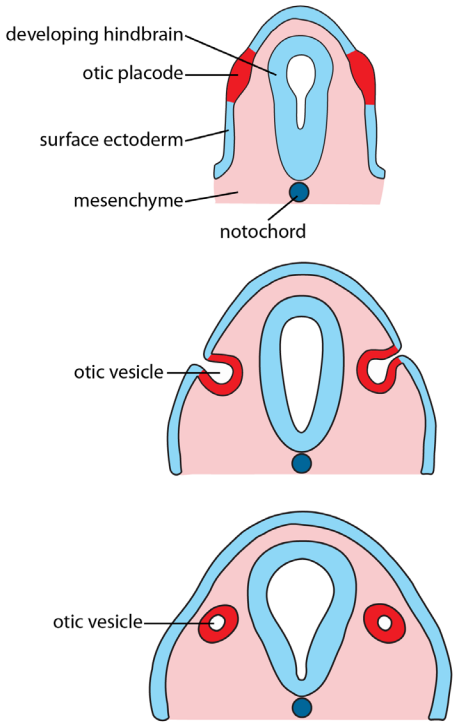


Figure 4. The otic placode.
A specialized area of the surface ectoderm called the otic placode is destined to form the otic vesicle and forms the basis of the cochlea. Early in development, it can be recognized as a thickened group of ectodermal cells (red) located near the hindbrain. Around Carnegie stage 13 (ca 6th week of gestation), the placode invaginates and pinches off from the surface to form the otic vesicle.

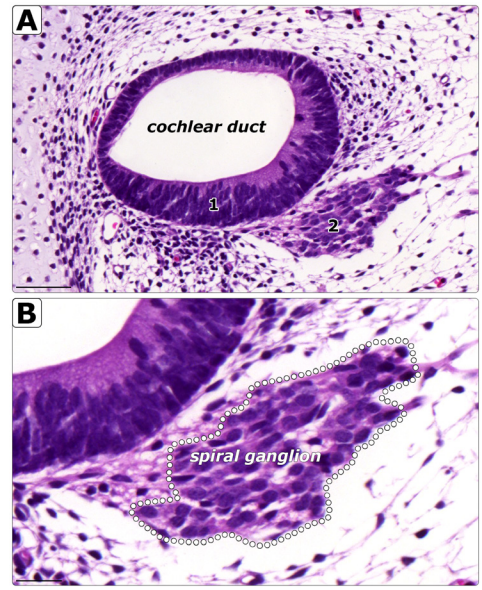


Figure 5. Human fetal cochlea at the 10th week of gestation.
(A) Hematoxylin-eosin staining of a transection through the lower basal turn. Both the epithelium of the cochlear duct (1) and the nearby spiral ganglion (2) are visible. Cells from the epithelium are microscopically undifferentiated at this stage. (B) Higher magnification of the area of the spiral ganglion (delineated with white dots). The large round nuclei belong to the developing spiral ganglion neurons. The smaller, darker and more elongated nuclei belong to the developing glial cells. Scalebars = 50 µm (A) and 20 µm (B).

and the cochlea. During a process called delamination, some cells from the otic vesicle/labyrinth detach from the otic epithelium and migrate into the surrounding mesenchyme, and from this group of cells the spiral ganglion neurons originate [3]. The cochlear part of the labyrinth (the cochlear duct) spirals around a central axis and reaches its final 2.5 turns at the end of the 10th or at the start of the 11th week of gestation [4, 5].

At this stage, the cells forming the epithelial lining of the cochlear duct (all derived from the otic placode/vesicle) are microscopically still undifferentiated (Figure 5A). The delaminated spiral ganglion neurons group together with the peripheral glial cells in the neighbouring spiral ganglion (Figure 5B). At the 12th week of gestation, a general developmental aspect of the cochlea can be observed: a spatiotemporal gradient in a basal-to-apical direction (Figure 6A). The development of the basal turn is ahead of that of the apical turn by one or two weeks, which is a consistent finding during maturation of the cochlea. Also, the spiral ganglion and the cochlear duct move away from one another, the scala vestibuli and tympani are formed, and the first hair cell becomes visible in the epithelial lining of the basal turn (Figures 6B-C). At 14 weeks of gestation, one row of inner hair cells and three rows of outer hair cells can be discerned (Figure 7). Although the major structures in the cochlea are readily recognizable, differentiation and maturation continue through subsequent stages of development. Based upon the structural development of the human fetal cochlea and insights gained from animal studies, it has been estimated that the onset of cochlear function occurs around 20 weeks of gestation [6, 7].

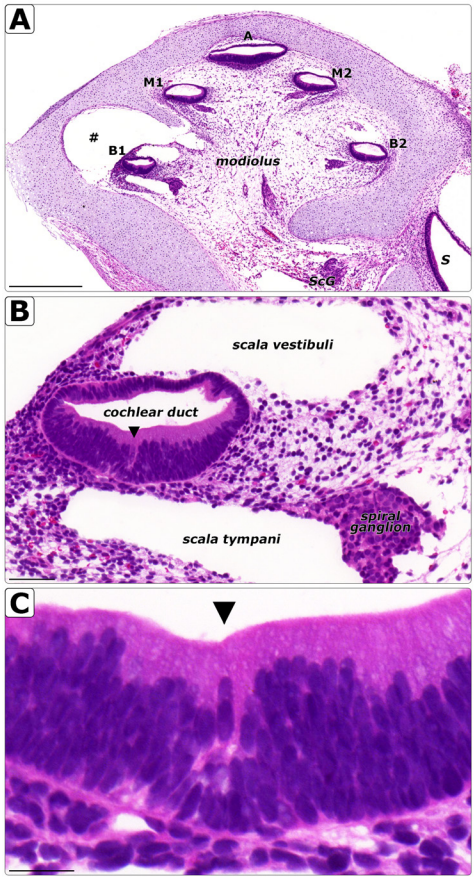


Figure 6. Human fetal cochlea at the 12th week of gestation. (A) Hematoxylin-eosin staining of a midmodiolar transection through the entire cochlea. (B) In the lower basal turn, the scala vestibuli and tympani have been formed, the distance between the spiral ganglion and the cochlear duct is increasing, and (C) the first hair cell becomes visible (arrow head). #, tissue artifact; B1, lower basal turn; B2, upper basal turn; M1, lower middle turn; M2, upper middle turn; A, apex; ScG, Scarpa's ganglion; S, saccule. Scalebars = 500 µm (A), 50 µm (B) and 20 µm (C).

Hearing: Loss

Worldwide, 360 million individuals suffer from disabling hearing loss[footnote3], which is over 5% of the world's total population [8]. Although this number also includes patients suffering from conductive hearing loss (the origin of which lies in the external or middle ear), a large part is of sensorineural origin. Sensorineural hearing loss (SNHL) is therefore the most prevalent sensorineural disorder afflicting human beings. SNHL can either be acquired or congenital. Of the acquired type, hearing loss due to aging (presbycusis), ototoxicity or acoustic trauma are well-known examples. Often, outer hair cells are primarily affected [1]. Congenital SNHL is the most common congenital disorder with a prevalence of 1 in every 1000 newborns in the UK and the Netherlands [9, 10]. In many countries, national neonatal screening programs to detect SNHL have therefore been implemented. Genetic (hereditary) factors are implicated in over two-thirds of patients afflicted by congenital SNHL cases, although exact numbers are not available due to our incomplete etiological understanding. Hereditary SNHL can be divided into syndromic and nonsyndromic forms. Although the search for responsible genes for SNHL is still ongoing, our knowledge has rapidly increased during the last few decades. Over 130 loci have been mapped and over 60 different genes have been identified to date (2014) [11][footnote4]. Nonsyndromic forms of hereditary SNHL are grouped into autosomal dominant (DFNA), autosomal recessive (DFNB), X-linked (DNFX) and mitochondrial subtypes. Unlike acquired SNHL, only a minority of mutations affect the hair cells in hereditary SNHL. Mutations have likewise been found in various other cell types involved in the function of the cochlea or the cochlear nerve.

Much can be learned from studies investigating gene expression patterns in experimental animals as well as from studies on developmental abnormalities in animal models of hereditary SNHL. However, this knowledge does not yet extend to the full scale of known mutations causing SNHL and only a limited number of studies have been performed on human tissues. Understanding etiologies and pathologies of disorders is essential to the advancement of therapeutic

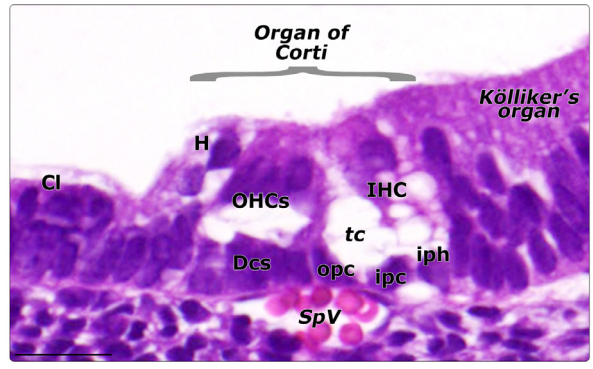


Figure 7. Human organ of Corti at the 14th week of gestation. Hematoxylin-eosin staining of a transection through the organ of Corti located in the lower basal turn. IHC, inner hair cell; OHCs, outer hair cells; H, Hensen's cells; Cl, Claudius cells; Dcs, Deiters' cells; opc, outer pillar cell; ipc, inner pillar cell; iph, inner phalangeal cell; SpV, spiral vessel; tc, tunnel of Corti. Scalebar = 20 μm.

options. For both acquired and congenital SNHL, increased knowledge of gene expression patterns and cell fate specification in the human inner ear has the potential to aid in the development of gene and cell-based therapeutic strategies.

Hearing: Regeneration

The options for improvement of hearing in patients affected by SNHL are generally limited to hearing aids, varying from 'simple' types worn behind the ear to cochlear implants requiring surgery for implantation. However, their function is largely dependent on the quality of the remaining cellular structures within the cochlea and the integrity of the cochlear nerve. Hair cell loss, strial dysfunction, or neuronal degeneration can severely limit the hearing aid's functionality. One remaining therapeutic option is the auditory brainstem implant: by bypassing the entire cochlea as well as the cochlear nerve, the brainstem is directly stimulated. However, as the quality of hearing with such an implant still remains very low [12], a different approach would be to induce tissue regeneration, i.e. to restore damaged hair cells or to regenerate the cochlear nerve. This might either improve the hearing aid's functionality, or could possibly restore hearing itself.

Several different approaches to achieve restoration of damaged cochlear structures are currently being investigated. One interesting option involves introducing neurotrophic factors (proteins that stimulate growth and survival of neurons) into the cochlea aiming to promote spiral ganglion neuron survival or even regrowth of their peripheral processes [13]. The authors speculate that application of exogenous neurotrophic factors enhances the function of cochlear implants or may even create direct contact between the electrode and the nerve fibers [14 – 16].

Another approach is gene therapy, for example to generate new hair cells from supporting cells. Introduction of viral vectors that induce expression of Atoh1 (the master regulator of hair cell differentiation) could convert targeted cells into new hair cells, potentially improving hearing [17 – 21]. However, it is difficult to target the right cells without affecting other cell types and disturbing cochlear architecture and function.

Regeneration of degenerated structures by stem cells is yet another, promising, approach. The rationale is that stem cells have migratory capabilities allowing them to reach appropriate locations, and that they subsequently differentiate into the desired cell type. Knowledge on the developmental origin of the damaged cell types as well as the factors that trigger differentiation is advantageous in the selection of the appropriate type of stem cell. Recently, otic progenitor cells induced from human embryonic stem cells were used in an animal model of SNHL, and led to an improvement in auditory thresholds [22]. Functional hair cells have also been cultured out of mouse embryonic stem cells [23]. These studies offer

more insight into inner ear development and pave the way for transplantation studies using in vitro grown hair cells.

Hearing: The hair follicle option

The development of stem cell based therapeutic strategies for restoration of auditory function starts with the search for the appropriate type of stem cell. In 2004 and 2005, two groups showed that pluripotent neural crest stem cells reside within the bulge of the hair follicle (Figure 8) in the whisker pads of adult mice. These cells were capable of differentiation into neurons, Schwann cells and melanocytes in vitro [24, 25]. Further studies showed that these cells could form neurons in vivo and promote axonal regeneration [26, 27]. Theoretically, these stem cells could be candidates to regenerate or repair the auditory nerve or its glial cells.

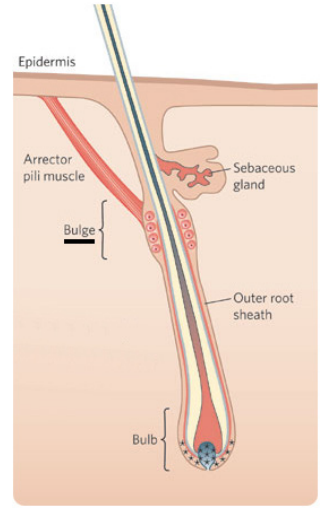


Figure 8. Schematic illustration of a transection through the hair follicle. Neural crest stem cells are thought to reside in the hair follicle bulge. *Reproduced with permission from Lin and Fisher, Nature, 2007.*

The use of neural crest stem cells residing in the hair follicle has several advantages over the use of other stem cells, such as embryonic or induced pluripotent stem cells. They are easily harvested, they are not oncogenic, and there are no ethical issues involved. More importantly, hair follicle derived neural crest stem cells reside in the adult body (at least in the mouse). Another advantage of these stem cells is that they have a neural crest-like phenotype, implying that they are already committed to follow a limited number of cellular lineages, thus reducing the risk of differentiation into unwanted cell types. Finally, when used in a therapeutic setting, these cells can be used for autologous transplantation without triggering unwanted immune responses in the host.

Aims and scope of this thesis

The aims and scope of this thesis are two-fold: (1) To gain more insight into the development of the human cochlea and (2) to investigate a possible stem cell strategy for the restoration of hearing. Although these two goals share little common ground at first sight, they are intimately associated with one another. When one pursues tissue regeneration, it is of huge advantage to have the blue print of the tissue's normal development, in order to avoid 'shooting in the dark'. Or, in other words, when something is broken, one needs to know how it normally functions in order to repair it. Knowing the origin of the degenerated cell type aids in selecting the proper replacement, and knowledge of the normal developmental steps helps in guiding a stem cell towards a specific cellular lineage.

Outline of this thesis

The first and largest part of this thesis investigates the normal development of the human cochlea. *Chapter 2* focuses on the neurosensory epithelium, from which the hair cells develop, and its developmental relation with the innervating spiral ganglion neurons. In *Chapter 3*, this investigation is extended towards the third cell type involved in the hair cell and spiral ganglion neuron triad: the glial cell. Here, the focus is on the developmental distribution of the peripheral glial cells and on the onset of myelination, one of the prerequisites of normal hearing. Focusing on one of the most undervalued cochlear structures that are involved in hearing, *Chapter 4* investigates the development of the stria vascularis and cochlear potassium regulation, including its relation to syndromic and nonsyndromic SNHL.

Chapters 5-7 are related to the neural crest stem cells residing in the hair follicle. *Chapter 5* serves as an introduction to this part of the thesis and as a short summary of the findings and implications of *Chapter 6*, which is solely about skin melanocytes. These insights are further elaborated in *Chapter 7*, where we investigate and identify cells growing in hair follicle bulge explant cultures. *Chapter 8*, the general discussion, combines and discusses Chapters 2-7 and speculates on one of the most intriguing aspects of human cochlear development: the onset of human hearing.

Footnotes:

1: The size and number of cochlear turns differ between mammals. The whale cochlea has 1.5 turns, a typical mouse cochlea has 2 turns, whereas the cochlear of elephants (similar to humans) has 2.5 turns. The guinea pig rules them all: it has 3.5-4.5 turns (for images and other animals, see: http://csi.whoi.edu/inner-ears-gallery).

2: Gestational age is equivalent to weeks post conception (fetal age) plus two weeks, as gestational age is measured from the first day of the last menstrual period.

3: According to the WHO's standards, disabling hearing loss refers to a hearing loss greater than 40 dB in the better hearing ear in adults and a hearing loss greater than 30 dB in the better hearing ear in children.

4: An extensive table on involved genes, their function, gene expression and hearing loss type as well as an image showing the location of these genes within the cochlea can be found in Morton and Nance, NEJM, 2006. Also, on the Hereditary Hearing Loss Homepage (hereditaryhearingloss.org) an interactive view of many causative genes and their expression is provided.

References

1. Merchant SN, Nadol JB: **Schuknecht's Pathology of the Ear.** 3rd edition. Shelton, CT: People's Medical Publishing House-USA; 2010.
2. O'Rahilly R: **The Early Development of the Otic Vesicle in Staged Human Embryos.** J Embryol Exp Morphol 1963, 11(December):741 – 55.
3. Rubel EW, Fritzsch B: **Auditory system development: primary auditory neurons and their targets.** Annu Rev Neurosci 2002, 25:51 – 101.
4. Moore JK, Linthicum FH: **The human auditory system: a timeline of development.** Int J Audiol 2007, 46:460 – 78.
5. Pujol R, Lavigne-Rebillard M: **Early stages of innervation and sensory cell differentiation in the human fetal organ of Corti.** Acta Otolaryngol Suppl 1985, 423:43 – 50.
6. Bibas AG, Xenellis J, Michaels L, Anagnostopoulou S, Ferekidis E, Wright A: **Temporal bone study of development of the organ of Corti: correlation between auditory function and anatomical structure.** J Laryngol Otol 2008, 122:336 – 42.
7. Pujol R, Lavigne-Rebillard M, Uziel A: **Development of the human cochlea.** Acta Otolaryngol Suppl 1991, 482:7 – 12; discussion 13.
8. Fact Sheet No300 [www.who.int]
9. NHSP: Annual Report NHS Newborn Hearing Screening Programme 2010-11. 2011.
10. Van der Ploeg CPB, Uilenburg NN, Kauffman-de Boer MA, Oudesluys-Murphy AM, Verkerk PH: **Newborn hearing screening in youth health care in the Netherlands: National results of implementation and follow-up.** Int J Audiol 2012, 51:584 – 90.
11. Hereditary Hearing Loss Homepage [http://hereditaryhearingloss.org]
12. Merkus P, Di Lella F, Di Trapani G, Pasanisi E, Beltrame M, Zanetti D, Negri M, Sanna M: **Indications and contraindications of auditory brainstem implants: Systematic review and illustrative cases.** Eur Arch Oto-Rhino-Laryngology 2014, 271:3 – 13.
13. Ramekers D, Versnel H, Grolman W, Klis SFL: **Neurotrophins and their role in the cochlea.** Hear Res 2012, 288:19 – 33.
14. Glueckert R, Bitsche M, Miller JM, Zhu Y, Prieskorn DM, Altschuler RA, Schrott-Fischer A: **Deafferentation-associated changes in afferent and efferent processes in the guinea pig cochlea and afferent regeneration with chronic intrascalar brain-derived neurotrophic factor and acidic fibroblast growth factor.** J Comp Neurol 2008, 507:1602 – 21.
15. Agterberg MJH, Versnel H, de Groot JCMJ, Smoorenburg GF, Albers FWJ, Klis SFL: **Morphological changes in spiral ganglion cells after intracochlear application**

of brain-derived neurotrophic factor in deafened guinea pigs. Hear Res 2008, 244:25 – 34.

16. Pettingill LN, Wise AK, Geaney MS, Shepherd RK: **Enhanced auditory neuron survival following cell-based BDNF treatment in the deaf guinea pig.** PLoS One 2011, 6:e18733.
17. Izumikawa M, Minoda R, Kawamoto K, Abrashkin KA, Swiderski DL, Dolan DF, Brough DE, Raphael Y: **Auditory hair cell replacement and hearing improvement by Atoh1 gene therapy in deaf mammals.** Nat Med 2005, 11:271 – 6.
18. Kawamoto K, Ishimoto S-I, Minoda R, Brough DE, Raphael Y: **Math1 gene transfer generates new cochlear hair cells in mature guinea pigs in vivo.** J Neurosci 2003, 23:4395 – 400.
19. Atkinson PJ, Wise AK, Flynn BO, Nayagam BA, Richardson RT: **Hair Cell Regeneration after ATOH1 Gene Therapy in the Cochlea of Profoundly Deaf Adult Guinea Pigs.** PLoS One 2014, 9:e102077.
20. Gubbels SP, Woessner DW, Mitchell JC, Ricci AJ, Brigande J V: **Functional auditory hair cells produced in the mammalian cochlea by in utero gene transfer.** Nature 2008, 455:537 – 41.
21. Kilpatrick LA, Li Q, Yang J, Goddard JC, Fekete DM, Lang H: **Adeno-associated virus-mediated gene delivery into the scala media of the normal and deafened adult mouse ear.** Gene Ther 2011, 18:569 – 78.
22. Chen W, Jongkamonwiwat N, Abbas L, Eshtan SJ, Johnson SL, Kuhn S, Milo M, Thurlow JK, Andrews PW, Marcotti W, Moore HD, Rivolta MN: **Restoration of auditory evoked responses by human ES-cell-derived otic progenitors.** Nature 2012, 490:278 – 282.
23. Koehler KR, Mikosz AM, Molosh AI, Patel D, Hashino E: **Generation of inner ear sensory epithelia from pluripotent stem cells in 3D culture.** Nature 2013, 500:217 – 21.
24. Sieber-Blum M, Grim M, Hu YF, Szeder V: **Pluripotent neural crest stem cells in the adult hair follicle.** Dev Dyn 2004, 231:258 – 69.
25. Amoh Y, Li L, Katsuoka K, Penman S, Hoffman RM: **Multipotent nestin-positive, keratin-negative hair-follicle bulge stem cells can form neurons.** Proc Natl Acad Sci U S A 2005, 102:5530 – 4.
26. Liu F, Zhang C, Hoffman RM: **Nestin-Expressing Stem Cells from the Hair Follicle Can Differentiate Into Motor Neurons and Reduce Muscle Atrophy after Transplantation to Injured Nerves.** Tissue Eng Part A 2013, 00:1 – 7.
27. Amoh Y, Hamada Y, Aki R, Kawahara K, Hoffman RM, Katsuoka K: **Direct transplantation of uncultured hair-follicle pluripotent stem (hfPS) cells promotes the recovery of peripheral nerve injury.** J Cell Biochem 2010, 110:272 – 7.


cochlea
cochlea

2

Neurosensory development and cell fate determination in the human cochlea

Locher
Frijns
van Iperen
de Groot
Huisman
Chuva de Sousa Lopes

Neural Development, 2013

Abstract

Background: Hearing depends on correct functioning of the cochlear hair cells, and their innervation by spiral ganglion neurons. Most of the insight into the embryological and molecular development of this sensory system has been derived from animal studies. In contrast, little is known about the molecular expression patterns and dynamics of signaling molecules during normal fetal development of the human cochlea. In this study, we investigated the onset of hair cell differentiation and innervation in the human fetal cochlea at various stages of development.

Results: At 10 weeks of gestation, we observed a prosensory domain expressing SOX2 and SOX9/SOX10 within the cochlear duct epithelium. In this domain, hair cell differentiation was consistently present from 12 weeks, coinciding with downregulation of SOX9/SOX10 to be followed several weeks later by downregulation of SOX2. Outgrowing neurites from spiral ganglion neurons were found penetrating into the cochlear duct epithelium prior to hair cell differentiation and directly targeted the hair cells as they developed. Ubiquitous Peripherin expression by spiral ganglion neurons gradually diminished and became restricted to the type II spiral ganglion neurons by 18 weeks. At 20 weeks, when the onset of human hearing is thought to take place, the expression profiles in hair cells and spiral ganglion neurons matched the expression patterns of the adult mammalian cochleae.

Conclusions: Our study provides new insights into the fetal development of the human cochlea contributing to our understanding of deafness and to the development of new therapeutic strategies to restore hearing.

Background

The cochlea houses two of the main cell types responsible for hearing: the hair cells, and the spiral ganglion neurons (SGNs). Damage to the cochlea is usually associated with degeneration and irreversible loss of these cell types, which ultimately leads to permanent sensorineural hearing loss, the most common type of deafness [1, 2]. In order to develop new therapeutic strategies, it is essential to have a better understanding of the normal molecular development of the human cochlea.

In the human embryo, the otic placode invaginates to form the otic vesicle (or otocyst) during week 6 of gestation (W6), equivalent to week 4 of fetal development [3]. In the subsequent weeks, the otic vesicle develops into both the vestibular organs and the cochlea. The cochlear duct spirals around a central axis and reaches its final 2.5 turns by W10 to W11 [4, 5]. At this stage, the epithelial lining of the cochlear duct is still undifferentiated. In mice, a dedicated area within the epithelium of the cochlear duct floor has been identified as the 'prosensory domain' [6]; this contains the precursors to the inner hair cells (IHCs), the outer hair cells (OHCs), and various types of surrounding supporting cells, which together form the organ of Corti (OC) [7, 8]. The prosensory domain is flanked by two other domains: Kölliker's organ (KO) and the future outer sulcus. Although the prosensory domain has not been formally described in humans, hair cells are first visible by W12 in the human fetus in the region where the OC will form [5]. The OC reaches its gross adult morphology around W20, which corresponds to the onset of auditory function [9-11].

Development of the prosensory domain into the OC coincides with the establishment of highly specialized innervation patterns by afferent type I and type II SGNs. In humans, multiple type I SGNs innervate single IHCs in a 'radial' organization, and make up 90 to 95% of the total population of SGNs, whereas single type II SGNs contact multiple OHCs in a 'spiral' organization [12]. In mice, SGNs project to both IHCs and OHCs until 6 to 7 days after birth when a clear distinction between type I and type II ganglion neurons takes place, just prior to the onset of hearing (postnatal week 2) [13, 14]. In humans, penetration of the SGN neurites into the cochlear neuroepithelium has been observed earlier than the first differentiation of hair cells by electron microscopy [5]. The peripheral neurites of the SGNs penetrate the basal turn around W11, and in the following weeks find their way to the developing hair cells and shape their synaptic connections [5, 15]. However, the separation of type I

and type II SGNs has not been investigated in humans.

Here, we investigated both the dynamics of development of human cochlear hair cells and their innervation. The spatial and temporal dynamics of hair cell differentiation was determined by examining the expression of three members of the SOX family, a group of genes involved with cell fate decisions: *SOX2*, *SOX9*, and *SOX10*. An example of early cell fate specification in the cochlear duct epithelium is the spatially restricted expression of SOX2 to the cells of the prosensory domain [8]. The functional importance of the SOX2 transcription factor in normal cochlear development is further illustrated by failure of the prosensory domain establishment in loss-of-function conditions [8], and underdevelopment of hair cells in gain-of-function conditions [16]. *Sox9* and *Sox10* are known to be expressed in the otic placode and the otic vesicle in frog and chick [17-20]. In mice, SOX9 is also expressed in the otic placode and otic vesicle and controls invagination [21], and both SOX9 and SOX10 have been found in the mouse cochlear duct epithelium [22-26]. Interestingly, in mice, Sox9 and Sox10 are downregulated before or upon hair cell differentiation, whereas Sox2 is downregulated gradually, although all three Sox genes remain expressed in the underlying supporting cells in the OC [8, 22, 23].

In humans, SOX2, SOX9, and SOX10 are likely to play an important role in cochlear development, as mutations in all three genes have been shown to cause sensorineural hearing loss [27-29]. However, although SOX10 expression has been reported in the human otic vesicle [30], expression patterns of these SOX transcription factors, and their dynamics upon hair cell differentiation, have not previously been determined in the (developing) human cochlea. In addition, the innervation of the IHCs and OHCs was in the current study investigated by comparing the dynamics of expression of Peripherin (PRPH), an intermediate filament protein that is expressed in type II SGNs, both in adult mouse and adult human cochleae [13, 31], along with the expression of class III β-Tubulin (TUBB3), a general SGN marker. The comprehensive description of the molecular and morphological events taking place in the cochlea as functional hearing develops may benefit the development of strategies for cochlear repair.

Results

The human prosensory domain is SOX2-positive

To determine whether a prosensory domain also exists during human development, we investigated the expression of SOX2 at W10.4 (week 10 and 4 days), a stage when the cochlear duct epithelium showed no clear morphological hair cell specification (Fig. 1A). At this point, nuclear SOX2 expression was already restricted to the human prosensory domain (Fig. 1B) and no expression was visible in other parts of the cochlear duct, except for cytoplasmic SOX2 expression in the lateral wall of the cochlear duct epithelium (Fig. 1B, asterisk). At W10.4, SOX9 not only overlapped with SOX2 in the prosensory domain, but showed uniform nuclear expression in all cells of the cochlear duct epithelium, similar to that described in the developing mouse cochlea [23]. SOX9 was also expressed in the Schwann cells of the adjacent spiral ganglion (Fig. 1C) and in the cartilage cells of the otic capsule (Fig. 1C).

Differentiating cochlear hair cells downregulated SOX9 and SOX10, followed by SOX2

At W12, the openings of the scala vestibuli and the scala tympani were observed, respectively, above and beneath the basal turn of the cochlear duct (Fig. 1D). The first morphological signs of hair cell differentiation were then visible exclusively in the basal turn, as a row of single cells that emerged facing the luminal aspect of the SOX2-positive prosensory domain (Fig. 1D, E). Immunostaining for myosin VIIA (MYO7A), a marker of hair cells, confirmed this lineage specification (Fig. 1F). Based on the position of the first hair cells at the border between the prosensory domain (SOX2-positive) and Kölliker's organ (SOX2-negative), we identified these cells as IHCs (Fig. 1E) and found that lineage specification to IHCs coincided with downregulation of SOX9 (Fig. 1F).

At W14 (2 weeks later) the SOX2-positive prosensory domain is developing into the OC, with maturation progressing in a basal-to-apical gradient. In the current study we found that solitary IHCs were differentiated in the apical and middle turns, whereas in the basal turn, not only were the IHCs visible, but all three rows of OHCs (O1, O2 and O3) had formed (Fig. 2A-I). In general, three rows of OHCs were present; however occasionally four rows of outer hair cells were detected. Upon hair cell specification, as confirmed by MYO7A expression, both IHCs and OHCs

showed specific downregulation of SOX9 (Fig. 2A-I), whereas the supporting cells underneath both IHCs and OHCs remained positive for boeth SOX2 and SOX9 (Fig. 2A-I).

In the basal turn of the W19 cochlea, all IHCs and OHCs had become negative for both SOX2 and SOX9, in contrast to the supporting cells in the OC and in some of the adjacent cells in Kölliker's organ, which expressed SOX2 (Fig. 2J, K), acquiring the mature SOX2/SOX9 expression pattern seen in the mouse OC [23, 32], which has yet to be investigated in the adult human cochlea. In the developing hair cells, the dynamics of SOX10 and SOX9 expression were identical (Fig. 3). Downregulation of SOX10 coincided directly with the first hair cell specification at W12, and expression was maintained in supporting cells (Fig. 3).

At W12 to W19, in the developing OC, either only the IHCs or the full set of IHCs and OHCs (O1, O2, and O3) were visible. Therefore, we next investigated whether the OHCs could be derived from the first differentiated IHCs by cell division. However, after performing immunostaining for proliferating cell nuclear antigen (PCNA), a marker of cycling cells, we found that all cells of the prosensory domain had exited the cell cycle at this stage (W10 to W12) (Fig. 4A, B). This strongly suggested that cells in the prosensory domain/OC do not proliferate, supporting the idea that the OHCs differentiate from cells in the prosensory domain, but are not progeny of the IHCs. At W14, most cells in the cochlear duct, including the OC cells, were PCNA negative (Fig. 4C).

Innervation of the cochlear duct by PRPH-positive neurites precedes hair cell differentiation

At W10.4, both PRPH-positive and TUBB3-positive neurites were present at the distal end of the spiral ganglion in the basal turn directly beneath the prosensory domain, but these neurites did not innervate into the epithelium of the cochlear duct (Fig. 5A). As there are no hair cells yet at this stage, no cells expressed MYO7A (Fig. 5B).

As at W10.4, both PRPH-positive and TUBB3-positive neurites where still located directly below the prosensory domain in the W12 apical turn (Fig. 5C). However, high magnification scanning revealed the presence of PRPH-positive and TUBB3-positive growth cones extending a few micrometers into the cochlear epithelium (Fig. 5C', white and black arrows, respectively), suggesting that in humans neurites penetrate the basement membrane prior to signs of hair cell differentiation, as

confirmed by the lack of MYO7A (Fig. 5D).

In the W12 middle turn, innervation by both PRPH and TUBB3 positive neurites advanced further into the epithelium (Fig. 5E). These neurites penetrated the basement membrane at multiple positions directly below the reorganizing prosensory domain, and seemed directed predominantly toward one specific cell type, most probably the first future hair cell to emerge, as the prosensory domain remained MYO7A-negative (Fig. 5F).

In the W12 basal turn, the neurites progressed upwards along different routes and contacted the base of the first differentiated MYO7A-positive hair cells, identified here as IHCs, at multiple positions along its basal side (Fig. 5G, H). Many neurites seemed to express both PRPH and TUBB3. Strikingly, single neurites positive for both PRPH and TUBB3 invaded the epithelium at a more lateral position, at the site of the future OHCs (Fig. 5G, yellow arrow), suggesting that innervation into the future OHC area precedes OHC differentiation, just as innervation into the IHC area precedes IHC differentiation.

PRPH-positive neurites become restricted to the OHC by W20.3

At W14, the middle turn showed only IHCs (Fig. 6A, B), whereas at W15, the middle turn showed the full complement of IHCs and OHCs. In both stages, the full complement of IHCs and OHCs was visible in the basal turn (Fig. 6C-F). At W14 to W15, there were observed abundant PRPH-positive and TUBB3-positive neurites targeting basically all the hair cells (IHCs and OHCs) in the middle and basal turns (Fig. 6A-F). At W15, all OHCs (O1, O2, and O3) were innervated by neurites that followed the basement membrane, and extended upwards in between supporting cells, and these neurites ended in a calyx-like cluster (Fig. 6E). Three-dimensional (3D) reconstructions showed that at W14 and W15, in contrast to W12, some of these PRPH-positive neurites contacting the OHCs had already acquired the characteristic 'spiral' organization, rather than penetrating the basement membrane perpendicularly toward the nearest OHC (see Additional file 1, see Additional file 2, see Additional file 3).

By W18, innervation by PRPH – positive neurites to the IHCs gradually diminished (Fig. 6G) and by W20.3, PRPH – positive neurites innervated the OHCs exclusively (Fig. 6H), similar to the specific innervation pattern of the adult cochlea [13, 31]. 3D reconstruction revealed the increased to complete 'spiral' organization of the PRPH – positive neurites innervating to the OHC (see Additional files 4, see

Additional file 5).

Ubiquitous PRPH expression becomes restricted to type II SGNs at W18

To further understand the separation of type I and type II SGNs in humans, we mapped the dynamics of PRPH expression in the developing spiral ganglion adjacent to the developing prosensory domain/OC. At W10 to W15, both PRPH and TUBB3 expression was visible throughout the spiral ganglion in the basal turn (Fig. 7A-C), with PRPH expression reaching a maximum at W12. PRPH-negative but TUBB3-positive nerve fibers were consistently found near the distal end of the ganglion, possibly representing the efferent, intra-ganglionic spiral bundles (Fig. 7, black arrows).

Strikingly, by W18, the spiral ganglion was found to be largely devoid of PRPH (Fig. 7D, E). Only some SGNs strongly expressed PRPH (Fig. 7D). Together with the observation that PRPH-positive neurites become confined to the OHCs and their increase in a spiral orientation, this suggests the emergence of *bona fide* type II SGNs at W18 to W20 in humans.

Initial innervation of the cochlear duct is not conserved between mouse and human

We have described here that innervation of the cochlear duct in humans started around W12 and involved the simultaneous penetration by PRPH-positive and TUBB3-positive neurites into the cochlear epithelium. To complement previous mouse studies that focused specifically on the expression of PRPH at late and post-natal stages of development (embryonic day 18 (E18) to post-natal day 7 (P7)) [13, 14], we investigated the expression dynamics of PRPH at the start of penetration of SGN neurites into the mouse cochlear duct and the onset of hair cell differentiation. At E13.5, TUBB3 was present only beneath the prosensory domain of the basal turn of the cochlear duct, as we found in humans at W10 (Fig. 8A, B). However, even though some of the neural structures outside the cochlea showed PRPH positivity (Fig. 8A, white arrow), as well as type II SGNs in adult mouse cochlea that had been processed identically in order to confirm correct immunoreactivity (data not shown), the spiral ganglia in the cochlea of E13.5 mice were completely PRPH-negative, in contrast to our findings in the human cochlea at W10. Two days later, at E15.5, innervation by TUBB3-positive neurites was clearly detected in the basal turn, but innervation by PRPH-positive neurites was still not seen (Fig. 8C-F). It

should be noted that in mice (and humans), innervation of the epithelium preceded hair cell differentiation, as only a single MYO7A-positive IHC was detected in the lower (B1) basal turn (Fig. 8E), but none was seen in the upper (B2) basal turn where neurites had already innervated into the epithelium.

Discussion

Differentiation of the IHC at W12

Using transmission electron microscopy, Pujol and Lavigne-Rebillard previously showed that the onset of first hair cell differentiation in the human fetal cochlea starts in W12 of gestation (that is, week 10 of fetal development) [5]. In the current study, we consistently observed epithelial reorganization in the prosensory domain concurrently with SOX9 downregulation and MYO7A expression in a single row of cells in the prosensory domain of the basal turn, indicating first (inner) hair cell differentiation at W12. However, in one cochlea from W11.4, there were identical changes in marker expression in one out of three sections of the basal turn (see Additional file 6: Figure S1), even though previous ultrastructural investigations had reported an undifferentiated poly-layered epithelium [5], suggesting that hair cell differentiation might already start at the end of W11.

Do SOX2 and SOX9/SOX10 differentially regulate hair cell differentiation?

In mammals and other vertebrates, it has been shown that hair cell differentiation is restricted to cells of the SOX2-positive prosensory domain [33]. Our data are in complete agreement with these observations, as we found that the developing human cochlea at W10.4 exhibited a SOX2-positive prosensory domain in which hair cell precursors subsequently differentiated into IHCs and OHCs in a radial and longitudinal gradient. Sox2 has been shown to act on Atoh1, the key transcription factor for hair cell differentiation [16]. Expression of Atoh1, and thereby hair cell fate commitment, is also under strict control of the Notch pathway [34]. Interestingly, there was downregulation of SOX9 and SOX10 coincident with the moment of first hair cell commitment, which was followed several weeks later by downregulation of SOX2. The same sequence of events for SOX9 and SOX2 has been previously reported in the developing mouse cochlear duct [23]. Together with our observations, this supports a distinct role for SOX9/SOX10 and SOX2 in hair cell fate commitment and an evolutionarily conserved mechanism of hair cell differentiation between mice and humans. It is known from studies in other tissues that Sox9 is directly controlled by Notch activity, for example in the developing nervous system, where it is involved in glial versus neuronal cell fate [35], and in the developing pancreas, where Sox9 and Notch regulate endocrine-versus-ductal cell fate [36]. Sox9 could possibly affect hair cell versus supporting cell fate in a similar,

Notch-dependent manner. Furthermore, we observed the expression of SOX2 by supporting cells in the human cochlea up to the final stage we investigated, at W20.3. As it is currently thought that Sox2 expression in supporting cells is linked to a dormant potential of hair cell diff erentiation [37], this validates (animal) research focusing on this pathway to restore hearing. SOX2 expression in the adult human cochlea remains to be investigated.

Innervation dynamics of the cochlear duct by PRPH-positive neurites

Hair cell development progresses hand in hand with the arrival and shaping of aff erent neurites into the cochlear duct epithelium [11]. In contrast to mice, human PRPH was expressed in SGNs prior to hair cell innervation, and the dynamics in the spiral ganglion correlated perfectly with the initial steps of innervation within the developing OC in humans. We found abundant PRPH expression at W12 and W15 in SGN cell bodies and in neurites reaching both the IHCs and OHCs. At W18, PRPH expression had become limited to cells generally located at the distal end of the spiral ganglion. It is well known that type II SGNs in the adult human cochlea are also found mainly in this area [12]. In addition, in the adult human cochlea, type II SGNs represent less than 10% of the total number of SGNs [12], and PRPH expression has been found to be restricted to this cell type [31]. In relation to our observations, it can therefore be concluded that PRPH expression becomes gradually restricted to type II SGNs by W18-W20.

Onset of human hearing by W20?

Complete absence of PRPH-positive neurites projecting to IHCs was observed at W20. At this gestational stage, the IHCs were abundantly innervated by TUBB3-positive neurites. The spiral orientation of neurites projecting to OHCs was already found at W14 to W15 and was prominently present at W20. These observations are in line with adult expression patterns and orientation, providing further support for the timing of onset of human cochlear function, which is thought to take place around W20 [9-11].

Conclusions

In conclusion, this work (summarized in fig. 9) provides some much needed insight into the development of the human cochlea. We have shown that a SOX2-positive prosensory domain exists within the fetal human cochlear duct. Furthermore, the results presented here support the notion that SOX2 and SOX9/SOX10 may have different roles in hair cell versus supporting cell fate determination. Our investigations into hair cell innervation have shown that both TUBB3-positive and PRPH-positive neurites penetrate the basement membrane of the cochlear epithelium as early as W12 and target the subsequent developing first hair cell. This in contrast to the mouse, in which PRPH expression is detected later. Finally, we determined that already by W18 to W20, PRPH expression distinguishes between type I and type II SGNs, in contrast to mice and other rodents in which this specialization occurs only during post-natal development of the cochlea [13, 14, 38]. Together, these results bring us closer to understanding the timing of some of the essential steps and the identification of some of the key molecular players during human cochlear development. Thus, we provide a basis for research focused on regeneration of the auditory system and restoration of hearing.

Methods

Ethics approval

The medical ethics committee of the Leiden University Medical Center approved this study (protocol 08.087), and informed consent was obtained in accordance with the WMA Declaration of Helsinki guidelines.

Tissue samples

In total, 27 human embryonic and fetal cochleae were collected from tissue obtained by elective termination of pregnancy (by vacuum aspiration, after obstetric ultrasonograpghy to determine gestational age in weeks and days) at various gestational stages (W10 to W20: W10, n = 4; W11, n = 1; W12, n = 4; W14, n = 4; W15, n = 2; W16, n = 1; W17, n = 4; W18, n = 4; W19, n = 2; W20, n = 1). Time between termination and collection was kept to a minimum, ranging from one to several hours. All cochlear specimens were fixed in 4% paraformaldehyde in PBS overnight at 4° C. Cochleae obtained before W14 were dehydrated in ethanol and embedded in paraffin wax using standard procedures. Cochleae from W14 and later were decalcified for 1 to 3 weeks in 10% EDTA disodium salt (pH 7.4) (Sigma-Aldrich, St Louis, MO, USA) in distilled water at 4° C, prior to ethanol dehydration and paraffin wax embedding. Sagittal sections from E13.5 and E15.5 mouse embryos (CBA/Bl6), were a generous gift from the McLaren Laboratry (Wellcome Trust/Cancer Research UK Gurdon Institute, University of Cambridge, Cambridge, UK) For these, E0.5 was designated as the first morning with a vaginal plug, and tissue was fixed in 4% paraformaldehyde in PBS overnight at 4° C before paraffin wax embedding.

Histology and immunofluorescence

The cochleae were sectioned (5 μm) in the sagittal plane using a RM2255 microtome (Leica). Sections were dewaxed in xylene, rehydrated in a descending ethanol series (100%, 90%, 80%, 70%), and rinsed in distilled water. Hematoxylin and eosin staining was performed by standard procedures to determine the morphology of each cochlea. For immunofluorescence, antigen retrieval was performed in 0.01 mol/l sodium citrate buffer (pH 6.0) for 12 minutes at 97° C using a microwave

oven and sections were allowed to cool to room temperature. The sections were subsequently blocked with 1% bovine serum albumin (BSA, Sigma-Aldrich) in PBS containing 0.05% Tween-20 (Promega, Leiden, the Netherlands) for 30 minutes, and incubated with primary antibodies diluted in blocking solution overnight at room temperature in a humidified chamber. The following day, the sections were incubated with secondary antibodies diluted in blocking solution for 2 hours at room temperature. Nuclei were stained with 4',6-diamidino-2-phenylindole (DAPI; Vector Laboratories Ltd., Peterborough, UK) or TO-PRO-3 (Life Technologies, Carlsbad, CA, USA), and sections were mounted in ProLong Gold (Life Technologies). The primary antibodies used in this study were mouse anti-MYO7A (1:40; 138-1 supernatant; DSHB, Iowa City, IA, USA), rabbit anti-SOX2 (1:200; ab5603), rabbit anti-PRPH (1:200; ab1530) (both Chemicon, Temecula, CA, USA); rabbit anti-SOX9 (1:200; ab5535, Millipore Corp., Bedford, MA, USA), goat anti-SOX10 (1:50; sc-17342), mouse anti-PCNA (1:500;, ab-56) (both Santa Cruz Biotechnologies, Santa Cruz, CA, USA), and mouse anti-TUBB3 (1:200; ab78078, Abcam, Cambridge, UK). The Alexa Fluor conjugated secondary antibodies used were 488 donkey anti-mouse (1:500; A-21202), 488 donkey anti-rabbit (1:500; A-21206), 488 donkey anti-goat (1:500; A-11055), 568 donkey anti-mouse (1:500; A-10037) and 568 donkey anti-rabbit (1:500; A-10042 (all Life Technologies)). For antibody specificity controls, primary antibodies were omitted.

Image acquisition and processing

Sections stained with hematoxylin and eosin were digitized using a Pannoramic MIDI scanner (3DHISTECH, Kisvárda, Hungary) and adjusted using Pannoramic Viewer (3DHISTECH). Confocal images were taken under a Leica TCS SP5 confocal inverted microscope (Leica Microsystems), operating with the Leica Application Suite Advanced Fluorescence software (LAS AF; Leica Microsystems). Sections were scanned throughout their full depth with Z-steps of 0.5 μm (or with a sampling density according to the Nyquist rate in the case of high magnification) and Z-projections were generated. Brightness and contrast adjustments, consistent with the image manipulation policy, were performed either in LAS AF or Adobe Photoshop CS6 (Adobe Systems Inc., San José, CA, USA). Amira (version 4.1; Visage Imaging, San Diego, CA, USA) was used for 3D reconstruction of entire Z-stacks.

Competing interests

The authors declare that they have no competing interest.

Authors' contributions

HL and SMC designed the experiments. HL and LI collected and processed the specimens. HL carried out the immunohistochemistry and fluorescent microscopy. All authors analyzed and interpreted the data. HL and SMC drafted the manuscript; LI, JCMJG, MAH and JHMF revized the manuscript. All authors read and approved the final manuscript.

Acknowledgements

We thank K Sprenkels, I Navarro, J Wiegant and AM van der Laan for technical support, CL Mummery for critical reading of the manuscript. We thank the Centre for Contraception, Abortion and Sexuality (CASA; Leiden, the Netherlands) for the human fetal material. Work in the laboratory of SCSL is supported by the Netherlands organization of Scientific Research (NWO) (ASPASIA 015.007.037) and Interuniversity Attraction Poles (IAP) (P7/07), and HL was supported by Stichting Het Heinsius-Houbolt Fonds.

References

1. Rask-Andersen H, Ekvall L, Scholtz A, Schrott-Fischer A: **Structural/audiometric correlations in a human inner ear with noise-induced hearing loss.** Hear Res 2000, **141:**129-139.
2. Merchant SN, Nadol Jr. JB: Schuknecht's Pathology of the Ear. 3rd Edition. Shelton, Connecticut, USA: People's Medical Publishing House-USA; 2010.
3. O'Rahilly R: **The early development of the otic vesicle in staged human embryos.** J Embryol Exp Morphol 1963, **11:**741-755.
4. Moore JK, Linthicum Jr. FH: **The human auditory system: a timeline of development.** Int J Audiol 2007, **46:**460-478.
5. Pujol R, Lavigne-Rebillard M: **Early stages of innervation and sensory cell differentiation in the human fetal organ of Corti.** Acta Otolaryngol Suppl 1985, **423:**43-50.
6. Groves AK, Fekete DM: **Shaping sound in space: the regulation of inner ear patterning.** Development 2012, **139:**245-257.
7. Fekete DM, Muthukumar S, Karagogeos D: **Hair cells and supporting cells share a common progenitor in the avian inner ear.** J Neurosci 1998, **18:**7811-7821.
8. Kiernan AE, Pelling AL, Leung KK, Tang AS, Bell DM, Tease C, Lovell-Badge R, Steel KP, Cheah KS: Sox2 is required for sensory organ development in the mammalian inner ear. Nature 2005, 434:1031-1035.
9. Bibas AG, Xenellis J, Michaels L, Anagnostopoulou S, Ferekidis E, Wright A: **Temporal bone study of development of the organ of Corti: correlation between auditory function and anatomical structure.** J Laryngol Otol 2008, **122:**336-342.
10. Pujol R, Lavigne-Rebillard M: **Sensory and neural structures in the developing human cochlea.** Int J Pediatr Otorhinolaryngol 1995, **32 Suppl:**S177-182.
11. Pujol R, Lavigne-Rebillard M, Uziel A: **Development of the human cochlea.** Acta Otolaryngol Suppl 1991, **482:**7-12; discussion 13.
12. Spoendlin H, Schrott A: **The spiral ganglion and the innervation of the human organ of Corti.** Acta Otolaryngol 1988, **105:**403-410.
13. Huang LC, Thorne PR, Housley GD, Montgomery JM: **Spatiotemporal definition of neurite outgrowth, refinement and retraction in the developing mouse cochlea.** Development 2007, **134:**2925-2933.
14. Barclay M, Ryan AF, Housley GD: **Type I vs type II spiral ganglion neurons exhibit differential survival and neuritogenesis during cochlear development.** Neural Dev 2011, **6:**33.
15. Lavigne-Rebillard M, Pujol R: **Hair cell innervation in the fetal human cochlea.** Acta Otolaryngol 1988, **105:**398-402.
16. Dabdoub A, Puligilla C, Jones JM, Fritzsch B, Cheah KS, Pevny LH, Kelley

MW: **Sox2 signaling in prosensory domain specification and subsequent hair cell diff erentiation in the developing cochlea.** Proc Natl Acad Sci U S A 2008, **105:**18396-18401.

17. Betancur P, Bronner-Fraser M, Sauka-Spengler T: **Genomic code for Sox10 activation reveals a key regulatory enhancer for cranial neural crest.** Proc Natl Acad Sci U S A 2010, **107:**3570-3575.
18. Betancur P, Sauka-Spengler T, Bronner M: **A Sox10 enhancer element common to the otic placode and neural crest is activated by tissue-specific paralogs.** Development 2011, **138:**3689-3698.
19. Saint-Germain N, Lee YH, Zhang Y, Sargent TD, Saint-Jeannet JP: **Specification of the otic placode depends on Sox9 function in Xenopus.** Development 2004, **131:**1755-1763.
20. Taylor KM, Labonne C: **SoxE factors function equivalently during neural crest and inner ear development and their activity is regulated by SUMOylation.** Dev Cell 2005, **9:**593-603.
21. Barrionuevo F, Naumann A, Bagheri-Fam S, Speth V, Taketo MM, Scherer G, Neubuser A: **Sox9 is required for invagination of the otic placode in mice.** Dev Biol 2008, **317:**213-224.
22. Breuskin I, Bodson M, Thelen N, Thiry M, Borgs L, Nguyen L, Lefebvre PP, Malgrange B: **Sox10 promotes the survival of cochlear progenitors during the establishment of the organ of Corti.** Dev Biol 2009, **335:**327-339.
23. Mak AC, Szeto IY, Fritzsch B, Cheah KS: **Diff erential and overlapping expression pattern of SOX2 and SOX9 in inner ear development.** Gene Expr Patterns 2009, **9:**444-453.
24. Watanabe K, Takeda K, Katori Y, Ikeda K, Oshima T, Yasumoto K, Saito H, Takasaka T, Shibahara S: **Expression of the Sox10 gene during mouse inner ear development.** Brain Res Mol Brain Res 2000, **84:**141-145.
25. Freyer L, Aggarwal V, Morrow BE: **Dual embryonic origin of the mammalian otic vesicle forming the inner ear.** Development 2011, **138:**5403-5414.
26. Wakaoka T, Motohashi T, Hayashi H, Kuze B, Aoki M, Mizuta K, Kunisada T, Ito Y: **Tracing Sox10-expressing cells elucidates the dynamic development of the mouse inner ear.** Hear Res 2013, **302C:**17-25.
27. Hagstrom SA, Pauer GJ, Reid J, Simpson E, Crowe S, Maumenee IH, Traboulsi EI: **SOX2 mutation causes anophthalmia, hearing loss, and brain anomalies.** Am J Med Genet A 2005, **138A:**95-98.
28. Savarirayan R, Robertson SP, Bankier A, Rogers JG: **Variable expression of campomelic dysplasia in a father and his 46, XY daughter.** Pediatr Pathol Mol Med 2003, **22:**37-46.
29. Elmaleh-Berges M, Baumann C, Noel-Petroff N, Sekkal A, Couloigner V, Devriendt K, Wilson M, Marlin S, Sebag G, Pingault V: **Spectrum of Temporal Bone**

Abnormalities in Patients with Waardenburg Syndrome and SOX10 Mutations. AJNR Am J Neuroradiol 2013, **34:**1257-1263.

30. Bondurand N, Kobetz A, Pingault V, Lemort N, Encha-Razavi F, Couly G, Goerich DE, Wegner M, Abitbol M, Goossens M: **Expression of the SOX10 gene during human development.** FEBS Lett 1998, **432:**168-172.
31. Liu W, Kinnefors A, Bostrom M, Rask-Andersen H: **Expression of peripherin in human cochlea.** Cell Tissue Res 2010, **342:**345-351.
32. Waldhaus J, Cimerman J, Gohlke H, Ehrich M, Muller M, Lowenheim H: **Stemness of the organ of Corti relates to the epigenetic status of Sox2 enhancers.** PLoS One 2012, **7:**e36066.
33. Neves J, Vachkov I, Giraldez F: **Sox2 regulation of hair cell development: incoherence makes sense.** Hear Res 2013, **297:**20-29.
34. Woods C, Montcouquiol M, Kelley MW: **Math1 regulates development of the sensory epithelium in the mammalian cochlea.** Nat Neurosci 2004, **7:**1310-1318.
35. Taylor MK, Yeager K, Morrison SJ: **Physiological Notch signaling promotes gliogenesis in the developing peripheral and central nervous systems.** Development 2007, **134:**2435-2447.
36. Shih HP, Kopp JL, Sandhu M, Dubois CL, Seymour PA, Grapin-Botton A, Sander M: **A Notch-dependent molecular circuitry initiates pancreatic endocrine and ductal cell differentiation.** Development 2012, **139:**2488-2499.
37. Burns JC, Corwin JT: **A historical to present-day account of efforts to answer the question: "what puts the brakes on mammalian hair cell regeneration?".** Hear Res 2013, **297:**52-67.
38. Hafidi A, Despres G, Romand R: **Ontogenesis of type II spiral ganglion neurons during development: peripherin immunohistochemistry.** Int J Dev Neurosci 1993, **11:**507-512.


cochlea
cochlea

3

Distribution and development of peripheral glial cells in the human fetal cochlea

Locher
de Groot
van Iperen
Huisman
Frijns
Chuva de Sousa Lopes

PLOS ONE, 2014

Abstract

The adult human cochlea contains various types of peripheral glial cells that envelop or myelinate the three different domains of the spiral ganglion neurons: the central processes in the cochlear nerve, the cell bodies in the spiral ganglia, and the peripheral processes in the osseous spiral lamina. Little is known about the distribution, lineage separation and maturation of these peripheral glial cells in the human fetal cochlea. In the current study, we observed immature Schwann cells expressing SOX10, SOX9 and S100B as early as 9 weeks of gestation (W9) in all three neuronal domains. We propose that these cells are the common precursor to both mature Schwann cells and satellite glial cells. Additionally, the immature Schwann cells located along the peripheral processes expressed NGFR, indicating a phenotype distinct from the immature Schwann cells located along the central processes. From W12, the spiral ganglion was gradually populated by satellite glial cells in a spatiotemporal gradient. In the cochlear nerve, radial sorting was accomplished by W22 and myelination started prior to myelination of the peripheral processes. The developmental dynamics of the peripheral glial cells in the human fetal cochlea is in support of a neural crest origin. Our study provides the first overview of the distribution and maturation of peripheral glial cells in the human fetal cochlea from W9 to W22.

Introduction

Schwann cells, the major type of peripheral glial cells (PGCs), envelop and/or myelinate the spiral ganglion neurons (SGNs) in the cochlea and are essential to normal hearing. Demyelinating diseases of the peripheral nervous system result in differences in the velocity of action potential propagation between individual nerve processes [1]. Depending on the degree of demyelination, this loss of neural synchrony leads to moderate sensorineural hearing loss or, if there is a complete conduction block, to deafness [2 – 4]. One major peripheral neuropathy affecting hearing is Charcot-Marie-Tooth disease, a genetically and clinically heterogeneous group of disorders which includes mutations in genes that are involved in myelination [5 – 8]. Other causes of demyelination of peripheral nerves, and hence potentially leading to sensorineural hearing loss, include autoimmune diseases such as the Guillain-Barré syndrome, and infectious diseases such as leprosy [9 – 12]. Loss of myelin may also be involved in the development of age-related sensorineural hearing loss [13].

Based on animal studies, it is commonly accepted that all PGCs derive from the neural crest and migrate along peripheral nerves to their target locations [14, 15]. There, Schwann cell precursors become immature Schwann cells, which subsequently differentiate into myelinating or non-myelinating Schwann cell phenotypes (Fig. 1A). Individual processes of peripheral neurons are singled out by pro-myelinating Schwann cells in a process known as radial sorting. Once ensheathment is completed, those Schwann cells will start to produce myelin, becoming myelinating Schwann cells [14]. The myelin sheath consists of multiple layers of tightly packed myelin surrounding individual nerve processes and functions to increase axonal conduction velocity [16]. Non-myelinating Schwann cells will envelop numerous unmyelinated neuronal processes, forming the so-called Remak bundles in which the individual nerve processes remain separated by cytoplasmic extensions of the non-myelinating Schwann cell [17, 18]. Although Schwann cell differentiation has been investigated extensively, less is known about the development of a third type of PGCs, satellite glial cells. Satellite glial cells are thought to play a role in the microenvironment, protecting, supporting and communicating with the neuronal cell bodies [19, 20]. Avian studies suggest that satellite glial cells and mature Schwann cells derive from a common precursor cell expressing the marker S100 [21] (Fig. 1A). The differentiation cascade that leads to the formation of satellite glial cells in humans remains to be investigated.

In the adult human cochlea, all three PGC types are intimately associated with SGNs. SGNs are bipolar or pseudo-unipolar neurons that transmit electrical signals encoding sound from cochlear hair cells to the brain. They are usually classified as type I SGNs (90-95% of the total population) and type II (5-10%) SGNs. In the adult human cochlea, both processes of the bipolar type I SGNs, the central process in the cochlear nerve (CN) and the peripheral process in the osseous spiral lamina (Fig. 1B), are enwrapped in myelin sheaths that are produced by myelinating Schwann cells [22, 23]. The second type of PGCs, the non-myelinating Schwann cells (Fig. 1B), ensheath but do not myelinate the central and peripheral processes of the type II SGNs [24, 25]. Neither type of Schwann cells ensheath the peripheral processes (that innervate the cochlear hair cells in the organ of Corti) beyond the habenula perforata [26]. In the spiral ganglion (SG), the cell bodies of the SGNs are enveloped by the third type of PGCs, the satellite glial cells (Fig. 1B). In contrast to most mammalian species, satellite glial cells in the human SG seldom myelinate the SGN cell bodies [13, 22, 27, 28].

PGCs have been observed using light microscopy in the human SG and along the central processes of SGNs from 11 weeks of gestation (W11, i.e. 9 weeks of fetal development) onwards [29]. Other reports have looked at earlier stages, but failed to discriminate between SGNs and PGCs in the SG [30]. Using electron-microscopy, it appeared that myelination of the central processes of the SGNs in the CN in humans starts at W20 [31]. At the peripheral processes, a study using Woelcke's iron-hematoxylin method [32] suggested that myelination starts in at W22, although transmission electron microscopy suggested that it commences at W24 [33]. However, it cannot be excluded that the onset of myelination of the peripheral processes is at an earlier stage, especially since younger specimens were not available to these authors.

In the present study, we investigated the distribution and maturation of PGCs in the human fetal cochlea from W9 to W22. Using immunohistochemistry, we observed immature Schwann cells in the cochlea as early as W9 and we defined their developmental phenotype in the three domains of the SGNs: (1) their central processes, (2) their cell bodies, and (3) their peripheral processes. Studies on Schwann cell development are not only important to investigate the onset of myelination (which is one indicator for the maturation of the auditory system and, hence, related to the onset of hearing), but are also needed to better understand the relationship of Schwann cells to auditory neuropathies, whether it be congenital disorders or disorders acquired during adult life.

Materials and Methods

Ethics Statement

The use of human fetal material for this study was approved by the Medical Ethical Committee of the Leiden University Medical Center (protocol 08.087) and informed written consent was obtained in accordance with the WMA Declaration of Helsinki guidelines.

Human fetal cochleae

Twenty-four fetal cochleas were isolated from human fetal material collected after elective abortion (using vacuum aspiration). Gestational age (in weeks and days) was determined using obstetric ultrasonography (W9, n=1; W10, n=2; W11, n=1; W12, n=2; W14, n=2; W15, n=2; W16, n=2; W17, n=3; W18, n=5; W19, n=2; W20, n=1; W22, n=1). The cochleas were isolated in PBS, fixed in 4% paraformaldehyde in PBS overnight at 4° C, decalcified and embedded in paraffin as previously described [34].

Immunofluorescence

The cochleas were cut (5 μm sections) in the sagittal plane using a RM2255 microtome (Leica). Sections were deparaffinized using standard procedures and immunohistochemistry was performed as previously described [34]. Briefly, sections were treated 12 minutes at 97° C with 0.01M sodium citrate buffer (pH 6.0) for antigen retrieval, blocked with 1% bovine serum albumin (Sigma-Aldrich) in PBS containing 0.05% Tween-20 (Promega), and consecutively incubated with primary and secondary antibodies diluted in blocking solution. Nuclei were stained with 4',6-diamidino-2-phenylindole (DAPI, Vector Laboratories). The primary antibodies used in this study were rabbit anti-myelin basic protein (MBP, 1:4000, A0623, DAKO), mouse anti-myosin VIIa (MYO7A, 1:40, 138-1 supernatant, DSHB), rabbit anti-nerve growth factor receptor (NGFR, 1:200, 07-476, Millipore), chicken anti-peripherin (PRPH, 1:200, ab39374, Abcam), rabbit anti-S100 calcium binding protein B (S100B, 1:200, ab52642, Abcam), rabbit anti-SOX9 (1:200, ab5535, Millipore), goat anti-SOX10 (1:50, sc-17342, Santa Cruz), and mouse anti-class III β-tubulin (TUBB3, 1:200, ab78078, Abcam). The secondary antibodies used were

Alexa Fluor (AF) conjugated immunoglobulins (Life Technologies): AF 488 donkey anti-mouse (A-21202), AF 488 donkey anti-rabbit (A-21206), AF 488 donkey anti-goat (A-11055), AF 488 goat anti-chicken (A-11039), AF 568 donkey anti-mouse (A-10037), AF 568 donkey anti-rabbit (A-10042), AF 647 donkey anti-mouse (A-31571), AF 647 donkey anti-rabbit (A-31573) and AF 647 donkey anti-goat (A-21447), all at 1:500 dilution. As antibody specificity controls, primary antibodies were omitted. Also, in the case of MBP stainings, rabbit immunoglobulin fraction (X0903, DAKO) was used as an additional negative control as we observed cytoplasmic fluorescence by SGN cell bodies at lower dilutions.

Image acquisition and processing

Confocal images were made with either a Leica TCS SP5 inverted or a Leica SP8 upright microscope, operating under the Leica Application Suite Advanced Fluorescence software (LAS AF) using Leica objectives (20x/0.5 dry HCX PL Fluotar; 40x/1.3 oil HC PL Apo; 63x/1.4 oil HC PL Apo; 100x/1.4 oil HCX PL Fluotar). Maximal projections were obtained from image stacks that were generated by scanning sections throughout their full depth with z-steps of 0.5 μm, or with a sampling density according to the Nyquist rate when image restoration (deconvolution) was applied using Huygens Professional version 4.3.1 software (Scientific Volume Imaging). Brightness and contrast adjustments consistent with image manipulation policies were performed either with LAS AF, ImageJ version 1.47a (National Institutes of Health, http://imagej.nih.gov/ij) or Adobe Photoshop CS6 (Adobe Systems) image-processing software.

Results

Human W9 fetal cochlea contains SOX9+/ SOX10+/S100B+ PGCs

To our knowledge, the presence of PGCs has not been reported in human fetal cochleas younger than W11 [29]. Here, we have investigated the distribution and phenotype of PGCs at W9, the youngest cochlear specimen we were able to obtain. At W9, the cochlear duct consisted of one full turn, the future basal turn. To identify PGCs, we immunostained for SOX10 (a nuclear marker for PGCs regardless of developmental stage [35, 36]), S100B (a cytoplasmic marker expressed in immature and mature Schwann cells but not in Schwann cell precursors [35]) and TUBB3 (a general marker of SGNs) (Fig. 1C-G). In the CN, abundant SOX10+/ S100B+ PGCs were detected surrounding essentially all central processes (Fig. 1G). SOX10+/S100B+ PGCs were also observed at the peripheral processes in the lower (B1) and the upper (B2) basal turn of the SG (Fig. 1G). In the SG, we identified SOX10+/S100B+ PGCs mainly along its edge and only a few in its center (Fig. 1G). Immunostaining for SOX9, a nuclear neural crest marker [37, 38], revealed a similar pattern of expression to SOX10 and S100B in PGCs (Fig. 1H-J), indicating that at W9 the majority of PGCs located along the neuronal processes have passed the SOX9+/SOX10+/S100B- progenitor phase and have developed into a more mature SOX9+/SOX10+/S100B+ phenotype. Based on their distribution density, these PGCs most likely migrate from the central processes to the peripheral processes along the periphery of the SG and may start colonizing the SG giving rise to the satellite glial cells.

SOX9+/ SOX10+/S100B+ PGCs invade the SG in a spatiotemporal gradient

The developing human cochlea is characterized by distinct temporal and a spatial gradients at various levels including hair cell development, organ of Corti maturation, and hair cell innervation [34]. Therefore, we investigated whether PGCs in the SG displayed a similar developmental pattern within the cochlea.

In the lower basal turn (B1) between W9 and W10.4, we observed an increased number of PGCs in the center of the SG (Fig. 1C-J and Fig. 2A-G), in agreement with our hypothesis that immature SOX9+/SOX10+/S100B+ PGCs colonize the SG, differentiating into satellite glial cells. At a higher magnification, the central region of the SG showed the formation of a network of PGCs between the cell bodies

of the SGNs (Fig. 2H-J). However, PGCs at this stage (W10.4) did not yet cluster with the cell bodies of the SGNs. S100B+ PGCs were present along the peripheral processes as far as the most distal tips of those processes, right underneath the prosensory domain of the cochlear duct (Fig. 2K-M). In addition to the SGNs, the epithelium of the cochlear duct also weakly immunostained for TUBB3, with the brightest fluorescence in the prosensory domain (Fig. 2B and 3B) or later in the hair cells [34].

By W12, dense immunostaining for S100B was observed in the lower basal turn (B1) of the SG (Fig. 3A-D, right arrow in D), suggesting the presence of many PGCs. In addition, a spatial gradient was visible in a basal-to-apical direction. From B1 to the upper middle turn (M2), S100B immunostaining was progressively less prominent in the center of the SG and PGCs were primarily present at the edge of the SG in M2 (Fig. 3A-D, left arrow in D). In agreement, immunostaining for SOX9 at W12 confirmed this basal to apical distribution of PGCs (Fig. 3E-L). We concluded that, similar to other aspects of cochlear development, PGCs also show distinct temporal and spatial gradients in colonizing the SG of the human fetal cochlea.

Satellite glial cells envelope SGN cell bodies between W12 and W14

The onset of envelopment of the cell bodies of the TUBB3+ SGNs by the S100B+ PGCs was observed at W12 in the basal turn of the SG (Fig. 4A-H, arrows) and by W14 the cell bodies of all SGNs in the SG were fully enveloped by S100B+ PGCs (Fig. 4I-L). By W18, this had become even more pronounced and S100B+ PGCs had become intimately associated with the SGNs (Fig. 4M-P).

During the process of envelopment, we also noticed changes in the PGC nuclei. At W12, DAPI staining showed that SGN nuclei were generally round whereas the nuclei of the enveloping PGCs tended to be more angular or crescent shaped (Fig. 5Q-R). At W14, this difference became more prominent. In addition, PGC nuclei started to get organized around and facing the cell bodies of the SGNs and exhibited bright yet diffuse DAPI staining (Fig. 5S-T). By W18, the differences between the PGC nuclei and SGN nuclei were even more pronounced, with round SGN nuclei containing prominent nucleoli (Fig. 5U-V), much like the morphology in adults. At W18, each SGN cell body was surrounded by one or more PGCs.

At W9, NGFR is expressed in PGCs along the peripheral processes

The low affinity nerve growth factor receptor (NGFR, also known as $p75^{NTR}$) is expressed by Schwann cells at various locations within the adult human cochlea [39] and is expressed in mice and rats throughout the neural crest and Schwann cell lineages [14]. Immunostaining for NGFR at W9 and W10.4 revealed two different PGC phenotypes in the developing human cochlea. In the lower basal turn (B1), PGCs along the peripheral SGN processes strongly expressed NGFR both at W9 (Fig. 5A-D) and W10.4 (Fig. 5E-I). NGFR immunostaining could even be detected along the most distal tips of the peripheral processes just underneath the cochlear duct (Fig. 5I, inset). In contrast, PGCs located at the central processes in the CN did not express NGFR (Fig. 5A-D). In addition, a few NGFR+ cells were detected in the SG at W9 (Fig. 5A-D, asterisk in D), but not at W10.4 (Fig. 5E-I) or later stages.

S100B+/NGFR+ PGCs cells do not penetrate the cochlear duct epithelium

Since we consistently observed PGCs at the distal tips of the outgrowing peripheral processes (Fig. 2K-M, inset 5I), we investigated whether they would initially follow the peripheral processes into the cochlear duct epithelium, although Schwann cells are known to be absent in the mature organ of Corti [26]. We have previously shown that penetration of peripheral processes into the cochlear duct epithelium is observed in all turns at W12 and that they targeted and innervated the developing (future) inner hair cell [34]. At W12 in the upper middle turn (M2), multiple S100+ PGCs were located directly outside the cochlear duct epithelium, and although some TUBB3+ neurites could be seen penetrating into the prosensory domain, S100B expression could not be observed beyond this border (Fig. 6A-C). In the lower basal turn (B1), many peripheral processes were found targeting the first developing hair cell within the cochlear duct epithelium (Fig. 6D-F, arrowhead). Here, S100B+ PGCs did not extend into the cochlear duct epithelium either. Immunostaining for NGFR confirmed these results (Fig. 6G-H, bold arrows). Expression of NGFR was also evident directly underneath the cochlear duct epithelium at W14, both in the basal and middle turns (Fig. 6I-N, bold arrows). Together, these findings indicate that PGCs do not follow the peripheral processes into the cochlear duct epithelium during development.

NGFR is expressed by pillar cells within the developing human organ of Corti.

Interestingly, just after the onset of the first hair cell differentiation at B1 of W12, we also observed weak NGFR expression within the cochlear duct epithelium in a group of cells located around the (future) inner hair cell, marked by MYO7A expression (Fig. 6G-H, thin arrows). At W14, similar weak NGFR expression was observed at M2 (Fig. 6I-J). At M1, expression was increased in the cell lateral to the inner hair cell, with a bright band at its apical surface, corresponding to the cuticular plate (Fig. 6K-L, thin arrows). At W14, the outer hair cells had also differentiated at B1 and strong NGFR expression was observed in the putative outer pillar cell (Fig. 6M-N, thin arrows). In contrast to the observed NGFR expression, none of the turns at W12-W14 showed any S100B expression in the developing organ of Corti (data not shown). In the subsequent weeks (i.e., up to W18), similar NGFR expression patterns were observed, both by the PGCs along the peripheral processes (Fig. 6O-Q) and within the organ of Corti (Fig. 6R-S).

Myelination has started in the W22 cochlear nerve

Immunostaining for S100B and TUBB3 demonstrated that PGCs enveloped and bundled groups of nerve fibers in the CN as early as W9 (Fig. 7A-C). At W22, immunostaining for S100B and TUBB3 revealed that within the CN many individual TUBB3+ cochlear nerve fibers were ensheathed by S100B+ PGCs (Fig. 7 D-G, upper inset in 7G), suggesting that these cells had differentiated into a promyelinating stage and that radial sorting was completed. In addition, Remak bundles, the final developmental stage of non-myelinating Schwann cells, were observed in the CN (Fig. 7G, lower inset). To investigate myelination, we analyzed the expression of MBP, a major component of the myelin sheath. We were unable to detect any MBP expression along the peripheral processes, nor within the SG nor within the CN up to W18 (data not shown). At W22, immunostaining for MBP revealed a few MBP+ tubular structures surrounding individual TUBB3+ cochlear nerve fibers, indicating that myelination in the CN had started at least by W22, but not before W18 (Fig. 7H-K). No MBP expression was observed within the SG or along the peripheral processes in any of the cochlear turns at W22 (Fig. 8A-E). To determine if the MBP+ central processes belonged to type I or type II SGNs, we immunostained the CN at W22 for MPB, TUBB3 and PRPH (which selectively labels type II SGNs in the adult human cochlea). In most cases, MBP+ structures were seen along TUBB3+/PRPH- cochlear nerve fibers (Fig 8F-O, upper inset in

O). However, MBP+ structures along TUBB3+/PRPH+ cochlear nerve fibers could also be observed, albeit only a few (Fig. 8K-O, lower inset in O).

Discussion

On the origin of PGCs in the human cochlea

The assumption that the cells within the cochlea are of dual embryonic origin has been based on classic experiments using spotted salamander larvae [40] and chick-quail chimeras [41]. These experiments indicated that whereas most of the SGNs are derived from the otic placode, PGCs have a neural crest origin. Recent research has further confirmed the neural crest origin for PGCs in the mouse cochlea [42, 43], suggesting that the PGC cell origin is conserved in vertebrates. The pattern of PGC distribution that we observed in humans at the early gestational stages (W9-12) is in agreement with the hypothesis of a neural crest origin, with neural crest cells or early derivatives migrating along the CN into the human cochlea and populating the SG. Although the human Schwann cell lineage remains to be fully delineated, expression of the calcium-binding protein S100 consistently marks the transition of Schwann cell precursors into immature Schwann cells in the rat [44, 45]. As S100B was already abundantly expressed at W9, we conclude that the PGCs in the human cochlea at this fetal stage have already differentiated into the immature Schwann cell phenotype. A more extensive descriptive investigation of marker expression (for example, as mentioned in [14, 38])) could further validate these results. In addition to S100B we have investigated glial-fibrillary acidic protein (GFAP), however this marker was found to be expressed by the SGNs rather than the PGCs (data not shown).

In avian embryos, previous studies have shown that both satellite glial cells and Schwann cells are derived from a S100+ common precursor cell [21, 46]. Based on the onset of association with SGNs, we hypothesize that the satellite glial cell phenotype arises in the human cochlea from W12 onwards, as modelled in Fig. 9. Before this stage, SOX9+/SOX10+/S100B+ PGCs can be found in and around the SG, matching an immature Schwann cell phenotype. Therefore, as in animals (reviewed in [14, 15, 21, 47]), our observations indicate that human satellite glial cells, myelinating Schwann cells and non-myelinating Schwann cells in the human cochlea also share a common precursor: the S100B+ immature Schwann cell.

Schwann cells along the peripheral processes, a role for NGFR?

Interestingly, the PGCs along the peripheral processes and along the central

processes in the CN have a different phenotype, as the former express NGFR whereas the latter do not. NGFR is a low-affinity receptor for all neurotrophins and can act alone or in conjunction with Trk-receptors. Among its functions are programmed cell death (apoptosis), cell survival, neurite outgrowth, myelination and Schwann cell migration as well as modulation of synaptic strength [48 – 50]. Although expression of NGFR has been reported in Schwann cells in the adult human cochlea [39], its exact functions in the cochlea remain unknown.

Mouse models have shown that deficiencies or mutations in NGFR are linked to progressive hearing loss, but have also indicated that NGFR is not required for development of hearing (as tested by auditory-evoked brainstem responses) in the first postnatal weeks [49, 51]. In a study exploring the development of neural innervation in the mouse cochlea in *ErbB2* null mutants, a Schwann cell receptor involved in survival and myelination, the cochlea was devoid of Schwann cells. Interestingly, in these mutant cochleas, the peripheral processes of SGNs did overshoot the organ of Corti, their target location [52]. The authors speculated that cochlear Schwann cells could normally provide containment signals guiding neurite outgrowth. Further evidence for this hypothesis comes from a study using a mouse model of peripheral nerve injury that showed strong up-regulation of NGFR by Schwann cells [53]. The resulting increase in NGFR lowered the amount of neurotrophins available to the injured neurons, thereby inhibiting the regenerating axons to penetrate from the dorsal root into the spinal cord.

Our data support the hypothesis of a role for Schwann cells in nerve containment, as we observed a close relationship between NGFR+ Schwann cells and peripheral processes, as early as W9. In addition, Schwann cells did not follow when peripheral processes started to penetrate and explore the cochlear duct epithelium at W12. Whether or not NGFR plays a role in the process of axon guidance within the cochlea remains to be investigated.

NGFR expression in the developing organ of Corti

In the adult human organ of Corti, expression of NGFR has not been reported [39]. However, studies in mice and rats have detected transient expression of NGFR in pillar cells, disappearing in the first postnatal week, prior to the onset of hearing in these animals [49, 54 – 56]. It is thought that hearing in the human foetus commences at W20 or later [57]; the NGFR expression we detected in the outer pillar cells at W18 support the view of the immaturity of the organ of Corti

at this stage. It has been proposed that NGFR expression plays a role in the differentiation or survival of hair and supporting cells and the formation of the tunnel of Corti [54]. Interestingly, we observed the strongest expression of NGFR in the cuticular plate of the outer pillar cell, that is exposed to the lumen of the cochlear duct. It is therefore plausible that these regulatory effects of NGFR are mediated by circulating (pro)neurotrophic factors in the fluid of the cochlea acting on the cuticular plate.

No transient myelination of SGNs by satellite glial cells

In contrast to other mammalian species, the majority of the cell bodies of the SGNs in the adult human are unmyelinated [13, 22, 27, 28]. Transient myelination of SGN cell bodies during human fetal development, from W14 onwards, has been suggested [29]. In the current study, we did not observe any MBP expression within the human SG between W15 and W22. As myelination of SGN cell bodies has also not been observed in human neonates or infants [22, 24], it is unlikely that SGNs undergo a period of transient myelination during human fetal development.

The onset of myelination within the human cochlea

In an extensive evaluation of the developing human fetal CN, it was reported that myelination of the central processes in the CN starts at W20 [31]. Myelination of the peripheral processes has been observed at W24 [33]. We investigated Schwann cells along peripheral processes up to W22, but did not detect MBP expression in any of the basal and middle turns. However, at W22 we observed MBP in the CN. Together, this shows that the onset of myelination of the CN, at W20, precedes myelination of the peripheral processes, which occurs between W22 and W24.

In the adult human cochlea, the number of type I SGNs correlates well with the number of myelinated nerve fibers within the CN and it is commonly accepted that the unmyelinated fibers represent type II SGNs [25]. As PRPH selectively immunostains the central processes of type II SGNs in the adult human cochlea [58], we examined whether all MBP+ structures surrounded PRPH-negative fibers. Indeed, most of the fibers surrounded by MBP did not express PRPH, but few exceptions were observed. This could indicate that some myelinated cochlear nerve fibers could be of type II SGN origin. However, as all SGNs express PRPH early in development [34], we favor the more plausible alternative explanation that

these structures represent (immature) type I SGNs in the process of downregulating PRPH.

In conclusion, our data provide a comprehensive overview of PGC development in the human fetal cochlea, which may add to our understanding of congenital disorders and auditory neuropathies and can be used as a basis to evaluate acquired changes during adult life.

Acknowledgements

We would like to thank J. Wiegant and A.M. van der Laan for technical support, C.L. Mummery for critical reading of the manuscript, and the Center for Contraception, Sexuality and Abortion (CASA) in Leiden and The Hague for the collection of the human fetal material.

References

1. Rowland LP: **Diseases of the motor unit. In Principles of Neural Science. 4th edition.** Edited by Kandel ER, Schwartz JH, Jessell TM. McGraw-Hill Companies; 2000:695 – 712.
2. Postelmans JTF, Stokroos RJ: **Cochlear implantation in a patient with deafness induced by Charcot-Marie-Tooth disease (hereditary motor and sensory neuropathies).** J Laryngol Otol 2006, 120:508 – 10.
3. Sambuughin N, de Bantel A, McWilliams S, Sivakumar K: **Deafness and CMT disease associated with a novel four amino acid deletion in the PMP22 gene.** Neurology 2003, 60:506 – 508.
4. El-Badry MM, Ding D, McFadden SL, Eddins AC: **Physiological eff ects of auditory nerve myelinopathy in chinchillas.** Eur J Neurosci 2007, 25:1437 – 46.
5. Bucci C, Bakke O, Progida C: **Charcot-Marie-Tooth disease and intracellular traff ic.** Prog Neurobiol 2012, 99:191 – 225.
6. d'Ydewalle C, Benoy V, Van Den Bosch L: **Charcot-Marie-Tooth disease: emerging mechanisms and therapies.** Int J Biochem Cell Biol 2012, 44:1299 – 304.
7. Berger P, Niemann A, Suter U: **Schwann cells and the pathogenesis of inherited motor and sensory neuropathies (Charcot-Marie-Tooth disease).** Glia 2006, 54:243 – 57.
8. Suter U, Scherer SS: **Disease mechanisms in inherited neuropathies.** Nat Rev Neurosci 2003, 4:714 – 26.
9. Koyuncu M, Celik O, Oztürk A, Saunders M: **Audiovestibular system, fifth and seventh cranial nerve involvement in leprosy.** Indian J Lepr 1994, 66:421 – 8.
10. Ooi WW, Srinivasan J: **Leprosy and the peripheral nervous system: basic and clinical aspects.** Muscle Nerve 2004, 30:393 – 409.
11. Takazawa T, Ikeda K, Murata K, Kawase Y, Hirayama T, Ohtsu M et al.,: **Sudden deafness and facial diplegia in Guillain-Barré Syndrome: radiological depiction of facial and acoustic nerve lesions.** Intern Med 2012, 51:2433 – 7.
12. Yuki N, Hartung H: Guillain-Barré syndrome. N Engl J Med 2012, 366:2294 – 304.
13. Xing Y, Samuvel DJ, Stevens SM, Dubno JR, Schulte BA, Lang H: **Age-related changes of myelin basic protein in mouse and human auditory nerve.** PLoS One 2012, 7:e34500.
14. Jessen KR, Mirsky R: **The origin and development of glial cells in peripheral nerves.** Nat Rev Neurosci 2005, 6:671 – 82.
15. Woodhoo A, Sommer L: **Development of the Schwann cell lineage: from the neural crest to the myelinated nerve.** Glia 2008, 56:1481 – 90.
16. Vabnick I, Shrager P: **Ion channel redistribution and function during development of the myelinated axon.** J Neurobiol 1998, 37:80 – 96.

17. Nave K-A, Salzer JL: **Axonal regulation of myelination by neuregulin 1.** Curr Opin Neurobiol 2006, 16:492 – 500.
18. Griff in JW, Thompson WJ: **Biology and pathology of nonmyelinating Schwann cells.** Glia 2008, 56:1518 – 31.
19. Hanani M: **Satellite glial cells in sympathetic and parasympathetic ganglia: in search of function.** Brain Res Rev 2010, 64:304 – 27.
20. Huang L-YM, Gu Y, Chen Y: **Communication between neuronal somata and satellite glial cells in sensory ganglia.** Glia 2013, 61:1571 – 81.
21. Le Douarin NM, Ziller C, Couly GF: **Patterning of neural crest derivatives in the avian embryo: in vivo and in vitro studies.** Dev Biol 1993, 159:24 – 49.
22. Ota CY, Kimura RS: **Ultrastructural study of the human spiral ganglion.** Acta Otolaryngol 1980, 89:53 – 62.
23. Spoendlin H: **Anatomy of cochlear innervation.** Am J Otolaryngol 1985, 6:453 – 67.
24. Arnold W: **The spiral ganglion of the newborn baby.** Am J Otol 1982, 3:266 – 9.
25. Spoendlin H, Schrott A: **Analysis of the human auditory nerve.** Hear Res 1989, 43:25 – 38.
26. Spoendlin H: **Anatomisch-pathologische Aspekte der Elektrostimulation des ertaubten Innenohres.** Arch Otorhinolaryngol 1979, 223:1 – 75.
27. Arnold W: **Myelination of the human spiral ganglion.** Acta Otolaryngol Suppl 1987, 436:76 – 84.
28. Tylstedt S, Kinnefors A, Rask-Andersen H: **Neural interaction in the human spiral ganglion: a TEM study.** Acta Otolaryngol 1997, 117:505 – 12.
29. Sánchez Del Rey A, Sánchez Fernández JM, Martínez Ibarguen A, Santaolalla Montoya F: **Morphologic and morphometric study of human spiral ganglion development.** Acta Otolaryngol 1995, 115:211 – 7.
30. Bibas AG, Hornigold R, Liang J, Michaels L, Anagnostopoulou S, Wright A: **The development of the spiral ganglion in the human foetus.** Folia Morphol (Warsz) 2006, 65:140 – 4.
31. Ray B, Roy TS, Wadhwa S, Roy KK: **Development of the human fetal cochlear nerve: a morphometric study.** Hear Res 2005, 202:74 – 86.
32. Moore JK, Linthicum FH: **Myelination of the human auditory nerve: diff erent time courses for Schwann cell and glial myelin.** Ann Otol Rhinol Laryngol 2001, 110(7 Pt 1):655 – 61.
33. Lavigne-Rebillard M, Pujol R: **Hair cell innervation in the fetal human cochlea.** Acta Otolaryngol 1988, 105:398 – 402.
34. Locher H, Frijns JHM, van Iperen L, de Groot JCMJ, Huisman MA, Chuva de Sousa Lopes SM: **Neurosensory development and cell fate determination in the human cochlea.** Neural Dev 2013, 8:20.
35. Mirsky R, Woodhoo A, Parkinson DB, Arthur-Farraj P, Bhaskaran A, Jessen KR: **Novel signals controlling embryonic Schwann cell development, myelination and**

dediff erentiation. J Peripher Nerv Syst 2008, 13:122 – 35.

36. Wakaoka T, Motohashi T, Hayashi H, Kuze B, Aoki M, Mizuta K, Kunisada T, Ito Y: **Tracing Sox10-expressing cells elucidates the dynamic development of the mouse inner ear.** Hear Res 2013, 302(May):17 – 25.
37. Sauka-Spengler T, Bronner-Fraser M: **A gene regulatory network orchestrates neural crest formation.** Nat Rev Mol Cell Biol 2008, 9:557 – 68.
38. D'Antonio M, Michalovich D, Paterson M, Droggiti A, Woodhoo A, Mirsky R, Jessen KR: **Gene profiling and bioinformatic analysis of Schwann cell embryonic development and myelination.** Glia 2006, 53:501 – 15.
39. Liu W, Glueckert R, Kinnefors A, Schrott-Fischer A, Bitsche M, Rask-Andersen H: **Distribution of P75 neurotrophin receptor in adult human cochlea-an immunohistochemical study.** Cell Tissue Res 2012, 348:407 – 15.
40. Yntema CL: **An experimental study of the origin of the cells which constitute the VIIth and VIIIth cranial ganglia and nerves in the embryo of Amblystoma punctatum.** J Exp Zool 1937, 75:75 – 101.
41. D'Amico-Martel A, Noden DM: **Contributions of placodal and neural crest cells to avian cranial peripheral ganglia.** Am J Anat 1983, 166:445 – 68.
42. Freyer L, Aggarwal V, Morrow BE: **Dual embryonic origin of the mammalian otic vesicle forming the inner ear.** Development 2011, 138:5403 – 14.
43. Sandell LL, Butler Tjaden NE, Barlow AJ, Trainor PA: **Cochleovestibular nerve development is integrated with migratory neural crest cells.** Dev Biol 2014, 385:200 – 10.
44. Woodhoo A, Dean CH, Droggiti A, Mirsky R, Jessen KR: **The trunk neural crest and its early glial derivatives: a study of survival responses, developmental schedules and autocrine mechanisms.** Mol Cell Neurosci 2004, 25:30 – 41.
45. Jessen KR, Brennan A, Morgan L, Mirsky R, Kent A, Hashimoto Y, Gavrilovic J: **The Schwann cell precursor and its fate: a study of cell death and diff erentiation during gliogenesis in rat embryonic nerves.** Neuron 1994, 12:509 – 27.
46. Dupin E, Baroffio A, Dulac C, Cameron-Curry P, Le Douarin NM: **Schwann-cell diff erentiation in clonal cultures of the neural crest, as evidenced by the anti-Schwann cell myelin protein monoclonal antibody.** Proc Natl Acad Sci U S A 1990, 87:1119 – 23.
47. Garratt AN, Britsch S, Birchmeier C: **Neuregulin, a factor with many functions in the life of a schwann cell.** Bioessays 2000, 22:987 – 96.
48. Green SH, Bailey E, Wang Q, Davis RL: **The Trk A, B, C's of Neurotrophins in the Cochlea.** Anat Rec (Hoboken) 2012, 295:1877 – 95.
49. Sato T, Doi K, Taniguchi M, Yamashita T, Kubo T, Tohyama M: **Progressive hearing loss in mice carrying a mutation in the p75 gene.** Brain Res 2006, 1091:224 – 34.
50. Ramekers D, Versnel H, Grolman W, Klis SFL: Neurotrophins and their role in the **cochlea.** Hear Res 2012, 288:19 – 33.

51. Brors D, Hansen S, Mlynski R, Volkenstein S, Aletsee C, Sendtner M, Ryan AF, Dazert S: **Spiral ganglion outgrowth and hearing development in p75-deficient mice.** Audiol Neurootol 2008, 13:388 – 95.

52. Morris JK, Maklad A, Hansen LA, Feng F, Sorensen C, Lee K-F, Macklin WB, Fritzsch B: **A disorganized innervation of the inner ear persists in the absence of ErbB2.** Brain Res 2006, 1091:186 – 99.

53. Scott ALM, Ramer MS: **Schwann cell p75NTR prevents spontaneous sensory reinnervation of the adult spinal cord.** Brain 2010, 133(Pt 2):421 – 32.

54. Gestwa G, Wiechers B, Zimmermann U, Praetorius M, Rohbock K, Köpschall I, Zenner HP, Knipper M: **Diff erential expression of trkB.T1 and trkB.T2, truncated trkC, and p75(NGFR) in the cochlea prior to hearing function.** J Comp Neurol 1999, 414:33 – 49.

55. Von Bartheld CS, Patterson SL, Heuer JG, Wheeler EF, Bothwell M, Rubel EW: **Expression of nerve growth factor (NGF) receptors in the developing inner ear of chick and rat.** Development 1991, 113:455 – 70.

56. Sano H, Mukai J, Monoo K, Close LG, Sato T-A: **Expression of p75NTR and its associated protein NADE in the rat cochlea.** Laryngoscope 2001, 111:535 – 8.

57. Bibas AG, Xenellis J, Michaels L, Anagnostopoulou S, Ferekidis E, Wright A: **Temporal bone study of development of the organ of Corti: correlation between auditory function and anatomical structure.** J Laryngol Otol 2008, 122:336 – 42.

58. Liu W, Kinnefors A, Boström M, Rask-Andersen H: **Expression of peripherin in human cochlea.** Cell Tissue Res 2010, 342:345 – 51.

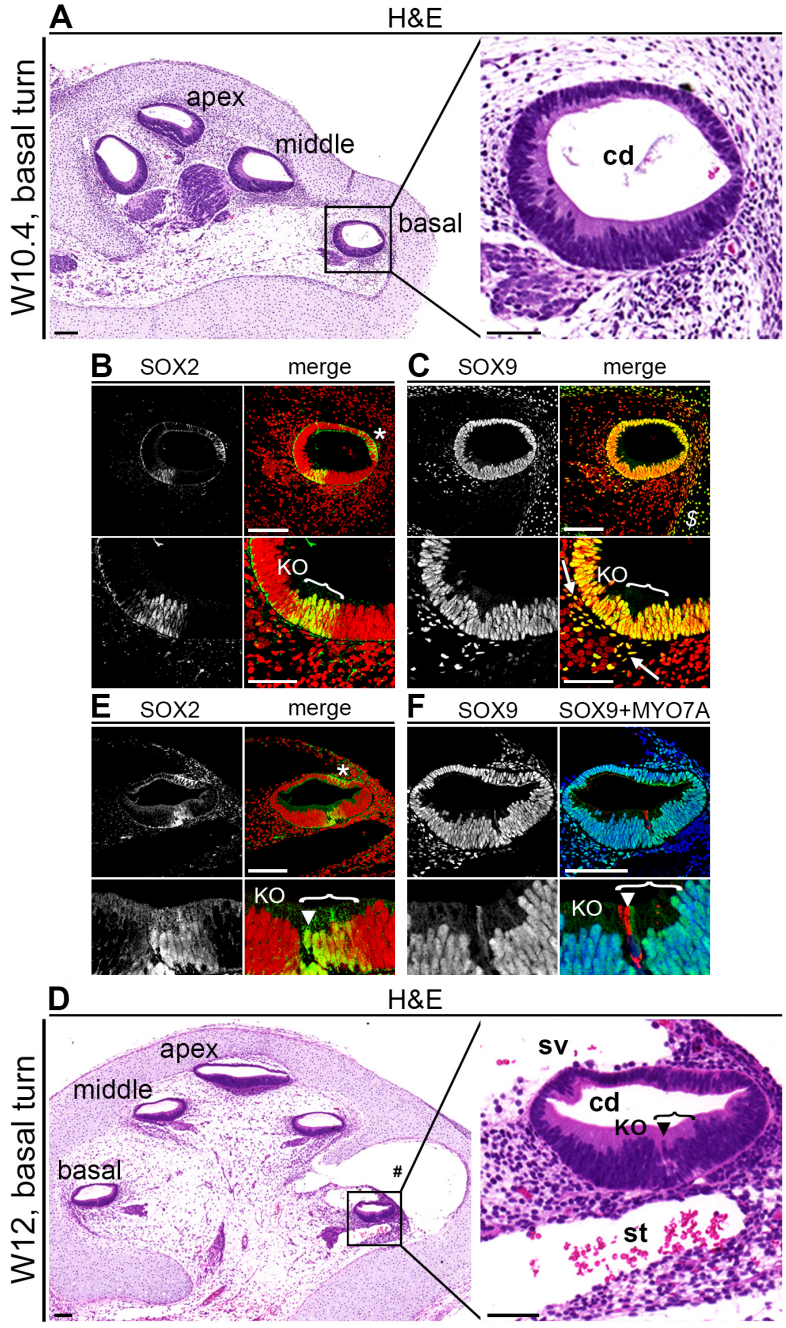


FIGURE 1. SOX2 AND SOX9 EXPRESSION IN HUMAN FETAL COCHLEA AROUND THE ONSET OF FIRST HAIR CELL DIFFERENTIATION.
(**A**) Hematoxylin and eosin (H&E) staining of a cochlea at W10.4 (week 10 and 4 days) with higher magnification (right panel) of the basal turn cochlear duct. (**B**) Basal turn of a W10.4 cochlea immunostained for SOX2, and magnification of the prosensory domain (bottom panels). Cell nuclei were visualized with TO-PRO-3 (red). (**C**) Basal turn of a W10.4 cochlea immunostained for SOX9, and magnification of the prosensory domain (bottom panels). Cell nuclei were visualized with TO-PRO-3 (red). (**D**) H&E staining of a W12 (week 12) cochlea with higher magnification (right panel) of the basal turn cochlear duct. (**E**) Basal turn of a W12 cochlea immunostained for SOX2, and magnification of the prosensory domain (bottom panels). Cell nuclei were visualized with TO-PRO-3 (red). (**F**) Basal turn of a W12 cochlea immunostained for SOX9 (green) and MYO7A (red), and magnification of the prosensory domain (bottom panels). Cell nuclei were visualized with DAPI (blue). #Tissue artifact; *, cytoplasmic SOX2 staining in the cochlear duct; $, SOX9 staining in the otic capsule; bracket, the prosensory domain; white arrow, Schwann cells of the spiral ganglion; arrowhead, inner hair cell. Abbreviations: cd, cochlear duct; KO, Kölliker's organ; sv, scala vestibuli; st, scala tympani. Scale bars = 100 μm (all lower magnifications) or 50 μm (all higher magnifications).

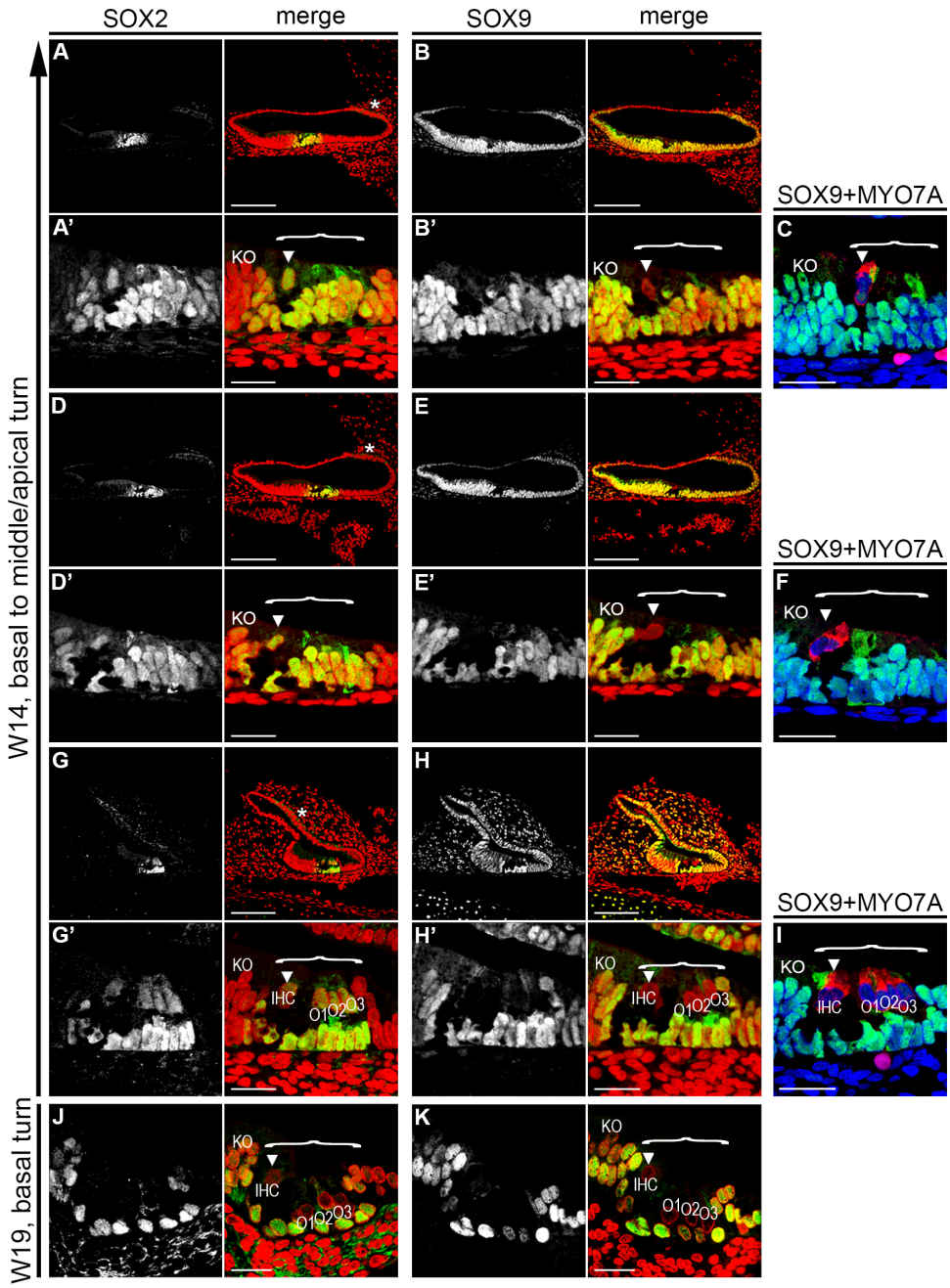


Figure 2. SOX2 and SOX9 expression during development of the human organ of Corti (OC).
(**A,B**) Apical turn of a W14 cochlea immunostained for (A) SOX2 and (B) SOX9 and magnification of the prosensory domain/OC (**A',B'**). Cell nuclei were visualized (red) with TO-PRO-3. (**C**) The prosensory domain/OC in the apical turn of a W14 cochlea immunostained for SOX9 (green) and MYO7A (red). Cell nuclei were visualized with DAPI (blue). (**D,E**) Middle turn of a W14 cochlea immunostained for (D) SOX2 and (E) SOX9, and (**D',E'**) magnification of the prosensory domain/OC. Cell nuclei were visualized with TO-PRO-3 (red). (**F**) The prosensory domain/OC in the middle turn of a W14 cochlea immunostained for SOX9 (green) and MYO7A (red). Cell nuclei were visualized with DAPI (blue). (**G,H**) Basal turn of a W14 cochlea immunostained for (G) SOX2 and (H) SOX9, and (**G',H'**) magnification of the prosensory domain/OC. (**I**) The prosensory domain/OC in the basal turn of a W14 cochlea immunostained for SOX9 (green) and MYO7A (red). Cell nuclei were visualized with DAPI (blue). (**J,K**) Basal turn of a W19 cochlea immunostained for (G) SOX2 and (H) SOX9. Cell nuclei were visualized with TO-PRO-3 (red). *Cytoplasmic SOX2 staining in the cochlear duct; bracket, the prosensory domain/OC; arrowhead, inner hair cell. Abbreviations: KO, Kölliker's organ; IHC, inner hair cell; O1, first row of outer hair cells; O2, second row of outer hair cells; O3, third row of outer hair cells. Scale bars = (A–K) 50 µm or (A'–H') 20 µm.

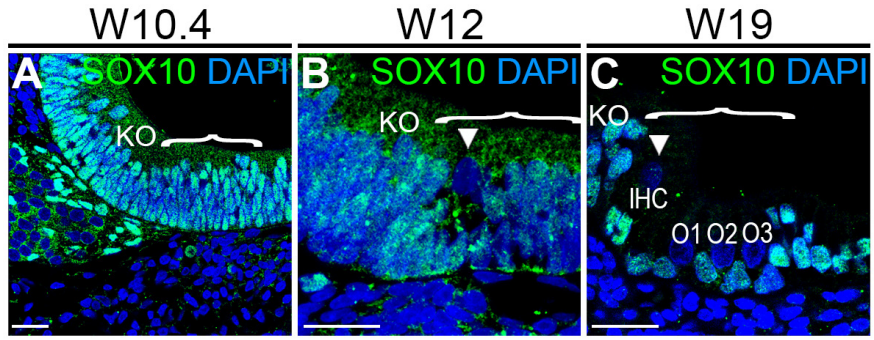


Figure 3. SOX10 expression during human organ of Corti (OC) development.
(A-C) Basal turn of a cochlea immunostained for SOX10 (green) at (A) W10.4, (B) W12 and (C) W19. Cell nuclei were visualized with DAPI (blue). Bracket, the prosensory domain/OC; arrowhead, inner hair cell. Abbreviations: KO, Kölliker's organ. Scale bars = 20 µm.

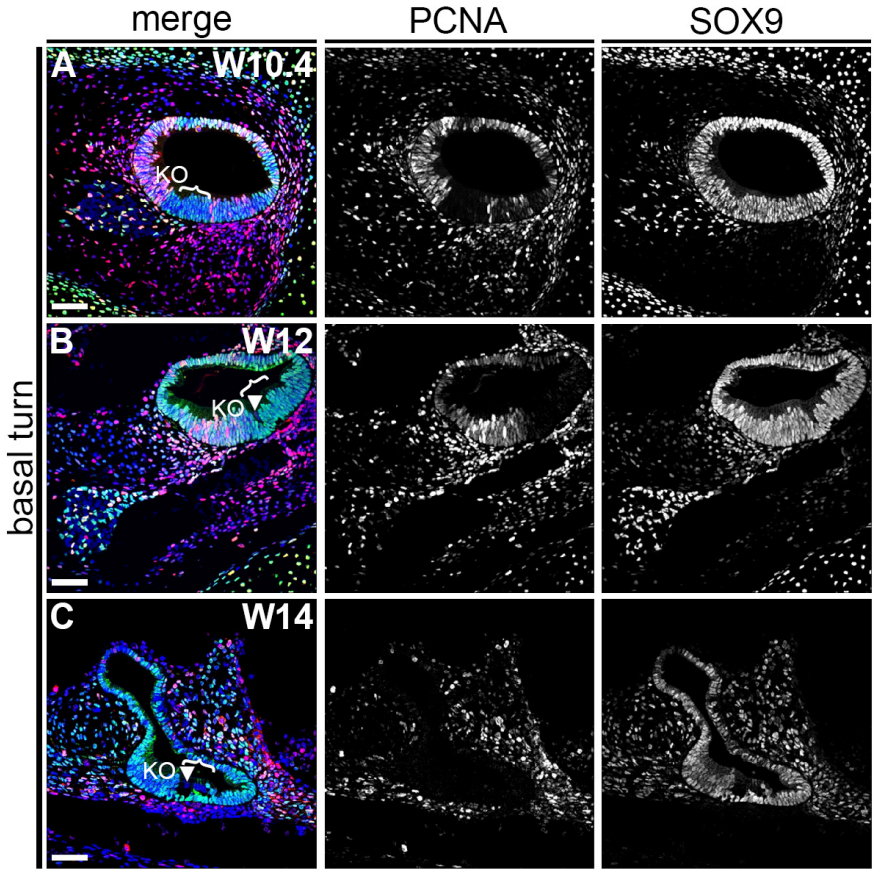


Figure 4. Proliferating cell nuclear antigen (PCNA) and SOX9 expression in the basal turn of W10.4 to W14 human fetal cochlea.
(A-C) Basal turn of a cochlea immunostained for PCNA (red) and SOX9 (green) at (A) W10.4, (B) W12 and (C) W14. Cell nuclei were visualized with DAPI (blue). Bracket, the prosensory domain/OC; arrowhead, inner hair cell. Abbreviations: KO, Kölliker's organ. Scale bars = 40 µm.

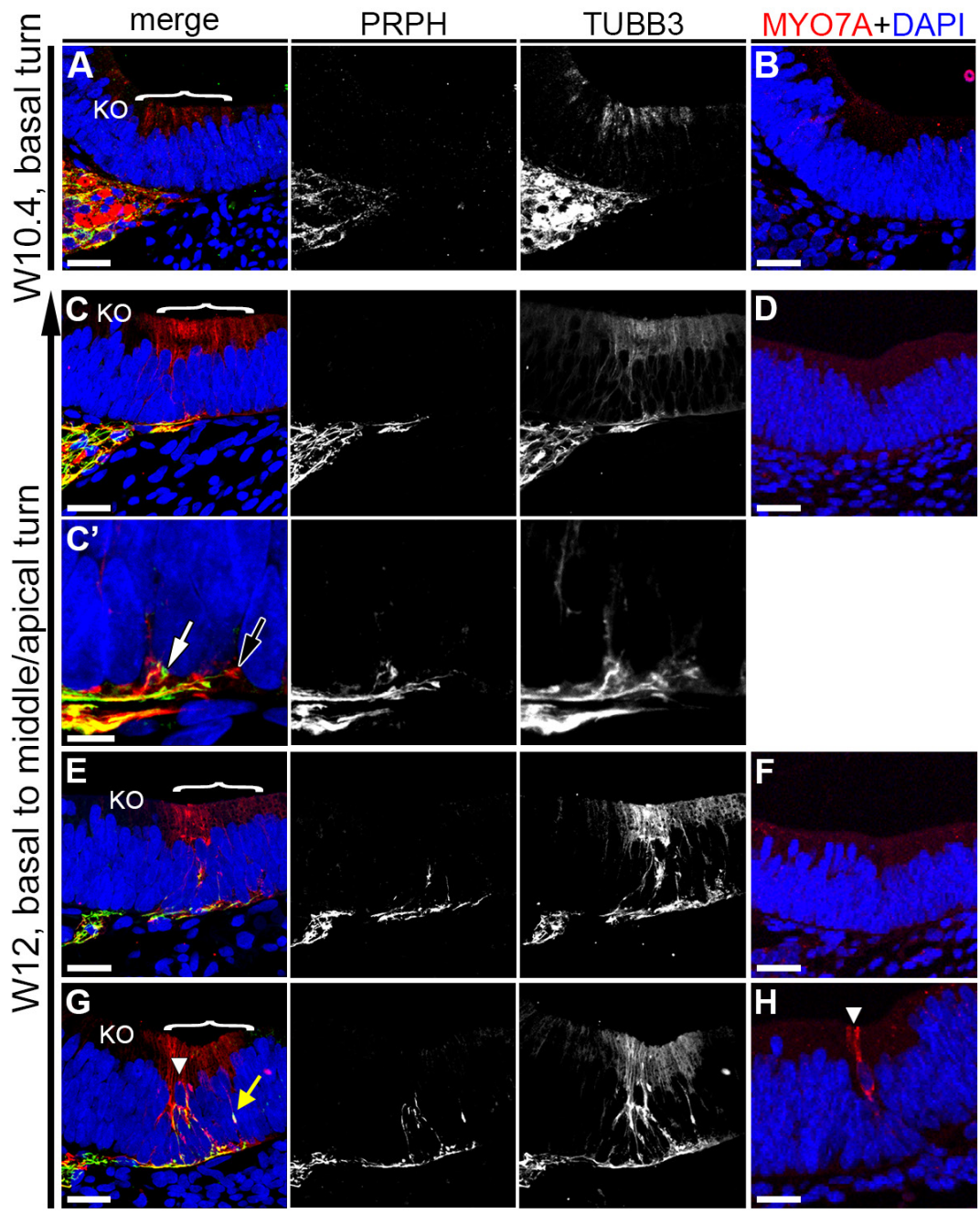


Figure 5. Dynamics of Peripherin (PRPH)-positive and class III β-Tubulin (TUBB3)-positive neurites during first hair cell differentiation. (**A,B**) Basal turn of a W10.4 (week 10 and 4 days) cochlea immunostained for (A) PRPH (green) and TUBB3 (red) and (B) MYO7A (red). (**C,D**) Apical turn of a W12 cochlea immunostained for (C) PRPH and TUBB3 and MYO7A (D). (**C'**) Magnification of the prosensory domain in (C). (**E,F**) Middle turn of a W12 cochlea immunostained for (E) PRPH and TUBB3 and (F) MYO7A. (**G,H**) Basal turn of a W12 cochlea immunostained for (G) PRPH and TUBB3 and (H) MYO7A. Cell nuclei were visualized with DAPI (blue). Bracket, the prosensory domain/OC; arrowhead, inner hair cell; white arrow, PRPH-positive growth cone; black arrow, TUBB3-positive growth cone; yellow arrow, PRPH/TUBB3-positive neurite. Abbreviations: KO, Kölliker's organ. Scale bars = (A-C, D-H) 20 µm or (C') 5 µm.

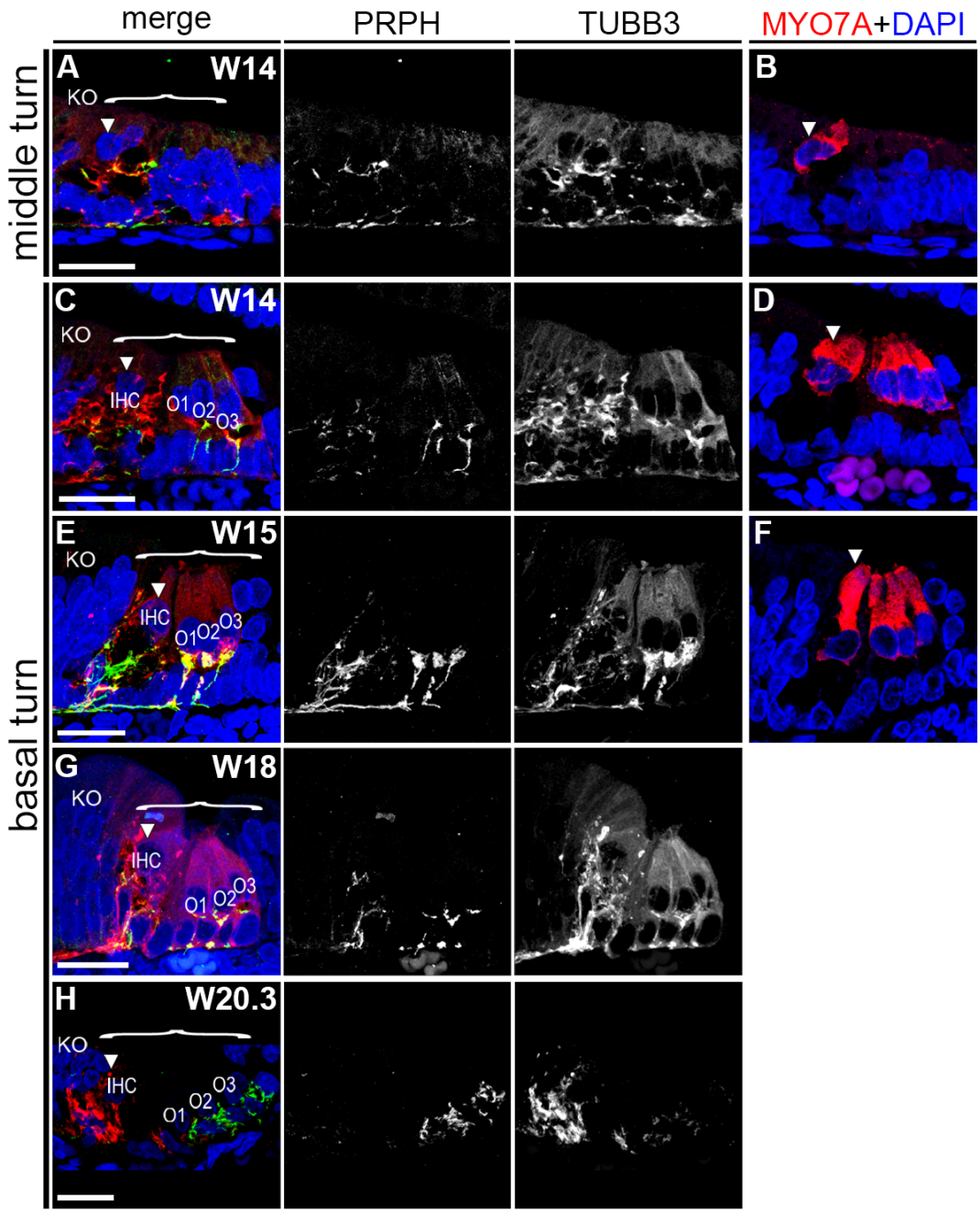


FIGURE 6. DYNAMICS OF PERIPHERIN (PRPH)-POSITIVE AND CLASS III B-TUBULIN (TUBB3)-POSITIVE NEURITES DURING ORGAN OF CORTI (OC) MATURATION.

(**A,B**) Middle turn of a W14 (week 14) cochlea immunostained for (A) PRPH (green) and TUBB3 (red) and (B) MYO7A (red). (**C,D**) Basal turn of a W14 cochlea immunostained for (C) PRPH and TUBB3 and (D) MYO7A. (**E,F**) Basal turn of a W15 cochlea immunostained for (E) PRPH and TUBB3 and (F) MYO7A. (**G**) Basal turn of a W18 cochlea immunostained for PRPH and TUBB3. (**H**) Basal turn of a W20.3 cochlea immunostained for PRPH and TUBB3. Cell nuclei were visualized with DAPI (blue). Bracket, the prosensory domain/OC; arrowhead, inner hair cell. Abbreviations: KO, Kölliker's organ; IHC, inner hair cell; O1, first row of outer hair cells; O2, second row of outer hair cells; O3, third row of outer hair cells. Scale bars = 20 µm.

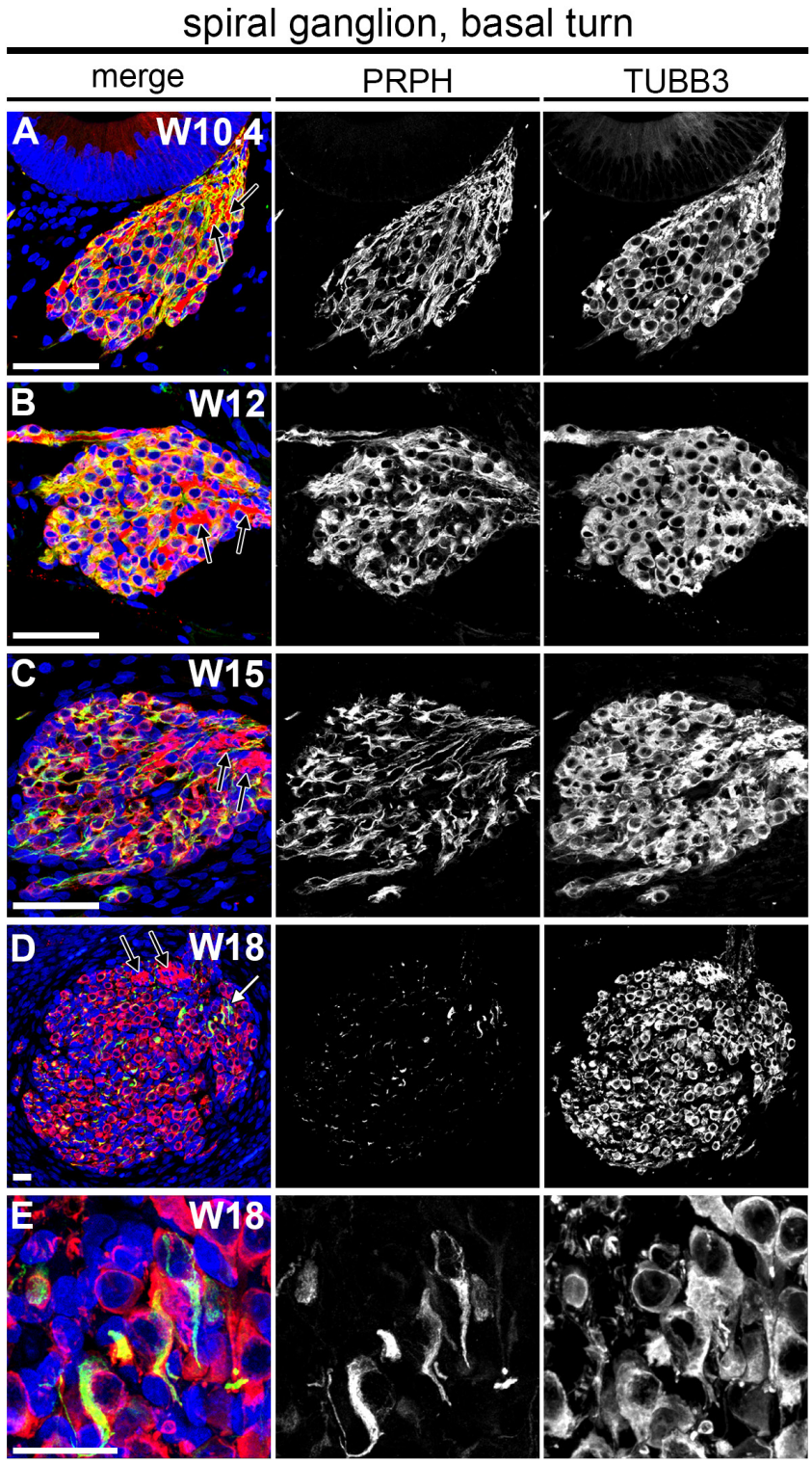


FIGURE 7. DYNAMICS OF PERIPHERIN (PRPH) AND CLASS III B-TUBULIN (TUBB3) EXPRESSION IN THE HUMAN FETAL SPIRAL GANGLION.
(A-E) Basal turn spiral ganglion immunostained for PRPH (green) and TUBB3 (red) at (A) W10.4 (week 10 and 4 days), (B) W12, (C) W15 and (D) W18. (E) Magnification of the basal turn spiral ganglion marked with a white arrow in (D). Cell nuclei were visualized with DAPI (blue). White arrow, PRPH-positive spiral ganglion neurons; black arrow, PRPH-negative and TUBB3-positive nerve fiber bundles. Scale bars = 20 µm.

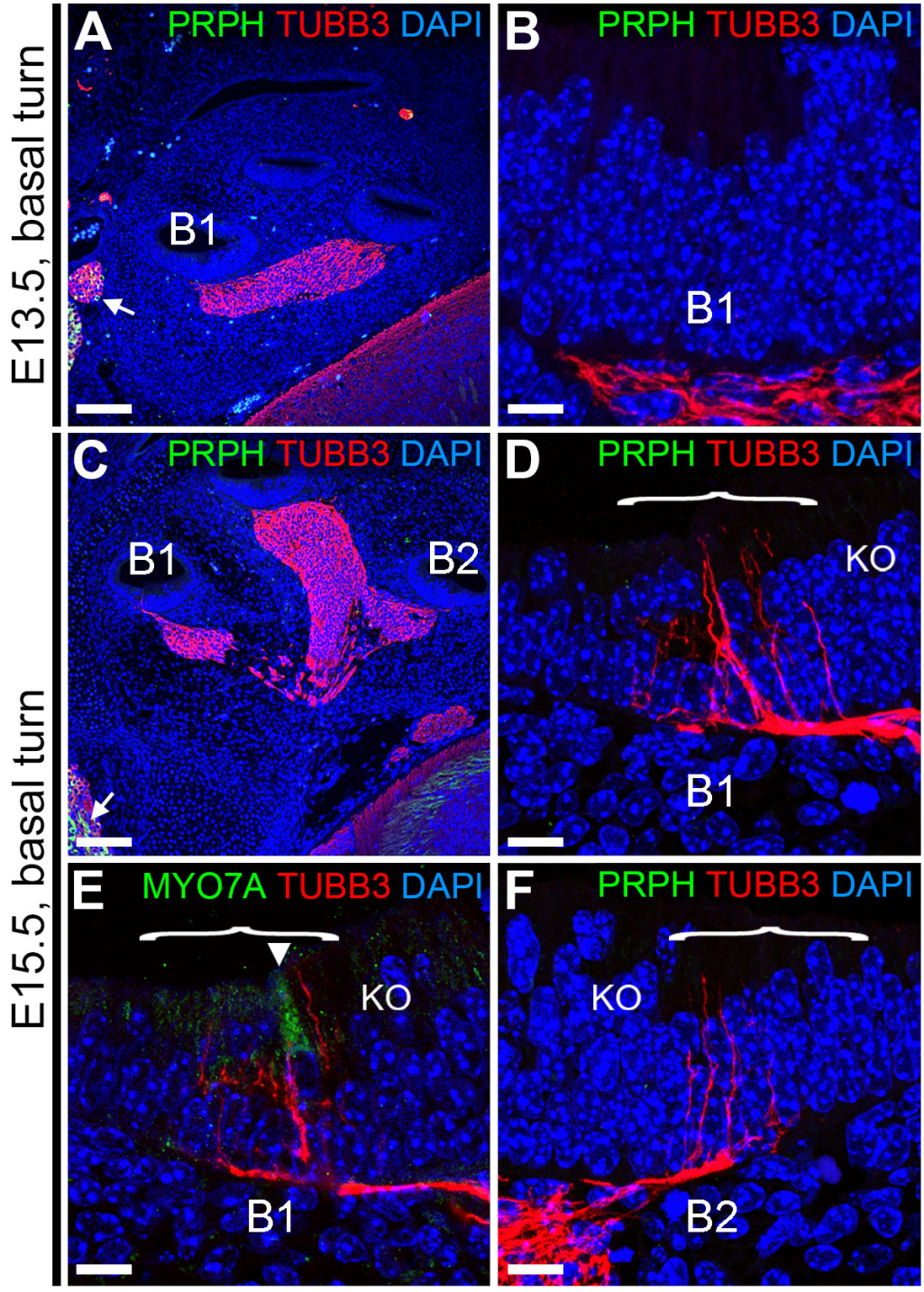


Figure 8. Peripherin (PRPH) and class III β-Tubulin (TUBB3) expression in embryonic day 13.5 (E13.5) and E15.5 mouse cochlea. (**A,B**) E13.5 mouse cochlea immunostained (A) for PRPH (green) and TUBB3 (red) and (B) magnification of the prosensory domain of basal turn B1. (**C-F**) E15.5 mouse cochlea (C) immunostained for PRPH and TUBB3, (D) magnification of the prosensory domain of basal turn B1, (E) magnification of the prosensory domain of basal turn B1 immunostained for TUBB3 (red) and MYO7A (green), and (F) magnification of the prosensory domain of basal turn B2 immunostained for PRPH (green) and TUBB3 (red). Cell nuclei were visualized with DAPI (blue). Bracket, the prosensory domain; arrowhead, inner hair cell. Abbreviations: KO, Kölliker's organ. Scale bars = (A,C) 100 μm or (B, D-F) 10 μm.

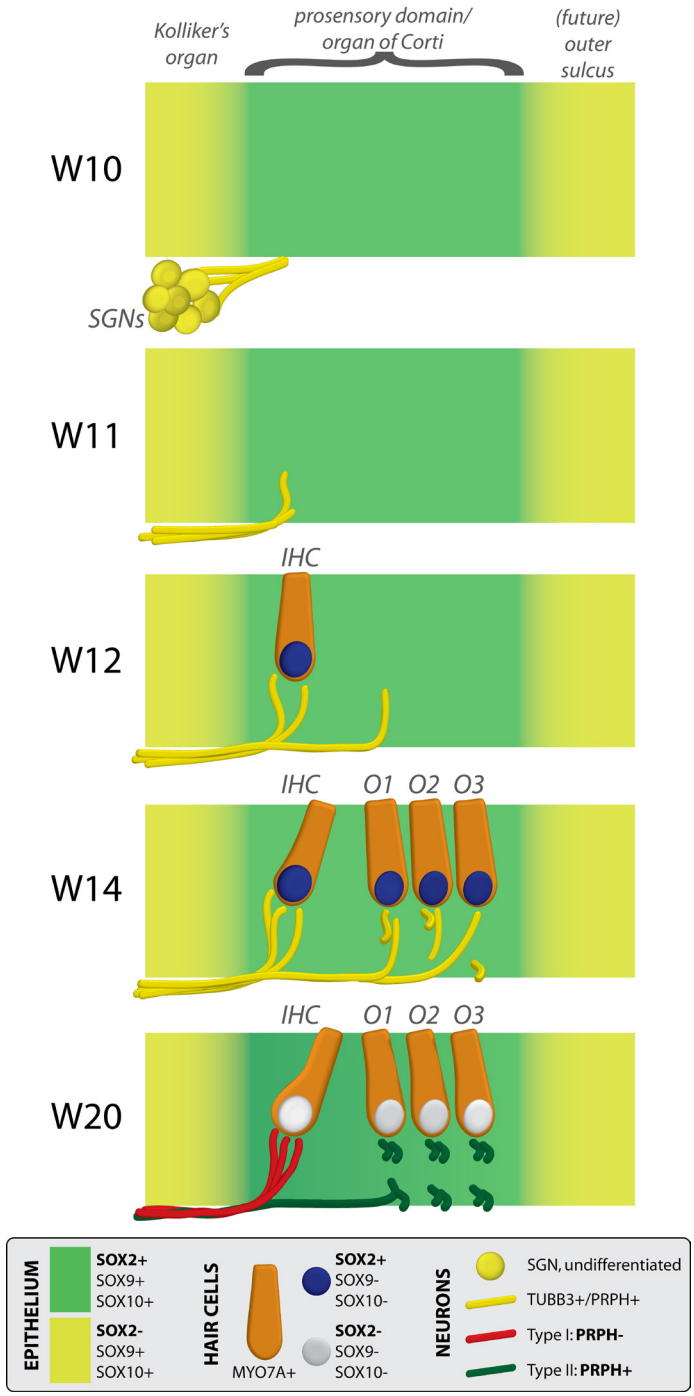
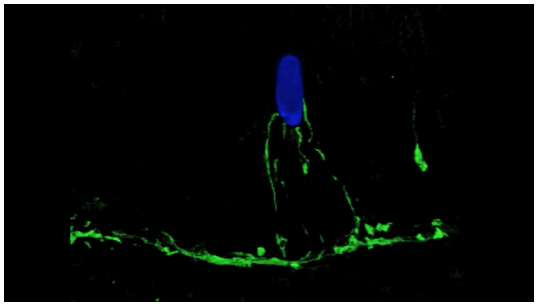
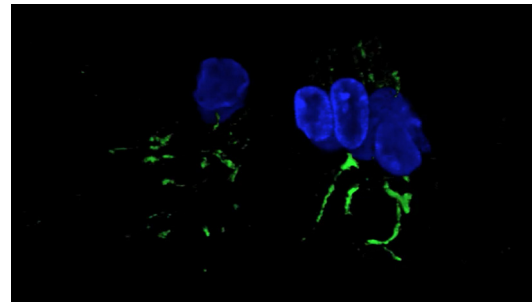


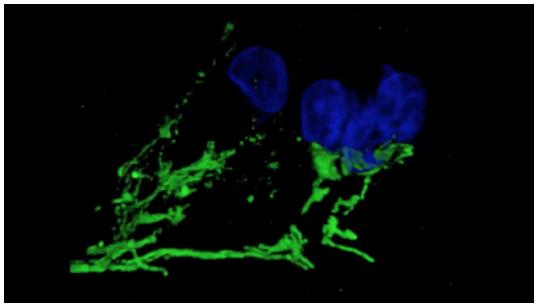
Figure 9. Schematic diagram of neurosensory development in the basal turn of the human fetal cochlea.
At W10 (week 10), SOX2 identifies the prosensory domain within the SOX9/SOX10+ cochlear duct epithelium. Neurites from the adjoining TUBB3+/PRPH+SGNs do not yet penetrate into the epithelium. Penetration starts at W11, prior to hair cell differentiation. At W12, the first MYO7A+/SOX9-/SOX10-/SOX2+ (inner) hair cell can be seen, and is contacted by multiple TUBB3+ and PRPH+neurites. Penetrating neurites are also found at the location of the future OHCs. At W14, both the IHCs and OHCs have differentiated, and neurites underneath the OHCs start to run in a spiral direction. At this stage, hair cells still express SOX2. At W20, SOX2 is downregulated in all hair cells, as opposed to the other cells in the organ of Corti. PRPH expression distinguishes between type I (PRPH-) and type II (PRPH+) neurites. Abbreviations: SGN, spiral ganglion neuron; IHC, inner hair cell; O1, first row of outer hair cells; O2, second row of outer hair cells; O3, third row of outer hair cells; OHC, outer hair cell.



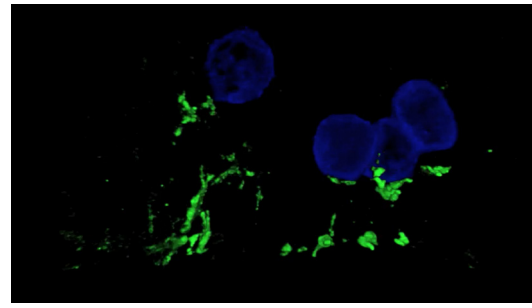
Additional file 1: Movie 1
Three-dimensional reconstruction showing the PRPH-positive neurites (green) and the nucleus of the inner hair cell (blue) of the prosensory domain/developing organ of Corti in the lower basal turn at W12, (week 12) corresponding to Figure 5G.
Format: M4V. Size: 3.4MB



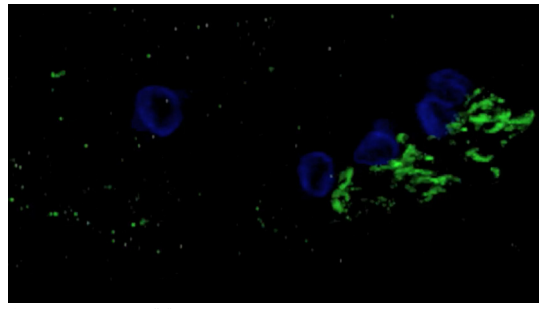
Additional file 2: Movie 2
Three-dimensional reconstruction showing the Peripherin (PRPH)-positive neurites (green) and the nuclei of the hair cells (blue) of the developing organ of Corti in the lower basal turn at W14 (week 14), corresponding to Figure 6C.
Format: M4V. Size: 3MB



Additional file 3: Movie 3
3D reconstruction showing the PRPH-positive neurites (green) and the nucleus of the inner hair cell (blue) of the developing organ of Corti in the lower basal turn at W15, corresponding to Figure 6E.
Format: M4V. Size: 3.8MB

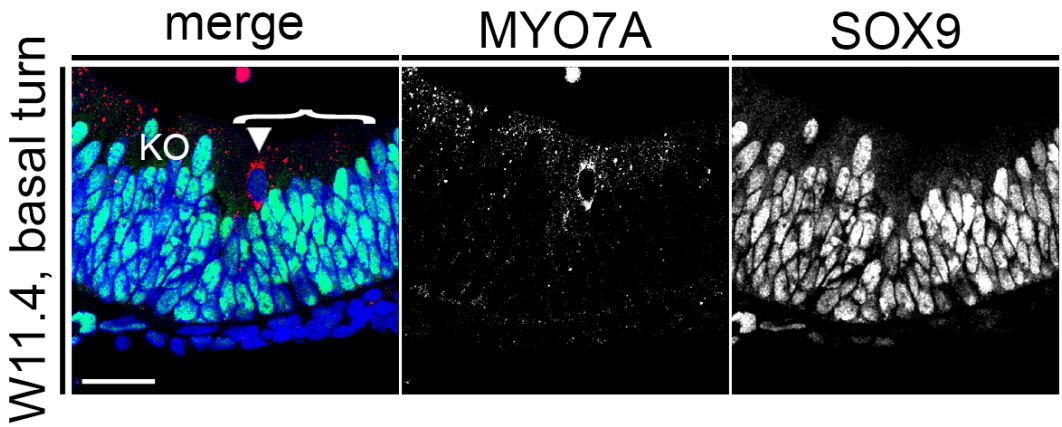


Additional file 4: Movie 4
Three-dimensional reconstruction showing the Peripherin (PRPH)-positive neurites (green) and the nucleus of the inner hair cell (blue) of the developing organ of Corti in the lower basal turn at W18 (week 18), corresponding to Figure 6G.
Format: M4V. Size: 4.1MB



Additional file 5: Movie 5
Three-dimensional reconstruction showing the Peripherin (PRPH)-positive neurites (green) and the nucleus of the inner hair cell (blue) of the developing organ of Corti in the lower basal turn at W20.3 (week 20.3), corresponding to Figure 6H.
Format: M4V. Size: 3.3MB

These additional movie files can be accessed online at the journal's website (www.neuraldevelopment.com)



Additional file 6: Figure S1. The onset of hair cell differentiation.
Confocal image of the prosensory domain within the lower basal turn of a W11.4 human fetal cochlea immunostained for MYO7A (red) and SOX9 (green). Nuclei were visualized (blue) with DAPI. Bracket, prosensory domain; arrowhead, inner hair cell. Scale bar = 20 μm.

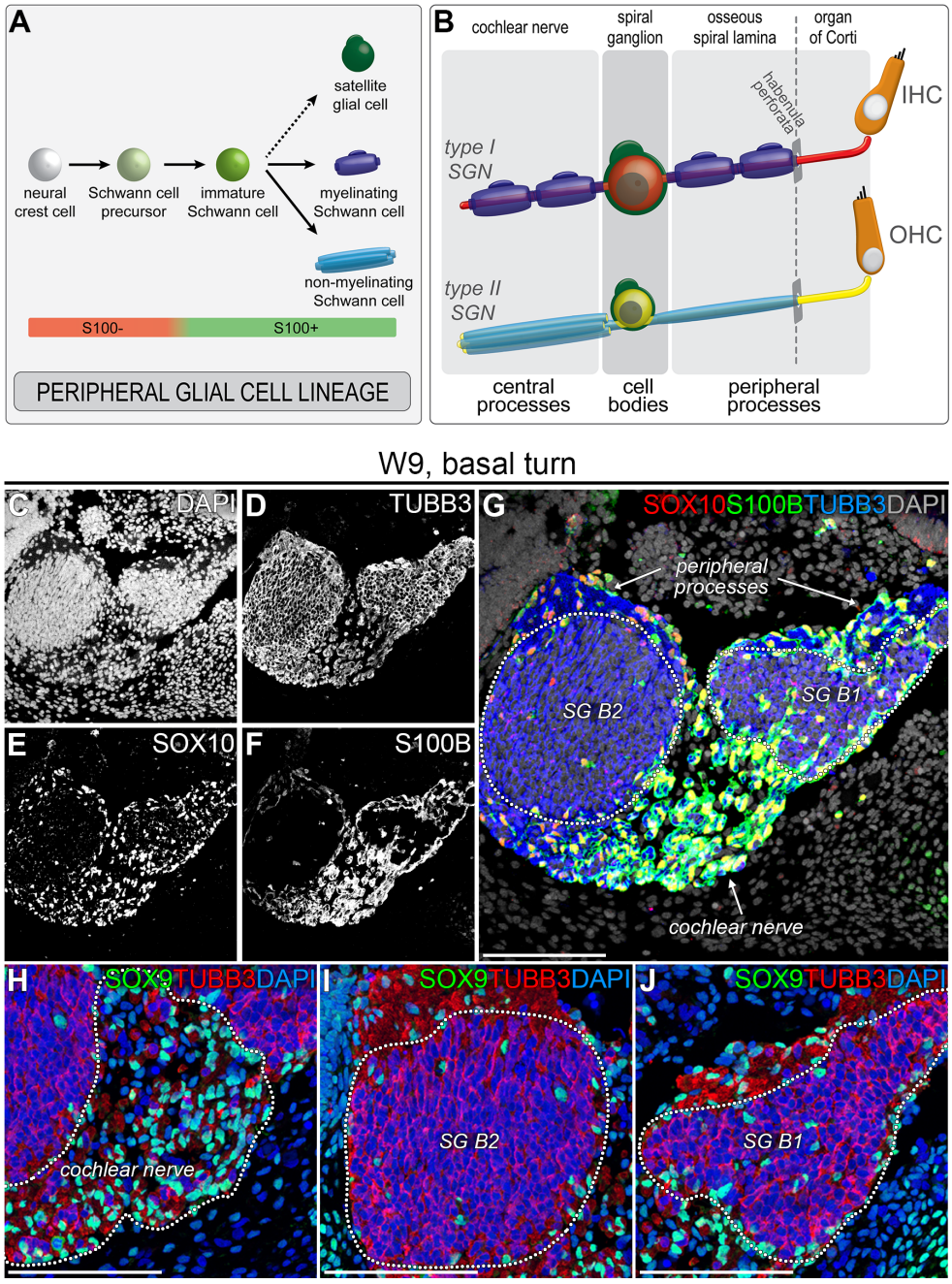


FIGURE 1. CAPTURING PGC DEVELOPMENT IN THE HUMAN COCHLEA.
(A) Schematic model of PGC development in the human fetal cochlea. Neural crest cells differentiate via a Schwann cell precursor stage into S100+ immature Schwann cells. The immature Schwann cells subsequently maturate into myelinating and non-myelinating Schwann cells, and (presumably) satellite glial cells. (B) Schematic illustration of the PGCs in the adult human cochlea. Satellite glial cells (green) envelop all SGN cell bodies. Non-myelinating Schwann cells (light blue) ensheath both the central and peripheral processes of the type II SGNs (yellow) that innervate the outer hair cells (OHC). Myelinating Schwann cells (dark blue) ensheath and myelinate both processes of the type I SGNs (red) that innervate the inner hair cells (IHC). Beyond the habenula perforata, in the organ of Corti, neither Schwann cell types ensheath the most distal part of the peripheral processes of type I and type II SGNs. (C-G) Confocal images of a cochlea at W9 showing DAPI (C), TUBB3 (D), SOX10 (E), and S100B (F) and the merged image (G). The spiral ganglion is delineated by the dotted line. (H-J) Confocal images of a cochlea at W9 showing the cochlear nerve (H), the spiral ganglion in the upper basal turn (I), and the spiral ganglion in the lower basal turn (J), delineated with dotted lines and immunostained with antibodies against SOX9 and TUBB3. Cell nuclei were visualized with DAPI. Abbreviations: B1, lower basal turn; B2, upper basal turn; SG, spiral ganglion. Scale bar = 100 µm.

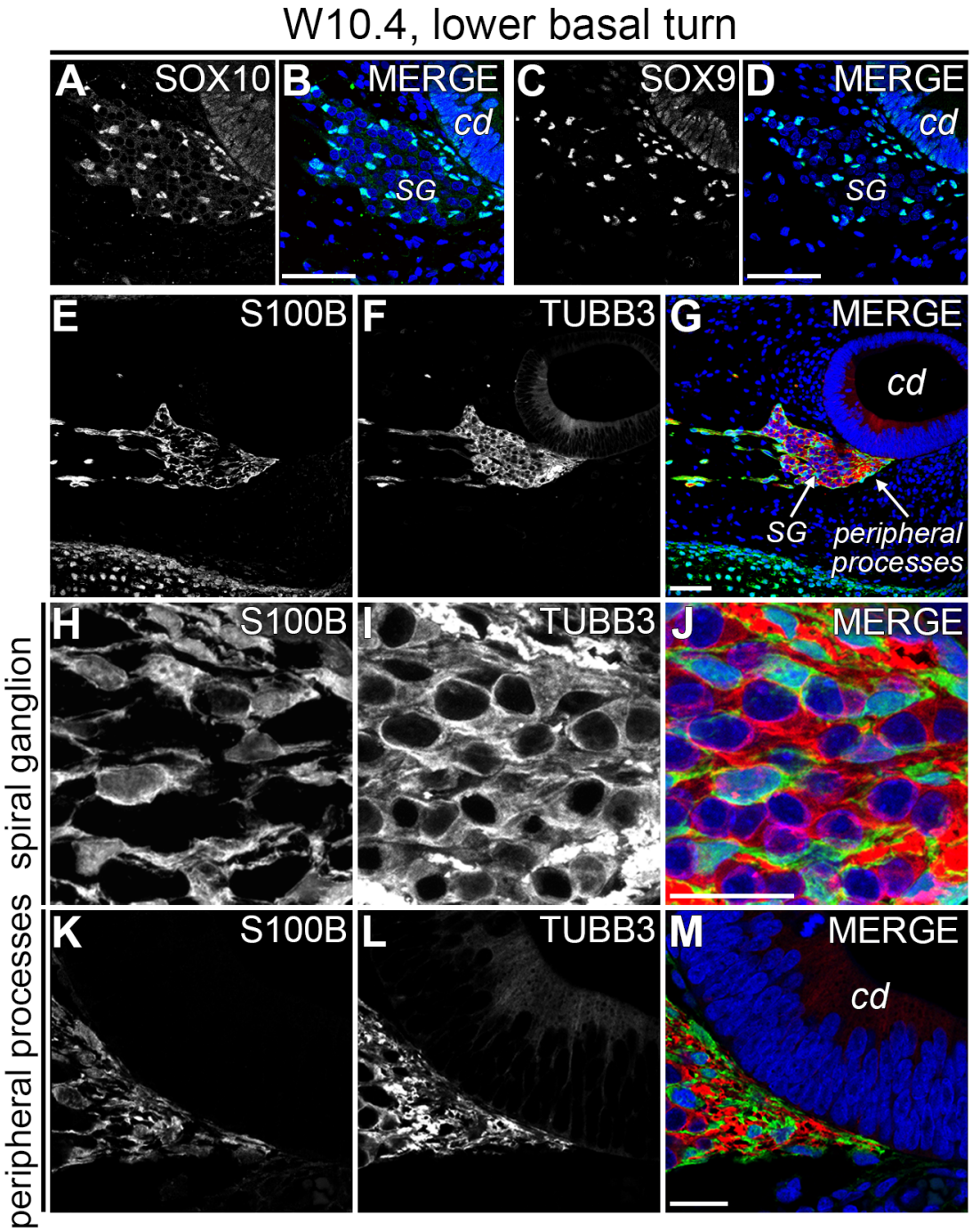


FIGURE 2. PGCS EXPRESSED SOX10, SOX9 AND S100B IN THE W10.4 HUMAN FETAL COCHLEA.
(A-B) Confocal images of the lower basal turn of a W10.4 cochlea immunostained for SOX10 and SOX10 merged with DAPI. (C-D) Confocal images of an adjacent section immunostained for SOX9 and SOX9 merged with DAPI. (E-G) Confocal images of the lower basal turn of a W10.4 cochlea immunostained for S100B (E) and TUBB3 (F) and the merged image with DAPI (G). (H-J) High-magnification view of the center of the spiral ganglion. (K-M) Detail of the peripheral processes at their distal end. Abbreviations: cd, cochlear duct; SG, spiral ganglion. Scale bar = 50 µm (A-G) or 20 µm (H-M).

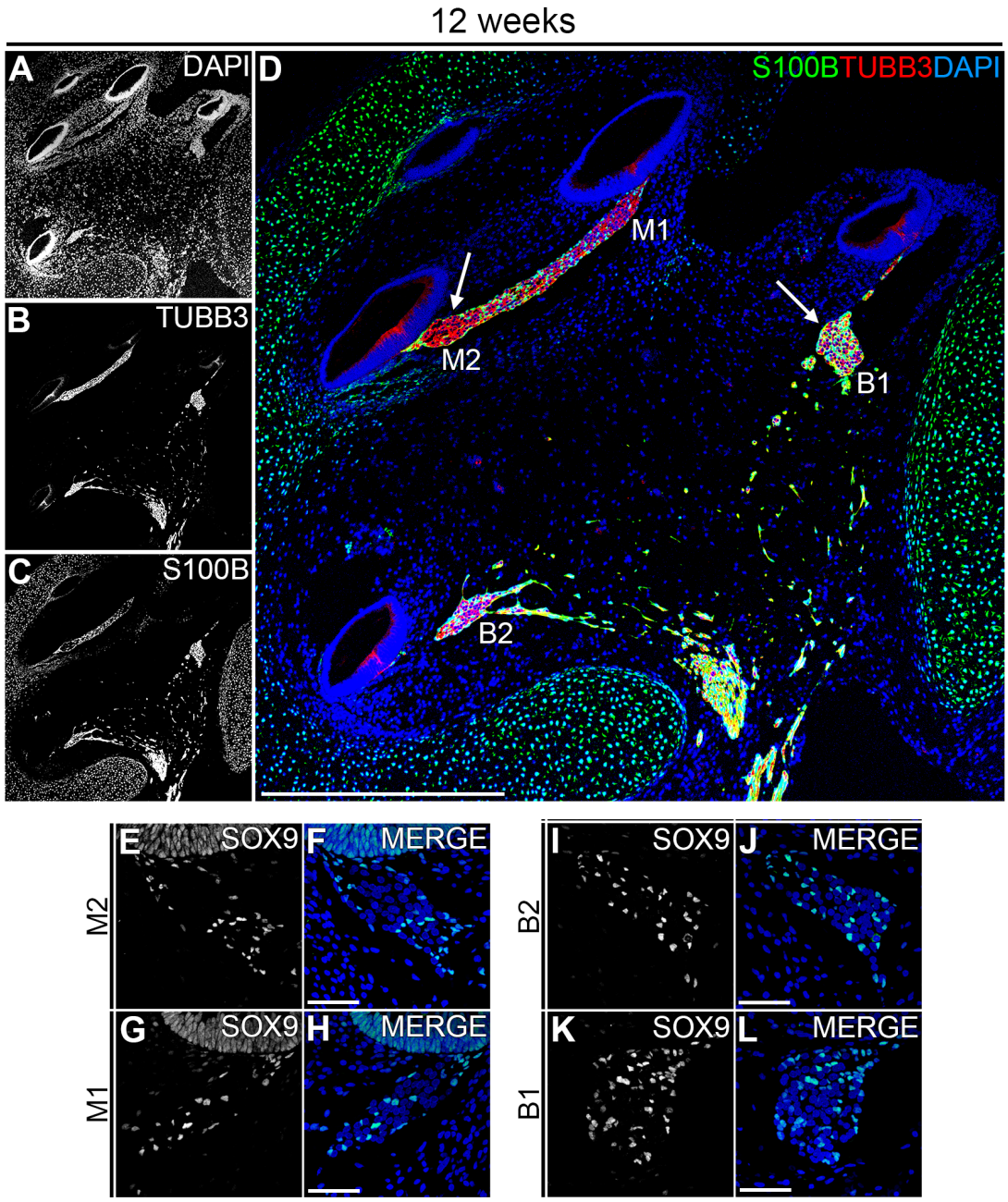


Figure 3. A spatial gradient of S100+/SOX9+ PGCs in the W12 human fetal cochlea.
(A-D) Confocal images of a cochlea at W12 showing DAPI (A) TUBB3 (B) and S100B (C) and the merged image (D). In D, the left arrow points to the spiral ganglion in the upper middle turn, whereas the right arrow points to the spiral ganglion in the lower basal turn. **(E-L)** Confocal images of a cochlea at W12 immunostained for SOX9 and SOX9 merged with DAPI showing the spiral ganglion at M2 (E-F), M1 (G-H), B2 (I-J) and B1 (K-L). Abbreviations: B1, lower basal turn; B2, upper basal turn; M1, lower middle turn; M2, upper middle turn. Scale bar = 500 µm (A-D) or 50 µm (E-L).

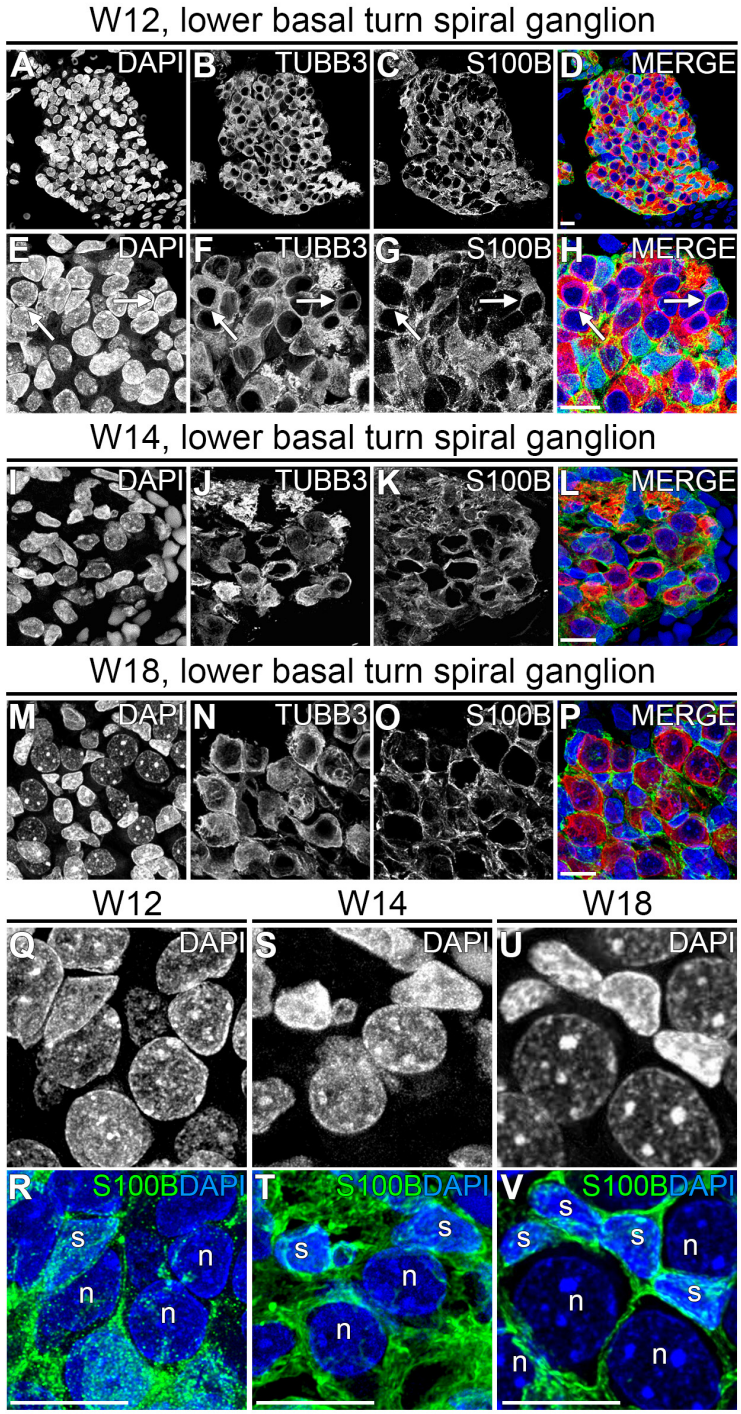


Figure 4. Development of satellite glial cells in the spiral ganglion.
(A-D) Deconvoluted confocal images of the spiral ganglion in the lower basal turn at W12 showing DAPI (A, blue), TUBB3 (B, red), S100B (C, green) and the merged image (D). **(E-H)** High-magnification view of the spiral ganglion. Arrows point to SGN cell bodies that are enwrapped by S100B+ satellite glial cells. **(I-L)** Deconvoluted confocal images of the spiral ganglion in the lower basal turn at W14 showing DAPI (I, blue), TUBB3 (J, red), S100B (K, green) and the merged image (L). **(M-P)** Deconvoluted confocal images of the spiral ganglion in the lower basal turn at W18 showing DAPI (M, blue), TUBB3 (N, red), S100B (O, green), and the merged image (P). **(Q-V)** High-magnification view of cell nuclei (DAPI) and S100B+ satellite glial cells within the spiral ganglion at W12 (Q-R), W14 (S-T) and W18 (U-V). Abbreviations: s, satellite glial cell; n, spiral ganglion neuron. Scale bar = 10 µm.

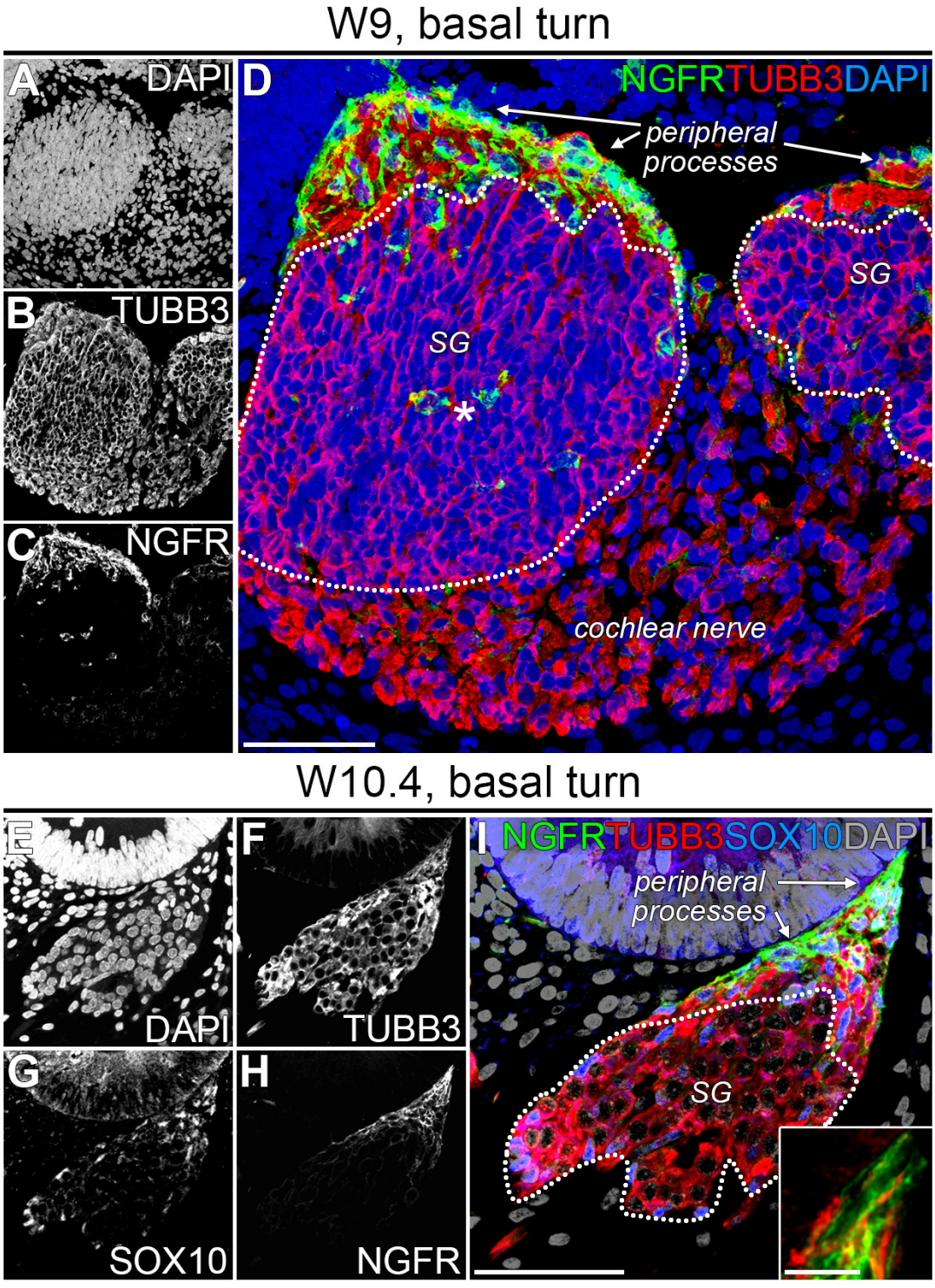


Figure 5. Immature Schwann cells along the peripheral processes express NGFR.
(A-D) Confocal images of the lower basal turn of a cochlea at W9 showing DAPI (A), TUBB3 (B) and NGFR (C) and the merged image (D). The spiral ganglion is delineated by the dotted line. The asterisk marks two NGFR+ cells in the center of the spiral ganglion. **(E-I)** Confocal images of the lower basal turn of a cochlea at W10.4 showing DAPI (E), TUBB3 (F), SOX10 (G) and NGFR (H) and the merged image (I). The spiral ganglion is delineated by the dotted line. The inset shows a deconvoluted, high-magnification view of TUBB3 and NGFR at the distal tips of the peripheral processes. Abbreviations: SG, spiral ganglion. Scale bar = 50 µm or 5 µm (inset in I).

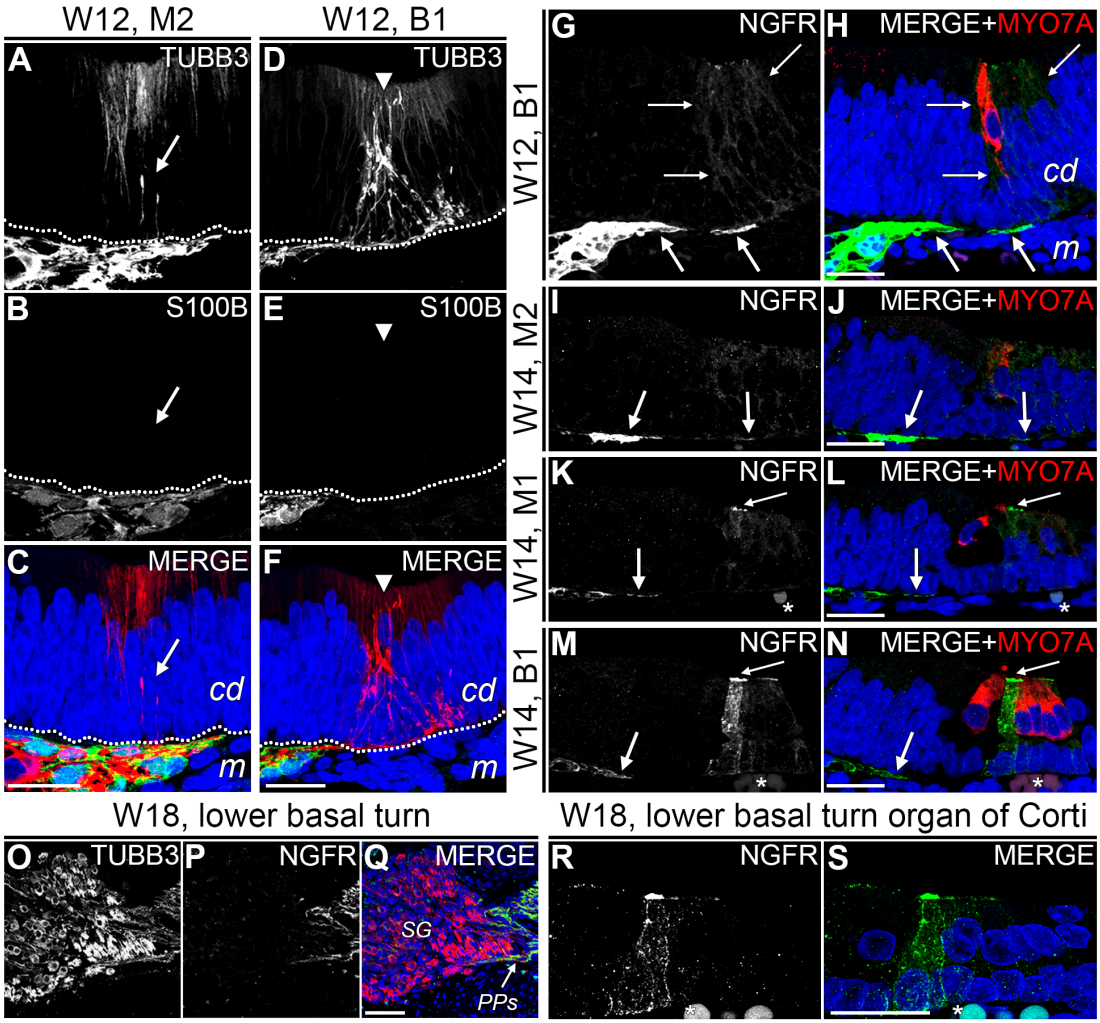


FIGURE 6. NGFR EXPRESSION IN THE COCHLEAR DUCT EPITHELIUM.
(A-C) Confocal images of the cochlear duct epithelium in the upper middle turn of a cochlea at W12 showing TUBB3 (A, red), S100B (B, green) and the merged image with DAPI (C). The arrow points to penetrating TUBB3+ peripheral processes. **(D-F)** Confocal images of the cochlear duct epithelium in the lower basal turn showing TUBB3 (D, red), S100B (E, green) and the merged image with DAPI (F). The arrowhead points to the first developing (inner) hair cell. **(G-H)** Confocal images of the cochlear duct epithelium of the lower basal turn of a cochlea at W12 showing NGFR (G, green) and the merged image with DAPI (H) and MYO7A (red). The bold arrows point to the NGFR+ Schwann cells. The thin arrows outline the epithelial cells that weakly express NGFR. **(I-J)** Upper middle turn of a cochlea at W14 showing NGFR (I, green) and the merged image (J) with DAPI (blue) and MYO7A (red). The bold arrows point to the NGFR+ Schwann cells. **(K-L)** Lower middle turn of a W14 cochlea immunostained for NGFR (K, green) and the merged image with DAPI (blue) and MYO7A (red). The bold arrow points to the NGFR+ Schwann cells. The thin arrow points to a bright band of NGFR. **(M-N)** Lower basal turn of a W14 cochlea immunostained for NGFR (M, green) and the merged image (N) with DAPI (blue) and MYO7A (red). The bold arrows point to the NGFR+ Schwann cells. The thin arrow points to a band brightly immunostained for NGFR. **(O-Q)** Confocal images of the spiral ganglion in the lower basal turn of a cochlea at W18 showing TUBB3 (O), NGFR (P, green) and the merged image with DAPI (Q). **(R-S)** Confocal images of the organ of Corti of a cochlea at W18 showing NGFR (R, green) and the merged image with DAPI (S). Abbreviations: cd, cochlear duct; m, mesenchyme; B1, lower basal turn; M1, lower middle turn; M2, upper middle turn; SG, spiral ganglion; PPs, peripheral processes. * = autofluorescence of erythrocytes. Scale bar = 20 µm (A-N, R-S) or 50 µm (O-Q).

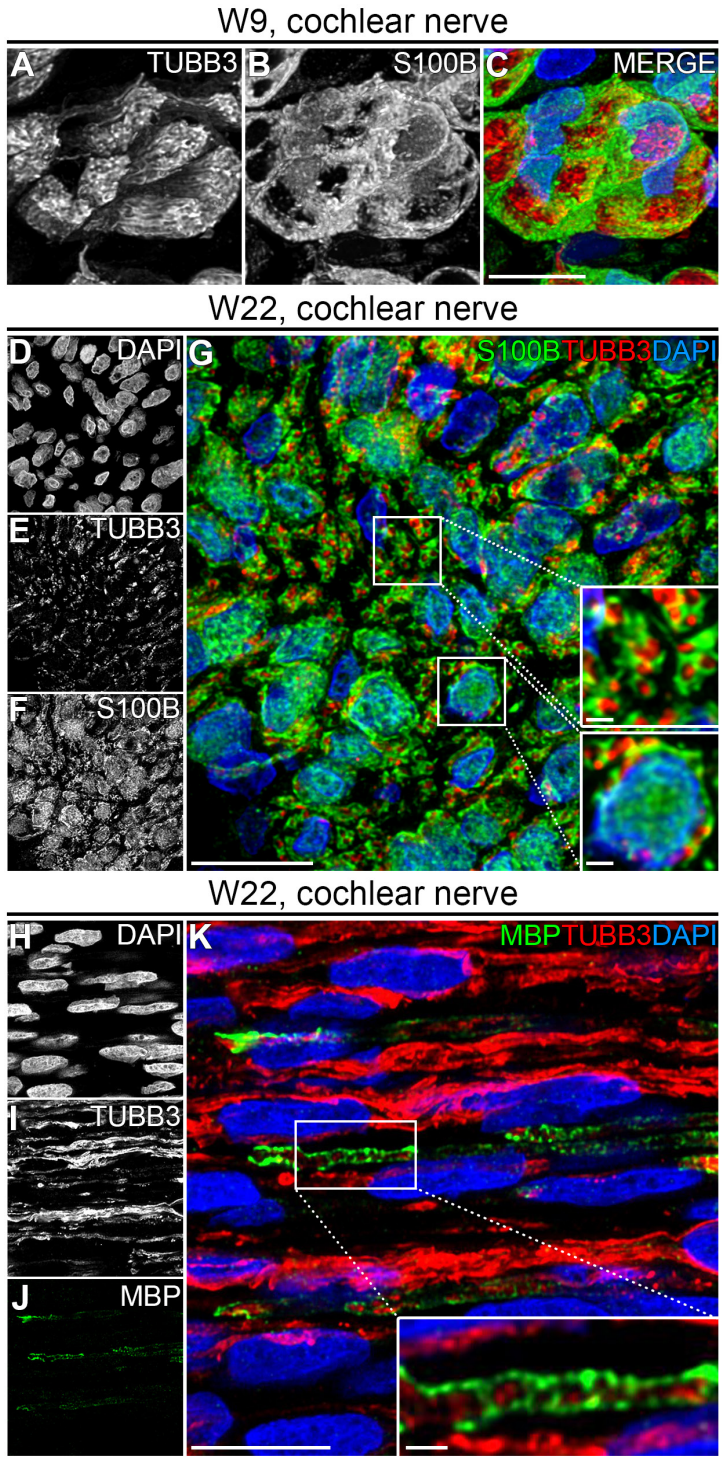


Figure 7. Terminal differentiation of Schwann cells in the cochlear nerve.
(A-C) Deconvoluted confocal images of the cochlear nerve at W9 showing TUBB3 (A, red), S100B (B, green), and the merged image with DAPI (C). **(D-G)** Deconvoluted confocal images of an axial transection of the cochlear nerve at W22 showing DAPI (D), TUBB3 (E), S100B (F) and the merged image (G). The upper inset in G shows a high-magnification of TUBB3+ cochlear nerve fibers each enveloped by S100B+ Schwann cells, the lower inset shows a Remak bundle. **(H-K)** Deconvoluted confocal images of a sagittal transection of the cochlear nerve at W22 showing DAPI (H), TUBB3 (I), MBP (J) and the merged image (K). The inset shows a high-magnification view of a myelinated nerve fiber. Scale bar = 10 µm or 1 µm (insets in G and K).

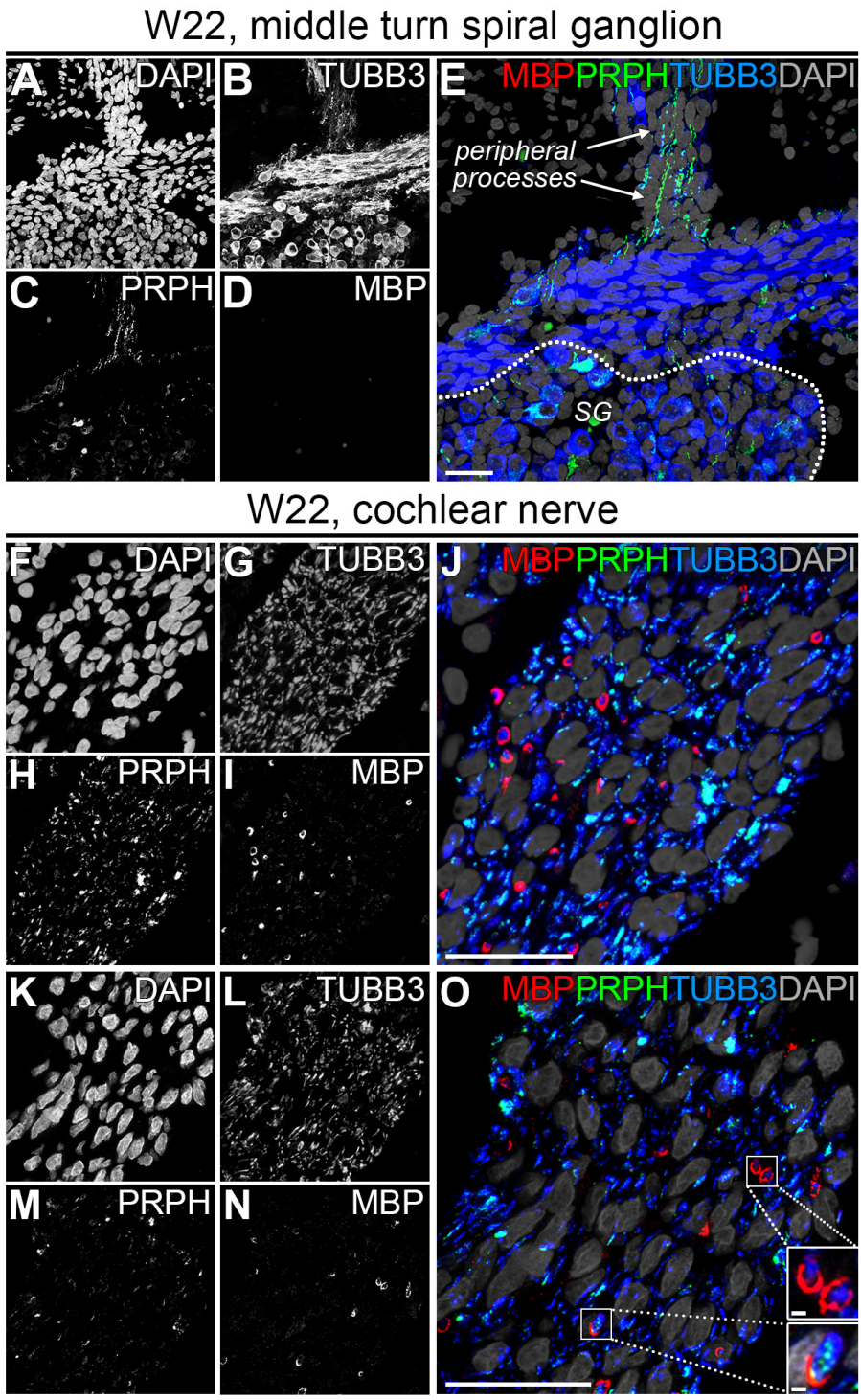


Figure 8. Myelination of spiral ganglion neurons at W22.
(A-E) Confocal images of a spiral ganglion in the middle turn of a cochlea at W22 showing DAPI (A), TUBB3 (B), PRPH (C), MBP (D) and the merged image (E). The spiral ganglion is delineated by the dotted line. **(F-J)** Confocal images of an axial transection of the cochlear nerve at W22 showing DAPI (F), TUBB3 (G), PRPH (H), MBP (I) and the merged image (J). **(K-O)** Deconvoluted confocal images of an axial transection of the cochlear nerve at W22 showing DAPI (K), TUBB3 (L), PRPH (M), MBP (N) and the merged image (O). Insets show TUBB3 (left), PRPH (middle) and the merge with MBP and DAPI (right) in high-magnifications examples of PRPH-/TUBB3+/MBP+ cochlear nerve fibers (upper inset) and PRPH+/TUBB3+/MBP+ cochlear nerve fibers (lower inset). Scale bar = 20 µm or 1 µm (insets in O).

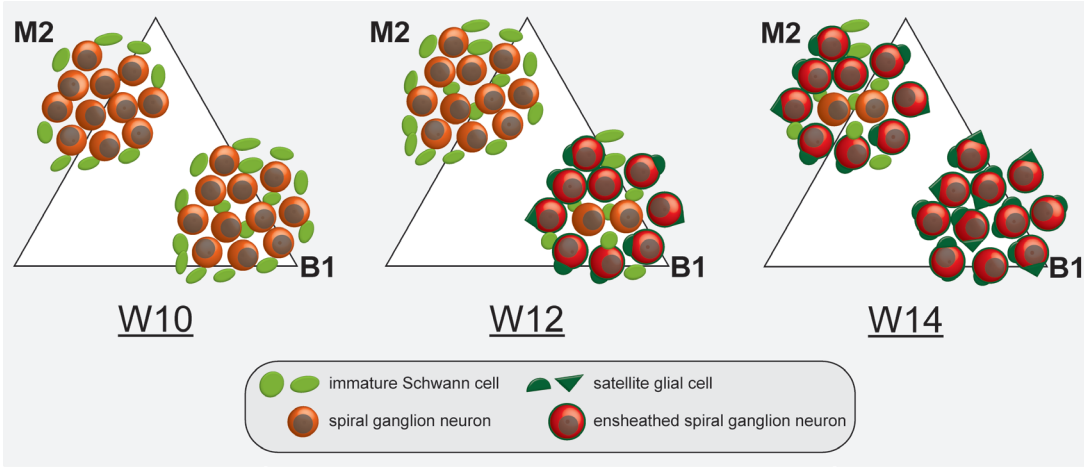


Figure 9. Model of satellite glial cell development in the human spiral ganglion.
Satellite glial cell development and the envelopment of the cell bodies of SGNs both occur in a temporal and spatial gradient within the spiral ganglion of the developing human fetal cochlea. W10: Immature Schwann cells (light green) can be found at the edges of the SG in the upper middle turn (M2). In addition, a few Schwann cells are located in between the SGNs (orange) in the lower basal turn. W12: The number of Schwann cells in between the SGNs has greatly increased in M2. Satellite glial cells (dark green) in B1 start to envelop the cell bodies of SGNs (red). The pattern in M2 at W12 resembles that in B1 at W10. W14: All SGN cell bodies in B1 are enveloped by one or more adjacent satellite glial cells. The pattern in M2 resembles that in B1 at W12.

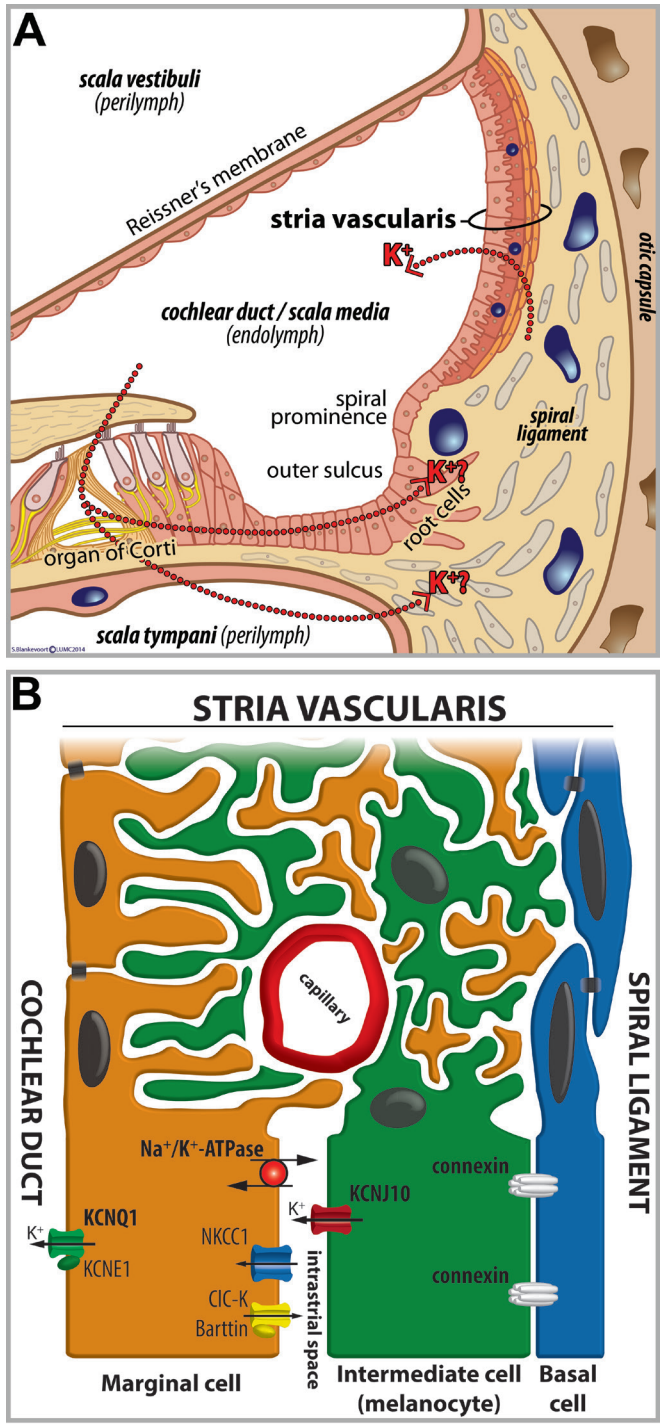


FIGURE 1. CAPTURING COCHLEAR POTASSIUM HOMEOSTASIS IN MAMMALS.
(A) A schematic illustration of a cross-section through the adult cochlea. The cochlear duct (or scala media) is filled with endolymph containing a high [K+] that is maintained by the stria vascularis. Potassium recycling is postulated to either occur via the supporting cells of the organ of Corti and the epithelial lining of the outer sulcus (Claudius cells and root cells), or through the perilymph of the scala tympani. *Picture courtesy of S.B. Blankevoort.*
(B) A schematic anatomical (upper half) and compartmental (lower half) model of the adult stria vascularis showing the three cellular layers and depicting the location of potassium regulating channels. The stria vascularis is electrochemically isolated from neighbouring structures by tight junctions (black bars).

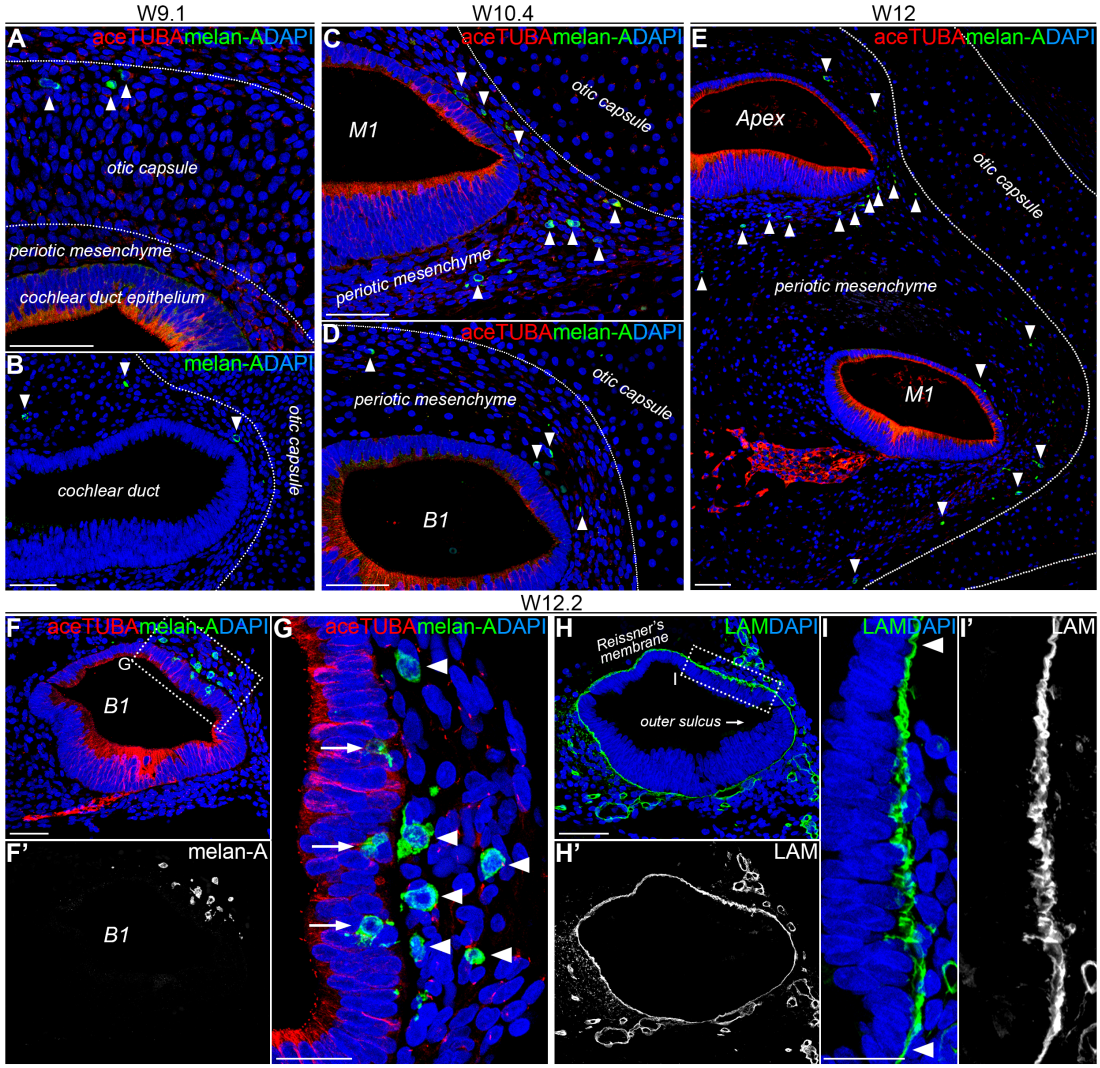


FIGURE 2. MIGRATION OF MELANOCYTES INTO THE STRIA VASCULARIS OF THE HUMAN FETAL COCHLEA.
(**A-B**) A cochlea at W9.1 immunostained for acetylated tubulin (aceTUBA) (red), melan-A (green) and DAPI (blue) (A) or melan-A (green) and DAPI (blue) (B). Arrowheads point to melan-A+ cochlear melanocytes. Scale bars = 50 µm. (**C**) The lower middle turn (M1) of a cochlea at W10.4 immunostained for aceTUBA (red), melan-A (green) and DAPI (blue). Scale bar = 50 µm. (**D**) The lower basal turn (B1) of a cochlea at W10.4 immunostained for aceTUBA (red), melan-A (green) and DAPI (blue). Scale bar = 50 µm. (**E**) The apical and lower middle turn of cochlea at W12 immunostained for aceTUBA (red), melan-A (green) and DAPI (blue). Scale bar = 50 µm. (**F-F'**) The lower basal turn of a cochlea at W12.2 immunostained for aceTUBA (red), melan-A (green) and DAPI (blue). The melan-A signal is shown separately in white in (F'). Scale bar = 50 µm. (**G**) Higher magnification of the outlined area in (F). Arrowheads point to melan-A+ melanocytes located in the periotic mesenchyme. Arrows point to melan-A+ melanocytes located in between the epithelial lining of the cochlear duct lateral wall (the future marginal cells of the stria vascularis). Scale bar = 20 µm. (**H-H'**) A similar section of the lower basal turn of a cochlea at W12.2 as depicted in (F), here immunostained for basement membrane protein laminin (LAM). The LAM signal is shown separately in white in (H'). Scale bar = 50 µm. (**I-I'**) Higher magnification of the developing stria vascularis outlined in (H). The arrowheads point to the smooth and continuous appearance of the basement membrane at the location of the bordering Reissner's membrane and the outer sulcus, as opposed to the irregular pattern observed in at the location of the future stria vascularis. The LAM signal is shown separately in white in (I') Scale bar = 20 µm.

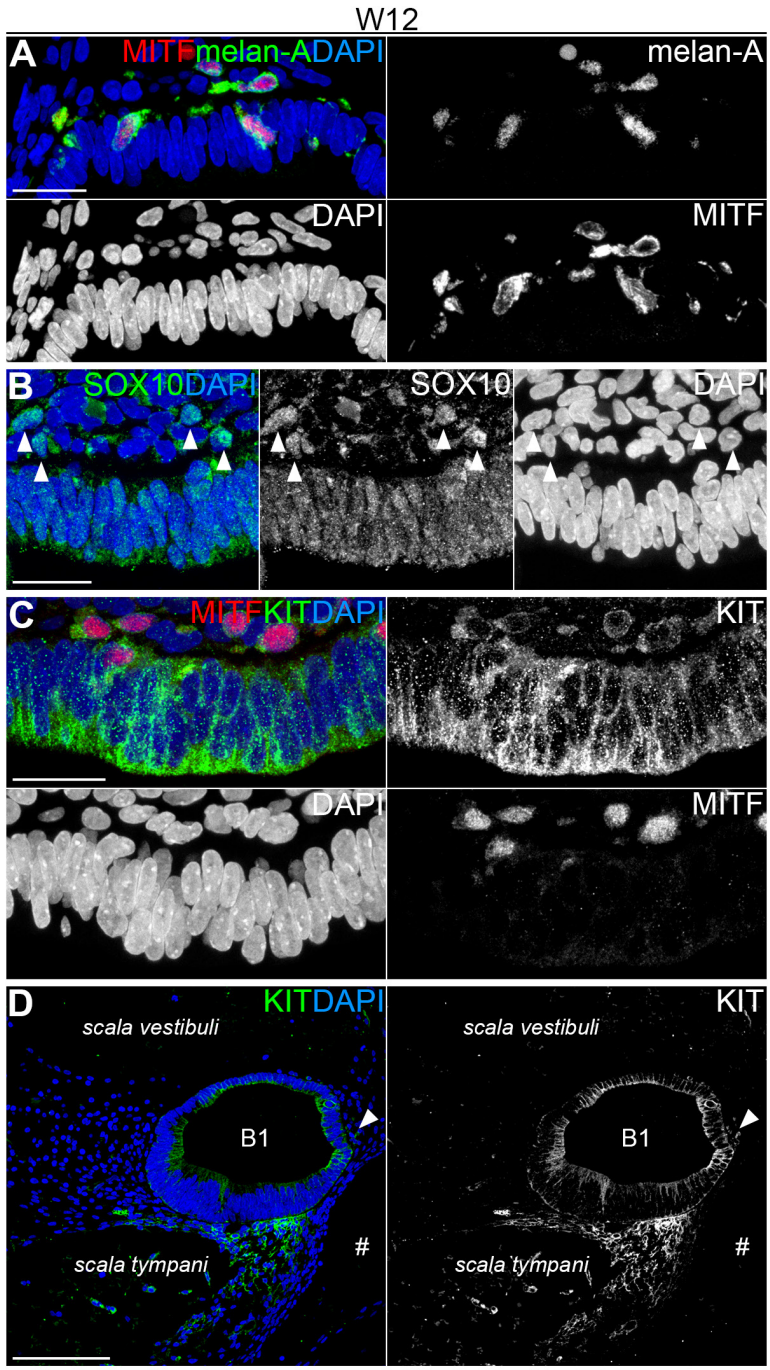


Figure 3. Expression of MITF, SOX10 and KIT.
(A) Lateral wall area of the lower basal turn of a cochlea at W12 immunostained for microphthalmia-associated transcription factor (MITF) (red), melan-A (green) and DAPI (blue), showing Melan-A+/MITF+ melanocytes in the periotic mesenchyme as well as in the developing stria vascularis. Signals are shown separately in white. Scale bar = 20 µm. **(B)** Lateral wall area of the lower basal turn of a cochlea at W12 immunostained for SOX10 (green) and DAPI (blue). Signals are shown separately in white. Arrowheads point to SOX10+ melanocytes located in the periotic mesenchyme. Scale bar = 20 µm. **(C)** Lateral wall area of the lower basal turn of a cochlea at W12 immunostained for MITF (red), KIT (green) and DAPI (blue), showing KIT+/MITF+ melanocytes in the periotic mesenchyme as well as in the developing stria vascularis. Signals are shown separately in white. Scale bar = 100 µm. **(D)** The lower basal turn of a cochlea at W12 immunostained for KIT (green) and DAPI (blue). The KIT signal is shown separately in white. The arrowhead points to KIT+ melanocytes in the periotic mesenchyme next to the developing stria vascularis. # = Tissue artifact. Scale bar = 20 µm.

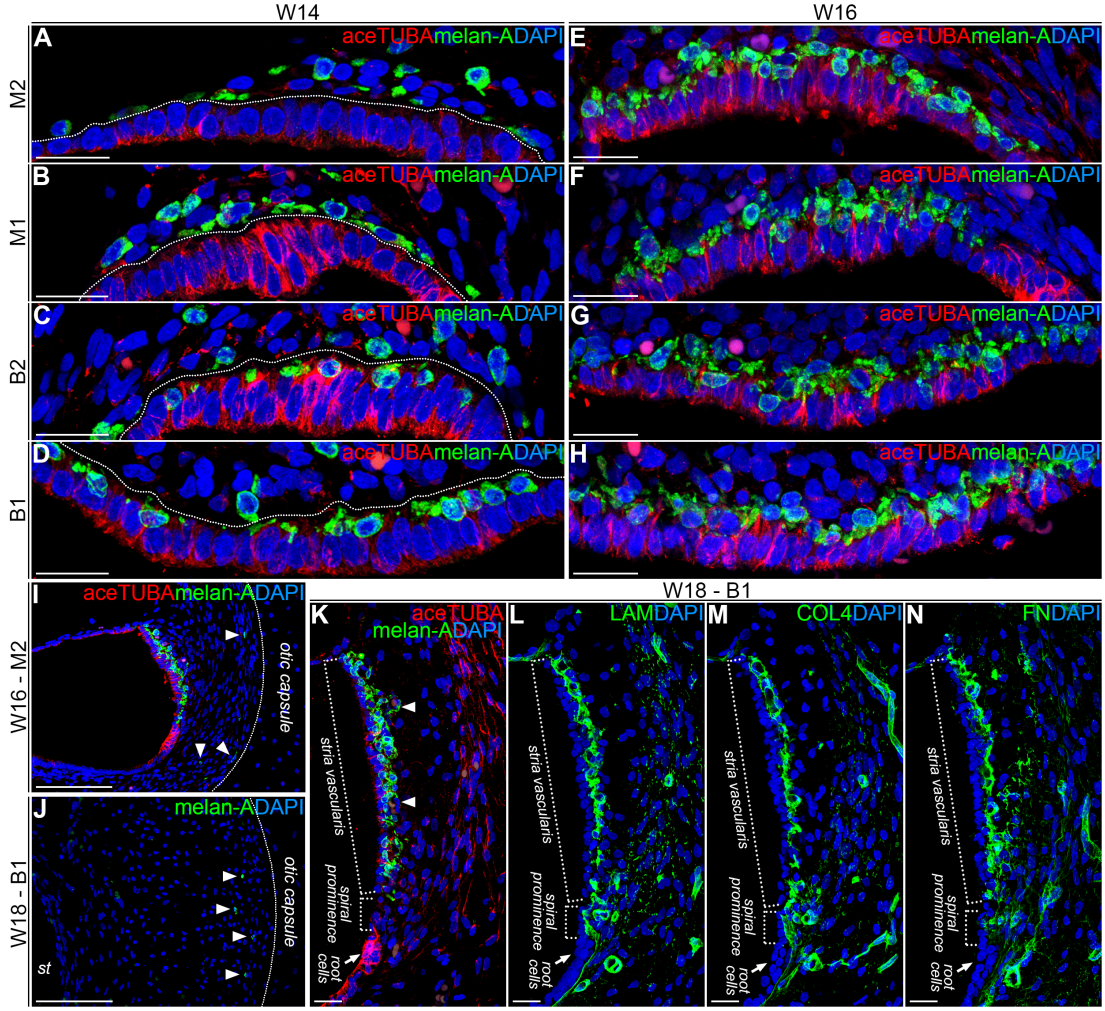


Figure 4. Maturation of the lateral wall in the human fetal cochlea.
(**A-D**) Lateral wall area of the upper middle (M2, (A)), lower middle (M1, (B)), upper basal (B2, (C)), and lower basal (B1, (D)) turn of a cochlea at W14 immunostained for acetylated tubulin (aceTUBA) (red), melan-A (green), and DAPI (blue). Scale bars = 20 µm. (**E-H**) Lateral wall area of the upper middle (E), lower middle (F), upper basal (G), and lower basal (H) turn of a cochlea at W16 immunostained for aceTUBA (red), melan-A (green), and DAPI (blue). Scale bars = 20 µm. (**I**) The upper middle turn of a cochlea at W16 immunostained for aceTUBA (red), melan-A (green), and DAPI (blue). Arrowheads point to melan-A+ melanocytes located in the periotic mesenchyme at the edges of the otic capsule. Scale bar = 100 µm. (**J**) The lower basal turn of a cochlea at W18 immunostained for melan-A (green) and DAPI (blue). Arrowheads point to melan-A+ melanocytes located in the periotic mesenchyme at the edges of the otic capsule. st = scala tympani. Scale bar = 100 µm. (**K**) The lower basal turn of a cochlea at W18 immunostained for aceTUBA (red), melan-A (green), and DAPI (blue). Arrowheads point to melan-A positive strial melanocytes around developing strial capillaries. Scale bar = 20 µm. (**L-N**) The lower basal turn of a cochlea at W18 immunostained for basement membrane proteins laminin (LAM) (L, green), collagen type IV (COL4) (M, green) and fibronectin (FN) (N, green), and DAPI (blue). Scale bars = 20 µm.

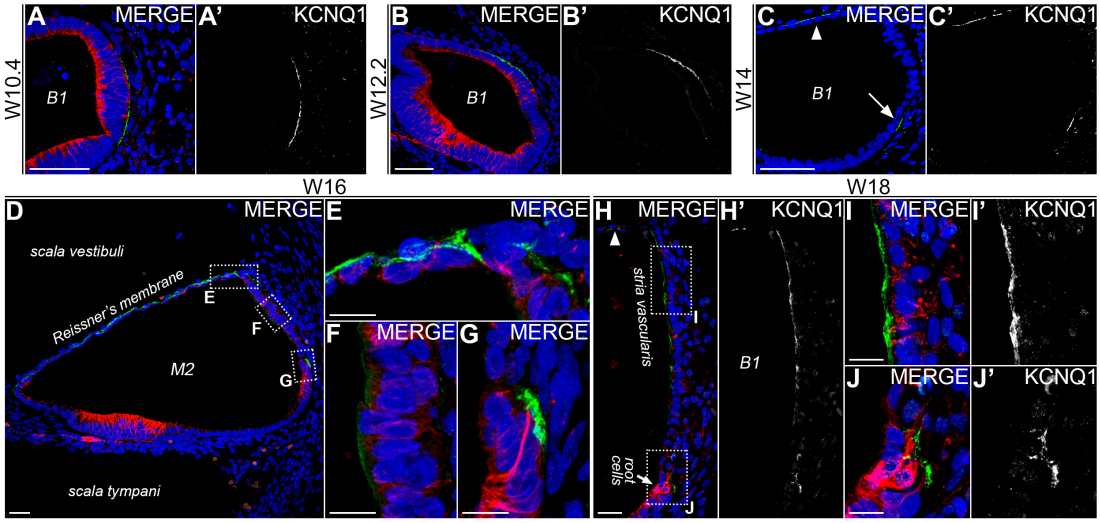


Figure 5. KCNQ1 expression in the human fetal cochlea.
(A-A') The lower basal turn of a cochlea at W10.4 immunostained for acetylated tubulin (aceTUBA) (red), voltage-gated potassium channel KCNQ1 (green), and DAPI (blue). The KCNQ1 signal is shown separately in white in (A'). Scale bar = 50 µm. **(B-B')** The lower basal turn of a cochlea at W12.2 immunostained for aceTUBA (red), KCNQ1 (green), and DAPI (blue). The KCNQ1 signal is shown separately in white in (B'). Scale bar = 50 µm. **(C-C')** The lower basal turn of a cochlea at W14 immunostained for aceTUBA (red), KCNQ1 (green), and DAPI (blue). The KCNQ1 signal is shown separately in (C'). The arrowhead points at KCNQ1 signals in the developing Reissner's membrane, the arrow points at KCNQ1 signals at the location of the future root cells. The KCNQ1 signal is shown separately in white in (C'). Scale bar = 50 µm. **(D)** The upper middle (M2) turn of a cochlea at W16 immunostained for aceTUBA (red), KCNQ1 (green), and DAPI (blue). Scale bar = 50 µm. **(E-G)** Higher magnifications of the outlined areas in (D), showing Reissner's membrane (E), the marginal cells of the stria vascularis (F) and the root cells in the outer sulcus (G). Scale bars = 20 µm. **(H-H')** The lower basal turn of a cochlea at W18 immunostained for aceTUBA (red), KCNQ1 (green), and DAPI (blue). The arrowhead points to Reissner's membrane. The KCNQ1 signal is shown separately in white in (H'). Scale bar = 20 µm. **(I-J')** Higher magnifications of the outlined areas in (H). KCNQ1 signals are shown separately in white in (I') and (J'). Scale bars = 10 µm.

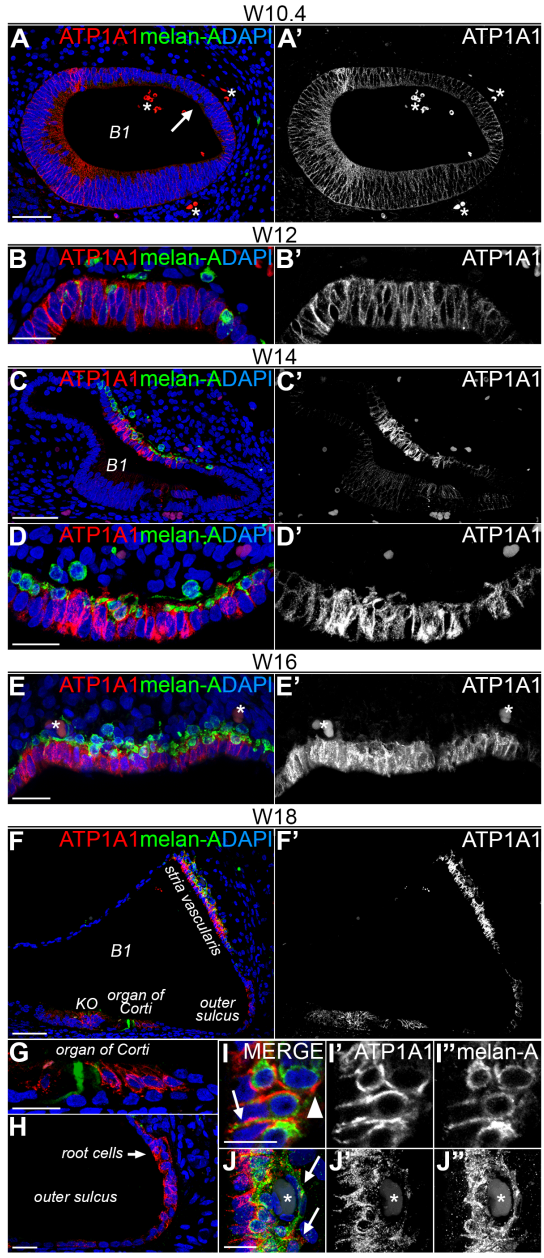


Figure 6. Expression of Na+/K+-ATPase in the human fetal cochlea.
(A) The lower basal turn of a cochlea at W10.4 immunostained for Na+/K+-ATPase ATP1A1 (red), melan-A (green), and DAPI (blue). The arrow points to the location of the future stria vascularis. The ATP1A1 signal is shown separately in white in (A'). * = autofluorescent erythrocytes. Scale bar = 50 µm. **(B)** The lateral wall in the lower basal turn of a cochlea at W12 immunostained for ATP1A1 (red), melan-A (green), and DAPI (blue). The ATP1A1 signal is shown separately in white in (B'). Scale bar = 20 µm. **(C)** The lower basal turn of a cochlea at W14 immunostained for ATP1A1 (red), melan-A (green), and DAPI (blue). The ATP1A1 signal is shown separately in white in (C'). Scale bar = 50 µm. **(D)** Higher magnification of the developing stria vascularis in (C). The ATP1A1 signal is shown separately in white in (D'). Scale bar = 20 µm. **(E)** The developing stria vascularis in the lower basal turn of a cochlea at W16 immunostained for ATP1A1 (red), melan-A (green), and DAPI (blue). The ATP1A1 signal is shown separately in white in (E'). * = autofluorescent erythrocytes. Scale bar = 20 µm. **(F)** The lower basal turn of a cochlea at W18 immunostained for ATP1A1 (red), melan-A (green), and DAPI (blue). The ATP1A1 signal is shown separately in white in (F'). Scale bar = 50 µm. **(G-H)** Higher magnifications of (F), showing the organ of Corti (G) and epithelial lining of the outer sulcus (H). Scale bars = 20 µm. **(I-J")** Higher magnifications of the stria vascularis in (F), with the separate signals of ATP1A1 (I' and J') and melan-A (I" and J") shown in white. The arrow in (I) point to a melan-A+ melanocyte process penetrating towards the lumen of the cochlear duct. The arrowhead in (I) points towards an ATP1A1+ structure around a melan-A+ melanocyte cell body. The arrows in (J) point towards ATP1A1+ structures around melan-A+ processes that encircle a developing capillary. * = autofluorescent erythrocytes. Scale bars = 20 µm.

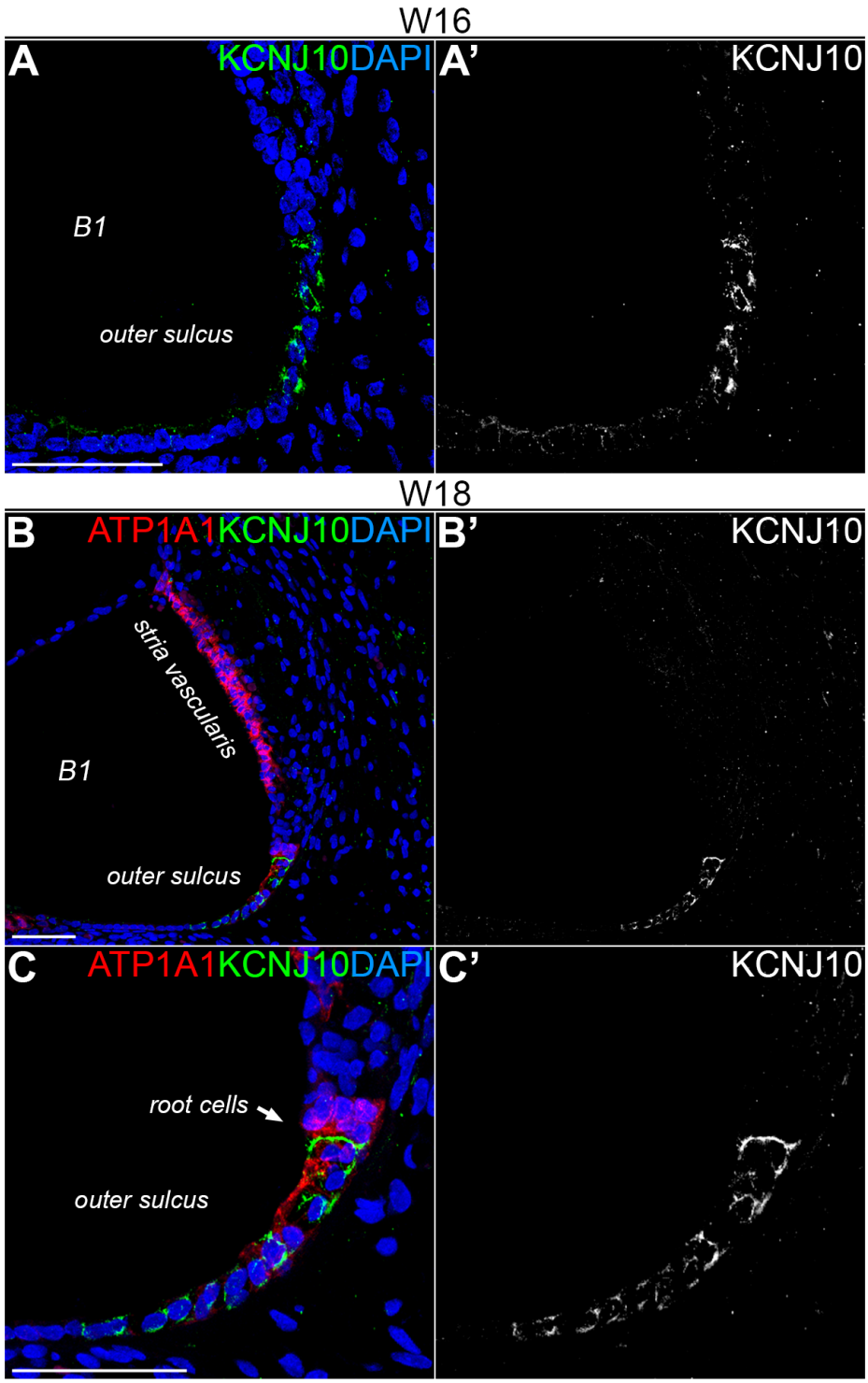


FIGURE 7. KCNJ10 EXPRESSION IN THE HUMAN FETAL COCHLEA.
(A) The epithelial lining in the lower basal turn outer sulcus of a cochlea at W16 immunostained for the inwardly-rectifying potassium channel KCNJ10 (green) and DAPI (blue). The KCNJ10 signal is shown separately in white in (A'). Scale bar = 50 µm. (B) The lower basal turn of a cochlea at W18 immunostained for sodium/potassium-transporting ATPase ATP1A1 (red), KCNJ10 (green), and DAPI (blue). The KCNJ10 signal is shown separately in white in (B'). Scale bar = 50 µm. (C) Higher magnification of the outer sulcus area in (B). The KCNJ10 signal is shown separately in white in (C'). Scale bar = 50 µm.

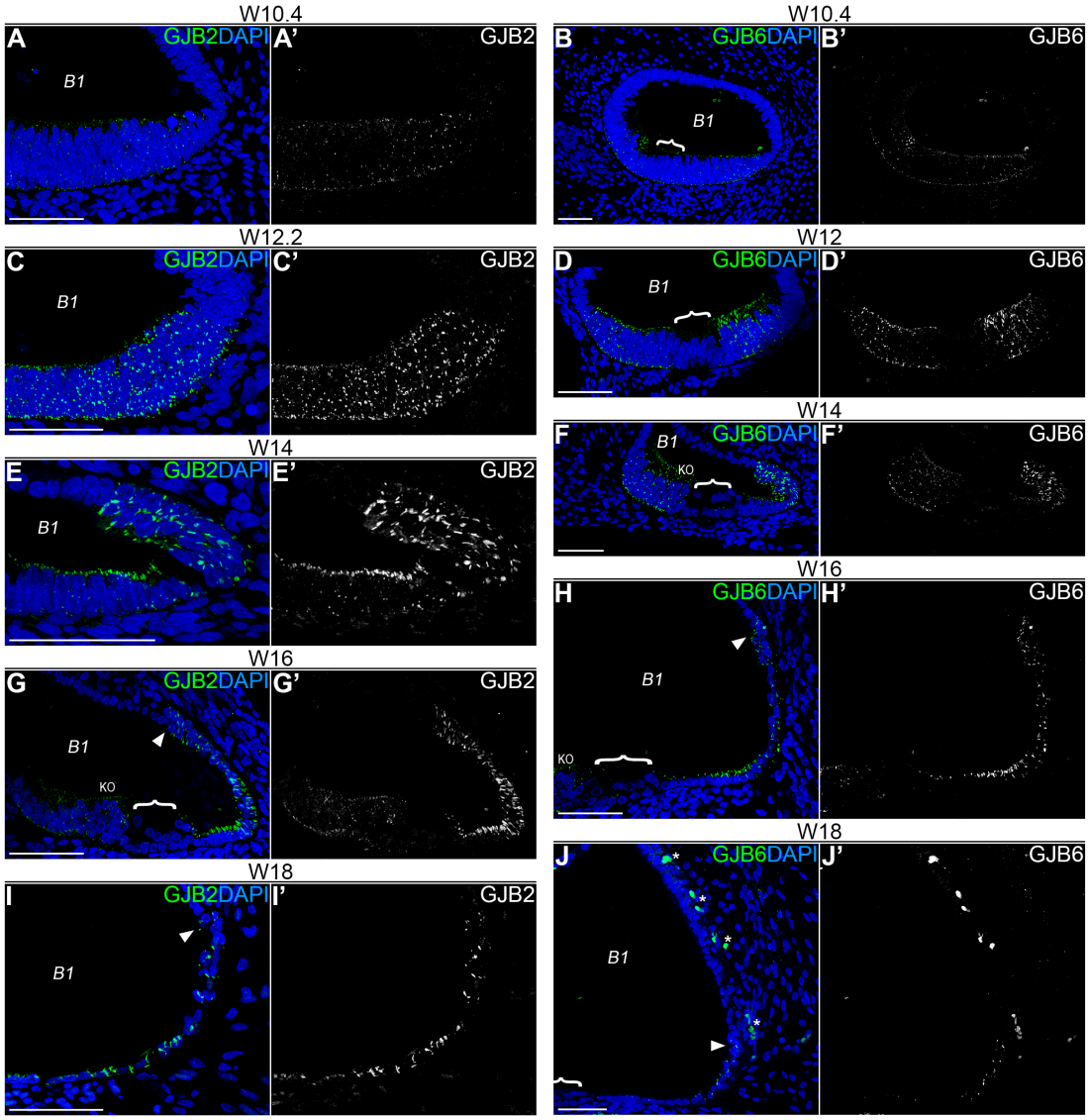


Figure 8. Epithelial expression of GJB2 and GJB6 in the cochlear duct.
(A-B) The lower basal turn cochlea at W10.4 immunostained for gap junction proteins GJB2 ((A), green) and GJB6 ((B), green) and DAPI (blue). GJB2 and GJB6 signals are shown separately in white in (A') and (B'), respectively. The bracket outlines the prosensory domain. Scale bars = 50 µm. **(C-D)** The lower basal turn cochlea at W12.2 immunostained for GJB2 ((C), green) and GJB6 ((D), green) and DAPI (blue). GJB2 and GJB6 signals are shown separately in white in (C') and (D'), respectively. The bracket outlines the prosensory domain. Scale bars = 50 µm. **(E-F)** The lower basal turn cochlea at W14 immunostained for GJB2 ((E), green) and GJB6 ((F), green) and DAPI (blue). GJB2 and GJB6 signals are shown separately in white in (E') and (F'), respectively. The bracket outlines the developing organ of Corti. KO = Kölliker's organ. Scale bars = 50 µm. **(G-H)** The lower basal turn cochlea at W14 immunostained for GJB2 ((G), green) and GJB6 ((H), green) and DAPI (blue). GJB2 and GJB6 signals are shown separately in white in (G') and (H'), respectively. The arrowheads points to the developing root cells. The bracket outlines the developing of Corti. KO = Kölliker's organ. Scale bars = 50 µm. **(I-J)** The lower basal turn cochlea at W14 immunostained for GJB2 ((I), green) and GJB6 ((J), green) and DAPI (blue). GJB2 and GJB6 signals are shown separately in white in (I') and (J'), respectively. The arrowheads points to the developing root cells. The bracket outlines the organ of Corti. * = autofluorescent erythrocytes. Scale bars = 50 µm.

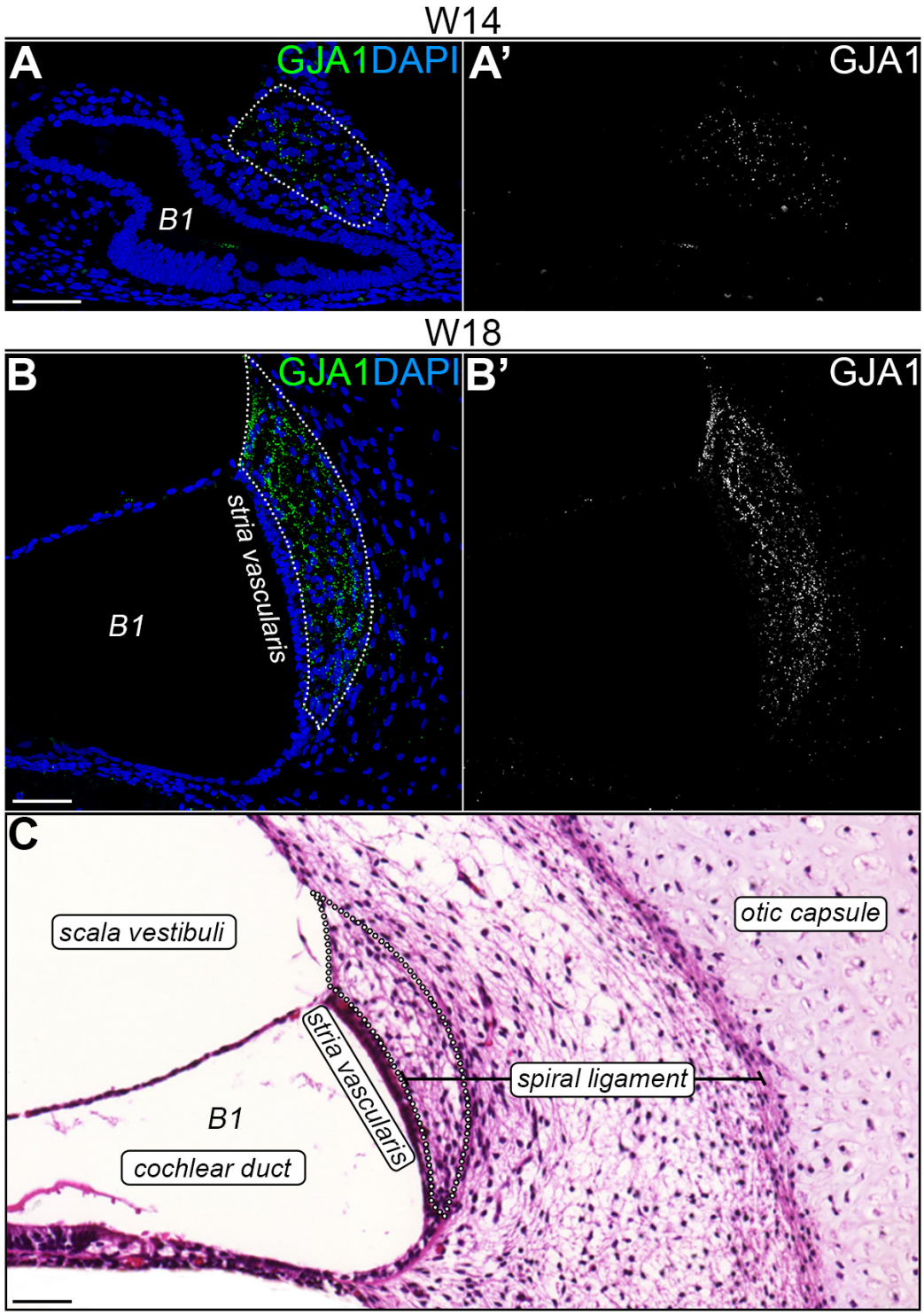


FIGURE 9. GJA1 IS EXPRESSED BY TYPE I FIBROCYTES IN THE HUMAN FETAL COCHLEA.
(A) The lower basal turn of a cochlea at W14 immunostained for the gap junction protein GJA1 (green) and DAPI (blue). The dotted line outlines the group of spiral ligament fibrocytes expressing GJA1. The GJA1 signal is shown separately in white in (A'). Scale bar = 50 µm. (B) The lower basal turn of a cochlea at W18 immunostained for GJA1 (green) and DAPI (blue). The dotted line outlines the group of spiral ligament fibrocytes expressing GJA1. The GJA1 signal is shown separately in white in (B'). Scale bar = 50 µm. (C) Hematoxylin and eosin staining of a similar section as shown in (B). The dotted line represents the area of GJA1-expressing fibrocytes in (B). Scale bar = 50 µm.

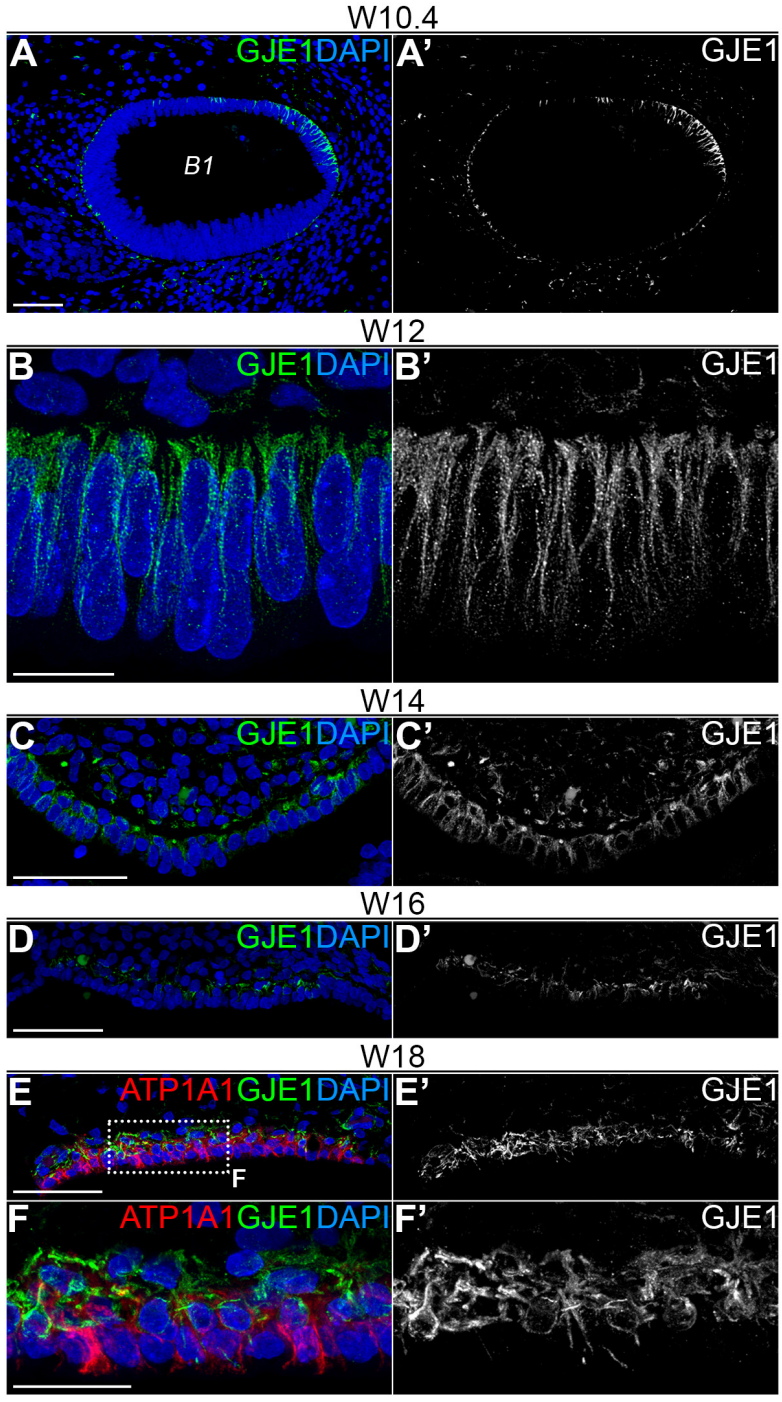


Figure 10. GJE1 expression dynamics during cochlear development in the human fetus.
(A) The lower basal turn of a cochlea at W10.4 immunostained for the gap junction protein GJE1 (green) and DAPI (blue). The GJE1 signal is shown separately in white in (A'). Scale bar = 50 µm. **(B)** The developing stria vascularis in the lower basal turn of a cochlea at W12 immunostained for GJE1 (green) and DAPI (blue). The GJE1 signal is shown separately in white in (B'). Scale bar = 10 µm. **(C)** The developing stria vascularis in the lower basal turn of a cochlea at W14 immunostained for GJE1 (green) and DAPI (blue). The GJE1 signal is shown separately in white in (C'). Scale bar = 50 µm. **(D)** The developing stria vascularis in the lower basal turn of a cochlea at W16 immunostained for GJE1 (green) and DAPI (blue). The GJE1 signal is shown separately in white in (D'). Scale bar = 50 µm. **(E)** The developing stria vascularis in the lower basal turn of a cochlea at W18 immunostained for GJE1 (green) and DAPI (blue). The GJE1 signal is shown separately in white in (E'). Scale bar = 50 µm. **(F)** Higher magnification of the area outlined in (E). The GJE1 signal is shown separately in white in (F'). Scale bar = 20 µm.

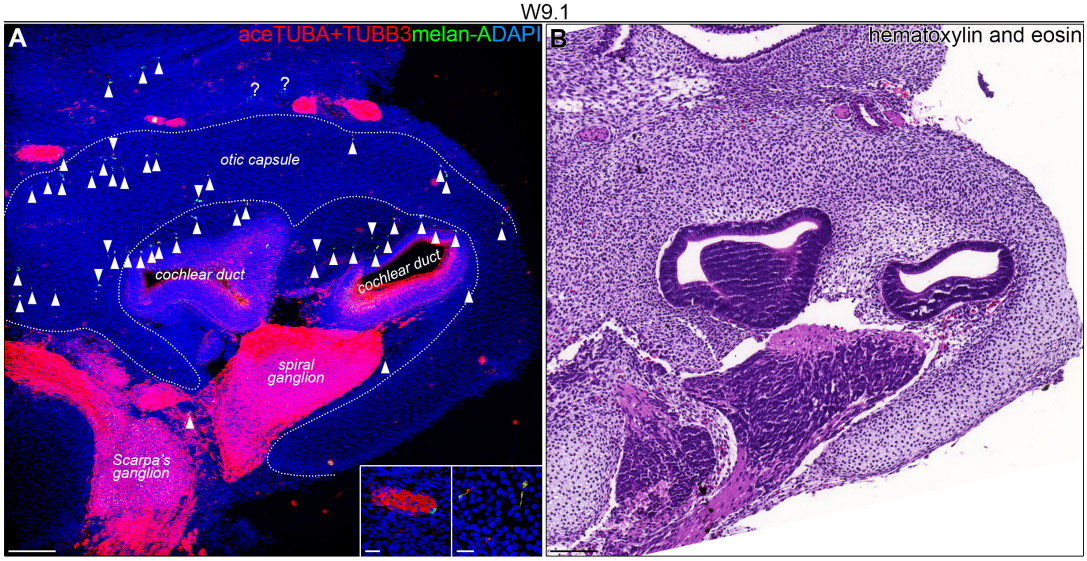


Figure S1. What is the embryonic origin of human cochlear melanocytes?
(**A**) Overview of a cochlea at W9.1 immunostained for class III beta-tubulin (TUBB3) (red), acetylated tubulin (aceTUBA) (red), melan-A (green), and DAPI (blue). The dotted lines outline the region of the developing otic capsule. The arrowheads points to melan-A+ cells. Question marks point to melan-A+ signals of unknown origin. The left inset is a higher magnification of the nervous structure shown in the upper left corner. The right image is a higher magnification of melan-A+/TUBB3+ melanocytes migrating through the otic capsule. Scale bar = 100 µm, or 10 µm (insets). (**B**) Hematoxylin and eosin staining of a consecutive section as shown in (A). Scale bar = 100 µm.

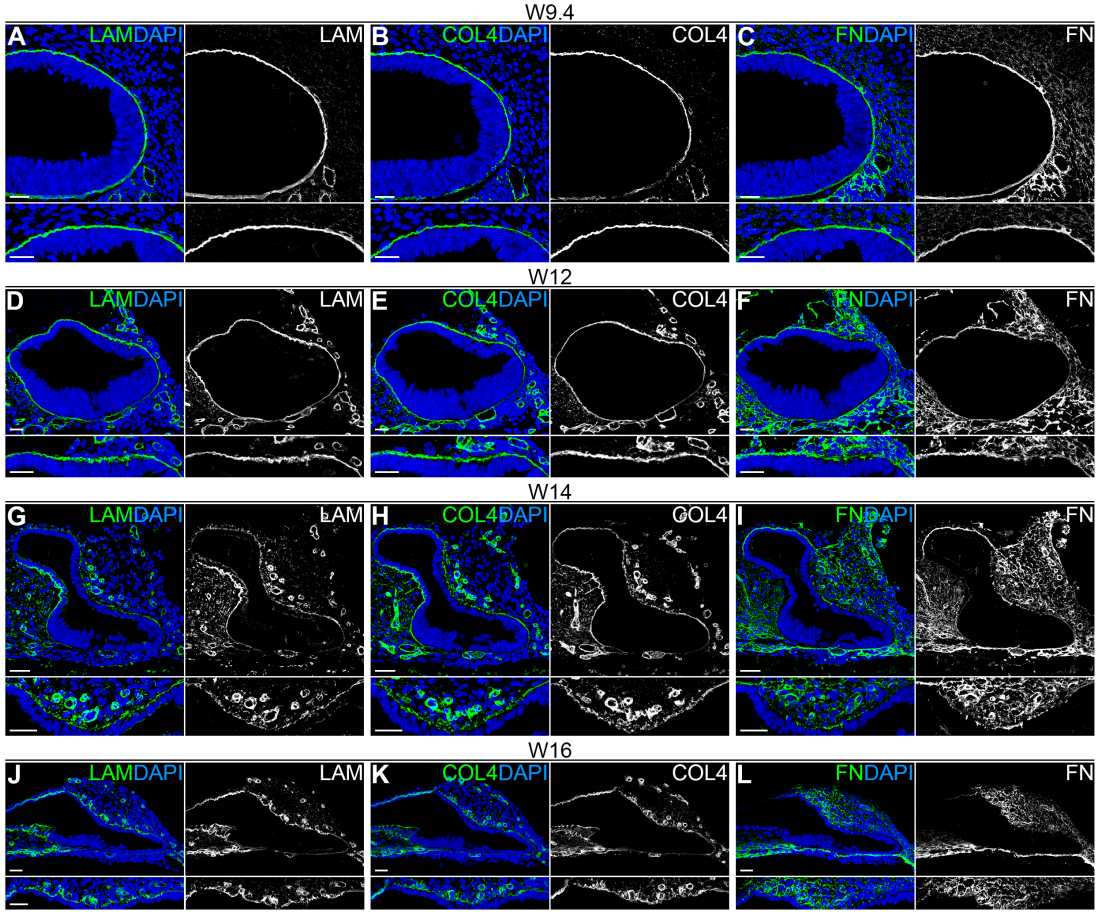


Figure S2. Basement membrane proteins in the developing human fetal cochlea.
(A-C) The lower basal turn of a cochlea at W9.4 immunostained for laminin (LAM) ((A), green), collage type IV (COL4) ((B), green), fibronectin (FN) ((C), green) and DAPI (blue). The LAM, COL4 and FN signals are shown separately in white. The lower panels show higher magnifications of the developing lateral wall. Scale bars = 20 µm. **(D-F)** As in (A-C), here at W12. Scale bars = 20 µm. **(G-I)** As in (A-C), here at W14. Scale bars = 20 µm. **(J-L)** As in (A-C), here at W16. Scale bars = 20 µm.

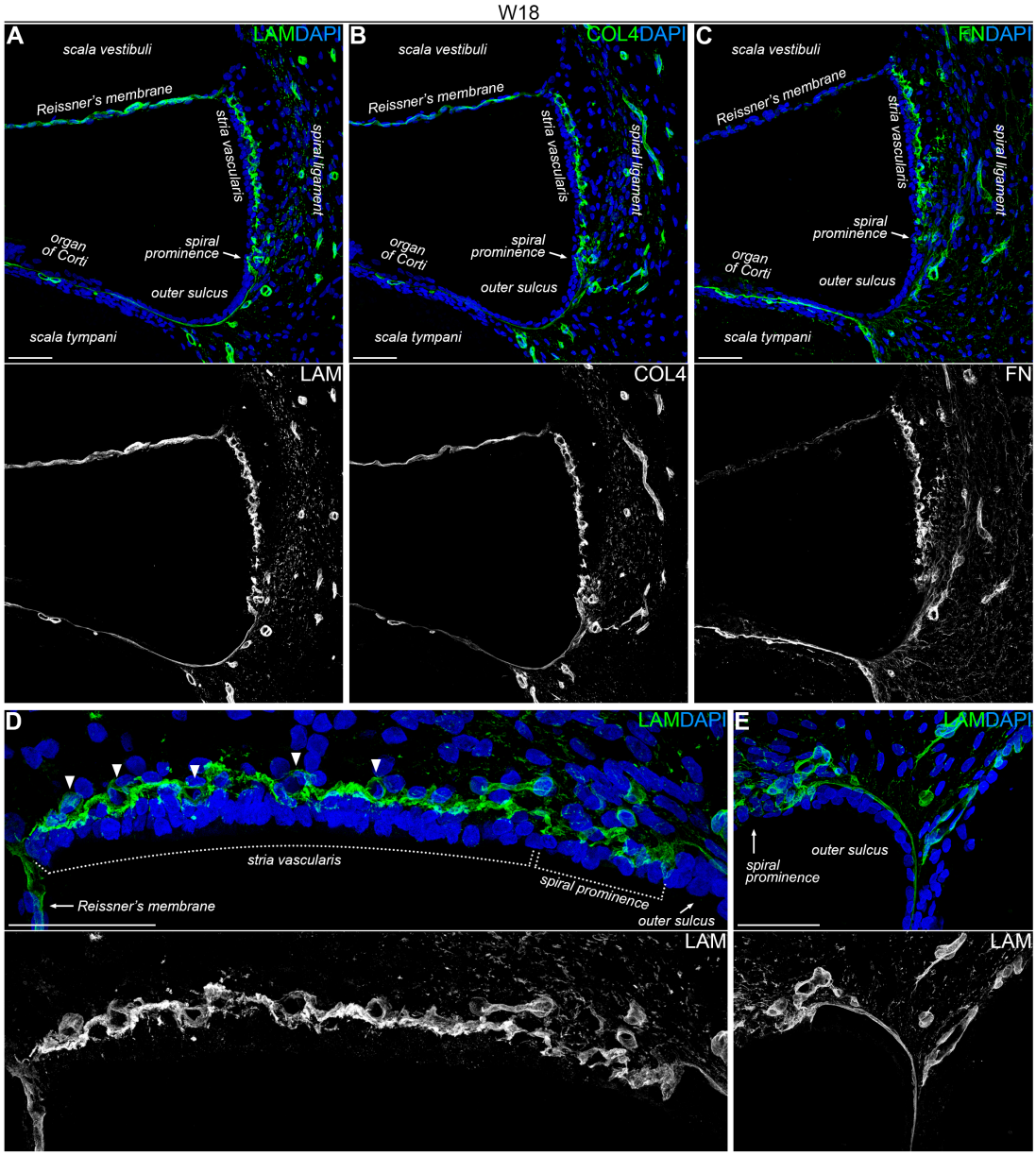


FIGURE S3. BASEMENT MEMBRANE PROTEINS IN THE HUMAN FETAL COCHLEA AT W18.
(**A-C**) The lower basal turn of a cochlea at W18 immunostained for laminin (LAM) ((A), green), collagen type IV (COL4) ((B), green), fibronectin (FN) ((C), green) and DAPI (blue). The LAM, COL4 and FN signals are shown separately in white. Scale bars = 50 µm. (**D-E**) Higher magnification of the stria vascularis (D) and outer sulcus (E) areas of (A). Scale bars = 50 µm.

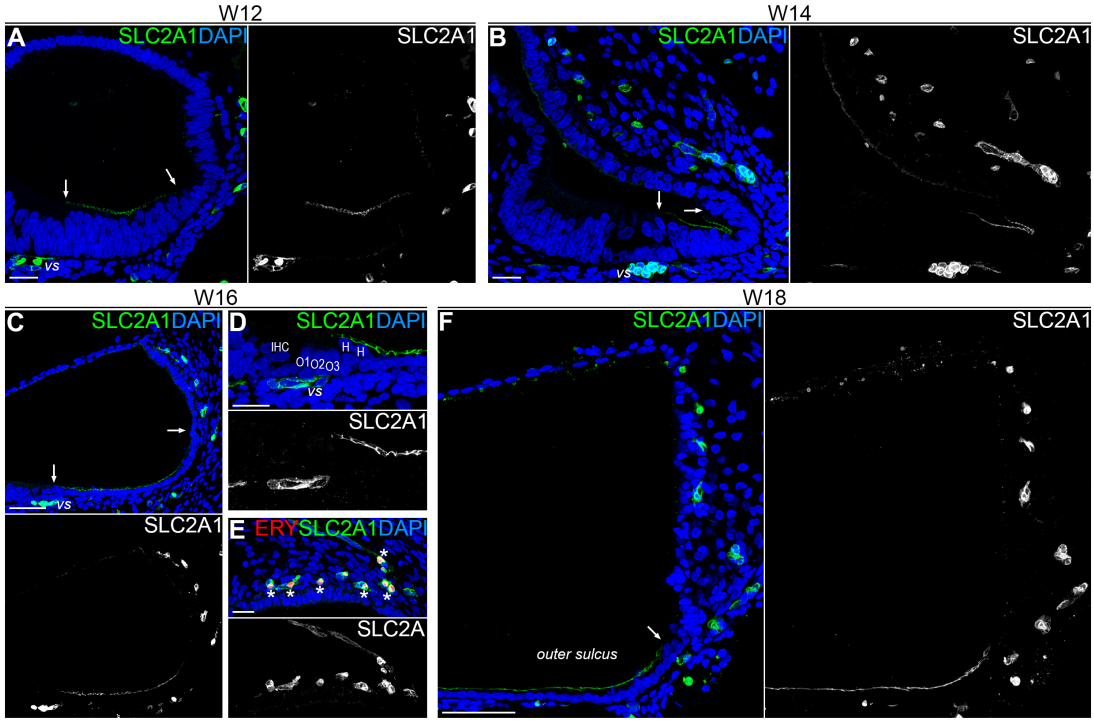
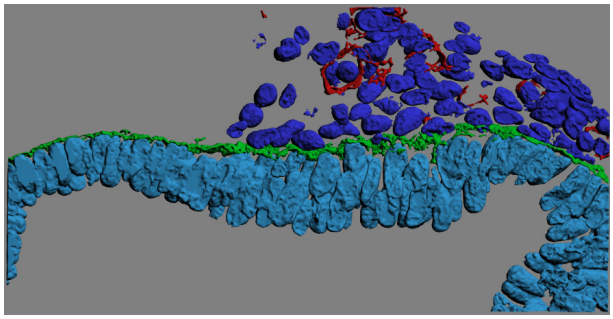
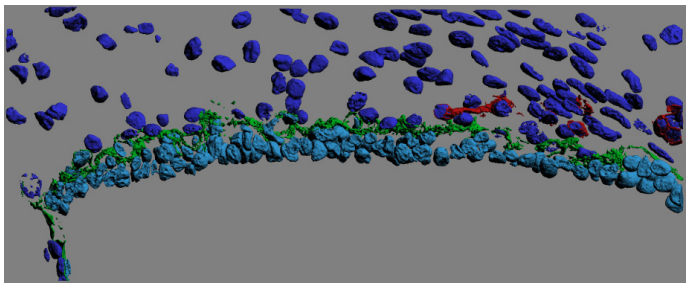


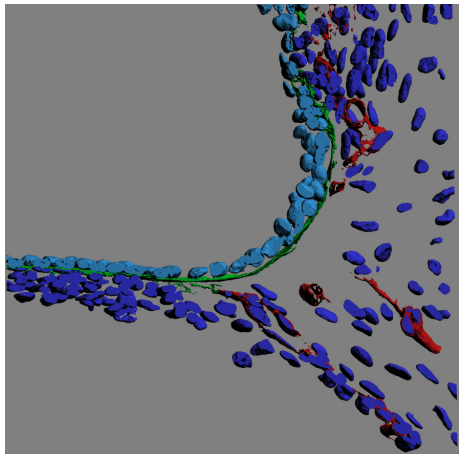
Figure S4. SLC2A1 expression in the human fetal cochlea.
(**A**) The lower basal turn of a cochlea at W12 immunostained for the glucose transporter SLC2A1 (green) and DAPI (blue). The SLC2A1 signal is shown separately in white. The arrows point to the medial and lateral edges of expression of SLC2A1 on the luminal membrane of the epithelial cells. vs = vas spirale (spiral vessel). Scale bar = 20 µm. (**B**) As in (A), here at W14. The SLC2A1 signal is shown separately in white. Scale bar = 20 µm. (**C**) As in (A), here at W16. The SLC2A1 signal is shown separately in white. Scale bar = 50 µm. (**D**) Higher magnification of the organ of Corti and lateral epithelial cells at W16. The SLC2A1 signal is shown separately in white. IHC = inner hair cells, O1 = first row of outer hair cells, O2 = second row of outer hair cells, O3 = third row of outer hair cells, vs = vas spirale (spiral vessel), H = Hensen's cells. Scale bar = 20 µm. (**E**) Higher magnification of the lateral wall and spiral ligament at W16. Asterisks point to auto-fluorescent erythrocytes (red) inside strial capillaries. The SLC2A1 signal is shown separately in white. Scale bar = 20 µm. (**F**) As in (A), here at W18). The SLC2A1 signal is shown separately in white. Scale bar = 50 µm.



Interactive PDF file 1. Irregular lateral wall basement membrane at W12.
Interactive three-dimensional reconstruction of the lateral wall of the basal turn of a cochlea at W12 immunostained for laminin (LAM), as shown in Figure 2H-I and Figure S2D. Cell nuclei in the epithelium are shown in light blue, nuclei in the mesenchymal area as shown in dark blue. The LAM of the lateral wall basement membrane is shown in green, that of vasculature in the mesenchymal area in red. The irregular appearance of the lateral wall basement membrane at the location of the future stria vascularis is shown in View1, in contrast to the smooth appearance of the basement membrane at other parts of the cochlear duct, such as the outer sulcus shown in View2.



Interactive PDF file 2. The lateral wall at W18.
Interactive three-dimensional reconstruction of the lateral wall of the basal turn of a cochlea at W18 immunostained for laminin (LAM), as shown in Figures 4L and S3D. Cell nuclei in the epithelial compartment are shown in light blue, nuclei in the mesenchymal area as shown in dark blue. The LAM of the lateral wall basement membrane (View1) and capillaries in the stria vascularis (View2) is shown in green, that of vasculature in the mesenchymal area in red. View3 shows the spiral prominence, View4 shows Reissner's membrane.



Interactive PDF file 3. The outer sulcus at W18.
Interactive three-dimensional reconstruction of the outer sulcus area of the basal turn of a cochlea at W18 immunostained for laminin (LAM), as shown in Figure S3E. Cell nuclei in the epithelial compartment are shown in light blue, nuclei in the mesenchymal area as shown in dark blue. The LAM of the epithelial basement membrane is shown in green, that of vasculature in the mesenchymal area in red. View1 shows the smooth appearance of the epithelial basement membrane at this location.

These interactive PDF files can be accessed online at the journal's website (http://onlinelibrary.wiley.com/journal/10.1002/(ISSN)1932-846X)

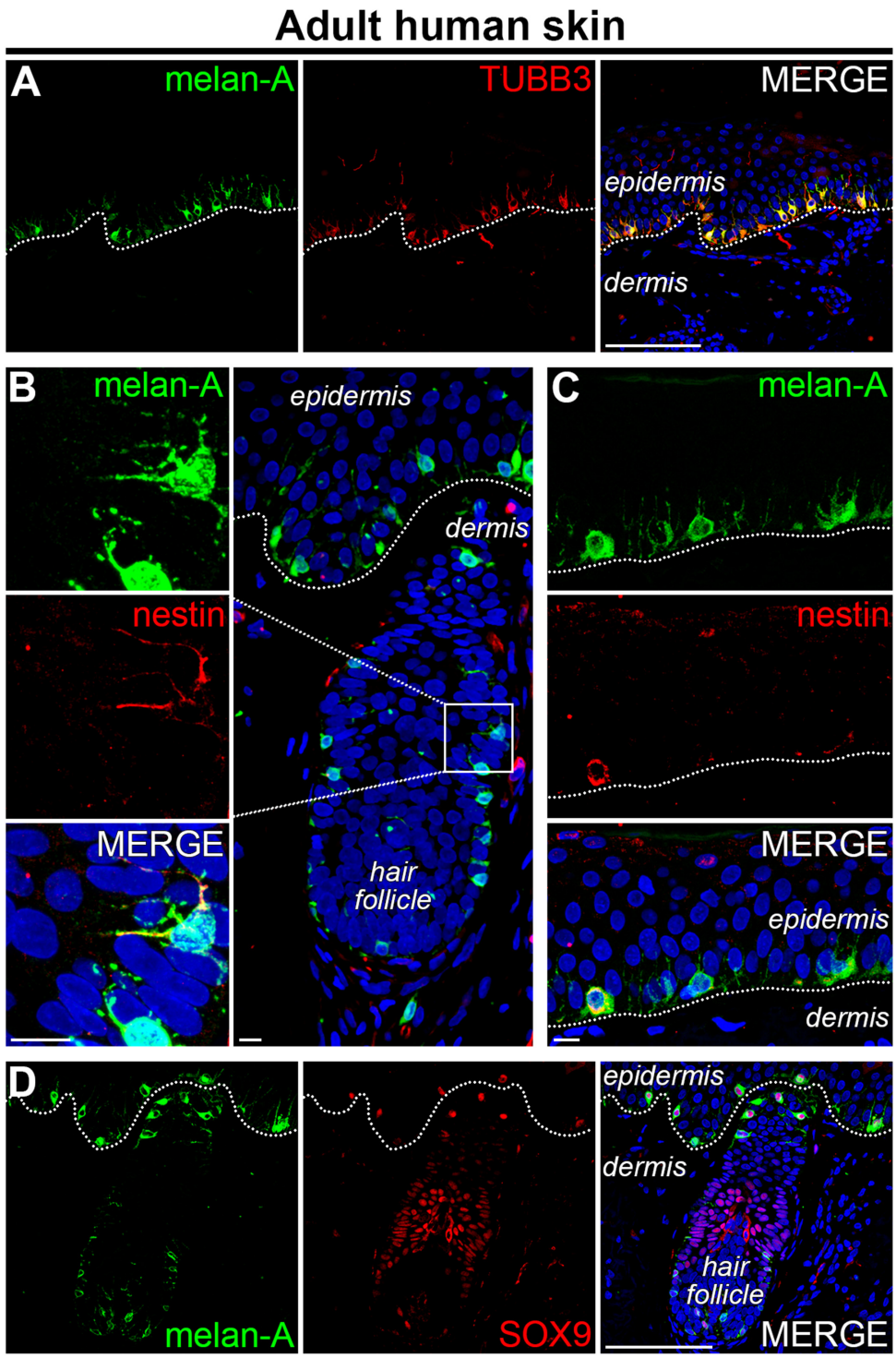


FIGURE 1. IN VIVO EXPRESSION OF MELANOCYTIC AND NEURONAL MARKERS IN THE HUMAN SKIN.
Confocal images of immunohistochemistry performed in 5 µm skin sections against various melanocytic and neuronal proteins. **(A)** Melanocytes express both melan-A and TUBB3. TUBB3, but not melan-A, is also expressed by dermal and epidermal nerve fibers. **(B,C)** Although most melanocytes do not express nestin, a few exceptions can be found, both in the hair follicle (B) and in the epidermis (C). **(D)** Melanocytes, but not neurons, express both melan-A and SOX9. The dashed line indicates the border between the dermis and the epidermis. In the merges, nuclei were stained blue with DAPI. Scale bar = 100 µm (A and D) or 10 (B and C).

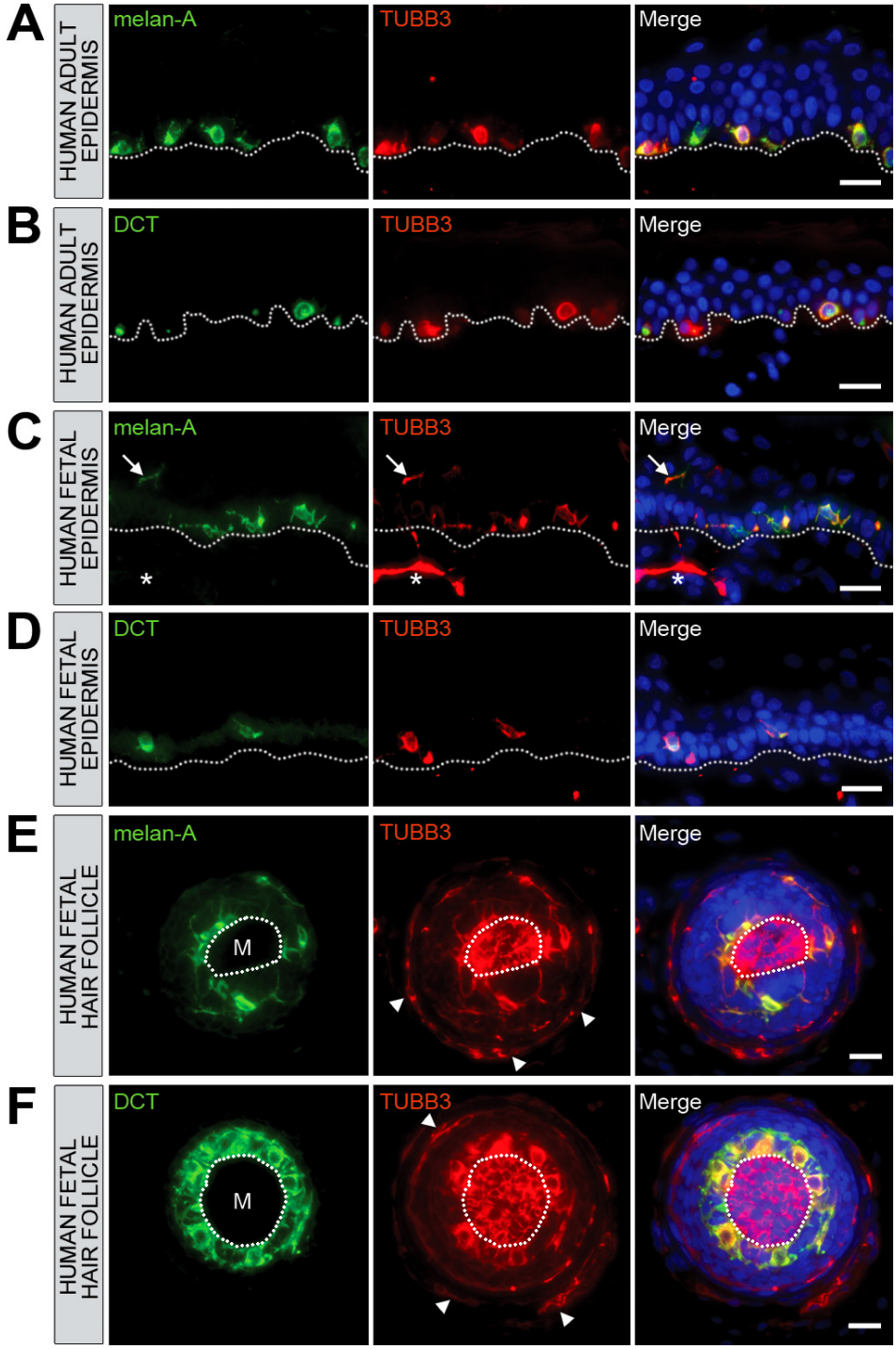


Figure 1. In vivo expression of TUBB3 in human epidermal and hair follicle melanocytes.
Immunohistochemistry was performed on deparaffinized sections of human adult and fetal scalp skin using antibodies to identify melanocytes (melan-A, DCT) and class III B-tubulin (TUBB3). **(A)** Adult epidermis stained for melan-A and TUBB3. **(B)** Adult epidermis immunostained for DCT and TUBB3. **(C)** Fetal epidermis immunostained for melan-A and TUBB3. Arrows: dendritic structure within the epidermis expressing both melan-A and TUBB3. Asterisk: TUBB3+ nerve fiber within the dermis. **(D)** Fetal epidermis immunostained for DCT and TUBB3. **(E)** Fetal hair follicle immunostained for melan-A and TUBB3. DP: Dermal papilla. Arrowheads: melan-A-/TUBB3+ cells **(F)** Fetal hair follicle immunostained for DCT and TUBB3. Arrowheads: DCT-/TUBB3+ cells. (A-F) White dotted lines indicate the basal layer of the skin (A-D) or the transition between the hair follicle matrix and medulla (E-F). Nuclei were stained blue with DAPI. Merge: overlay of fluorescent images. Scale bars = 20 μm.

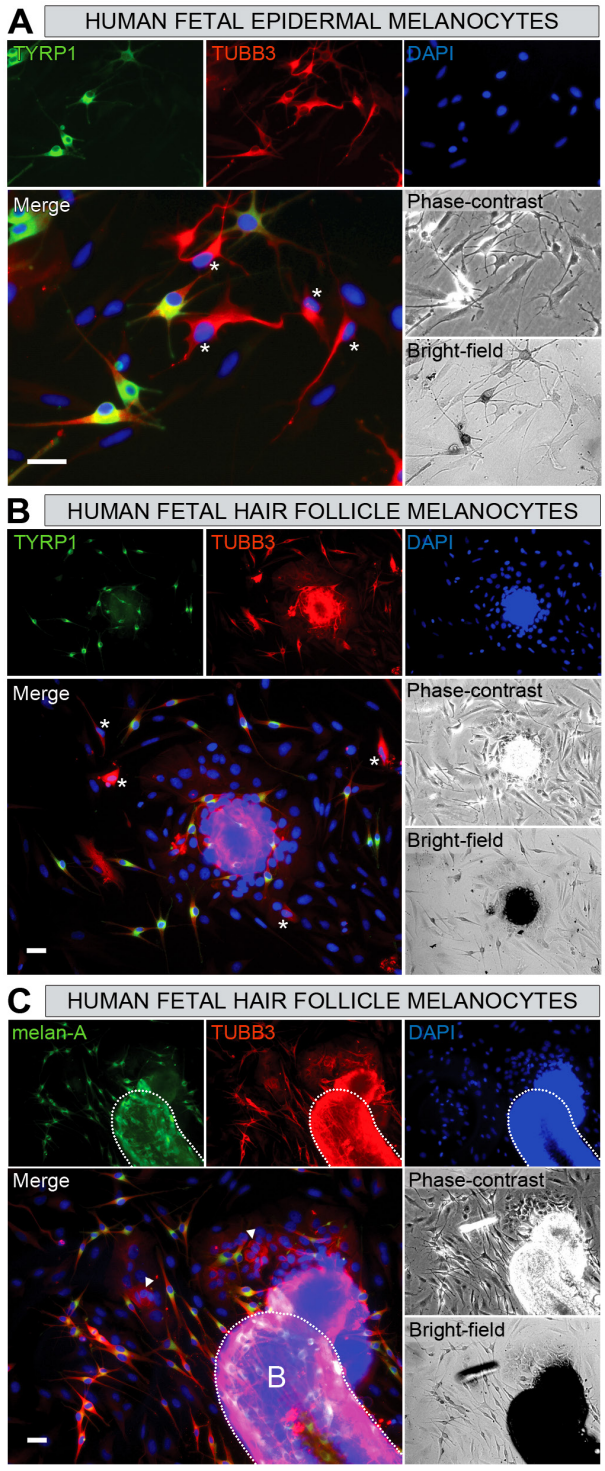


Figure 2. In vitro expression of TUBB3 in human epidermal and hair follicle melanocytes.
Immunostaining was performed on cultures of human fetal scalp skin using antibodies to identify melanocytes (TYRP1 and melan-A) and class III B-tubulin (TUBB3). **(A)** Cultured epidermal melanocytes immunostained for TYRP1 and TUBB3. Asterisks identify TYRP1-/TUBB3+ cells. **(B)** Cultured hair follicle melanocytes immunostained for TYRP1 and TUBB3. Asterisks identify TYRP1-/TUBB3+ cells. **(C)** Cultured cells immunostained for melan-A and TUBB3. White dotted lines outline hair follicle bulb (B). (A-C) Nuclei are stained blue with DAPI. Merge: overlay of fluorescent images. Phase contrast: phase contrast microscopy. Bright field: bright field microscopy. Scale bars = 20 μm.

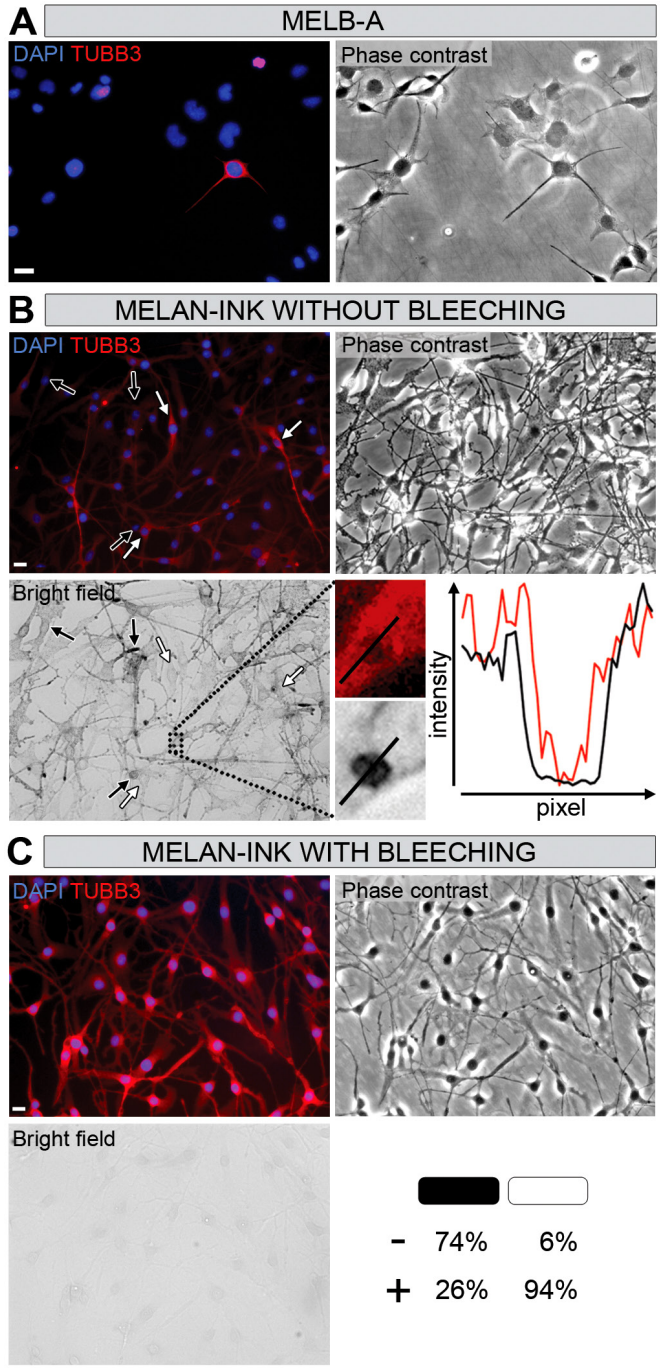
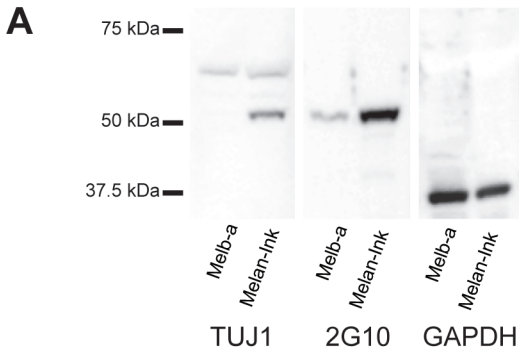


FIGURE 3. IMMUNOSTAINING OF TUBB3 IN THE MOUSE MELANOCYTE LINEAGE.
TUBB3 expression was investigated in two immortalized murine melanogenic cell lines. Melb-a cells are clonal, nonpigmented melanoblasts. Melan-Ink4a2 cells cultures contain both nonpigmented and pigmented melanocytes. **(A)** Cultured melb-a cells immunostained for TUBB3. **(B)** Cultured melan-Ink4a2 cells immunostained for TUBB3 without bleaching. Arrows identify a selection of non-pigmented, fluorescent (white arrows) and pigmented, non-fluorescent (black arrows) melanocytes. The graph depicts intensity values over identical lines plotted in the magnified areas. Red line: TUBB3 fluorescence intensity; Black line: intensity measured under bright field microscopy. Scaling on the vertical axis is normalized to maximum intensity. **(C)** Similar to figure B, but after bleaching with potassium permanganate and oxalic acid (see Materials and Methods). Table: black rectangle = without bleaching; white rectangle = with bleaching; 'minus sign' = non-fluorescent cells, 'plus sign' = bright fluorescent cells. (A-B) Nuclei are stained blue with DAPI.. Phase contrast, phase contrast microscopy. Bright field: bright field microscopy. Scale bars = 20 µm.



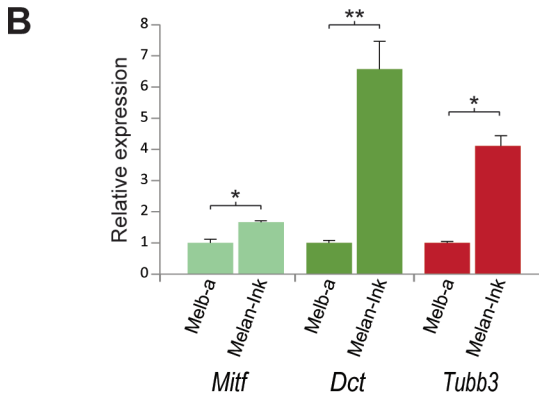


Figure 4. Western blot and quantitative RT-PCR analysis of TUBB3 expression in the melanocyte lineage.
(A) Representative Western blots of TUBB3 expression in melb-a and melan-Ink4a2 cells using two different monoclonal antibodies, TUJ1 and 2G10. Both antibodies recognize the C-terminal end of the protein. TUBB3 has a molecular weight of ~50 kDa. GAPDH was used as loading control. **(B)** Quantitative RT-PCR analysis of melb-a and melan-Ink4a2 cell lysates. The figure shows the expression levels of RNA from two genes regulating melanogenesis, Mitf and DCT, as well as the RNA levels for TUBB3. All PCR products are normalized against averages of Hprt and Gapdh controls, and shown as relative expression levels against melb-a RNA. *p < 0.05; **p < 0.01.

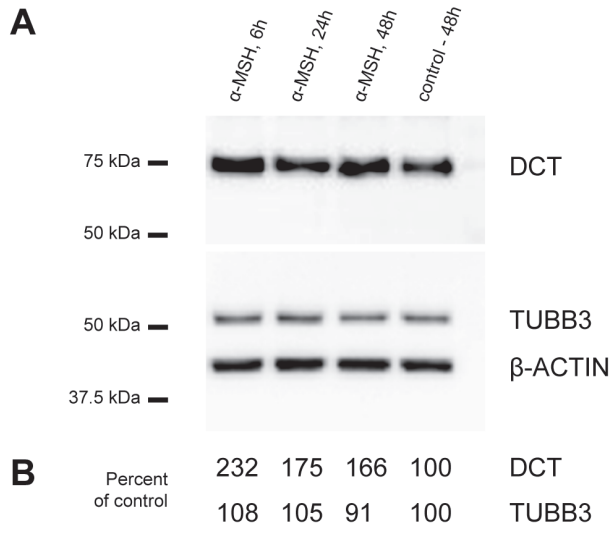


Figure 5. Western blot analysis of DCT and TUBB3 expression after a-MSH stimulation in normal human melanocytes.
(A) Representative Western blots showing DCT and TUBB3 expression in human melanocytes after stimulation with a-MSH for 6, 24 and 48 hours. The same blots were incubated with a monoclonal antibody against B-actin to correct for equal loading. **(B)** The intensity of the bands in (A) was measured using Quantity One 1-D analysis and the resulting change in expression is given in percentage of the unstimulated control, corrected for loading.

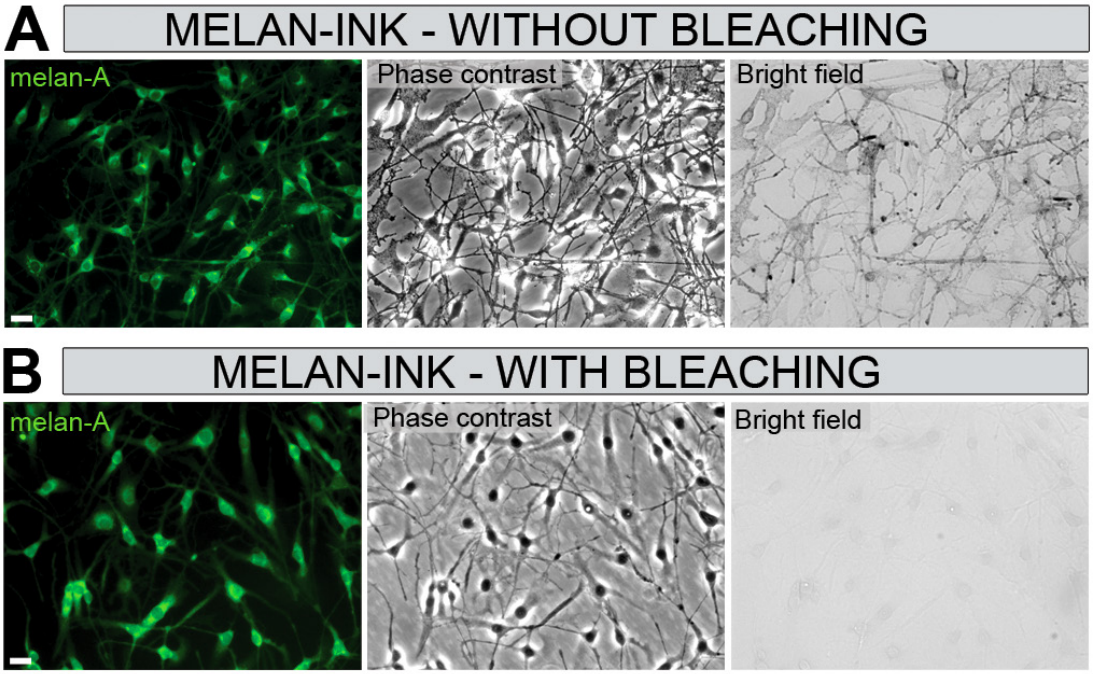


FIGURE S1. MELAN-A IMMUNOREACTIVITY WITHOUT AND WITH BLEACHING.
(A) Cultured melan-Ink4a2 cells immunostained for Melan-A, without bleaching, and (B) with bleaching. (A-B) Phase contrast: phase contrast microscopy. Bright field: bright field microscopy. Scale bars = 20 µm.

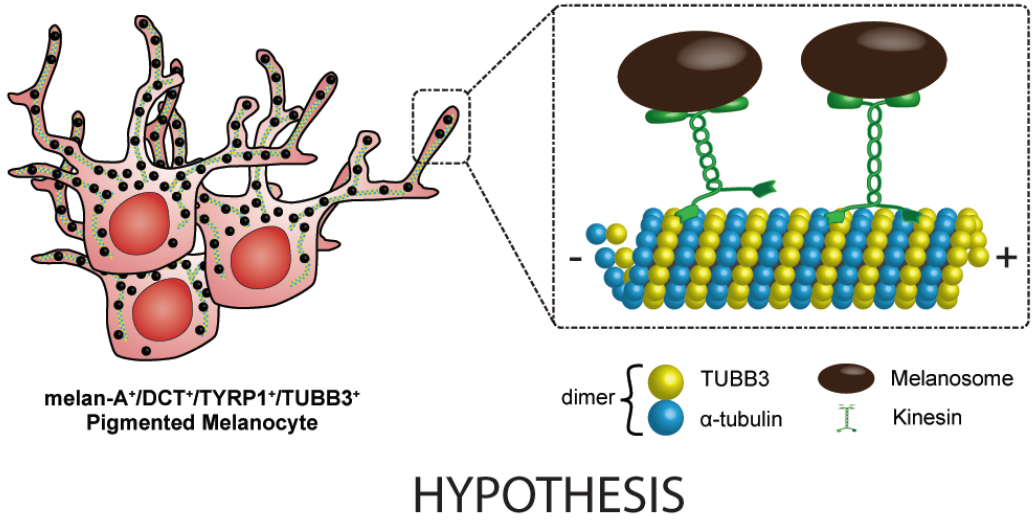


FIGURE S2. HYPOTHESIZED MODEL OF TUBB3 FUNCTION IN MELANOSOME TRANSPORT.
Melanin containing melanosomes are transported by kinesins towards the plus end of microtubules composed of B-tubulin and TUBB3 dimers.

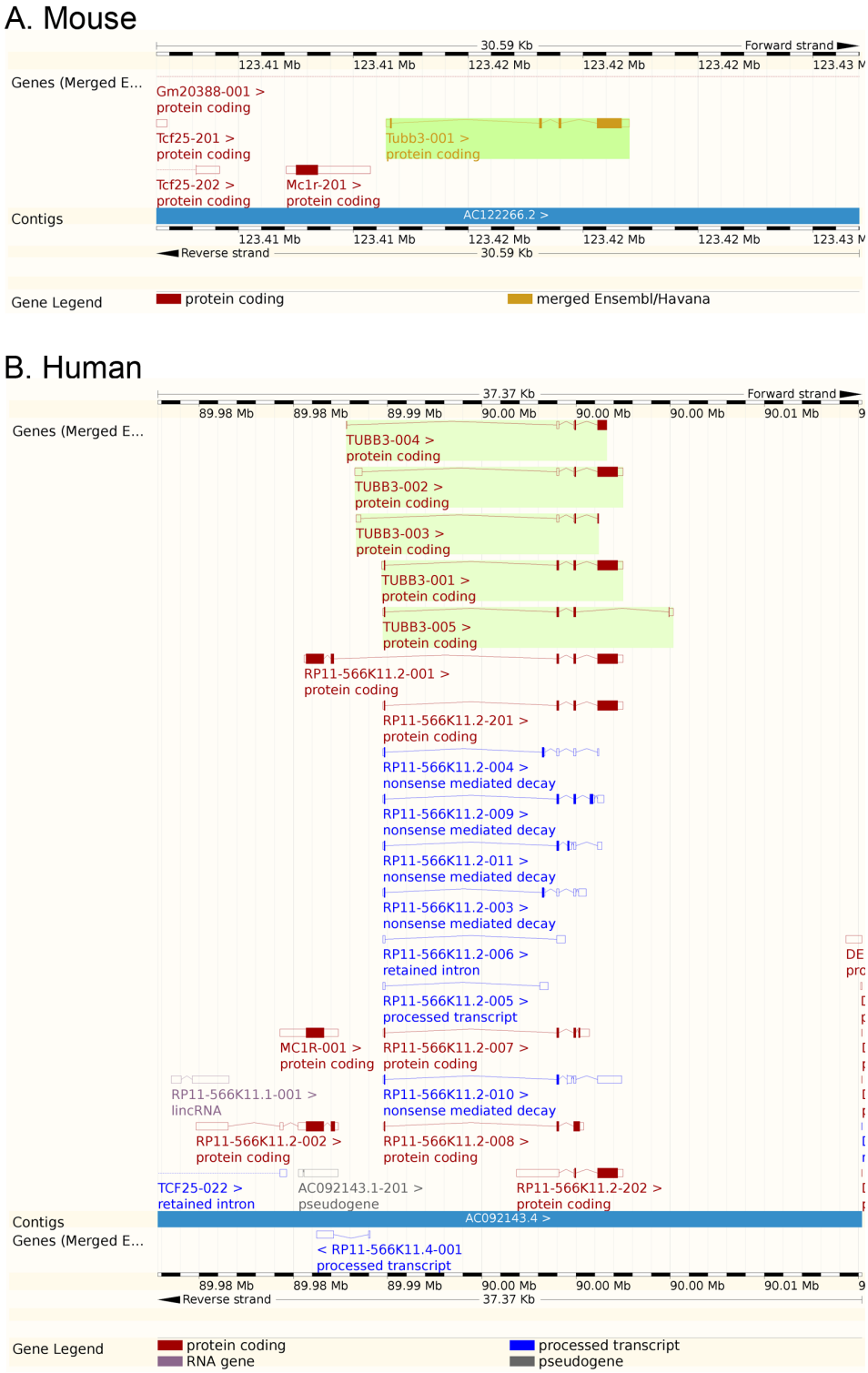


FIGURE S3. TUBB3 TRANSCRIPTS IN MICE AND HUMANS.
(A) In mice, only one protein transcript is known. (B) In humans, there are five known protein transcripts with additions MC1R/TUBB3 chimeric transcripts. Figures are taken from Ensembl (Flicek et al., 2012).

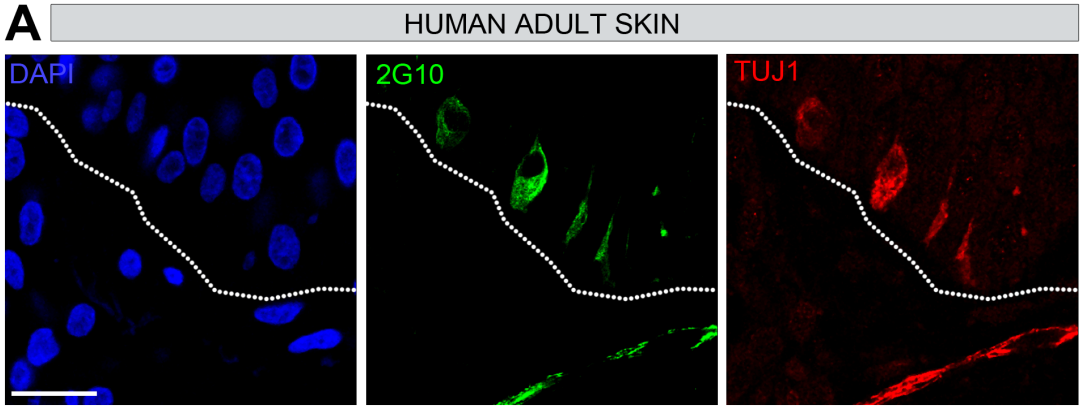


Figure S4. Double immunostaining of 2G10 and TUJ1 antibodies.
(**A**) Human skin stained both with 2G10 and TUJ1. Both monoclonal anti-TUBB3 antibodies stain identical structures within the dermis (nerve fiber with Schwann cell nucleus) and the epidermis (melanocytes). Nuclei are stained blue with DAPI. Scale bar = 20 µm.

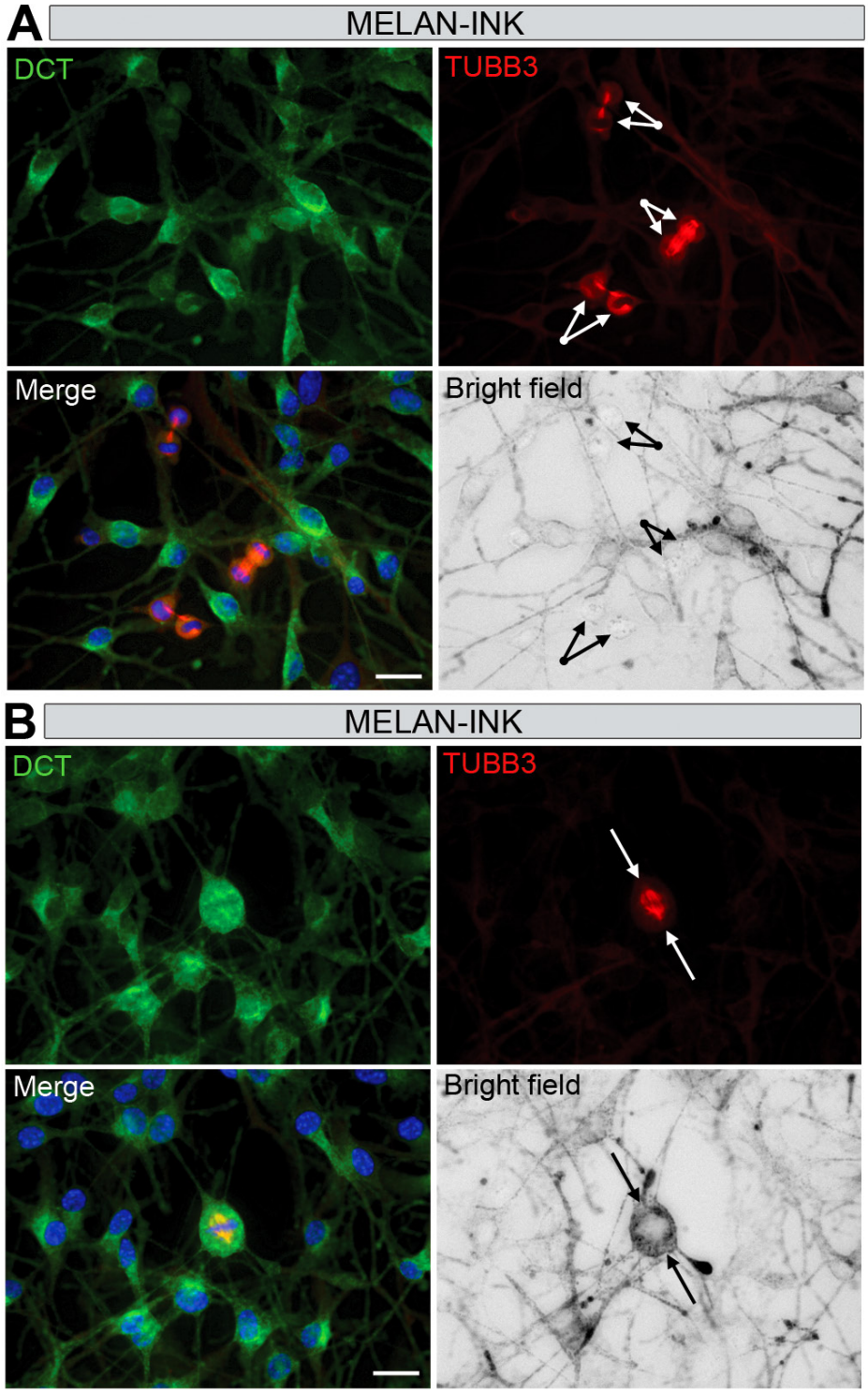


Figure S5. Presence of TUBB3 in mitotic spindles of both non-pigmented and pigmented melanocytes.
(**A**) Cultured melan-Ink4a2 cells immunostained for both DCT and TUBB3. Arrows point to dividing non-pigmented cells. (**B**) Similar to figure A, but arrows indicate a dividing pigmented melanocyte. (A-B) TUBB3 fluorescence can be observed in surrounding cells, but are barely visible here due to the intense emission from the mitotic spindles. Nuclei are stained blue with DAPI. Merge: overlay of fluorescent images. Bright field: bright field microscopy. Scale bars = 20 µm.

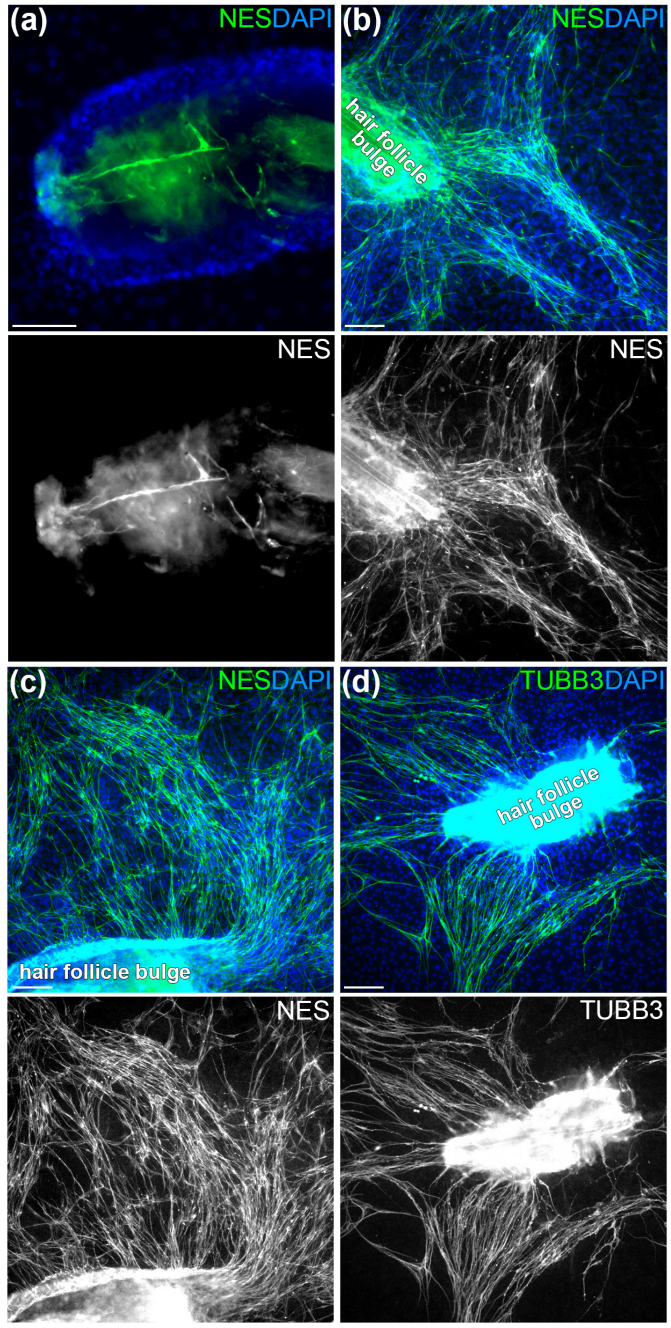


Figure 1. Nestin-positive and TUBB3-positive cells migrate from the hair follicle bulge.
(a) Hair follicle bulge at the start of the culture, showing elongated nestin-positive (NES) cells (green) residing within the explant. **(b-c)** After four weeks in culture, numerous nestin-positive cells (green) are found growing in tracks extending from the bulge explant. **(d)** Hair follicle bulge explants after 4 four weeks of culture immunostain for TUBB3 in a pattern similar to that of nestin. Cell nuclei are stained blue with DAPI. Scalebars = 100 µm (a) or 200 µm (b-d).

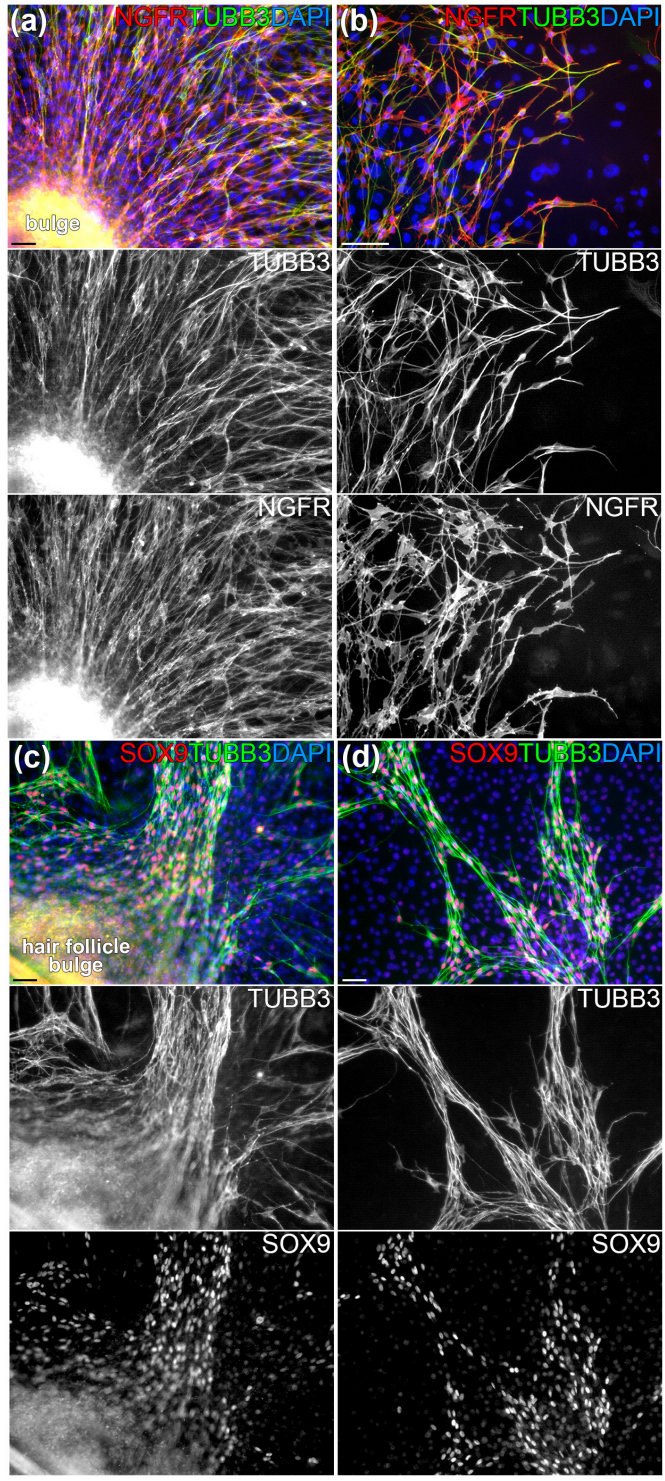


Figure 2. TUBB3-positive hair follicle bulge cells co-express NGFR and SOX9.
(a-b) Double-immunostaining for TUBB3 (green) and NGRF (red) showing that both proteins are expressed in the same subgroup of cells. **(c-d)** Double-immunostaining for TUBB3 (green) and SOX9 (red). The strong co-expression of SOX9 indicates that the TUBB3-positive cells are of melanoglial, rather than neuronal, origin. Cell nuclei are stained blue with DAPI. Scalebars = 50 µm.

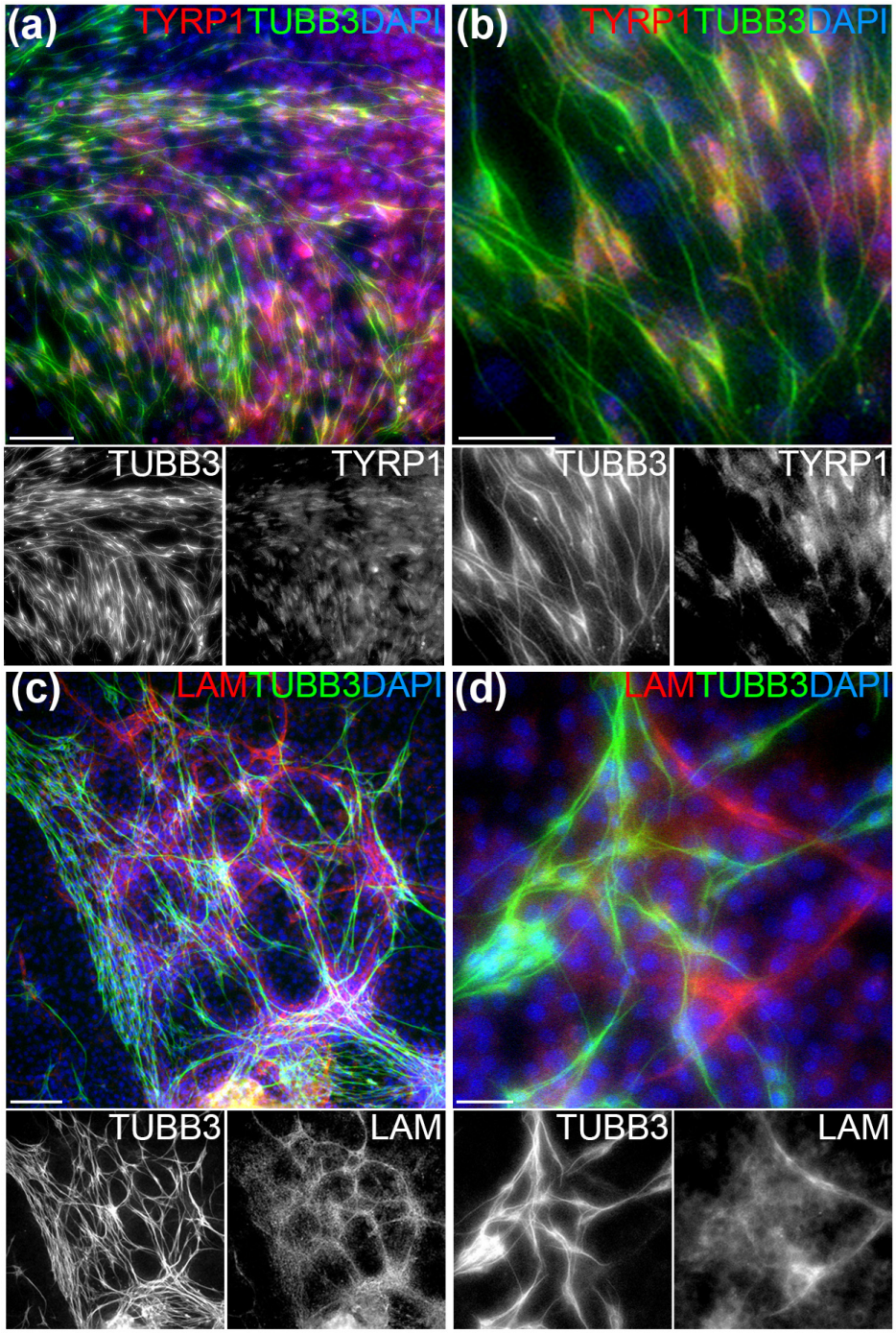


Figure 3. Melanocyte and glial marker expression of TUBB3-positive cells.
(a) Hair follicle bulge explant after 4 weeks of culture immunostained for TUBB3 (green) and TYRP1 (red), showing weak expression of TYRP1 in the TUBB3-positive cells. **(b)** Higher magnification of the lower left area in (a). **(c-d)** Double-immunostaining for TUBB3 (green) and laminin (red) shows a subpopulation of laminin-positive cells largely growing along the same migration patterns of the TUBB3-positive cells. Cell nuclei are stained blue with DAPI. Scalebars = 200 µm (a, c), 100 µm (b) or 20 µm (d).


cochlea
cochlea

4

Development of the stria vascularis and potassium regulation in the human fetal cochlea: insights into hereditary sensorineural hearing loss

Locher
de Groot
van Iperen
Huisman
Frijns
Chuva de Sousa Lopes

Developmental Neurobiology, 2015

Abstract

Sensorineural hearing loss (SNHL) is one of the most common congenital disorders in humans, afflicting one in every thousand newborns. The majority is of heritable origin, and can be divided in syndromic and nonsyndromic forms. Knowledge of the expression profile of affected genes in the human fetal cochlea is limited, and as many of the gene mutations causing SNHL likely affect the stria vascularis or cochlear potassium homeostasis (both essential to hearing), a better insight into the embryological development of this organ is needed to understand SNHL etiologies. We present an investigation on the development of the stria vascularis in the human fetal cochlea between 9 and 18 weeks of gestation (W9-W18), and show the cochlear expression dynamics of key potassium-regulating proteins. At W12, MITF+/SOX10+/KIT+ neural-crest-derived melanocytes migrated into the cochlea and penetrated the basement membrane of the lateral wall epithelium, developing into the intermediate cells of the stria vascularis. These melanocytes tightly integrated with Na^+/K^+-ATPase-positive marginal cells, which started to express KCNQ1 in their apical membrane at W16. At W18, KCNJ10 and gap junction proteins GJB2/CX26 and GJB6/CX30 were expressed in the cells in the outer sulcus, but not in the spiral ligament. Finally, we investigated GJA1/CX43 and GJE1/CX23 expression, and suggest that GJE1 presents a potential new SNHL associated locus. Our study helps to better understand human cochlear development, provides more insight into multiple forms of hereditary SNHL, and suggests that human hearing does not commence before the third trimester of pregnancy.

Introduction

According to recent estimates of the World Health Organization, more than 5% of the world's total population suffer from some form of disabling hearing loss [1]. A large part of this hearing loss is of sensorineural nature, making sensorineural hearing loss (SNHL) the most prevalent sensorineural disorder in humans. SNHL is also the most common congenital disorder, with a prevalence of 1 in every 1000 newborns in the UK and the Netherlands (with a bilateral hearing loss $\geqslant$ 40 dB [2, 3]). Of these, over two-thirds can be attributed to genetic factors. Hereditary SNHL can be classified in syndromic (~25%) and nonsyndromic (~75%) forms [4].

Examples of syndromic SNHL include Pendred's syndrome ([MIM 274600], combining hearing loss and goiter [5, 6]), Waardenburg syndrome (hearing loss and pigmentation abnormalities [7, 8]) and Jervell and Lange-Nielsen syndrome ([MIM 220400 and MIM 612347], hearing loss and cardiac symptoms [9]). In nonsyndromic SNHL, associations with obvious abnormalities of the external ear or symptoms other than hearing loss cannot be found, but the heterogeneity of loci and genes is high: over 130 loci have been mapped and over 60 different genes have been implicated presently (Van Camp & Smith). Nonsyndromic forms are grouped in autosomal dominant (DFNA), autosomal recessive (DFNB), X-linked (DNFX) and mitrochondrial subtypes. The most commonly affected gene causing nonsyndromic hearing loss (both in autosomal recessive DFNB1A [MIM 220290] and in autosomal dominant DFNA3A [MIM 601544]) is *gap junction beta 2* (*GJB2*, [MIM 121011]), the gene encoding the connexin 26 protein (CX26) [11, 12]. Depending on the studied population, 20-50% of all recessive nonsyndromic SNHL cases can be attributed to a mutation in *GJB2* [13, 14]. For a comprehensive overview of other affected genes we refer to recent reviews [15 – 19].

In SNHL, the disorder lies either in the cochlea itself, or in any of the retrocochlear auditory structures. Cochlear hair cells are responsible for converting sound into electrical signals that travel to the brainstem via the cochlear nerve [20]. Hair cell function depends on the endocochlear potential, a positive extracellular potential ($\approx$80-100 mV relative to perilymph) in the endolymph of the cochlear duct (or scala media), generated by an unusually high concentration of potassium ions (K^+) [21]. These ions are secreted into the endolymph by specialized cells within the stria vascularis, located in the lateral wall of the cochlear duct [22]. The stria vascularis is highly vascularized and consists of three layers of distinct cell types: the marginal

cells, the intermediate cells (melanocytes), and the basal cells [23, 24]. It is generally accepted that the depolarizing K^+ flow causing hair cell activation in the organ of Corti is recycled back to the stria vascularis via the epithelial lining of the cochlear duct and the spiral ligament fibrocytes, and/or through the perilymph, as depicted in Figure 1. To maintain the endocochlear potential, this recycling system requires a specific distribution of cochlear cell types as well as selective ion channels and gap-junctions [25, 26].

Therefore, it is not surprising that many gene mutations causing SNHL either result in functional changes of the ion channels involved in K^+ homeostasis or cause an abnormal cellular morphology in the cochlea. Although progress has been made in identifying the genes responsible for SNHL in humans, knowledge on their actual expression in the human cochlea is limited and only a few studies have investigated the morphological development of the stria vascularis in the human fetal cochlea [27, 28]. In this paper, we address both aspects, focussing on the embryonic development of the lateral wall in the human fetal cochlea. We show the expression profiles of several genes involved in syndromic and nonsyndromic SNHL (Table 1) between 9 and 18 weeks of gestation (W9-W18). More specifically, we have investigated the development of the different cell types in the stria vascularis and studied the expression of K^+-regulating and gap junction proteins. Together, our data gives insight in hereditary SNHL and provides a basis for K^+-recycling models in the human cochlea.

Table 1 Selected Genes and Association with Syndromic and Nonsyndromic Sensorineural Hearing Loss

Gene	MIM	SNHL in Genetic Disorder *(MIM)*
MITF	156845	Waardenburg syndrome, type 2A *(193510)*
		Waardenburg syndrome/ocular albinism, digenic *(103470)*
		Tietz albinism-deafness syndrome *(103500)*
SOX10	602229	Waardenburg syndrome, type 4C *(613266)*
		Waardenburg syndrome, type 2E *(611584)*
		PCWH syndrome *(609136)*
		Kallman syndrome with deafness *(not defined)*
KIT	164920	Piebaldism *(172800)*
KCNQ1 (KVLQT1)	607542	Jervell and Lange-Nielsen syndrome *(220400)*
KCNJ10 (K_{ir}4.1)	602208	Enlarged vestibular aqueduct, digenic *(600791)*
		SESAME syndrome *(612780)*
GJB2 (CX26)	121011	DFNA3A *(601544)*
		DFNB1A *(220290)*
		Hystrix-like ichthyosis with deafness *(602540)*
		Keratitis-ichthyosis-deafness syndrome *(148210)*
		Bart-Pumphrey syndrome *(149200)*
		Keratoderma, palmoplantar, with deafness *(148350)*
		Vohwinkel syndrome *(124500)*
GJB6 (CX30)	604418	DFNA3B *(612643)*
		DFNB1B *(612645)*
		DFNB1A, digenic *(220290)*
GJA1 (CX43)	121014	DFN not defined
GJE1 (CX23)	Not defined	Unknown

Methods

Tissue samples

Human fetal cochleas were collected from tissues obtained by elective abortion (healthy subjects, no medical indication) using vacuum aspiration. Prior to the procedure, obstetric ultrasonography was used to determine the gestational age in weeks and days. Of all collected cochleas, we discarded those which where mechanically damaged or showed marked tissue degeneration, upon inspection by light-microscopy. Cochleas of the following gestational ages were collected and used: W9, W9.1, W10.4 (2x), W12 (2x), W12.2, W14 (2x), W16 (2x), W18 (3x). The cochleas were obtained in PBS, fixed in 4% paraformaldehyde in PBS overnight at 4° C, decalcified and embedded in paraffin as previously described [29]. The use of human fetal material was approved by the Medical Ethical Committee of the Leiden University Medical Center (protocol 08.087). Informed written consent was obtained in accordance with the WMA Declaration of Helsinki guidelines.

Immunohistochemistry

The cochleas were cut in 5 or 10 μm thick sections in the sagittal plane using a RM2255 microtome (Leica). Deparaffinization and immunohistochemistry were carried out as previously described [29]. Briefly, antigen retrieval was performed (see below) and sections were consecutively incubated with primary and secondary antibodies diluted in blocking solution consisting of 1% bovine serum albumin (Sigma-Aldrich) and 0.05% Tween-20 (Promega) in PBS. Nuclei were stained with 4',6-diamidino-2-phenylindole (DAPI, Vector Laboratories). The primary antibodies used in this study were mouse anti-acetylated tubulin (aceTUBA, 1:500, T6793, Sigma), rabbit anti-collagen type IV (COL4, 1:200, AB748, Chemicon), rabbit anti-fibronectin (FN, 1:400, F3648, Sigma-Aldrich), rabbit anti-GJA1 (1:1000, C6219, Sigma), rabbit anti-GJA1 (1:2000, ACC-201, Alomone labs), rabbit anti-GJB2 (1:100, ACC-212, Alomone labs), rabbit anti-GJB6 (1:100, PA511640, Thermo Scientific), rabbit anti-GJE1 (1:1000, NBP2-14051, Novus biologicals), goat anti-KCNJ10 (1:100, NBP1-70371), rabbit anti-KCNQ1 (1:200, ab65092, Abcam), rabbit anti-KCNQ1 (1:100, APC-022, Alomone labs), rabbit anti-KIT (1:100, A4502, Dako), rabbit anti-laminin (LAM, 1:200, Z009701, Dako), rabbit anti-melan-A (1:500, NBP1-30151, Novus), mouse anti-microphthalmia-associated transcription factor (MITF, 1:100, M3621, Dako), mouse anti-Na+/K+-ATPase α1 (ATP1A1, 1:200, α6F, Developmental Studies

Hybridoma Bank), rabbit anti-solute family carrier 2, member 1 (SLC2A1, 1:500, ab15309, Abcam) and goat anti-SOX10 (1:50, sc-17342, Santa Cruz Biotechnology). Prior to immunostaining for COL4, LAM and FN antibodies, antigen retrieval was performed by incubating sections for 5 minutes with 20 μg/ml proteinase K (Promega) in Tris-EDTA-CaCl2 buffer (pH8.0). In all other cases, tissue sections were treated for 12 minutes at 97 ° C with 0.01M sodium citrate buffer (pH 6.0) and allowed to cool down. The secondary antibodies used were Alexa Fluor (AF) conjugated immunoglobulins (Life Technologies): AF 488 donkey anti-mouse (A-21202), AF 488 donkey anti-rabbit (A-21206), AF 488 donkey anti-goat (A-11055), AF 568 donkey anti-mouse (A-10037), and AF 568 donkey anti-rabbit (A-10042), all at a 1:500 dilution. As antibody specificity controls, primary antibodies were routinely omitted (negative control), isotype controls were performed (negative control) and immunostainings were performed on adult mouse cochlea (positive control). On human fetal tissue, at least three separate immunostaining experiments were performed with each primary antibody. To further verify specificity, all immunostaining results were checked to confirm the appropriate cellular location of the fluorescent signals and tissue expression patterns were compared to previous studies using experimental animals, if available.

Image acquisition and processing

Confocal images were acquired with a Leica SP8 confocal laser scanning microscope operating under the Leica Application Suite Advanced Fluorescence software (LAS AF) using Leica objectives (40x/1.3 oil HC PL Apo or 63x/1.4 oil HC PL Apo). Maximal projections were obtained from image stacks with a z-step size of 0.5 μm. Brightness and contrast adjustments consistent with image manipulation policies were performed either with LAS AF, Fiji (ImageJ version 1.48k [30]) or Adobe Photoshop CS6 (Adobe Systems) image-processing software.

Results

Melanocytes invade the lateral wall epithelium at W12 and develop into the intermediate cells

The cochlear melanocytes that form the intermediate cell layer of the stria vascularis are thought to originate from the neural crest. In order to investigate the formation of the three cell layers of the stria vascularis, we first determined the cochlear location of melanocytes and monitored their invasion into the lateral wall epithelium during embryonic development of the human fetal cochlea. Immunostaining for melan-A ([MIM 605313], a marker of melanocytes) and acetylated α-tubulin (aceTUBA, which labels various types of epithelial and neural cells) allowed us to visualize melanocyte location and general cochlear architecture. At W9.1, the melan-A+ melanocytes were located both in the part of the periotic mesenchyme that will develop into the otic capsule (called hereafter: otic capsule), and in the part of the periotic mesenchyme that will form the spiral ligament and the spiral limbus (called hereafter: periotic mesenchyme), but not in the epithelium of the cochlear duct (Figure 2A-B, Figure S1). More specifically, most melanocytes were found in the apical half of the developing cochlea situated above the cochlear duct, and only a few could be observed in the periotic mesenchyme bordering the lateral wall epithelium, i.e. the future stria vascularis (Figure 2B, right arrowhead). Immunostaining for basement membrane proteins laminin (LAM) (Figure S2A), collagen type IV (COL4) (Figure S2B) and fibronectin (FN) (Figure S2C) at W9.4 showed a strictly continuous and smooth basement membrane, further confirming the mesenchymal location of the melanocytes. At W10.4, the cochlear duct had spiralled twice around the central axis of the cochlea and melan-A+ melanocytes were observed exclusively in the periotic mesenchyme of the future middle and basal turns (Figure 2C-D, arrowheads). When compared to W9.1, more melanocytes were located close to the lateral wall epithelium.

At W12, melan-A+ melanocytes were observed in all cochlear turns. In the apical and middle turns, melanocytes were still located exclusively to the periotic mesenchyme (Figure 2E). However, in the basal turn, melanocytes were observed both in the periotic mesenchyme (Figure 2F and arrowheads in Figure 2G) and in the lateral wall epithelium of the cochlear duct (the future stria vascularis), indicating that they had penetrated through the basement membrane (arrows in Figure 2G). This finding is in agreement with the observation that the basement

membrane at this location showed irregular staining patterns for LAM, COL4 and FN, in contrast to its smooth and continuous appearance near the developing Reissner's membrane and at the location of the outer sulcus (Figure 2H-I and three-dimensional reconstruction provided in Interactive PDF file 1).

Melanocytes in the stria vascularis express MITF, SOX10 and KIT

Next, we investigated the expression of two genes, *MITF* [MIM 156845] and *SOX10* [MIM 602229] that are expressed in the melanocytic lineage. At W12, MITF was expressed in all turns in both the melan-A+ melanocytes in the periotic mesenchyme and in the melanocytes that had invaded the developing stria vascularis (Figure 3A). Previously, we have shown that SOX10+ cells are present in the spiral ganglion and throughout the cochlear epithelium [31]. In the present study, we also detected SOX10 expression in the presumptive melanocytes bordering the stria vascularis (Figure 3B, arrowheads).

Double immunostaining for MITF and KIT [MIM 164920], the latter protein being expressed in both the neural crest and the melanocytic lineage, at W12 showed that KIT was expressed by all MITF+ melanocytes (Figure 3C). In addition, KIT expression was found in the cochlear duct epithelium, in a few remaining mesenchymal cells within the developing scala tympani (Figure 3C-D), and in the spiral ganglion (data not shown).

In the developing stria vascularis, melanocytes integrate with the marginal cells in a spatiotemporal order

At W12, we detected a clear spatial gradient in the location of melanocytes, with epithelial invasion commencing in the basal turn (Figure 2E-F). To monitor this development, we immunostained cochleas at W14, W16 and W18 for melan-A and aceTUBA. At W14, melan-A+ melanocytes were still confined to the periotic mesenchyme in both the upper middle (M2) and lower middle (M1) turns (Fig 4A, B). In the upper basal turn (B2), melanocytes were observed invading the lateral wall epithelium (Figure 4C) and in the lower basal turn (B1) most melanocytes were found integrating with the developing marginal cells (Figure 4D). At W16, integrating melanocytes were found in greater numbers and observed throughout all turns (Figure 4E-H). In addition to melanocytes in or near the lateral wall epithelium, we also consistently observed the presence of melan-A+ melanocytes

along the edges of the otic capsule, here shown in the M2 turn at W16 (Figure 4I, arrowheads) and the B1 turn at W18 (Figure 4J, arrowheads). At W18, melanocytes were found tightly integrated with the developing marginal cells in the B1 turn, and some melanocyte processes were also observed around the developing strial capillaries (Figure 4K, arrowheads). Expression patterns of aceTUBA (Figure 4K) and the basement membrane proteins LAM, COL4 and FN better accentuated the development of other regions in the lateral wall epithelium (Figure 4L-N, Figure S2D-L and Figure S3, and three-dimensional reconstruction provided in Interactive PDF files 2 and 3). In particular, with these immunostainings the spiral prominence is clearly emerging, thereby demarcating the stria vascularis from the future root cells in the outer at W18.

Until W18, SLC2A1+ basal cells were not detected in the stria vascularis

In the stria vascularis, in addition to the marginal cells and the melanocytes, we also investigated the formation of the third and innermost strial layer, i.e., the basal cells. However, until W18, we were unable to detect any basal cells by immunostaining for solute family carrier 2, member 1 (SLC2A1, also known as GLUT1, [MIM 138140]), a glucose transporter known to be expressed by the rodent cochlear basal cells and vascular endothelial cells [32]. SLC2A1 expression was found in the developing human stria vascularis but this expression was confined to capillaries and erythrocytes (Figure S4). Interestingly, we did observe consistent expression of SLC2A1 on the apical (luminal) membranes of all epithelial cells between the organ of Corti and the spiral prominence (Hensen's cells in the organ of Corti as well as Claudius' cells and root cells in the outer sulcus) at all studied stages (from W12 to W18, Figure S4).

Dynamics of KCNQ1 in the developing human cochlear duct

To investigate the onset of expression and developmental distribution of ion channels and enzymes involved in cochlear K^+ transport and the generation of the endocochlear potential, we immunostained for the K^+ channel protein KCNQ1 [MIM 607542]. At W10.4 (Figure 5A) and W12.2 (Figure 5B), reactivity was observed at the basement membrane delineating the lateral wall epithelium. At W14, this pattern had changed to reactivity in the developing Reissner's membrane (arrowhead in Figure 5C) and the future outer sulcus (arrow in Figure 5C). From W16 (Figure 5D, 5F) to W18 (Figure 5H, 5I) increased KCNQ1 expression was observed at the

apical (luminal) membrane of the developing marginal cells in the stria vascularis, in addition to reactivity in Reissner's membrane (Figure 5E, 5H) and the future root cells of the outer sulcus (Figure 5G, 5J). However, a different anti-KCNQ1 antibody clone (Alomone) that also recognizes the C-terminus of KCNQ1 did not show any reactivity in Reissner's membrane or in the root cells of the outer sulcus. It did, however, show identical reactivity in the developing marginal cells at W16 and W18 (data not shown). Although we cannot explain this difference as both antibodies should recognize the same KCNQ1 transcript, expression of KCNQ1 in Reissner's membrane has been reported previously [33].

Dynamics of Na^+/K^+ ATPase in the developing cochlear duct

Already at W10.4, immunostaining for the alpha-1 subunit of Na^+/K^+-ATPase (ATP1A1, [MIM 182310]) was observed in different degrees throughout the entire epithelium of the cochlear duct, with a moderate intensity in the future stria vascularis (Figure 6A). However, at W12 ATP1A1 expression increased in the developing stria vascularis on the basolateral membranes of the developing marginal cells (Figure 6B). At W14 and W16, ATPA1 expression became even more prominent and was located in cells adjacent to the increasing numbers of invading melan-A+ melanocytes (Figure 6C-E). Immunostaining diminished in most parts of the epithelium, and at W18 ATP1A1 expression was found on the basolateral membranes of the marginal cells, on the basolateral membranes of the developing hair cells in the organ of Corti, as well as on both the apical and basolateral membranes of the Claudius' cells and the root cells in the outer sulcus (Figure 6F-H). Curiously, at this stage, pillar cells in the organ of Corti were also consistently found to stain positive for melan-A in the basal turn, although these are not of melanocytic origin (Figure 6G). Focusing on the stria vascularis, we found melan-A+ melanocyte processes penetrating between the marginal cells towards the lumen of the cochlear duct (Figure 6I, arrow). We also observed ATP1A1 expression around the melan-A+ melanocyte cell bodies (Figure 6I, arrowhead) and around melanocyte processes encircling the strial capillaries (Fig 6J, arrows).

KCNJ10 expression is confined to the outer sulcus at W18

From W16 onwards, we observed KCNJ10 in the future root cells cells of the outer sulcus (Figure 7). However, we did not observe KCNJ10 expression by strial melanocytes at any of the investigated stages (data not shown).

Distribution of GJB2, GJB6, GJA1 and GJE1 in the human fetal cochlea

To investigated the developmental expression of gap junction proteins we immunostained for GJB2 (CX26), GJB6 (CX30, [MIM 604418]), GJA1 (CX43 [MIM 121014]), all known to be expressed in the human cochlea [34 – 36], and GJE1 (CX23 [MIM unknown]), which expression pattern has not been investigated previously in the cochlea (see Discussion).

Throughout the investigated stages (W10.4-W18), the GJB2 and GJB6 expression patterns remained identical to each other (Figure 8). At W10, immunostaining for GJB2 and for GJB6 showed a diffuse and punctated pattern in both Kölliker's organ and the cells of the future outer sulcus (Figure 8A, B). By W12, expression of GJB2 and GJB6 had greatly increased and could clearly be observed on both sides of the developing organ of Corti (Figure 8C, D). In the subsequent weeks, up to W18, this pattern remained consistent as both in the Kölliker's organ and in the cells lining the outer sulcus (Claudius' cells and future root cells) expression of GJB2 and GJB6 was observed (Figure 8E-J). Although expression of both GJB2 and GJB6 has been reported in the spiral ligament fibrocytes in the adult human cochlea [35], no expression could be observed in these cells at least up to W18 (Figure 8J). We also did not detect expression in the organ of Corti itself.

Table 2 Spatiotemporal Expression Patterns of Investigated Proteins in the Developing Human Fetal Cochlea

Protein	Expression
SLC2A1 (GLUT1)	W12–W18: apical membrane of epithelial cells between organ of Corti and root cells in the outer sulcus (i.e. Hensen's cells, Claudius cells), capillaries, erythrocytes
ATP1A1	W10: throughout cochlear duct epithelium W12: increased expression in lateral wall epithelium W14–W18: basolateral membranes of marginal cells, basolateral membranes of inner and outer hair cells, basolateral membranes of epithelial cells in outer sulcus, Kölliker's organ.
KCNQ1 (KVLQT1)	W10–W12: basement membrane lateral wall epithelium W14: Reissner's membrane, developing root cells in outer sulcus W16–W18: apical membrane marginal cells, Reissner's membrane, developing root cells in outer sulcus
KCNJ10 ($K_{ir}4.1$)	W10–W14: no expression observed W16–W18: epithelial cells in outer sulcus, including root cells
GJB2 (CX26)	W10–W12: increased expression in epithelium of cochlear duct floor, with the exemption of the prosensory domain W14–W18: expression in Kölliker's organ and epithelial cells in outer sulcus
GJB6 (CX30)	Identical pattern to GJB2
GJA1 (CX43)	W10–W12: no expression observed W14–W18: increased expression in type I fibrocytes in the spiral ligament
GJE1 (CX23)	W10–W12: basolateral membranes of epithelial cells in lateral wall W14: basolateral membranes of marginal cells, melanocytes W16–W18: exclusive to melanocytes

Immunostaining for GJA1 showed weak expression by a significant subgroup of spiral ligament fibrocytes at W14 (Figure 9A). In the subsequent weeks, this expression became more prominent and at W18 could be clearly defined as belonging to the type I fibrocytes (Figure 9B, C).

Immunostaining for GJE1 revealed a dynamic pattern of expression during human cochlear development. At W10.4 and W12, strong expression of GJE1 was observed in the basolateral membranes of the future marginal cells (Figure 10A, B). Interestingly, at W14, expression was observed both in the lateral wall epithelium and in some of the cells in the adjacent periotic mesenchyme, presumably melanocytes (Figure 10C). At W16, expression of GJE1 was downregulated by the developing marginal cells and became exclusively limited to those adjacent cells (Figure 10D). Double immunostaining at W18 for GJE1 and ATP1A1 confirmed the melanocytic origin of the signal, as no overlap in GJE1 and ATP1A1 was observed (Figure 10E, F).

An overview of the observed spatiotemporal expression patterns of selected proteins in this study is presented in Table 2.

Discussion

Are human cochlear melanocytes derived from the neural crest?

The developmental pattern of melanocyte distribution observed in the human fetal cochlea closely follows that of the mouse, where it is generally accepted that cochlear melanocytes are derived from the neural crest [37 – 39]. Therefore, we suggest that the melanocytes in the human cochlea are also derived from the neural crest. However, in all species analysed so far, the migratory route taken by melanocytes to arrive in the cochlea remains unknown. As cochlear development in humans progresses slower than in mice (as a rule of thumb, 1 day of rodent cochlear development corresponds to 1 week in humans), this permits a more explicit visualization of developmental events. Recently, it has been reported that cranial melanocytes can arise from Schwann cell precursors migrating together with outgrowing nerves [40, 41]. As Schwann cell precursors arrive in the cochlea via the cochlear nerve [42], it is tempting to propose that melanocytes (precursors) may travel along the same path. However, our data on melanocyte migration towards their target location in the cochlea, which to our knowledge has not been shown before in such clarity, suggests that cochlear melanocytes in humans migrate through the periotic mesenchyme from the opposite side. In agreement, several studies in mice embryos show the presence of neural crest derivatives or melanocytes near this part of the otic vesicle around embryonic day 10.5 [37 – 39, 41, 42]. Therefore, although the peripheral glial cells in the cochlea originate from the migratory wave of neural crest cells from rhombomere 4, we now hypothesize that cochlear melanocytes originate from a different wave of neural crest cells, namely those delaminating from the region at rhombomere 6, at the location of the developing glossopharyngeal nerve (cranial nerve IX) and the third pharyngeal arch.

Cochlear melanocytes, a major player in syndromic SNHL

Intermediate cells in the stria vascularis were identified as melanocytes in 1977, although their exact function was unknown at that time [24]. The involvement of cochlear melanocytes in generating the endocochlear potential was recognized later in a studies with 'viable dominant spotting' mouse mutants, with a mutation in the *W* locus [43, 44]. Shortly hereafter, *Kit* was found to be the gene product of the *W* locus [45, 46], and it was shown to primarily affect the survival of migratory melanoblasts [47]. In humans, *KIT* mutations can result in the neurocristopathy (a

pathology affecting normal neural crest development) piebaldism [MIM 172800], a disorder characterized by areas of skin and hair devoid of melanocytes. Although most of these patients have a heterozygous mutation, deafness has been observed in rare cases of both heterozygous and homozygous mutations [48, 49]. We show that KIT is expressed by strial melanocytes in the human fetal cochlea, suggesting that SNHL due to *KIT* mutations in humans is caused by mechanisms similar to those in mouse *Kit* mutants.

Another neurocristopathy affecting melanocyte development with pigment abnormalities and SNHL is the genetically heterogeneous Waardenburg syndrome (WS), the most common type of autosomal dominant SNHL in humans. Its four subtypes are based on clinical symptoms and multiple causative genes have been identified [8]. We show here that in the human fetal cochlea, MITF expression is confined to melanocytes (Figure 3A, 3C). Therefore, it is likely that cochlear melanocytes are responsible for SNHL in WS with *MITF* mutations (causing type IIa WS [MIM 193510]), and/or *PAX3* mutations (a gene regulating *MITF*, causative for type I WS [MIM 193500] and type III WS [MIM 148820]). In addition to *MITF*, mutations in *SOX10* can also cause type II WS in next to type IVc WS [MIM 613266] [50, 51], whereas *SOX10* has recently also been identified to play a role in Kallmann syndrome with deafness (KS, [MIM 147950, 244200, 308700, 610628, 612370, and 612702]) [52]. SOX10 expression, however, is not exclusively limited to melanocytes in the human fetal cochlea (Figure 3B). We recently observed additional expression throughout the human fetal cochlear duct epithelium [29] and in all peripheral glial cells [31]. Although it is likely that melanocytes play a major role in SNHL in WS or KS due to *SOX10* mutations, it cannot be excluded that other SOX10+ cell types in the cochlea are involved as well. Taken together, the melanocytic expression of MITF, SOX10 and KIT in the human fetal cochlea help to explain the aforementioned hereditary hearing disorders and underscore the important role of this cochlear cell type in syndromic SNHL.

The endocochlear potential and its relation to hereditary SNHL

Hearing depends on the highly positive endocochlear potential, generated by the interplay of various ion channels and transporters in the cell types of the stria vascularis (reviewed in [25, 53]). The location of these proteins along the membranes of the different cells of the adult stria vascularis is depicted in Figure 1B. Disrupting the function of any of these proteins (including connexin proteins) in

the stria vascularis or at other locations in the cochlea where they are thought to be involved in K+ homeostasis results in immediate SNHL [54 – 56]. In many cases of both syndromic (as mentioned above) and nonsyndromic SNHL, the endocochlear potential is likely to be affected.

The marginal cells in the stria vascularis express the voltage-gated potassium channel KCNQ1 (or KCNE1, [MIM 176261]). Mutations in *KCNQ1* cause the autosomal recessive Jervell and Lange-Nielsen syndrome [MIM 220400], characterized by SNHL and cardiac abnormalities (long QT syndrome) [9, 57]. In this syndrome, there is an impaired K^+ secretion into the endolymph by the KCNQ1/KCNE1 channel complex on the apical membranes of the marginal cells in the stria vascularis, as confirmed in a mouse model with the homozygous mutants being completely deaf [58]. Since a low number of functional channels still result in normal hearing in heterozygous patients [59], it can be surmised that, to cause deafness, mutations in *KCNQ1* have to inactive the channel complex completely so that the total K^+-secretion is reduced to a minimum. On the basolateral membranes of the marginal cells, K^+ uptake from the intrastrial space (the narrow fluid-containing space between the marginal cells and the melanocytes) is mediated by the sodium-potassium pump Na^+/K^+-ATPase [60] and the $Na^+2Cl^-K^+$ cotransporter (NKCC). Na^+/K^+-ATPase is known to be expressed in the adult human stria vascularis [61] and inhibition of Na^+/K^+-ATPase directly suppresses the endocochlear potential in guinea pigs [55, 62]. We found first expression of KCNQ1 on the luminal membranes of the marginal cells at W16. At W18, we observed that the cell processes from the developing marginal cells (expressing ATP1A1) and the strial melanocytes intermingle and form an intricate network together with the capillaries. The developmental expression of KCNQ1 and ATP1A1 indicates that both K^+ uptake and secretion could be mediated by marginal cells as early as W16-W18.

The pivotal role of strial melanocytes in the generation of the endocochlear potential is to secrete K+ ions into the intrastrial space and hence they express the inward-rectifying potassium channel KCNJ10 (also known as Kir4.1, [MIM 602208]) [63, 64]. In contrast to the potassium channels of the marginal cells, we did not observe any KCNJ10 expression in strial melanocytes up to the last stage we investigated, W18. As inhibition of this receptor directly suppresses the endocochlear potential [55], it is likely that the endocochlear potential is not yet generated at this stage. KCNJ10 is implicated in multiple syndromic disorders with SNHL. Loss-of-function mutations in *KCNJ10* cause SESAME syndrome ([MIM 612780], also called EAST syndrome), a disorder characterized by SNHL, electrolyte imbalance,

seizures, ataxia and mental retardation. Here, the hearing loss is likely due to disrupted function of strial melanocytes [65]. KCNJ10 is also implicated in SNHL in autosomal recessive deafness-4 (DFNB4) with enlarged vestibular aqueduct (EVA) [MIM 600791], and in autosomal recessive Pendred syndrome [MIM 274600]. In Pendred syndrome, *SLC26A4* [MIM 605646] mutations account for the majority of cases [66]. The dysfunction of its protein, PENDRIN, results in loss of KCNJ10 expression in the melanocytes of the stria vascularis and subsequent loss of the endocochlear potential [67, 68]. However, mutations in *KCNJ10* itself have also been linked directly to Pendred syndrome [69]. Interestingly, KCNJ10 has also been described in the root cells of the outer sulcus, both in the adult rodent and human cochlea [64, 70]. Also, the expression pattern of KCNJ10 that we observed in the outer sulcus during cochlear development matches the known expression pattern of PENDRIN in the outer sulcus of the adult mouse cochlea [67, 71]. This provides a striking link between the two proteins and could help to explain the etiology of SNHL in Pendred syndrome.

Several connexins (Cx, gap junction proteins) are expressed at various locations in the cochlea and are thought to be implicated in K^+ recycling [25, 72]. Mutations in connexins are a major cause of hereditary SNHL [18]. The most frequent causative gene for nonsyndromatic SNHL is *GJB2* (CX26) [18]. Although less frequent, mutations in *GJB6* (CX30) [73, 74] and *GJA1* (CX43) [75, 76] have also been linked to SNHL. These gap junction proteins are thought to play a role in maintaining cochlear ion homeostasis and the endocochlear potential, as shown in *Gjb6*-deficient mice [56], by passively recycling K^+ ions back to the stria vascularis. The observed expression in the developing human cochlea is in support of this model. However, an interesting note can be made with regard to the observed glucose transporter (SLC2A1) expression on the luminal membranes of the outer sulcus cells. As this part of the cochlea does not have its own vascularization, one could speculate that receptor expression at this luminal location functions to take up glucose circulating in the endolymph, suggesting a rather more active role for these cells with regard to cochlear K^+ homeostasis (with a potential role for the Na^+/K^+-ATPase?).

Finally, GJE1 has not been previously investigated in the human cochlea. *GJE1* encodes the connexin 23 protein, and should not be confused with CX29/CX30.2, which used to be called *GJE1* but recently has been renamed to *GJC3* [MIM 611925]). In the developing human fetal cochlea, we observed dynamic GJE1 expression in the lateral wall, shifting from the developing marginal cells to the melanocytes between W14-W16. We speculate that GJE1 could be a suitable candidate gene for

non-syndromic SNHL, especially as a many causes of hereditary deafness remain presently unknown [77].

Maturation of the lateral wall and the onset of human hearing

In many rodent species, development of hearing extends beyond birth and the onset of hearing occurs after birth (in an altricial manner). In contrast, hearing development in humans progresses at a much slower rate, but the cochlea and hearing function are complete before birth (precocial hearing development). Although cochlear size and degree of spiralization differs between species, the morphological appearance of the various cochlear tissues and structures as well as the subsequent protein expression profiles are very similar. Therefore, based on similarities in morphology and protein expression patterns in adult mammalian cochleas, we conclude that the human fetal cochlea at W18 demonstrates a nearly adult phenotype, but that some essential elements for functionality are still missing. Most notably, strial melanocytes do not yet express KCNJ10, basal cells are immunohistochemically undefined, root cells have not developed their root-like basolateral processes, and GJB2 and GJB6 are not yet observed in the spiral ligament. This implies that the endocochlear potential cannot be generated at this stage and, therefore, that the human fetus at W18 is still unable to hear. Although W20 has been proposed by us [29, 31] and others [78 – 80] as the onset of human hearing based on the maturation of the organ of Corti and the cochlear nerve, it is more likely that hearing commences a few weeks later, which is in line with otoacoustic emission measurements [81] and auditory brainstem responses in preterm infants [82, 83].

In mice and gerbils, the appearance of the endocochlear potential has been observed just prior to their onset of hearing [43, 84], and coincides with morphological maturation of gap and tight junctions. Even although their auditory system does not become functional before birth, the sequence of morphological maturation is similar to what we observe in human fetuses. In view of these findings, extrapolation of our observations to later fetal stages suggests that the endocochlear potential, and therefore hearing, in the human fetus does not emerge before the third trimester of pregnancy.

Conclusion

We have investigated the complex embryonic development of the lateral wall in the human fetal cochlea with respect to the expression of several genes that are known to be involved both in syndromic and nonsyndromic SNHL, providing an etiological basis for these hearing disorders in humans. Although hereditary SNHL can be caused by specific mutations in various genes involved in cochlear K^+ transport, we would like to underline the major functional role of melanocytes in the cochlea and the generation of the endocochlear potential. We suggest that many cases of hereditary SNHL can be attributed to a disturbed development or migration of neural-crest-derived melanocytes.

Acknowledgments

We would like to thank J. Wiegant and A.M. van der Laan for technical support, S.B. Blankevoort (anatomical, medical illustrator of the LUMC) for his work on figure 1A, and the Center for Contraception, Sexuality and Abortion (CASA) in Leiden and The Hague for the collection of the human fetal material. Work in the lab of SCSL is supported by the Netherlands Organisation for Scientific Research (NWO, ASPASIA 015.007.037, www.nwo.nl/aspasia) and the Interuniversity Attraction Poles (IAP, P7/07). HL is supported by the Stichting Het Heinsius-Houbolt Fonds, the Netherlands.

Web Resources

Online Mendelian Inheritance in Man (OMIM), http://www.omim.org/

Hereditary Hearing Loss Homepage, http://hereditaryhearingloss.org/

GeneReviews: Deafness and Hereditary Hearing Loss Overview, http://www.ncbi.nlm.nih.gov/books/NBK1434/

References

1. **Fact Sheet No300** [www.who.int]
2. **NHSP: Annual Report NHS Newborn Hearing Screening Programme 2010-11.** 2011.
3. Van der Ploeg CPB, Uilenburg NN, Kauff man-de Boer MA, Oudesluys-Murphy AM, Verkerk PH: **Newborn hearing screening in youth health care in the Netherlands: National results of implementation and follow-up.** Int J Audiol 2012, 51:584 – 90.
4. Morton CC, Nance WE: **Newborn hearing screening--a silent revolution.** N Engl J Med 2006, 354:2151 – 64.
5. Pendred V: **Deaf-mutism and Goitre.** Lancet 1896, 148:532.
6. Bizhanova A, Kopp P: **Genetics and phenomics of Pendred syndrome.** Mol Cell Endocrinol 2010, 322:83 – 90.
7. Waardenburg PJ: **A new syndrome combining developmental anomalies of the eyelids, eyebrows and nose root with pigmentary defects of the iris and head hair and with congenital deafness.** Am J Hum Genet 1951, 3:195 – 253.
8. Pingault V, Ente D, Dastot-Le Moal F, Goossens M, Marlin S, Bondurand N: **Review and update of mutations causing Waardenburg syndrome.** Hum Mutat 2010, 31:391 – 406.
9. Jervell A, Lange-Nielsen F: **Congenital deaf-mutism, functional heart disease with prolongation of the Q-T interval and sudden death.** Am Heart J 1957, 54:59 – 68.
10. **Hereditary Hearing Loss Homepage** [http://hereditaryhearingloss.org]
11. Kelsell DP, Dunlop J, Stevens HP, Lench NJ, Liang JN, Parry G, Mueller RF, Leigh IM: **Connexin 26 mutations in hereditary non-syndromic sensorineural deafness.** Nature 1997, 387:80 – 3.
12. Denoyelle F, Weil D, Maw MA, Wilcox SA, Lench NJ, Allen-Powell DR, et al.: **Prelingual deafness: high prevalence of a 30delG mutation in the connexin 26 gene.** Hum Mol Genet 1997, 6:2173 – 7.
13. Linden Phillips L, Bitner-Glindzicz M, Lench N, Steel KP, Langford C, Dawson SJ, Davis A, Simpson S, Packer C: **The future role of genetic screening to detect newborns at risk of childhood-onset hearing loss.** Int J Audiol 2013, 52:124 – 33.
14. Hilgert N, Smith RJH, Van Camp G: **Forty-six genes causing nonsyndromic hearing impairment: which ones should be analyzed in DNA diagnostics?** Mutat Res 2009, 681:189 – 96.
15. Angeli S, Lin X, Liu XZ: **Genetics of hearing and deafness.** Anat Rec (Hoboken) 2012, 295:1812 – 29.
16. Hilgert N, Smith RJH, Van Camp G: **Function and expression pattern of nonsyndromic deafness genes.** Curr Mol Med 2009, 9:546 – 64.

17. Shearer EA, Smith RJH: **Genetics: advances in genetic testing for deafness.** Curr Opin Pediatr 2012, 24:679 – 86.
18. **Deafness and Hereditary Hearing Loss Overview** [http://www.ncbi.nlm.nih.gov/books/NBK1434/]
19. Stelma F, Bhutta MF: **Non-syndromic hereditary sensorineural hearing loss: review of the genes involved.** J Laryngol Otol 2014, 128:13 – 21.
20. Hudspeth AJ: **How the ear's works work.** Nature 1989, 341:397 – 404.
21. Smith CA, Lowry OH, Wu ML: **The electrolytes of the labyrinthine fluids.** Laryngoscope 1954, 64:141 – 53.
22. Patuzzi R: **Ion flow in stria vascularis and the production and regulation of cochlear endolymph and the endolymphatic potential.** Hear Res 2011, 277:4 – 19.
23. Kimura RS, Schuknecht HF: **The ultrastructure of the human stria vascularis.** I. Acta Otolaryngol 1970, 69:415 – 27.
24. Hilding DA, Ginzberg RD: **Pigmentation of the stria vascularis. The contribution of neural crest melanocytes.** Acta Otolaryngol 1977, 84:24 – 37.
25. Zdebik AA, Wangemann P, Jentsch TJ: **Potassium ion movement in the inner ear: insights from genetic disease and mouse models.** Physiology (Bethesda) 2009, 24:307 – 16.
26. Adachi N, Yoshida T, Nin F, Ogata G, Yamaguchi S, Suzuki T, Komune S, Hisa Y, Hibino H, Kurachi Y: **The mechanism underlying maintenance of the endocochlear potential by the K+ transport system in fibrocytes of the inner ear.** J Physiol 2013, 591(Pt 18):4459 – 72.
27. Lavigne-Rebillard M, Bagger-Sjöbäck D: **Development of the human stria vascularis.** Hear Res 1992, 64:39 – 51.
28. Bibas A, Liang J, Michaels L, Wright A: **The development of the stria vascularis in the human foetus.** Clin Otolaryngol Allied Sci 2000, 25:126 – 9.
29. Locher H, Frijns JHM, van Iperen L, de Groot JCMJ, Huisman MA, Chuva de Sousa Lopes SM: **Neurosensory development and cell fate determination in the human cochlea.** Neural Dev 2013, 8:20.
30. Schindelin J, Arganda-Carreras I, Frise E, Kaynig V, Longair M, Pietzsch T, Preibisch S, Rueden C et al.: **Fiji: an open-source platform for biological-image analysis.** Nat Methods 2012, 9:676 – 82.
31. Locher H, de Groot JCMJ, van Iperen L, Huisman MA, Frijns JHM, Chuva de Sousa Lopes SM: **Distribution and development of peripheral glial cells in the human fetal cochlea.** PLoS One 2014, 9:e88066.
32. Ito M, Spicer SS, Schulte BA: **Immunohistochemical localization of brain type glucose transporter in mammalian inner ears: comparison of developmental and adult stages.** Hear Res 1993, 71:230 – 8.
33. Kim SH, Kim KX, Raveendran NN, Wu T, Pondugula SR, Marcus DC: **Regulation of ENaC-mediated sodium transport by glucocorticoids in Reissner's membrane**

epithelium. Am J Physiol Cell Physiol 2009, 296:C544 – 57.

34. Kammen-Jolly K, Ichiki H, Scholtz AW, Gsenger M, Kreczy A, Schrott-Fischer A: **Connexin 26 in human fetal development of the inner ear.** Hear Res 2001, 160:15 – 21.
35. Liu W, Boström M, Kinnefors A, Rask-Andersen H: **Unique expression of connexins in the human cochlea.** Hear Res 2009, 250:55 – 62.
36. Liu W, Glueckert R, Linthicum FH, Rieger G, Blumer M, Bitsche M, Pechriggl E, Rask-Andersen H, Schrott-Fischer A: **Possible role of gap junction intercellular channels and connexin 43 in satellite glial cells (SGCs) for preservation of human spiral ganglion neurons : A comparative study with clinical implications.** Cell Tissue Res 2013.
37. Wakaoka T, Motohashi T, Hayashi H, Kuze B, Aoki M, Mizuta K, Kunisada T, Ito Y: **Tracing Sox10-expressing cells elucidates the dynamic development of the mouse inner ear.** Hear Res 2013, 302(May):17 – 25.
38. Steel KP, Davidson DR, Jackson IJ: **TRP-2/DT, a new early melanoblast marker, shows that steel growth factor (c-kit ligand) is a survival factor.** Development 1992, 115:1111 – 9.
39. Freyer L, Aggarwal V, Morrow BE: **Dual embryonic origin of the mammalian otic vesicle forming the inner ear.** Development 2011, 138:5403 – 14.
40. Adameyko I, Lallemend F, Aquino JB, Pereira JA, Topilko P, Müller T, Fritz N, Beljajeva A, et al.: **Schwann cell precursors from nerve innervation are a cellular origin of melanocytes in skin.** Cell 2009, 139:366 – 79.
41. Adameyko I, Lallemend F, Furlan A, Zinin N, Aranda S, Kitambi SS, et al.: **Sox2 and Mitf cross-regulatory interactions consolidate progenitor and melanocyte lineages in the cranial neural crest.** Development 2012, 139:397 – 410.
42. Sandell LL, Butler Tjaden NE, Barlow AJ, Trainor PA: **Cochleovestibular nerve development is integrated with migratory neural crest cells.** Dev Biol 2014, 385:200 – 10.
43. Steel KP, Barkway C: **Another role for melanocytes: their importance for normal stria vascularis development in the mammalian inner ear.** Development 1989, 107:453 – 63.
44. Steel KP, Barkway C, Bock GR: **Strial dysfunction in mice with cochleo-saccular abnormalities.** Hear Res 1987, 27:11 – 26.
45. Chabot B, Stephenson DA, Chapman VM, Besmer P, Bernstein A: **The proto-oncogene c-kit encoding a transmembrane tyrosine kinase receptor maps to the mouse W locus.** Nature 1988, 335:88 – 9.
46. Geissler EN, Ryan MA, Housman DE: **The dominant-white spotting (W) locus of the mouse encodes the c-kit proto-oncogene.** Cell 1988, 55:185 – 92.
47. Cable J, Jackson IJ, Steel KP: **Mutations at the W locus affect survival of neural crest-derived melanocytes in the mouse.** Mech Dev 1995, 50:139 – 50.

48. Kilsby AJ, Cruwys M, Kukendrajah C, Russell-Eggitt I, Raglan E, Rajput K, Loshe P, Brady AF: **Homozygosity for piebaldism with a proven KIT mutation resulting in depigmentation of the skin and hair, deafness, developmental delay and autism spectrum disorder.** Clin Dysmorphol 2013, 22:64 – 7.
49. Spritz RA, Beighton P: **Piebaldism with deafness: molecular evidence for an expanded syndrome.** Am J Med Genet 1998, 75:101 – 3.
50. Bondurand N, Dastot-Le Moal F, Stanchina L, Collot N, Baral V et al.: **Deletions at the SOX10 gene locus cause Waardenburg syndrome types 2 and 4.** Am J Hum Genet 2007, 81:1169 – 85.
51. Baral V, Chaoui A, Watanabe Y, Goossens M, Attie-Bitach T, Marlin S, Pingault V, Bondurand N: **Screening of MITF and SOX10 regulatory regions in Waardenburg syndrome type 2.** PLoS One 2012, 7:e41927.
52. Pingault V, Bodereau V, Baral V, Marcos S, Watanabe Y, Chaoui A, Fouveaut C, Leroy C, et al.: **Loss-of-Function Mutations in SOX10 Cause Kallmann Syndrome with Deafness.** Am J Hum Genet 2013, 92:707 – 24.
53. Hibino H, Nin F, Tsuzuki C, Kurachi Y: **How is the highly positive endocochlear potential formed? The specific architecture of the stria vascularis and the roles of the ion-transport apparatus.** Pflugers Arch 2010, 459:521 – 33.
54. Cohen-Salmon M, Ott T, Michel V, Hardelin JP, Perfettini I, Eybalin M, Wu T, Marcus DC, Wangemann P, Willecke K, Petit C: **Targeted ablation of connexin26 in the inner ear epithelial gap junction network causes hearing impairment and cell death.** Curr Biol 2002, 12:1106 – 11.
55. Nin F, Hibino H, Doi K, Suzuki T, Hisa Y, Kurachi Y: **The endocochlear potential depends on two K+ diff usion potentials and an electrical barrier in the stria vascularis of the inner ear.** Proc Natl Acad Sci U S A 2008, 105:1751 – 6.
56. Teubner B, Michel V, Pesch J, Lautermann J, Cohen-Salmon M, Söhl G, Jahnke K, Winterhager E, Herberhold C, Hardelin J, Petit C, Willecke K: **Connexin30 (Gjb6)-deficiency causes severe hearing impairment and lack of endocochlear potential.** Hum Mol Genet 2003, 12:13 – 21.
57. Neyroud N, Tesson F, Denjoy I, Leibovici M, Donger C, Barhanin J, Fauré S, Gary F, Coumel P, Petit C, Schwartz K, Guicheney P: **A novel mutation in the potassium channel gene KVLQT1 causes the Jervell and Lange-Nielsen cardioauditory syndrome.** Nat Genet 1997, 15:186 – 9.
58. Lee MP, Ravenel JD, Hu RJ, Lustig LR, Tomaselli G, Berger RD, et al.: **Targeted disruption of the Kvlqt1 gene causes deafness and gastric hyperplasia in mice.** J Clin Invest 2000, 106:1447 – 55.
59. Wollnik B, Schroeder BC, Kubisch C, Esperer HD, Wieacker P, Jentsch TJ: **Pathophysiological mechanisms of dominant and recessive KVLQT1 K+ channel mutations found in inherited cardiac arrhythmias.** Hum Mol Genet 1997, 6:1943 – 9.

60. Schulte BA, Adams JC: **Distribution of immunoreactive Na+,K+-ATPase in gerbil cochlea.** J Histochem Cytochem 1989, 37:127 – 34.
61. Weber PC, Cunningham CD, Schulte BA: **Potassium recycling pathways in the human cochlea.** Laryngoscope 2001, 111:1156 – 65.
62. Kuijpers W, Bonting SL: **The cochlear potentials. I. The effect of ouabain on the cochlear potentials of the guinea pig.** Pflugers Arch 1970, 320:348 – 58.
63. Ando M, Takeuchi S: **Immunological identification of an inward rectifier K+ channel (Kir4.1) in the intermediate cell (melanocyte) of the cochlear stria vascularis of gerbils and rats.** Cell Tissue Res 1999, 298:179 – 83.
64. Eckhard A, Gleiser C, Rask-Andersen H, Arnold H, Liu W, Mack A, Müller M, Löwenheim H, Hirt B: **Co-localisation of K(ir)4.1 and AQP4 in rat and human cochleae reveals a gap in water channel expression at the transduction sites of endocochlear K(+) recycling routes.** Cell Tissue Res 2012, 350:27 – 43.
65. Scholl UI, Choi M, Liu T, Ramaekers VT, Häusler MG, Grimmer J, Tobe SW, Farhi A, Nelson-Williams C, Lifton RP: **Seizures, sensorineural deafness, ataxia, mental retardation, and electrolyte imbalance (SeSAME syndrome) caused by mutations in KCNJ10.** Proc Natl Acad Sci U S A 2009, 106:5842 – 7.
66. Everett LA, Glaser B, Beck JC, Idol JR, Buchs A, Heyman M, Adawi F, Hazani E, Nassir E, Baxevanis AD, Sheffield VC, Green ED: **Pendred syndrome is caused by mutations in a putative sulphate transporter gene (PDS).** Nat Genet 1997, 17:411 – 22.
67. Wangemann P, Itza EM, Albrecht B, Wu T, Jabba S V, Maganti RJ, Lee JH, Everett LA, Wall SM, Royaux IE, Green ED, Marcus DC: **Loss of KCNJ10 protein expression abolishes endocochlear potential and causes deafness in Pendred syndrome mouse model.** BMC Med 2004, 2:30.
68. Ito T, Li X, Kurima K, Choi BY, Wangemann P, Griffith AJ: **Slc26a4-insufficiency causes fluctuating hearing loss and stria vascularis dysfunction.** Neurobiol Dis 2014, 66:53 – 65.
69. Yang T, Gurrola JG, Wu H, Chiu SM, Wangemann P, Snyder PM, Smith RJH: **Mutations of KCNJ10 together with mutations of SLC26A4 cause digenic nonsyndromic hearing loss associated with enlarged vestibular aqueduct syndrome.** Am J Hum Genet 2009, 84:651 – 7.
70. Jagger DJ, Nevill G, Forge A: **The Membrane Properties of Cochlear Root Cells are Consistent with Roles in Potassium Recirculation and Spatial Buffering.** J Assoc Res Otolaryngol 2010, 448:435 – 448.
71. Royaux IE, Belyantseva IA, Wu T, Kachar B, Everett LA, Marcus DC, Green ED: **Localization and Functional Studies of Pendrin in the Mouse Inner Ear Provide Insight About the Etiology of Deafness in Pendred Syndrome.** JARO - J Assoc Res Otolaryngol 2003, 4:394 – 404.
72. Kelly JJ, Forge A, Jagger DJ: **Development of gap junctional intercellular**

communication within the lateral wall of the rat cochlea. Neuroscience 2011, 180:360 – 9.

73. Del Castillo I, Villamar M, Moreno-Pelayo MA, del Castillo FJ, Alvarez A, Tellería D, Menéndez I, Moreno F: **A deletion involving the connexin 30 gene in nonsyndromic hearing impairment.** N Engl J Med 2002, 346:243 – 9.
74. Grifa A, Wagner CA, D'Ambrosio L, Melchionda S, Bernardi F, Lopez-Bigas N, Rabionet R, Arbones M, Monica MD, Estivill X, Zelante L, Lang F, Gasparini P: **Mutations in GJB6 cause nonsyndromic autosomal dominant deafness at DFNA3 locus.** Nat Genet 1999, 23:16 – 8.
75. Liu XZ, Xia XJ, Adams J, Chen ZY, Welch KO, Tekin M, Ouyang XM, Kristiansen A, Pandya A, Balkany T, Arnos KS, Nance WE: **Mutations in GJA1 (connexin 43) are associated with non-syndromic autosomal recessive deafness.** Hum Mol Genet 2001, 10:2945 – 51.
76. Hong H-M, Yang J-J, Shieh J-C, Lin M-L, Li M-L, Li S-Y: **Novel mutations in the connexin43 (GJA1) and GJA1 pseudogene may contribute to nonsyndromic hearing loss.** Hum Genet 2010, 127:545 – 51.
77. Korver AMH, Admiraal RJC, Kant SG, Dekker FW, Wever CC, Kunst HPM, Frijns JHM, Oudesluys-Murphy AM: **Causes of permanent childhood hearing impairment.** Laryngoscope 2011, 121:409 – 16.
78. Bibas AG, Xenellis J, Michaels L, Anagnostopoulou S, Ferekidis E, Wright A: **Temporal bone study of development of the organ of Corti: correlation between auditory function and anatomical structure.** J Laryngol Otol 2008, 122:336 – 42.
79. Pujol R, Lavigne-Rebillard M: **Sensory and neural structures in the developing human cochlea.** Int J Pediatr Otorhinolaryngol 1995, 32:S177 – S182.
80. Pujol R, Lavigne-Rebillard M, Uziel A: **Development of the human cochlea.** Acta Otolaryngol Suppl 1991, 482:7 – 12; discussion 13.
81. Chabert R, Guitton MJ, Amram D, Uziel A, Pujol R, Lallemant J-G, Puel J-L: **Early maturation of evoked otoacoustic emissions and medial olivocochlear reflex in preterm neonates.** Pediatr Res 2006, 59:305 – 8.
82. Van Straaten HL, Tibosch CH, Dorrepaal C, Dekker FW, Kok JH: **Efficacy of automated auditory brainstem response hearing screening in very preterm newborns.** J Pediatr 2001, 138:674 – 8.
83. Lary S, Briassoulis G, de Vries L, Dubowitz LM, Dubowitz V: **Hearing threshold in preterm and term infants by auditory brainstem response.** J Pediatr 1985, 107:593 – 9.
84. Souter M, Forge A: **Intercellular junctional maturation in the stria vascularis: possible association with onset and rise of endocochlear potential.** Hear Res 1998, 119:81 – 95.

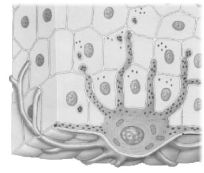
Supplemental Material and Methods

Immunohistochemistry

An additional primary antibody used in the supplementary data is mouse anti-TUBB3 (1:500, 2G10, Ab78078, Abcam).

Image acquisition, processing and reconstruction

Image restoration (deconvolution) was applied to scans shown in Figure S3. These maximal projections were obtained from images stacks acquired at sampling density according to the Nyquist rate. Deconvolution was performed using Huygens Professional version 4.3.1 software (Scientific Volume Imaging). Three-dimensional (3D) reconstructions were made from deconvoluted image stacks using AMIRA 5.3.3 (Visage Imaging), and interactive PDF files were created using Adobe Acrobat Pro Extended version 9.5.5. (Adobe Systems). For clarity, erythrocytes present in the scala vestibuli and scala tympani were manually masked with black pixels in Figure S4F. To generate the image in Figure S1A, ten consecutive tissue sections were scanned and their subsequent maximum projections were overlain manually.



5

TUBB3:
Neuronal marker or melanocyte mimic?

Locher
Frijns
Huisman
Chuva de Sousa Lopes

Cell Transplantation, 2014

Dear editor:

Identifying neuronal derivatives of stem cells is essential for both basic research and future applications in regenerative medicine targeting neurodegenerative diseases. Erroneous identification could result in the transplantation of inappropriate cell types, thus directly affecting clinical outcome.

Stem cell and neurobiology researchers widely regard the class III β-tubulin protein (TUBB3), a member of the microtubule family, as being selectively expressed in neuronal cells. Antibodies against this protein are therefore often used to identify cells of the neuronal lineage or to quantify neuronal cells within cell cultures. The most renowned anti-TUBB3 antibody is the monoclonal TUJ1, with other examples including clones TU-20 and 2G10.

Nevertheless, we propose reconsidering the use of TUBB3 as a marker for neurons when melanocytes are potentially present or being formed. Why? Research in our own lab indicated that melanocytes were formed in studies on neuronal differentiation. Intrigued, we investigated and detected high TUBB3 expression during melanocyte differentiation *in vitro* and *in vivo* [1] in both human foetal and adult melanocytes (see Figure 1A for an example in the human skin). In agreement, two other articles [2, 3] have described the expression of TUBB3 in chick and mouse melanoblasts, indicating that TUBB3 expression is clearly not restricted to neurons and should therefore not be regarded as a standard for neuronal identification, but rather as a broader marker of the neural lineage (both neural crest and neural tube derivatives).

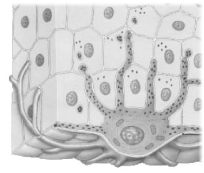
Furthermore, double-labelling combinations of microtubule-associated protein 2 (MAP2) and TUBB3 (used to identify cells as *"neurons"*) or tyrosine hydroxylase (TH) and TUBB3 (used to identify cells as *"dopaminergic neurons"*) are not fail-safe as melanocytes can express both MAP2 and TH. Melanocytes can also express nestin (considered to be a neural stem cell marker although its presence in endothelial cells has also been reported), which together with TUBB3 is often used to identify *"neuronal precursor cells"* (Figure 1B and 1C). Thus, using these combinations of markers may result in cells being incorrectly identified as neurons. The same is true for neurotrophins (NGF, BDNF, NT3 or NT4) and neurotrophic receptors (Trks and NGFR (p75NTR)) [4]. Even functional ion channels (sodium, potassium or calcium) of various types have been identified in the melanocyte [5].

Melanocytes and neurons are both derived from the neural plate (more specifically, all neurons from the peripheral nervous system and melanocytes are derived from the neural crest), share morphological features (e.g. an extensive dendritic tree) and to a large extent express the same biomarkers. If melanocytes are potentially present in the experimental system of interest, another method of identification should be sought. One option is to rule out melanocytes, for example by taking advantage of markers present in melanocytes but not in mature neurons such as melan-A or sex-determining region Y box 9 (SOX9) (Figure 1D). The other option is to irrefutably demonstrate successful derivation of neurons by their true neuronal hallmark: the action potential.

Or is it?

References

1. Locher H, de Rooij KE, de Groot JCMJ, Doorn R Van, Gruis N a, Löwik CWGM, Chuva de Sousa Lopes SM, Frijns JHM, Huisman MA: **Class III β-tubulin, a novel biomarker in the human melanocyte lineage.** Diff erentiation 2013, 85:173 – 181.
2. Adameyko I, Lallemend F, Aquino JB, Pereira JA, Topilko P, Müller T, Fritz N, Beljajeva A, Mochii M, Liste I, Usoskin D, Suter U, Birchmeier C, Ernfors P: **Schwann cell precursors from nerve innervation are a cellular origin of melanocytes in skin.** Cell 2009, 139:366 – 79.
3. Adameyko I, Lallemend F, Furlan A, Zinin N, Aranda S, Kitambi SS, Blanchart A, Favaro R, Nicolis S, Lübke M, Müller T, Birchmeier C, Suter U, Zaitoun I, Takahashi Y, Ernfors P: **Sox2 and Mitf cross-regulatory interactions consolidate progenitor and melanocyte lineages in the cranial neural crest.** Development 2012, 139:397 – 410.
4. Yaar M, Park H-Y: **Melanocytes: a window into the nervous system.** J Invest Dermatol 2012, 132(3 Pt 2):835 – 45.
5. Plonka PM, Passeron T, Brenner M, Tobin DJ, Shibahara S, Thomas A, Slominski A, Kadekaro AL, Hershkovitz D, Peters E, Nordlund JJ, Abdel-Malek Z, Takeda K, Paus R, Ortonne JP, Hearing VJ, Schallreuter KU: **What are melanocytes really doing all day long...?** Exp Dermatol 2009, 18:799 – 819.



6

Class III β-tubulin, a novel biomarker in the human melanocyte lineage

Locher
de Rooij
de Groot
van Doorn
Gruis
Löwik
Chuva de Sousa Lopes

Diff erentiation, 2013

Abstract

It is generally thought that class III β-tubulin expression is limited to cells of the neural lineage and is therefore often used to identify neurons amongst other cell types, both *in vivo* and *in vitro*. Melanocytes are derived from the neural crest and share both morphological features and functional characteristics with peripheral neurons. Here, we show that these similarities extend to class III β-tubulin (TUBB3) expression, and that human melanocytes express this protein both *in vivo* and *in vitro*. In addition, we studied the expression of class III β-tubulin in two murine melanogenic cell lines and show that expression of this protein starts as melanoblasts mature into melanocytes. Melanin bleaching experiments revealed close proximity between melanin and TUBB3 proteins. *In vitro* stimulation of primary human melanocytes by α-MSH indicated separate regulatory mechanisms for melanogenesis and to TUBB3 expression. Together, these observations imply that human melanocytes express TUBB3 and that this protein should be recognized as a wider marker for multiple neural crest-derived cells.

Introduction

Over the last several years, there has been a notable increase in interest in the culture of skin and skin stem cells, in part for the generation of skin substitutes, in part with view to understanding cutaneous pathologies. It is of great importance to be able to identify the different skin cell subtypes accurately in culture in order to fully understand their biology. A widely used biomarker in this context is class III β-tubulin (TUBB3), which is generally thought to be expressed only in cells of the neural lineage.

Microtubules are one of the main classes of cytoskeletal filaments involved in cellular morphology, motility, division and intracellular transport. They are composed of assemblies of heterodimers one α- and one β-tubulin subunit [1, 2]. There are multiple β-tubulin isotypes and their expression is tissue-specific and depends on the developmental stage [3]. Isotype TUBB3 was first described in avian and mammalian species [4]. Antibodies directed against TUBB3 epitopes distinguished between neurons and glial cells [5, 6], so that it became a standard biomarker for neuronal identification. TUBB3 expression is often used to identify neuronal cells in skin-derived and (epidermal) stem cell cultures. *In vivo* it is used to trace the dendritic processes of neurons in the dermis and epidermis, of which the cell bodies are located elsewhere.

TUBB3 is not exclusively neuron-specific. It is, albeit weakly, expressed in testicular and a few other tissue types [3, 7]. Recently, it was shown to be present in cultures of mesenchymal and epithelial cells [8]. A variety of solid tumors such as ovarian tumors, lung tumors and malignant melanomas also express TUBB3 and it has been suggested that this tubulin isotype is associated with cellular drug resistance [9]. Tubb3 has also been found expressed in developing melanoblasts in mouse and chicken embryo's [10, 11]. Interestingly, in a recent study positive immunoreactivity for the TUBB3 protein was reported in cells in the basal layer of normal human adult epidermis [12]. Although it is suggestive that these cells could be melanocytes, no confirmation has been provided. This is of importance as an identical epidermal immunostaining pattern can be found in a study on human epidermal innervation [13]. A potential TUBB3 expression by melanocytes could therefore mislead neuronal cell identification when using antibodies directed against TUBB3.

In the present study, we have resolved this issue by showing that TUBB3 is expressed in human epidermal and hair follicle melanocytes, both *in vivo* and *in vitro*, and

therefore have identified TUBB3 as a novel marker of melanocytes. In addition, we have explored its relation to melanocyte differentiation and melanogenesis. Because melanocytes do express TUBB3, this has major implications in interpreting results of cultured skin and skin stem cells, as well as in studies on skin innervation.

Materials and Methods

Tissue samples

Human adult retroauricular tissue was obtained during surgery on a 70-year-old female patient. Fetal scalp skin was collected from tissue of 20 weeks gestational age obtained by elective abortion. Both cases were approved by the Medical Ethical Committee of the Leiden University Medical Center (fetal tissue: P08.087) and informed consent was obtained in accordance with the Declaration of Helsinki guidelines. Skin specimens were fixed in 4% formaldehyde in PBS overnight at 4 ^{0}C followed by ethanol dehydration and embedding in paraffin wax using standard procedures.

Cell culture

Fetal scalp skin was mechanically dissociated and cultured for seven days in RPMI 1640 (Life Technologies, Carlsbad, CA, USA) containing 10% fetal bovine serum (FBS) GOLD (PAA Laboratories GmbH, Pasching, Austria), 200 nM 12-O-tetradecanoylphorbol 13-acetate (TPA, Sigma-Aldrich, Saint Louis, MO, USA), 200 pM cholera toxin (CT, Sigma-Aldrich), 10 ng/ml stem cell factor (SCF, R&D Systems, Inc., MN, USA), GlutaMAX (Life Technologies) and antibiotic antimycotic solution (Sigma-Aldrich). Cultures were maintained in a humidified incubator with 5% CO_2 at 37 ^{0}C. Medium was changed every third day.

Melb-a cells were cultured in RPMI with 10% FBS, 20 ng/ml SCF, 10 ng/ml bFGF (R&D Systems, Inc.), GlutaMAX and antibiotic antimycotic solution. Melan-Ink4a2 cells were cultured in RPMI containing 10% FBS, 200 nM TPA, 200 pM CT, 10 ng/ml SCF, GlutaMAX and antibiotic antimycotic solution. Both cell lines were maintained in a humidified incubator with 10% CO2 at 37 ^{0}C. Medium was changed every other day, and cells were passaged using TrypLE Express (Life Technologies) upon reaching 90% confluency.

Primary normal human melanocytes were cultured in Ham's F10 supplemented with 100 U/ml penicillin, 100 U/ml streptomycin and 292 µg/ml L-glutamine (Invitrogen, Breda, the Netherlands), 1% Ultroser G (Biosepra, Fremont, CA, USA), 5 ng/ml endothelin-1 (Sigma-Aldrich), 5 ng/ml basic-FGF (Sigma-Aldrich), 30 µg/ml CT, 33 µM IBMX (Sigma-Aldrich) and 8 nM TPA. Melanocytes were cultured in a humidified incubator with 7.5% CO_2 at 37 ^{0}C. Medium was changed every

other day, and cells were passaged using 0.01% Trypsin (Life Technologies) upon reaching 90% confluency. Melanocytes were stimulated with 109 U alpha-MSH (Sigma-Aldrich) for 6, 24 and 48 hours.

Immunochemistry and image processing

Paraffin sections (5 μm) of skin specimen were deparaffinized in xylene, rehydrated in a descending ethanol series (100%, 90%, 80%, 70%), and rinsed in distilled water. Antigen unmasking was performed in 0.01M sodium citrate buffer (pH 6.0) for 12 minutes at 97 ^{0}C using a microwave oven. Sections were blocked with 1% bovine serum albumin (BSA, Sigma-Aldrich) in PBS containing 0.05% Tween-20 (Promega, Madison, WI) for 30 minutes, and incubated with primary antibodies (appropriately diluted in BSA/Tween-20/PBS) overnight at room temperature in a humidified chamber. Secondary antibodies were diluted in 1% normal goat serum (NGS, DAKO, Glostrup, Denmark) in Tween-20/PBS, and sections were incubated for 1 hour at room temperature. Nuclei were stained with 4',6-diamidino-2-phenylindole (DAPI) and sections were mounted in ProLong Gold (Molecular Probes, Life Technologies). Cultures were fixed in 1% formaldehyde in PBS overnight at 4 ^{0}C and, when necessary, stored in PBS. Bleaching was performed in 2% potassium permanganate solution for 30 minutes followed by 0.5% oxalic acid solution for 10 minutes. Cells were permeabilized with ice-cold methanol for 10 minutes, blocked in 5% NGS and 0.05% Tween-20 in PBS, and incubated with primary antibodies (appropriately diluted in NGS/Tween-20/PBS) overnight at 4 ^{0}C. Next, the cells were incubated with fluorochrome-conjugated secondary antibodies (diluted in NGS/Tween-20/PBS) for 1 hour at room temperature and followed by nuclear staining with DAPI added to Vectashield mounting medium (Vector Laboratories, Burlingame, CA). Primary and secondary antibodies, and their dilutions, are listed in Table S1. In all double stainings with melanocytic markers, monoclonal anti-TUBB3 2G10 was used. Due to technical limitations, DCT was used to identify the pigmented melanocytes in deparaffinized sections whereas TYRP1 was used to identify these cells in culture. These enzymes catalyze subsequent steps in melanin biosysthesis. Human dermal fibroblast cultures (HDF-a, ScienCell, Carlsbad, CA, USA) were used as a negative tissue control whereas in specificity controls the primary antibody was omitted. Brightfield, phase contrast and fluorescent images were taken with either a DM5500 microscope and camera (Leica Microsystems, Rijswijk, the Netherlands) or an Olympus IX70 microscope (Olympus, Zoeterwoude, the Netherlands) equipped with a Leica DFC340 FX camera (Leica) using LAS

AF software (Leica). Brightness and contrast adjustments and cell counting was performed using ImageJ 1.45s (National Institutes of Health, http://imagej.nih.gov/ij).

Western blot analysis

For Western blotting, p34 melb-a and p19 melan-Ink4a2 cells were lysed in ice cold lysis buffer (50 mM Tris-HCl (pH 7.5), 100mM NaCl, 0.2% Tween-20, supplemented with 1 mini protease inhibitor cocktail tablet (Roche, Basel, Switzerland) per 10 ml). Human melanocytes were harvested for Western analysis in lysis buffer M-per (Thermo Scientific, Rockford, IL), supplemented with 1 tablet PhosSTOP and 1 tablet protease inhibitor (Roche) per 10 ml. Protein concentration was determined using a Pierce BCA Protein assay kit (Thermo Scientific). Equal amounts of protein were loaded on a 10% SDS-PAGE gel, separated for 90 minutes at 100 V and blotted onto polyvinylidene difluoride membranes (Immobilon-P, Millipore, Bedford, MA) for 90 minutes at 300 mA. Membranes were blocked with 3% non-fat dry milk (Elk skimmed instant milk powder; FrieslandCampina, the Netherlands) in TBS containing 0.01% Tween-20 (TBST, pH 7.5) for 1 hour at room temperature followed by incubation with the primary antibodies TUJ1 (1:2000, Covance, Princeton, NJ), 2G10 (1:400, Abcam, Cambridge, UK) and DCT (1:1000, Abcam) overnight at 4 ^{0}C. GAPDH (1:2000, Santa Cruz Biotechnology Inc, Santa Cruz, CA) and β-actin (1:5000, Sigma-Aldrich, St. Louis, MO) were used as loading controls. Subsequently, the membranes were inubated with horseradish peroxidase-conjugated secondary antibodies (Promega) for 1 hour at room temperature in TBST. Protein was detected with SuperSignal West Pico Chemiluminescent Substrate (Thermo Scientific) using a Gel Doc XR System (Bio-Rad, Hercules, CA). Quantity One 1-D Analysis software (Bio-Rad) was used to determine band intensity for analysis of protein expression levels in the human melanocytes.

qRT-PCR Analysis

RNA from p34 melb-a and p19 melan-Ink4a2 cell cultures was isolated using RNA-Bee (Tel-Test Inc., Friendswood, TX) according to the manufacturer's instructions. Primers against *Mitf*, *Dct* and *Tubb3* were designed with Primer-BLAST (http://www.ncbi.nlm.nih.gov/tools/primer-blast). A complete list of the primers used can be found in Table S2. cDNA was generated by incubating 1 μg RNA with 500 ng Random Hexamers (Promega), supplemented with H2O to 10 μl, for 10 minutes

at 70 ^{0}C. Per sample, 100 units M-MLV reverse transcriptase, 1.25 µl 10 mM dNTP mix, 20 units RNAsin ribonuclease inhibitor and 1x buffer (all from Promega) were mixed, incubated at room temperature for 10 minutes, and heated for 50 minutes at 45 ^{0}C and 10 minutes at 70 ^{0}C. Real-time PCR was performed using the IQ5 Real Time PCR Detection System (Bio-Rad) with an initial denaturation step of 15 minutes at 95 ^{0}C followed by 40 cycles of 15 seconds at 95 ^{0}C, 30 seconds at 60 ^{0}C and 30 seconds at 72 ^{0}C. Cycle threshold values were attained and relative expression levels of mRNA were normalized to the housekeeping genes *Hprt* and *Gapdh* and calculated by the ΔΔCT method. qRT-PCRs were performed on two independent samples of each cell line and three technical replicas were performed for each sample.

Statistical analysis

Results are expressed as the mean ± standard deviation. Two-tailed, paired Student's *t*-tests were used to determine statistical significance. A value of $p < 0.05$ was considered to be statistically significant. Analysis was performed using Microsoft Excel 2010 (Microsoft, Redmond, WA).

Primary Antibodies

Antibody	*Host*	*Clone*	*Dilution*	*Company*	*Catalog number*
Melan-A	Rabbit	A19-P	1:200	Novus Biologicals	NBP1-30151
DCT	Rabbit	-	1:200	Abcam	Ab74073
TYRP1	Rabbit	-	1:50	Santa Cruz Biotechnology	sc-25543
TUBB3	Rabbit	TUJ1	1:1000	Covance	MRB-435P
TUBB3	Mouse	2G10	1:200	Abcam	Ab79078

Secondary antibodies

Antibody	*Dilution*	*Company*
Alexa Fluor 488 goat anti-rabbit IgG (H+L)	1:200	Life Technologies
Alexa Fluor 555 goat anti-mouse IgG (H+L)	1:200	Life Technologies
Alexa Fluor 647 goat anti-mouse IgG (H+L)	1:200	Life Technologies

Table S1. List of primary and secondary antibodies for immunochemistry.

GENE	*FORWARD PRIMER*	*REVERSE PRIMER*
Mitf	5'-GGGGCTGCCTGAAACCTTGCT-3'	5'-TACCTGGTGCCTCTGAGCTTGC-3'
Dct	5'-TGACCGTGAGCAATGGCCGA-3'	5'-GGCCGGTCCAGCCGAACTTG-3'
Tubb3	5'-CCGCGTGAAGTCAGCATGAGGG-3'	5'-CCGCTGGGGTCTATGCCGTG-3'
Hprt	5'-TTGCTCGAGATGTCATGAAGGAGA-3'	5'-AGCAGGTCAGCAAAGAACTTATAG-3'
Gapdh	5'-TGCACCACCAACTGCTTAGC-3'	5'-GGCATGGACTGTGGTCATGAG-3'

TABLE S2. LIST OF PRIMERS.

Results

TUBB3 is expressed in human epidermal melanocytes *in vivo*

To confirm the TUBB3 expression reported by Akasaka et al. in the basal layer of human epidermis and to investigate if this was indeed localized to melanocytes, we analyzed human epidermal skin sections by immunohistochemistry for both TUBB3 and two melanocytic markers, melanoma-specific antigen 1 (melan-A) and dopachrome tautomerase (DCT). Melan-A (also known as MART-1) is a protein present both in non-pigmened and in pigmented melanocytes. DCT (also known as tyrosinase-related protein 2, TYRP2) is an enzyme involved in melanogenesis and is a direct target of microphthalmia-associated transcription factor (MITF) and therefore specifically marks the early and terminally differentiated pigment producing melancoytes. In adult human epidermis, most melan-A+ and DCT+ cells in the basal layer of the epidermis immunostained for TUBB3 (Figures 1A and 1B). TUBB3 expression was seen in 83.7% $\pm$ 5.4 (n = 49) of the melan-A+ cells and in all of the DCT+ cells (n = 21). There were also TUBB3+ cells in the basal layer that did not immunostain for melan-A (6.8% $\pm$ 5.0, n = 44) nor for DCT (43.2% $\pm$ 19.3, n = 37). Fetal scalp skin at 20 weeks of gestational age showed a similar staining pattern. Already, melan-A+/TUBB3+ and DCT+/TUBB3+ melanocytes were found in the basal layer (Figures 1C and 1D) and the majority of melan-A+ and DCT+ cells expressed TUBB3 (98.0% $\pm$ 3.0 (n = 50) and 100.0% (n = 27), respectively). Of the TUBB3+ cells, 3.9% $\pm$ 3.4 (n = 51) did not immunostain for melan-A, whereas 42.6% $\pm$ 5.5 (n = 47) were negative for DCT. Taken together, these data show that normal human epidermal non-pigmented and terminally differentiated pigmented melanocytes express TUBB3 *in vivo*.

We also observed TUBB3+ dendritic-like structures in the epidermis (Figure 1C, arrow) which we assumed to be epidermal nerve endings and therefore be of neuronal origin. Interestingly, many of these structures were also melan-A+ (Figure 1C, arrow). Since the dermal nerve fibers did not stain for melan-A (Figure 1C, asterisk), we conclude that these intraepidermal melan-A+/TUBB3+ structures are melanocytic dendrites rather than free nerve endings.

Human hair follicle melanocytes express TUBB3 *in vivo*

Our observations in epidermal melanocytes raised the question of whether hair

follicle melanocytes also expressed TUBB3. In the hair follicle, non-pigmented melanocytes reside within the bulge/sub-bulge area and the outer root sheet of the infundibulum [14 – 16]. They are thought to be the source of the mature melanocytes located around the dermal papilla and lower portion of the medulla, which provide pigment to the hair shaft keratinocytes. In fetal scalp hair follicles, melan-A+ and DCT+ melanocytes were seen in the hair matrix surrounding the basal area of the medulla (Figure 1E-F). As epidermal melanocytes, these hair follicle melanocytes immunostained for TUBB3 (Figures 1E-1F). In addition, TUBB3 expression was observed in cells of the outer root sheath (Figures 1E and 1F, arrowheads). These TUBB3+ cells, however, were negative for melan-A and DCT and it could be surmised that these cells are non-pigmented melanocytes which are known to reside in this area. TUBB3 immunostaining was also seen in the hair shaft medulla keratinocytes (Figure 1E-F, *M*). In summary, in the human hair follicle melan-A+/TUBB3+ and DCT+/TUBB3+ melanocytes were observed in the hair matrix, whereas melan-A-/TUBB3+ and DCT-/TUBB3+ cells were found in the outer root sheath of the hair follicle bulb.

Fetal epidermal and hair follicle melanocytes express TUBB3 *in vitro*

Based on the *in vivo* expression of TUBB3 in both epidermal and hair follicle melanocytes, we anticipated that TUBB3 would also be expressed *ex vivo/ in vitro* in these cells. For this purpose, human fetal scalp skin which contained an abundance of pigmented hair follicles was mechanically dissociated and cultured for seven days in standard culture medium containing additional factors (SCF, TPA and CT, see *Materials and Methods*) to support the whole range of differentiated melanocytes, including the non-pigmented, early-pigmented and the terminally differentiated pigmented melanocytes. This resulted in heterogeneous cultures containing keratinocytes, fibroblasts and melanocytes. The melanocytic cells were identified by means of different types of light microscopy. Using phase-contrast microscopy, melanocytes could be recognized by their bipolar or multipolar dendrites and the halo surrounding their cell body (Figure 2). Bright-field microscopy was used to detect pigment inclusions (Figure 2). Using both approaches, epidermal and hair follicle melanocytes could be distinguished on basis of the criteria formulated by Tobin et al. [17] who showed that cultured epidermal melanocytes have 3-6 dendrites, whereas cultured hair follicle melanocytes are mostly bipolar. Definite confirmation was provided by immunofluorescent staining for tyrosine-related protein 1 (TYRP1) and melan-A.

As expected, we were able to identify TYRP1+/TUBB3+ pigmented epidermal melanocytes in the dissociated skin cultures (Figure 2A). Interestingly, TYRP1-/TUBB3+ cells were also observed (Figure 2A, asterisks). Morphologically, these non- or early-pigmented melanocytes were similar to the TYRP1+/TUBB3+ cells, but they were less dark under bright-field microscopy. Bipolar hair follicle melanocytes were present in large numbers and were TYRP1+/TUBB3+ (Figure 2B). In close proximity to these cells, some bipolar TYRP1-/TUBB3+ were also found (Figure 2B, asterisks). Melan-A staining showed similar results; bipolar melan-A+/TUBB3+ cells were clearly growing out of the hair follicle bulb (Figure 2C). There were no melan-A-/TUBB3+ cells with similar morphology, but some TUBB3 expression was seen in cells with a morphology reminiscent of keratinocytes (Figure 2C, arrowheads). This data show that, as *in vivo*, both human epidermal and hair follicle melanocytes express TUBB3 *in vitro* and that expression starts before initiation of melanogenesis.

Expression of TUBB3 starts upon differentiation of melanoblasts into mature melanocytes

In neurons of the central nervous system TUBB3 expression decreases as the cells mature and can therefore be used to identify young developing neurons. In the peripheral nervous system, however, the opposite is found: TUBB3 levels increase with neuronal cell maturation in dorsal root ganglia[18]. Our experiments with human melanocytes show that TUBB3 is expressed in the end stages of the melanocytic lineage (non-pigmented and pigmented melanocytes). However, expression in the undifferentiated, melanoblast stage remains inconclusive. To further examine this relationship of TUBB3 expression within the melanocytic lineage, we analyzed two widely-used immortalized mouse melanocytic cell lines derived from the C57BL/6J strain. Melb-a is a clonal line of melanoblasts, which do not produce melanin [19]. Using bright-field microscopy, cells could not be seen due to the obvious lack of pigment inclusions (data not shown), confirming their immature state. Although most cells were negative for TUBB3 (Figure 3A), rare TUBB3+ cells could be observed. Interestingly, these TUBB3+ cells demonstrated a more differentiated cell morphology by the presence of dendrites and a halo surrounding their cell bodies. TUBB3- cells were generally flat with few and short dendrites, or none at all (Figure 3A).

To analyze TUBB3 expression in mature murine melanocytes, we used melan-Ink4a2

cells[20]. Cells of this line produce different amounts of melanin, so both non-pigmented and pigmented melanocytes are present which can be visualized under bright field microscopy (Figure 3B). TUBB3 immunostaining showed a gradient of strong to almost no fluorescence (Figure 3B). Our data suggests that there is an inverse relationship between TUBB3 fluorescence and melanin production; cells that showed the brightest TUBB3 fluorescence contained only little or no melanin at all, as evident from the immunofluorescence and bright-field images (Figure 3B, white arrows), whereas the darkest cells demonstrated little or no TUBB3 fluorescence at all (Figure 3B, black arrows). When we analyzed line plots over areas containing large amounts of melanin, we indeed found a relation between fluorescent intensity (Figure 3B, graph, red line) and bright field intensity (graph, black line).

We questioned whether this observed inversed relation of TUBB3 immunostaining and pigment inclusion would be caused by either a down-regulation of TUBB3 upon terminal differentiation, as is the case in neurons from the central nervous system, or by the pigment itself blocking emission of TUBB3 fluorescence, in which case TUBB3 expression would actually be sustained upon terminal differentiation. When we analyzed line plots within cells over areas containing large amounts of melanin, we found a relation between fluorescent intensity (Figure 3B, graph, red line) and bright field intensity (graph, black line), suggestive that the pigment itself blocked fluorescence. Similar line plot profiles were seen with secondary antibodies of different wavelengths (data now show). To further test this, we treated formaldehyde-fixed melan-Ink4a2 cells with potassium permanganate and oxalic acid to bleach the melanin (Figure 3B, bright field). After subsequent immunostaining, TUBB3 fluorescence was significantly increased (Figure 3C). Bright TUBB3 immunostaining was present in nearly all cells (94.2% $\pm$ 3.2, n = 142), whereas in the untreated samples only about a quarter of the cells (25.9% $\pm$ 12.3, n = 192, $p < 0.001$ between groups) were clearly visible (Figure 3B-C). These data indicate that TUBB3 is not only upregulated upon differentiation of melanoblasts into melanocytes, but that this tubulin isotype remains expressed during terminal differentiation into mature pigment-producing melanocytes.

To verify the immunocytochemistry findings, we performed both Western blot and qRT-PCR experiments on the melb-a and melan-Ink4a2 cell lines. Western blotting analysis using two different, commonly used, monoclonal antibodies against TUBB3 (TUJ1 and 2G10) showed corresponding bands at the predicted molecular weight of approximately 50 kDa (Figure 4A). In the case of TUJ1, no band was found in the melb-a cells, whereas a clear band was present in the melan-Ink4a2 cells. Antibody

2G10 showed bands in both cell types with a much higher protein expression in the melan-Ink4a2 cells. Using qRT-PCR we determined *Mitf*, *Dct* and *Tubb3* RNA levels (Figure 4B). *Mitf* and *Dct*, both key molecules in melanogenesis, were 1.67 ± 0.04 and 6.58 ± 0.89 fold increased ($p < 0.03$ and $p < 0.002$) in melan-Ink4a2 cells compared to melb-a cells, again confirming their more differentiated state. Tubb3 was also found in both cell lines, with a 4.12 ± 0.32-fold higher expression level in the melan-Ink4a2 cells ($p < 0.02$). In summary, immunocytochemistry, Western blot and qRT-PCR data indicated that TUBB3 expression starts when melanoblasts commit to the melanocyte lineage and differentiate into pigment producing melanocytes.

α-MSH stimulation does not increase TUBB3 expression in cultured human melanocytes

As TUBB3 expression in the melanocytic lineage coincides with the induction of melanin, we questioned if the melanogenesis pathway could also regulate TUBB3 expression. To assess this, we cultured primary human melanocytes and stimulated the cells with alpha-melanocyte-stimulating hormone (α-MSH) for 6 hours, 24 hours or 48 hours. After exposure, we performed quantitative western blot analysis for DCT and TUBB3 expression on the cell lysates. As α-MSH binds to the melanocortin 1 receptor (MC1R), which in turn promotes transcription of the MITF transcription factor, an observed increase in expression of the MITF target gene DCT would indicate a successful stimulation of the melanogenesis pathway. DCT expression was found to be increased (232%, 175% and 166% after 6 hours, 24 hours and 48 hours, respectively) confirming successful stimulation (Figure 5). In contrast, TUBB3 showed no concomitant increase in expression (108%, 105% and 91%, respectively (Figure 5)). Combined, no association between TUBB3 expression and induction of melanogenesis could be found.

Discussion

In this study, we show that TUBB3 is not only expressed within peripheral neurons but also in the melanocytic lineage. In melanocytes, TUBB3 expression was found both in human epidermal and hair follicle melanocytes. Using skin sections, we showed that nearly all melan-A+ and DCT+ melanocytes express TUBB3. Conversely, TUBB3+ cells in the basal layer of the epidermis were almost always melan-A+, although many did not express DCT. Similar results were found in cultured human fetal epidermal and hair follicle melanocytes. In the melanocytic lineage, melan-A is expressed both by non-pigmented and pigmented melanocytes. However, DCT and TYRP1 are not expressed before terminal diff erentiation into pigment producing melanocytes. This indicates that TUBB3 is widely expressed within the melanocyte lineage, with expression starting before pigment production. Indeed, when we investigated TUBB3 expression in mouse melanoblasts and melanocytes, most melanoblasts did not (as yet) express TUBB3 whereas both non-pigmented and pigmented melanocytes did express TUBB3. This implicates that expression of TUBB3 starts around the point of time where melanoblasts commit to the melanocyte lineage (Figure 5).

Like peripheral neurons, melanocytes are derived from the neural crest. There are also other similarities, both in morphology and functional characteristics. Both cell types have small, round cell bodies and multiple dendritic processes. Both can express similar receptors (e.g. $p75^{NTR}$ and c-Kit) and therefore respond to identical cytokines and neurotrophins [21]. Furthermore, both melanins (produced by melanocytes) and catecholamines (e.g. dopamine, produced by neurons) are derived from tyrosine, and both melanosomes and synaptic vesicle precursors are transported over microtubules by kinesins. In turn, melanosomes and neurotransmitters are both released from their dendrites or axons. Presently, there is an emerging concept that melanocytes could potentially be used to represent neuronal cells in disease model systems. In this light, the expression of neuron-specific TUBB3 in melanocytes might not be so surprising. In the skin, TUBB3 expression is considered to be of neuronal origin, whether it be intraepidermal free nerve endings or nerves projecting to Merkel cells, Langerhans cells or even melanocytes [22 – 24]. As we show that at least a part of these endings belong to melanocytes, it is of great interest to further investigate the extent of TUBB3 expression by skin melanocytes, examine their relationship with surrounding cells and investigate expression of other neuronal biomarkers.

TUBB3 has now been found expressed in chicken, mouse and human melanocytes. This evolutionary conservation is suggestive of an important role of TUBB3 in these cells. We observed initiation of TUBB3 expression in the melanocytic lineage around the time of diff erentiation into pigment producing melanocytes. Melanocyte development as well as the UV-induced pigmentation response are regulated by the MITF transcription factor that modulates multiple diff erentiation and melanin biosynthesis genes. We questioned whether TUBB3 expression could be regulated by the same pathway and stimulated cultured human melanocytes with α-MSH, known to induce MITF expression. Whereas expression of the MITF target gene DCT was induced by α-MSH stimulation, there was no associated increase in TUBB3 expression. Therefore, TUBB3 does not seem to be regulated by the MITF-pathway which regulates melanocyte development and pigmentation response. This is in line with results of studies examining MITF target genes, which consistently found that TUBB3 was not among the targets of this transcription [25 – 27].

Using a well-established bleaching protocol, we show that fluorescent signals emitted by TUBB3 stainings are blocked by melanin. This was in contrast to control experiments with melan-A immunostaining which did not show this clear relationship (Figure S1), indicating that the melanin specifically interfered with the TUBB3 fluorescence. Therefore, we conclude that the diminished TUBB3 fluorescence was caused by specific co-localization of melanin. This could indicate a novel role of TUBB3 in melanosomal transport. It is known that mature melanosomes are transported by kinesin and dynein motor proteins (Marks & Seabra, 2001). These proteins use microtubule tracks to travel in a bi-directional way (Wu et al., 1998). Also, by specifically disrupting microtubules, it has been shown that melanosome transport is microtubule dependent [28]. Potentially, TUBB3 could be the corresponding β-unit isotype (Figure S2). However, its role in cellular processes remains to be investigated.

A recent study by Dalziel et al. (2011) showed that TUBB3 is physically located immediately downstream of MC1R (Figure S3). This receptor binds to melanocortins and plays an important role in melanogenesis through its ability to influence MITF transcription. Aside from showing that TUBB3 is located immediately downstream of MC1R, in itself suggesting a role within melanocytes, Dalziel and colleagues found that chimeric proteins are transcribed by intergenic splicing between these two genes. The monoclonal TUBB3 antibodies used in our study, TUJ1 and 2G10, both recognize the C-terminus of the TUBB3 protein (epitopes EAQGPK [30] and MYEDDEEESEAQGPK [31]) and immunostain the same structures (Figure S4).

In chick and mice, *Tubb3* has only one protein product. In humans, aside from the chimeric proteins, there are four additional TUBB3 isoforms (Figure S3). Both antibodies will recognize at least isoforms 1 and 2 and the chimeric transcript RP11-566K11.2-001. Currently, these antibodies react both with neuronal and melanocytic cells. However, it could be that both cell types express different isoforms of the TUBB3 protein. It will be interesting to investigate the exact expression of these isoforms in normal human neurons and melanocytes to find out whether different and/or identical isoforms are present in these cell types. Together, our results and these findings suggest a dynamic role for TUBB3 in multiple aspects of melanocytic function.

Finally, in addition to TUBB3 expression in melanocytes, we have also observed its presence in hair follicle medulla keratinocytes *in vivo*. Expression of TUBB3 in the mitotic spindle of cultured keratinocytes and fibroblasts has been previously reported [8], something we have observed as well in our cultured melanocytes (Figure S5). This indicates that this biomarker, especially in the skin, cannot be reliably used to differentiate between neuronal cells and other neural crest and ectodermal cell types. Primary skin cultures and differentiation studies on skin stem cells or even (induced) pluripotent stem cells might be prone to this identification issue. Aside from identifying neurons, TUBB3 can be used as a much wider marker of neural crest derived and epithelial cells.

Acknowledgements

We thank L. van Iperen for technical support and Prof. dr. C.L. Mummery for critical reading of the manuscript. Cell lines melb-a (Sviderskaya et al., 1995) and melan-Ink4a2 (Ha et al., 2007) were kindly provided by the Wellcome Trust Functional Genomics Cell Bank (St George's, University of London, UK). This research was supported by the Heinsius Houbolt Fund, the Netherlands Organization for Scientific Research (NWO Aspasia 015.007.037) and the Netherlands Institute for Regenerative Medicine (NIRM, FES0908).

References

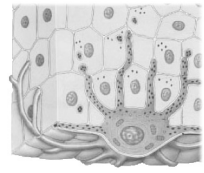
1. Bryan J, Wilson L: **Are cytoplasmic microtubules heteropolymers?** Proc Natl Acad Sci U S A 1971, 68:1762 – 6.
2. Downing KH, Nogales E: **Tubulin and microtubule structure.** Curr Opin Cell Biol 1998, 10:16 – 22.
3. Ludueña RF: **Multiple forms of tubulin: different gene products and covalent modifications.** Int Rev Cytol 1998, 178:207 – 75.
4. Sullivan KF, Cleveland DW: **Identification of conserved isotype-defining variable region sequences for four vertebrate beta tubulin polypeptide classes.** Proc Natl Acad Sci U S A 1986, 83:4327 – 31.
5. Geisert EE, Frankfurter A: **The neuronal response to injury as visualized by immunostaining of class III beta-tubulin in the rat.** Neurosci Lett 1989, 102:137 – 41.
6. Moody SA, Quigg MS, Frankfurter A: **Development of the peripheral trigeminal system in the chick revealed by an isotype-specific anti-beta-tubulin monoclonal antibody.** J Comp Neurol 1989, 279:567 – 80.
7. Burgoyne RD, Cambray-Deakin MA, Lewis SA, Sarkar S, Cowan NJ: **Differential distribution of beta-tubulin isotypes in cerebellum.** EMBO J 1988, 7:2311 – 9.
8. Jouhilahti E-M, Peltonen S, Peltonen J: **Class III beta-tubulin is a component of the mitotic spindle in multiple cell types.** J Histochem Cytochem 2008, 56:1113 – 9.
9. Mariani M, Shahabi S, Sieber S, Scambia G, Ferlini C: **Class III β-tubulin (TUBB3): more than a biomarker in solid tumors?** Curr Mol Med 2011, 11:726 – 31.
10. Adameyko I, Lallemend F, Aquino JB, Pereira JA, Topilko P, Müller T, Fritz N, Beljajeva A, Mochii M, Liste I, Usoskin D, Suter U, Birchmeier C, Ernfors P: **Schwann cell precursors from nerve innervation are a cellular origin of melanocytes in skin.** Cell 2009, 139:366 – 79.
11. Adameyko I, Lallemend F, Furlan A, Zinin N, Aranda S, Kitambi SS, Blanchart A, Favaro R, Nicolis S, Lübke M, Müller T, Birchmeier C, Suter U, Zaitoun I, Takahashi Y, Ernfors P: **Sox2 and Mitf cross-regulatory interactions consolidate progenitor and melanocyte lineages in the cranial neural crest.** Development 2012, 139:397 – 410.
12. Akasaka K, Maesawa C, Shibazaki M, Maeda F, Takahashi K, Akasaka T, Masuda T: **Loss of class III beta-tubulin induced by histone deacetylation is associated with chemosensitivity to paclitaxel in malignant melanoma cells.** J Invest Dermatol 2009, 129:1516 – 26.
13. Lauria G, Borgna M, Morbin M, Lombardi R, Mazzoleni G, Sghirlanzoni A, Pareyson D: **Tubule and neurofilament immunoreactivity in human hairy skin: markers for intraepidermal nerve fibers.** Muscle Nerve 2004, 30:310 – 6.

14. Tobin DJ, Slominski A, Botchkarev VA, Paus R: **The fate of hair follicle melanocytes during the hair growth cycle.** J Investig Dermatol Symp Proc 1999, 4:323 – 32.
15. Botchkareva NV, Khlgatian M, Longley BJ, Botchkarev VA, Gilchrest BA: **SCF/c-kit signaling is required for cyclic regeneration of the hair pigmentation unit.** FASEB J 2001, 15:645 – 58.
16. Nishimura EK: **Melanocyte stem cells: a melanocyte reservoir in hair follicles for hair and skin pigmentation.** Pigment Cell Melanoma Res 2011, 24:401 – 10.
17. Tobin DJ, Bystryn JC: **Different populations of melanocytes are present in hair follicles and epidermis.** Pigment Cell Res 1996, 9:304 – 10.
18. Jiang YQ, Oblinger MM: **Differential regulation of beta III and other tubulin genes during peripheral and central neuron development.** J Cell Sci 1992, 103 (Pt 3:643 – 51.
19. Sviderskaya EV, Wakeling WF, Bennett DC: **A cloned, immortal line of murine melanoblasts inducible to differentiate to melanocytes.** Development 1995, 121:1547 – 57.
20. Ha L, Ichikawa T, Anver M, Dickins R, Lowe S, Sharpless NE, Krimpenfort P, Depinho RA, Bennett DC, Sviderskaya E V, Merlino G: **ARF functions as a melanoma tumor suppressor by inducing p53-independent senescence.** Proc Natl Acad Sci U S A 2007, 104:10968 – 73.
21. Yaar M, Park H-Y: **Melanocytes: a window into the nervous system.** J Invest Dermatol 2012, 132(3 Pt 2):835 – 45.
22. Hosoi J, Murphy GF, Egan CL, Lerner EA, Grabbe S, Asahina A, Granstein RD: **Regulation of Langerhans cell function by nerves containing calcitonin gene-related peptide.** Nature 1993, 363:159 – 63.
23. Hara M, Toyoda M, Yaar M, Bhawan J, Avila EM, Penner IR, Gilchrest BA: **Innervation of melanocytes in human skin.** J Exp Med 1996, 184:1385 – 95.
24. Chateau Y, Misery L: **Connections between nerve endings and epidermal cells: are they synapses?** Exp Dermatol 2004, 13:2 – 4.
25. Cheli Y, Ohanna M, Ballotti R, Bertolotto C: **Fifteen-year quest for microphthalmia-associated transcription factor target genes.** Pigment Cell Melanoma Res 2010, 23:27 – 40.
26. Levy C, Khaled M, Fisher DE: **MITF: master regulator of melanocyte development and melanoma oncogene.** Trends Mol Med 2006, 12:406 – 14.
27. Hoek KS, Schlegel NC, Eichhoff OM, Widmer DS, Praetorius C, Einarsson SO, Valgeirsdottir S, Bergsteinsdottir K, Schepsky A, Dummer R, Steingrimsson E: **Novel MITF targets identified using a two-step DNA microarray strategy.** Pigment Cell Melanoma Res 2008, 21:665 – 76.
28. Wu X, Bowers B, Rao K, Wei Q, Hammer JA: **Visualization of melanosome dynamics within wild-type and dilute melanocytes suggests a paradigm for myosin V function In vivo.** J Cell Biol 1998, 143:1899 – 918.

29. Dalziel M, Kolesnichenko M, Pires das Neves R, Iborra F, Goding C, Furger A: **Alpha-MSH regulates intergenic splicing of MC1R and TUBB3 in human melanocytes.** Nucleic Acids Res 2011, 39:2378 – 92.

30. Lee MK, Tuttle JB, Rebhun LI, Cleveland DW, Frankfurter A: **The expression and posttranslational modification of a neuron-specific beta-tubulin isotype during chick embryogenesis.** Cell Motil Cytoskeleton 1990, 17:118 – 32.

31. Spano AJ, Frankfurter A: **Characterization of anti-beta-tubulin antibodies.** Methods Cell Biol 2010, 95:33 – 46.



7

Hair follicle bulge cultures yield class III β-tubulin-positive melanoglial cells

Locher
Saadah
de Groot
de Groot
Frijns
Huisman

Histochemistry and Cell Biology, *2015*

Abstract

Class III β-tubulin (TUBB3)-positive cells from the hair follicle bulge are thought to be neuronal cells derived from a local neural crest stem cell. However, TUBB3 has recently been shown to be expressed in the melanocytic lineage. To evaluate the neural-crest-associated immunophenotype of TUBB3-positive cells from hair follicle bulge explants, we dissected hair follicle bulges out from mouse whisker pads and cultured for one month and assessed outgrowing cells by means of immunocytochemistry using the biomarkers TUBB3, nestin, NGFR, SOX9, TYRP1 and laminin. Large amounts of TUBB3-positive cells could be cultured that co-expressed nestin, NGFR, SOX9 and, to a lesser degree, TYRP1, matching a melanoglial phenotype. In addition, a small population of TUBB3-negative but laminin-positive cells was found, which presumably are of glial origin. It can be concluded that cells of melanoglial origin can easily be obtained from hair follicle bulge explants. These cells may be of use in experimental animal or human disease and wound healing models. Notably, the TUBB3-positive cells are of melanoglial rather than neuronal origin.

Introduction

Stem cells that are harvested from adult human tissues are considered the gold standard for autologous cell-based therapies[1]. Adult human neural-crest-derived stem cells (NCSCs) are promising candidates for the use in regenerative medicine; niches have been described in the dorsal root ganglia, gut epithelium, cornea epithelium, heart muscle, inferior turbinate, dental and periodontal tissue, and the hair follicle bulge[2]. The advantage of hair follicle bulge stem cells is that they can be harvested in a minimally invasive way and that they can be isolated without proteolysis.

Nestin-positive cells from the hair follicle bulge area have been reported to be multipotent stem cells and able to differentiate into various neural-crest-derived lineages[3, 4]. It has been claimed that these nestin-positive cells differentiate into neuronal cells specifically expressing TUBB3, a widely used neural biomarker.

However, it has recently been demonstrated that mouse and human melanocytes also express TUBB3[5 – 7]. As melanocytes, similar to peripheral neurons, derive from the neural crest, we wondered whether the TUBB3-positive cells cultured from hair follicle bulge explants could be such melanocytes. If so, we should be extremely reticent about TUBB3-positive cells cultured from hair follicle bulge explants, presumed to be committed towards the neuronal lineage.

To address this issue, we investigated the immunophenotype of the cells migrating out of mouse hair follicle bulge explants by immunostaining with biomarkers specific for the neural crest and glial and melanocytic lineages.

Material and Methods

Specimens

Hair follicles were dissected from the whisker pads of surplus C57BL/6 mice (n=7; 126 hair follicles), which were obtained from the LUMC central Animal Facility. Their use was approved by the LUMC Animal Experiments Committee (DEC permit 10172).

Cell cultures

Hair follicle bulges were isolated from mouse whisker pads according to a protocol previously described by Sieber-Blum et al.3. In summary, hair follicles were dissected out from the whisker pads, the follicle was transected below and above the bulge region and a longitudinal incision was made in the capsule. The bulge was rolled out of the capsule and explants were transferred to 6-well cell culture plates pre-coated with collagen I (Sigma-Aldrich) and allowed to attach for 1 hour at 37° C in a humidified incubator with 5% CO2 prior to addition of culture medium. Culture medium consisted of alpha MEM (Bio-Whittaker) containing 5% chicken embryo extract (Seralab), 10% fetal bovine serum (Life Technologies), 1% GlutaMAX (Life Technologies) and 1% antibiotic/antimycotic solution (Sigma-Aldrich). Medium was refreshed every other day. To allow as many cells as possible to migrate out of the explant, cultures were maintained for 4 weeks followed by fixation in 1% formaldehyde in phosphate-buffered saline for 30 minutes and immunocytochemistry. Cell lines RT4D6P2T (schwannoma cells; ATCC) and melan-Ink4a2 (melanocytes; Wellcome Trust Functional Genomics Cell Bank) were used as positive controls, and were cultured according to manufacturer's instructions.

Immunocytochemistry

Immunocytochemical protocols were similar to the ones described previously[5]. Primary antibodies used in this study were rabbit anti-laminin (1:200, Z009701, Dako), mouse anti-nestin (1:200, Biosensis, M-1385-100), rabbit anti-SOX9 (1:500, Millipore, AB5535), rabbit anti-NGFR (1:200, Millipore, 07-476), mouse anti-TUBB3 (1:200, Abcam, ab78078) and rabbit anti-TYRP1 (1:50, Santa Cruz Biotechnology, sc-25543). Secondary antibodies were Alexa Fluor 488 goat anti-

rabbit (1:500, Invitrogen, A-11034) and Alexa Fluor 555 goat anti-mouse (1:500, Invitrogen, A-21422). To confirm secondary antibody specificity, negative controls were included in which the primary antibodies were omitted. Images were made with an Olympus IX70 microscope equipped with a Leica DFC340 FX camera using LAS AF software (Leica).

Brightness and contrast adjustments consistent with image-manipulation policies were performed with either LAS AF, ImageJ version 1.47a (National Institutes of Health, http://imagej.nih.gov/ij) or Adobe Photoshop CS6 (Adobe Systems) image-processing software.

Results

At the start of the culture, some cells residing within the hair follicle bulge stained positively for nestin, a marker commonly used to identify NCSCs (Fig. 1A). After 4 weeks, extensive outgrowth of nestin-positive bi- or tripolar cells migrating out of the explant was observed in each culture (Figs. 1B-C). Similar patterns were seen after immunostaining for TUBB3 (Fig. 1D). The nestin- and TUBB3-positive cells are positioned on top or in between of a matrix of flattened polyhedral cells. Based on previous immunophenotyping in similar culture experiments, these cells can be identified as pan-Cytokeratin- and cytokeratin15-positive keratinocytes (results not shown).

To further establish the immunophenotype and identity of these nestin- and TUBB3-positive cells, we performed double immunostaining for TUBB3 together with various markers of the early neural crest, Schwann cell and melanocyte lineages. All TUBB3-positive cells co-expressed nerve growth factor receptor (NGFR, also often named $p75^{NTR}$) (Figs. 2A-B) and (sex determining region Y)-box 9 (SOX9) (Figs. 2C-D), indicating that these cells are of the melanoglial lineage. Double immunostaining for TUBB3 and tyrosinase-related protein 1 (TYRP1), a protein involved in melanin synthesis, revealed a high degree of co-expression of TUBB3 and (albeit weakly) TYRP1 (Figs. 3A-B). Double immunostaining for TUBB3 and laminin, an early Schwann cell marker, showed many TUBB3-positive cells and laminin-positive cells, but co-expression was never observed, suggesting two different cell populations. Remarkably, these cells seemed to migrate along the same tracks (Figs. 3C-D).

Discussion

Based upon our previous results[5], we initially assumed that the TUBB3-positive cells migrating out of the hair follicle bulge explant would be melanocytes. Our results show, however, that the TUBB3-positive cells migrating out of the hair follicle bulge co-expressed nestin, NGFR and SOX9, indicative of a melanoglial identity, notwithstanding their TUBB3 expression which is generally thought to be limited to neuronal cells.

To investigate whether these cells were actually committed to either a melanocytic or glial cell fate, we performed additional double immunostainings for TUBB3 together with pertinent lineage markers for each respective cell type, i.e. TYRP1 for melanocytes and laminin for glial cells, resulting in diverse findings. TUBB3-positive cells showed weak TYRP1 co-expression and the most plausible explanation is that these cells belong to a population of intermediate cells, which seem to show a tendency to the melanocytic commitment. Double immunostaining with antibodies against TUBB3 and laminin revealed a second population consisting of TUBB3-negative and laminin-positive cells, suggesting that these cells belong to the Schwann cell lineage.

The hair follicle bulge accommodates several different (stem) cell populations[8]. In addition, in the vibrissae this region is abundantly innervated by multiple sensory nerve endings[9, 10]. Given the immunophenotype of the cells in our cultures, we hypothesize that both populations originate either from Schwann cells located in the proximal nerve stump or sensory nerve endings[10 – 12], or from melanocyte stem cells in the bulge[13, 14], both displaying an intermediate status between glial and melanocytic cell fate choice.

Recently, a nestin-positive cell population has been shown to reside between the basal membrane and the outer root sheath in the area just above the bulge, exhibiting long processes forming a crown around the whole hair follicle[15]. These cells are closely associated with terminal nerve endings and are thought to be similar to nestin-positive type-II terminal Schwann cells of the piloneural collar[12]. Interestingly, the first paper reports that these nestin-positive cells co-express NGFR, and that this nestin- and NGFR-positive cell population shares histological characteristics and immunological markers with the nestin-positive, multipotent stem cells from the bulge-isthmus region of hair follicles[4]. The authors assume that these cells all represent a single cell type originating from the piloneural collars.

Therefore, it is conceivable that the TUBB3- and NGFR-positive cells found in our cultures originate from the same source, i.e., Schwann cells from the hair follicle sensory nerve endings, existing in an intermediate phase between a Schwann cell precursor and a melanocyte, as has been described previously[16]. It then seems plausible to assume that the TUBB3-negative but laminin-positive cells represent a population of more mature Schwann cells, although these different populations share a common predecessor. Whether the TUBB3-positive melanoglial cells are derived from this population by dedifferentiation or from distinct melanocyte stem cells located in the hair follicle bulge remains to be elucidated.

Interestingly, it has been reported that nestin- and NGFR-positive cells, identified as nerve-terminal- associated NCSCs and located around the hair follicle bulge, contribute cells to regenerating dermis following skin injury[17]. These nestin- and NGFR-positive cells are probably key to wound healing, for it has been shown that normal innervation is prerequisite for completely healing of injured skin[18]. As the nestin- and NGFR-positive in our study can be cultured easily, they could be used in future studies using wound-healing models.

In this study we have demonstrated that hair follicle bulge explants yield TUBB3-positive cells of melanoglial lineage, which sheds a new light on the different populations of (stem) cells that have been proposed to reside in the hair follicle bulge. Especially, the use of TUBB3 as a specific marker of neuronal identity should be considered with great caution, because cells of a melanoglial phenotype also do express TUBB3.

Acknowledgements

This research was supported by grants from the Heinsius Houbolt Foundation. Cell line melan-Ink4a2[19] was kindly provided by the Wellcome Trust Functional Genomics Cell Bank.

References

1. Prasongchean W, Ferretti P: **Autologous stem cells for personalised medicine.** N Biotechnol 2012, 29:641 – 50.
2. Kaltschmidt B, Kaltschmidt C, Widera D: **Adult craniofacial stem cells: sources and relation to the neural crest.** Stem Cell Rev 2012, 8:658 – 71.
3. Sieber-Blum M, Grim M, Hu YF, Szeder V: **Pluripotent neural crest stem cells in the adult hair follicle.** Dev Dyn 2004, 231:258 – 69.
4. Amoh Y, Mii S, Aki R, Hamada Y, Kawahara K, Hoffman RM, Katsuoka K: **Multipotent nestin-expressing stem cells capable of forming neurons are located in the upper, middle and lower part of the vibrissa hair follicle.** Cell Cycle 2012, 11:3513 – 7.
5. Locher H, de Rooij KE, de Groot JCMJ, Doorn R Van, Gruis NA, Löwik CWGM, Chuva de Sousa Lopes SM, Frijns JHM, Huisman MA: **Class III β-tubulin, a novel biomarker in the human melanocyte lineage.** Differentiation 2013, 85:173 – 181.
6. Akasaka K, Maesawa C, Shibazaki M, Maeda F, Takahashi K, Akasaka T, Masuda T: **Loss of class III beta-tubulin induced by histone deacetylation is associated with chemosensitivity to paclitaxel in malignant melanoma cells.** J Invest Dermatol 2009, 129:1516 – 26.
7. Adameyko I, Lallemend F, Furlan A, Zinin N, Aranda S, Kitambi SS, Blanchart A, Favaro R, Nicolis S, Lübke M, Müller T, Birchmeier C, Suter U, Zaitoun I, Takahashi Y, Ernfors P: **Sox2 and Mitf cross-regulatory interactions consolidate progenitor and melanocyte lineages in the cranial neural crest.** Development 2012, 139:397 – 410.
8. Jaks V, Kasper M, Toftgård R: **The hair follicle-a stem cell zoo.** Exp Cell Res 2010, 316:1422 – 8.
9. Takahashi-Iwanaga H: **Three-dimensional microanatomy of longitudinal lanceolate endings in rat vibrissae.** J Comp Neurol 2000, 426:259 – 69.
10. Maklad A, Fritzsch B, Hansen LA: **Innervation of the maxillary vibrissae in mice as revealed by anterograde and retrograde tract tracing.** Cell Tissue Res 2004, 315:167 – 80.
11. Kaucká M, Adameyko I: **Non-canonical functions of the peripheral nerve.** Exp Cell Res 2014, 321:17 – 24.
12. Woo S-H, Baba Y, Franco AM, Lumpkin EA, Owens DM: **Excitatory glutamate is essential for development and maintenance of the piloneural mechanoreceptor.** Development 2012, 139:740 – 8.
13. Dupin E, Real C, Glavieux-Pardanaud C, Vaigot P, Le Douarin NM: **Reversal of developmental restrictions in neural crest lineages: transition from Schwann cells to glial-melanocytic precursors in vitro.** Proc Natl Acad Sci U S A 2003, 100:5229 –

33.

14. Wong CE, Paratore C, Dours-Zimmermann MT, Rochat A, Pietri T, Suter U, Zimmermann DR, Dufour S, Thiery JP, Meijer D, Beermann F, Barrandon Y, Sommer L: **Neural crest-derived cells with stem cell features can be traced back to multiple lineages in the adult skin.** J Cell Biol 2006, 175:1005 – 15.

15. Djian-Zaouche J, Campagne C, Reyes-Gomez E, Gadin-Czerw S, Bernex F, Louise A, Relaix F, Buckingham M, Panthier J-J, Aubin-Houzelstein G: **Pax3(GFP) , a new reporter for the melanocyte lineage, highlights novel aspects of PAX3 expression in the skin.** Pigment Cell Melanoma Res 2012, 25:545 – 54.

16. Adameyko I, Lallemend F: **Glial versus melanocyte cell fate choice: Schwann cell precursors as a cellular origin of melanocytes.** Cell Mol Life Sci 2010, 67:3037 – 55.

17. Johnston APW, Naska S, Jones K, Jinno H, Kaplan DR, Miller FD: **Sox2-Mediated Regulation of Adult Neural Crest Precursors and Skin Repair.** Stem Cell Reports 2013, 1:38 – 45.

18. Kumar A, Brockes JP: **Nerve dependence in tissue, organ, and appendage regeneration.** Trends Neurosci 2012, 35:691 – 9.

19. Ha L, Ichikawa T, Anver M, Dickins R, Lowe S, Sharpless NE, Krimpenfort P, Depinho RA, Bennett DC, Sviderskaya EV, Merlino G: **ARF functions as a melanoma tumor suppressor by inducing p53-independent senescence.** Proc Natl Acad Sci U S A 2007, 104:10968 – 73.


cochlea
cochlea

8

DISCUSSION

Human cochlear embryology

On the origin of cell types in the human cochlea

The first aim of this thesis was to gain more insight into the developing human fetal cochlea. The adult cochlea contains cells derived from different embryonic regions: the otic placode, the mesoderm, and the neural crest. To establish the exact origin of a cell type one has to perform lineage-tracing experiments, either by using the classic, chimeric, transplantation and dye injection approaches or by using more modern genetic fate-mapping methods. Although lineage tracing in the human fetus is difficult due to both ethical and technical reasons, experiments on the salamander [1], chicken [2], and rodent [3] have shown similar embryonic origins of various cochlear cell types in these three species. All immunostainings presented in this dissertation on the human fetal cochlea, as shown in Chapters 2-4, match the expression patterns (when available) of the developing cochlea in other vertebrate species. This strongly supports the hypothesis that the origin of all cell types in the vertebrate cochlea, including the human, is highly conserved. Animal data in combination with the data presented in Chapters 2-4 result in a model of the origin of cell types in the human cochlea, described in the following paragraphs and summarized in Table 1.

Cell type	Origin
Cochlear duct epithelium	Otic placode (cranial placode)
Spiral ganglion neurons	Otic placode (cranial placode)
Peripheral glial cells	Neural crest
Strial melanocytes (intermediate cells)	Neural crest
Basal cells of the stria vascularis	Unknown (likely mesoderm)
Interdental cells	Unknown (otic placode or neural crest?)
Fibrocytes	Periotic mesenchyme (mesoderm)
Otic capsule	Periotic mesenchyme (mesoderm)
Blood vessels	Periotic mesenchyme (mesoderm)

Table 1. The embryonic origin of various cochlear cell types

Cochlear duct epithelium

Most of the cochlea is derived from the otic placode and develops via the otic vesicle stage into both the vestibular labyrinth and the cochlear duct. It is therefore likely that all epithelial cells lining the cochlear duct are derived from the otic placode. Counterclockwise (Figure 1), starting at the organ of Corti, these cells are: hair cells and various types of supporting cells, Hensen's cells, Claudius' cells, outer sulcus root cells, the epithelial cells of the spiral prominence, the marginal cells of the stria vascularis, the epithelial cells of Reissner's membrane, interdental cells, and the inner sulcus cells (or Kölliker's organ in the fetus). All these different cell types develop from a more or less undifferentiated epithelium which at the 10th week of gestation (W10) expresses SOX9 and SOX10, with additional SOX2 expression in the prosensory domain (Chapter 2).

Spiral ganglion neurons

Spiral ganglion neurons (SGNs) are, like the epithelial lining of the cochlear duct, also derived from the otic placode. Proneural cells delaminating from the

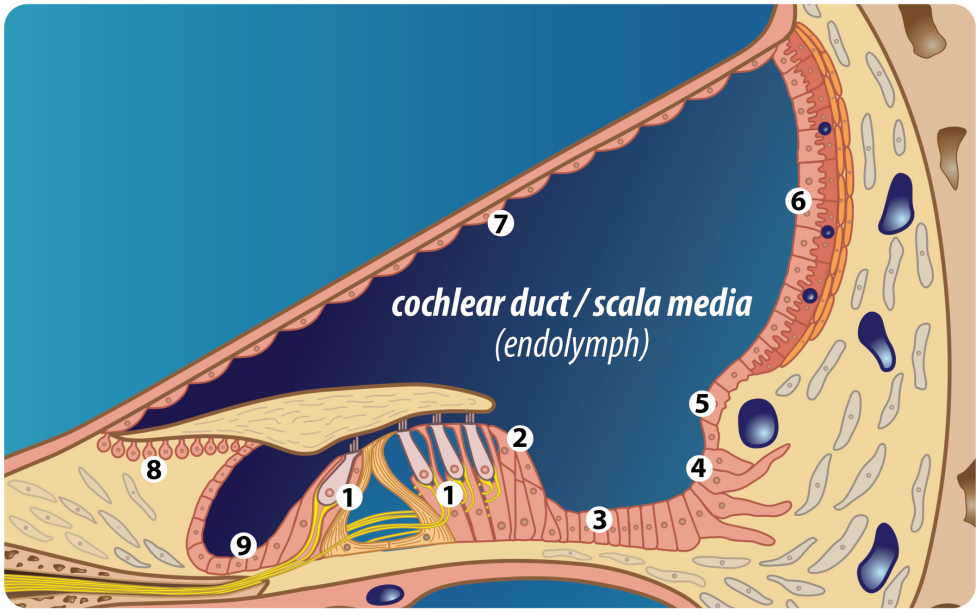


Figure 1. Schematic illustration of the cochlear duct / scala media.
1: hair cells, 2: Hensen's cells, 3: Claudius' cells, 4: outer sulcus root cells, 5: epithelial cells of the spiral prominence, 6: marginal cells of the stria vascularis, 7: epithelial cells of Reissner's membrane, 8: interdental cells in the spiral limbus, 9: inner sulcus cells. *Picture courtesy of S.B. Blankevoort.*

otic vesicle start to form the statoacoustic ganglion, which in humans presumably occurs around Carnegie stage 13 (~32 days of fetal age, during the 6th week of gestation) [4]. As maturation advances, the cochlear spiral ganglion separates from the vestibular neurons (Scarpa's ganglion) and type-I and type-II SGNs gradually appear. As we could not acquire cochlear specimens of fetal stages before W9, we were unable to visualize the key event of delamination. We did, however, shed new light on the onset of type-I versus type-II SGN identity in the human cochlea, as from W18 onwards, the intermediate filament peripherin became restrictively expressed in groups of cells representing type-II SGNs, suggesting that they share a common progenitor (Chapter 2).

Peripheral glial cells and melanocytes

Presently, at least two neural crest-derived cell types are known to be present in the cochlea: (1) peripheral glial cells and (2) specialized melanocytes.

A neural crest origin of the peripheral glial cells in the cochlea has been investigated in multiple studies, both recently by genetic tracing studies in the mouse [5, 6] and longer ago by tissue transplantation studies in the salamander and chicken [1, 2]. As shown in Chapter 3, the distribution and developmental pattern of peripheral glial cells in the human fetal cochlea matches with the postulate of a neural crest origin. The importance of these glial cells cannot be underestimated, as they (or their precursors) not only guide the central processes of SGNs towards their correct position within the brain [7], but are also essential for synchronous activity of SGNs in the adult cochlea, a prerequisite for normal hearing [8]. An intriguing question remaining to be answered is the exact route that is taken by the neural crest-derived peripheral glial cells to reach and enter the cochlea. The cellular distribution pattern we observed at W9 indicates that the peripheral glial cells migrate via the vestibulocochlear nerve (the 8th cranial nerve) into the human fetal cochlea. However, as SGNs originate from the otic placode, there has to be a moment during embryonic development when these two cell populations encounter one another for the first time. Interestingly, the vestibulocochlear ganglion and the geniculate ganglion (the ganglion of the facial nerve, n. VII) are in close proximity to one another early during development [9]; also see Figure 2). As the facial nerve and the geniculate ganglion receive their neural crest-derived cell population from a migratory stream of neural crest cells originating from rhombomere 4[footnote1] (Figure 3A), it is likely that the peripheral glial cells populating the cochlea also originate

from this migratory stream of neural crest cells [2, 6, 10, 11].

As proposed in Chapter 4, cochlear melanocytes might be derived from a different migratory stream of neural crest cells, this one originating from rhombomere 6. This is supported by images from several studies in mouse embryos in which, although not mentioned by the authors, neural crest (derived) cells are clearly visible on the apical side of the developing otic vesicle, i.e. the side facing rhombomere 6 [3, 5, 6, 12, 13]. In the human fetus at W9.1, melanocytes are present both around the nervous tissue at the apical side of the developing cochlea (at this stage likely part of the glossopharyngeal nerve (n. IX)), within the developing otic capsule, and in the mesenchyme bordering the developing stria vascularis (Chapter 4, Figure S1A). The glossopharyngeal nerve itself originates partly from an epibranchial placode and partly from delaminating neural crest cells, both of which are derived from rhombomere 6 [11, 14]. Taken together, we therefore believe that cochlear melanocytes originate from the stream of migrating neural crest cells from rhombomere 6 before travelling through the developing otic capsule and finding

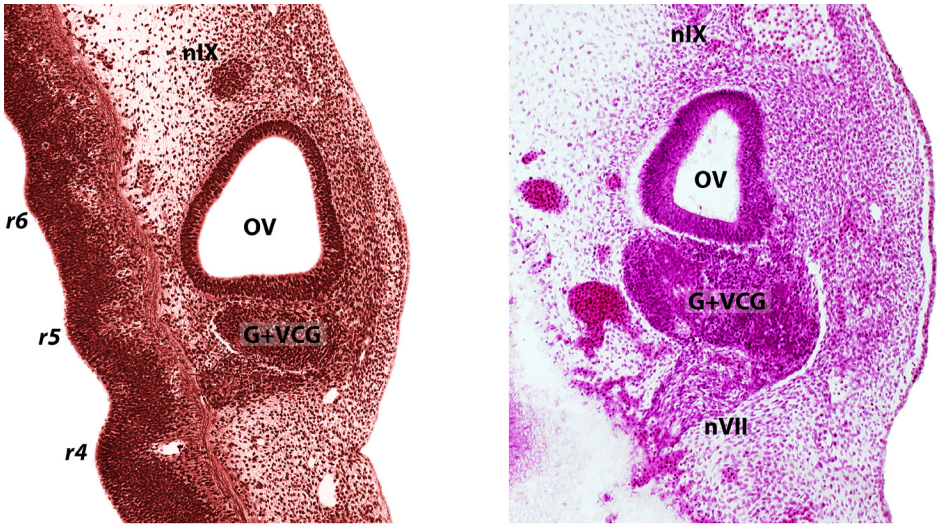


Figure 2. Sections through human fetuses at Carnegie stages 14 and 15.
r4-6: rhombomeres 4-6, G+VCG: geniculate ganglion and the vestibulocochlear ganglion, OV: otic vesicle, n. VII: facial nerve, n. IX: glossopharyngeal nerve. *Images modified and reproduced with permission from the Virtual Human Embryo website: http://www.ehd.org/virtual-human-embryo/*

their way to the lateral wall epithelium during the early embryonic development. A model of these migratory streams of neural crest cells is shown in Figure 3B. Future studies are needed to test this model.

Cell types with unknown origin

There are two cell types residing in the cochlea whose the exact embryonic origin remains unknown: (1) the basal cells and (2) the interdental cells.

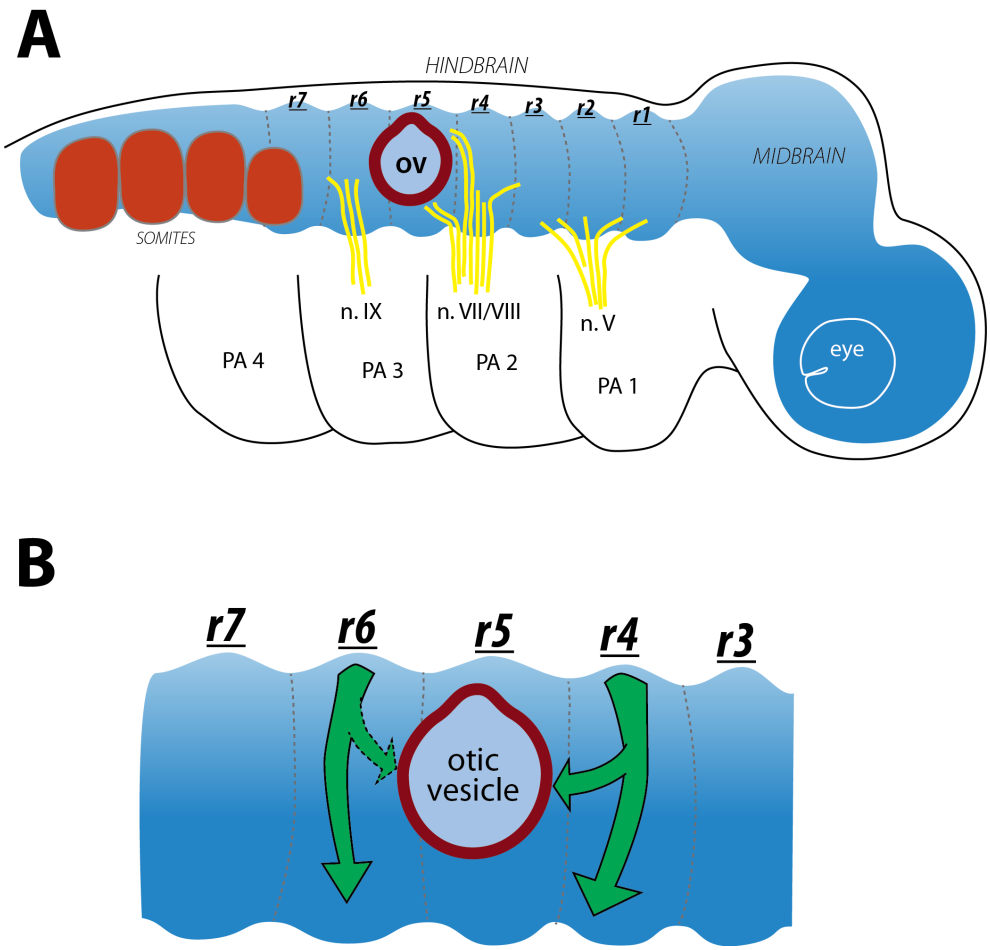


Figure 3. Schematic illustration of the hindbrain and otic vesicle in the human fetus.
(A) Overview showing the otic vesicle (OC) and its position relative to the rhombomeres (r1-7), the developing cranial nerves n. V, n. VII/VIII and n. IX and the pharyngeal arches (PA1-4). **(B)** Migratory streams of neural crest cells delaminating from the regions at rhombomeres 4 and 6, with their proposed contribution to the development of the cochlea.

Basal cells

The origin of the basal cells in the stria vascularis remains unknown as little research has been done on these cells (the exact location of the basal cells within the cochlea is shown in Chapter 4, Figure 1). Theoretically, there are three possible sites of origin: (1) they belong to the mesenchymal portion of the cochlea (as do the bordering fibrocytes in the spiral ligament), (2) they originate from the neural crest (as the strial melanocytes), and (3) they are derived from the otic placode (differentiating from the marginal cells). The first option is the most likely one, as basal cells have never been identified in lineage-tracing studies of the otic placode or neural crest.

Interdental cells

Interdental cells are located in the spiral limbus and most likely play an additional role in potassium homeostasis [15] as they express KCNJ10 on their apical (luminal) membranes [16]. A recent study in mice traces interdental cells to a shared lineage with spiral ganglion neurons, suggesting an otic placode origin [17]. However, the same study also groups them with the intermediate cells (melanocytes), which clearly have a different (neural crest) origin. This contradiction needs to be resolved to conclusively confirm their origin. Neural crest lineage-tracing studies in the cochlea have never observed cells that migrate to the spiral limbus, which would argue against a neural crest origin of the interdental cells. Nonetheless, they would have been easily overlooked as this specific region has not been investigated at the proper embryonic or fetal stages, and as multiple lineage markers are expressed in both the neural crest and the otic placode, hampering discrimination between the two.

Stem cell regeneration

Cochlear regeneration using stem cells

The second aim of this thesis was to pursue a possible stem cell strategy for the restoration of hearing. To successfully regenerate damaged or lost cochlear structures by means of stem cell-based therapies, one has first to select the appropriate stem cell source. Two general approaches may be considered: (1) taking advantage of

stem cells residing in the adult cochlea itself, and (2) introducing exogenous stem cells into the damaged cochlea.

Cochlear stem cells

There are several lines of evidence suggesting that the adult mammalian cochlea still contains stem cells. In the 1980s it was discovered (against expectations) that adult birds are able to regenerate hair cells in their damaged basilar papillae, i.e., the hearing organ in birds [18, 19]. Later, it became clear that in various vertebrate species, ranging from amphibians to fish, hair cells are able to regenerate or are continuously produced [20]. Hair cells in the vestibular organs likewise renew throughout life in birds as well as in most other non-mammalian vertebrates. The supporting cells in the sensory epithelium were found to be the source of the new hair cells. Unfortunately, spontaneous hair cell regeneration in mammals seems to have been lost during evolution, except for the limited capability for hair cell renewal in the vestibular organs of rodents. Although the exact reason remains unknown, it is suggested that this loss has been a trade-off with the development of the unique but intricate architecture of the organ of Corti in which regeneration has become too challenging [21].

Since the discovery that hair cells in birds can regenerate, numerous studies have focused on identifying the key regulators of hair cell specification, differentiation and regeneration in order to induce hair cell (re)generation in mammals. Major players that have been identified presently are the Notch/Jagged signaling pathway, transcription factors Atoh1 and Sox2 and cell cycle regulatory protein $p27^{Kip1}$ [22]. Since it has been shown that new hair cells are derived from Sox2-expressing supporting cells, an important question is to ask if the human organ of Corti still contains SOX2-positive cells supporting cells. Experiments from Chapter 2 showed that these supporting cells in the human fetal cochlea do express SOX2 positive up to the latest stage investigated (W19). Whether or not they retain their SOX2 expression in the adult cochlea remains to be seen. If so, successful experimental therapies in animal studies could benefit potential human trials.

Another interesting note is be made regarding regeneration of other cochlear structures. At present, there is no evidence whatsoever for regeneration of, for example, spiral ganglion neurons or cells in the stria vascularis by means of innate cochlear stem cells. Does this mean that there are no such cells? Intriguingly, we know that there are melanocytes residing in the spiral ligament (as shown in

Chapter 4) or in the modiolus (data not shown). Why exactly are those cells present at these sites, and are they or could they serve as a local source of stem cells?

Exogenous stem cells

The other stem cell option to consider in cochlear regeneration is the transplantation of exogenous stem cells into the damaged cochlea, which should be able to migrate to the appropriate site and differentiate into the desired cell type. Therefore, it is essential to know the embryonic origin of the cells that need to be replaced, especially since it is unlikely that a neural crest stem cell will differentiate into an otic placode-derived hair cell or that a stem cell from the central nervous system will differentiate into a myelinating Schwann cell from the peripheral nervous system. As stem cells come in multiple flavours, extensive knowledge of the molecular basis of cell fate is a prerequisite for selecting the appropriate stem cell type. For example, the transcription factors Pax2 and Pax8 are expressed in the otic placode, whereas cochlear neural crest precursors express Pax3. A Pax2-/Pax3+/Pax8- stem cell most likely will not differentiate into a hair cell, as it is destined to develop in another cell lineage (more extensively reviewed in [23]). However, this cell type could very well be the stem cell of choice for the formation of new peripheral glial cells.

As the otic placode is formed very early during embryological development, the most likely candidates for otic placode-derived cell induced regeneration (such as hair cell or spiral ganglion cell regeneration) are the pluripotent stem cells. Promising candidate stem cells are the induced-pluripotent stem cells (iPSCs) [24] as these cells resemble in many aspects an early embryonic cell type still able to differentiate into most cell lineages. An additional advantage is that iPSCs can be derived from adult tissue of the patient himself. Another option would be to use human embryonic stem cells, which have recently been shown to have a restorative effect on auditory function when introduced in an animal model with auditory neuropathy [25]. Although transplantation proved effective in that study, immune responses can be expected when using such cells in a human transplantation setting. Stem cells such as patient-specific iPSCs will most likely not have this adverse effect if used autologously. Other important reasons to consider in selecting a stem cell source for regeneration purposes is the tendency of stem cells to form tumors after transplantation, and the lineage distance between the stem cell and the desired, differentiated, cell type. A larger distance results in a higher number of

differentiation steps needed and consequently a higher chance that the stem cell will deviate from its requested path. To circumvent this problem, a stem cell type could be selected that is more differentiated but retains stem cell characteristics, such as neural crest stem cells (NCSCs). Evidently in the case of NCSCs, their suitability to regenerate hair cells or spiral ganglion neurons is limited, but they could prove to be the appropriate choice when it comes to regeneration of peripheral glial cells or cochlear melanocytes.

Hair follicle stem cells

Beginning in 2004, researchers began reporting that adult hair follicles contain NCSCs [26, 27]. As mentioned previously, this could have an enormous therapeutic potential, as it is thought that these cells are still able to differentiate into multiple important cell lineages and because they can be easily harvested from patients. In one of the original studies a *Wnt1*-cre/R26R compound transgenic mouse was used [26]. In hair follicle bulge cultures, TUBB3-positive cells were found showing X-gal activity, meaning that these cells (had) expressed *Wnt1*. The authors mentioned that neural crest cells express *Wnt1* transiently, and therefore concluded that the TUBB3-positive cells (which were identified as neurons) originated from NCSCs. However, as shown in Chapters 5-7, we suggest that there are no bona fide NCSCs in the adult hair follicle and that the interpretations made in their study were likely based on an extended expression of TUBB3 in multiple neural crest derivatives, including the melanocytic lineage (Chapters 5-7). Furthermore, *Wnt1* is not only expressed transiently in the neural crest but also in the melanocytic lineage, where it controls differentiation, proliferation and tumor initiation [28, 29]. Therefore, an alternative conclusion about the presence of TUBB3-positive cells in adult hair follicles could be that TUBB3-positive cells from those original studies were melanoblasts/melanocytes rather than neurons. In that perspective, the TUBB3-positive cells could originate from melanocyte stem cells residing in the bulge, or could be dedifferentiated Schwann cells (Chapter 7). Remarkably, no study so far has convincingly shown expression of other neuron-exclusive markers or recorded action potentials (Chapter 5) from *in vitro* hair follicle bulge-derived cells.

Even though it seems plausible that there is no true neural crest stem cell located in the hair follicle bulge and that these cells do not differentiate into neurons, hair-follicle bulge derived cells might retain their therapeutic potential when it comes to regeneration of other neural crest derived cell types such as melanocytes

or peripheral glial cells. This reasoning and our work from Chapters 5-7 support the hypothesis that different groups of neural crest descendants exist in the hair follicle bulge region, which may act jointly to achieve tissue restoration [30, 31].

Nevertheless, whether neural crest-derived neurons are the right candidate to replace damaged SGNs remains an open question. SGNs are derived from the otic placode and not from the neural crest like most other neurons from the peripheral nervous system. Therefore, cell regeneration with neurons derived from neural crest stem cells might not result in cells with the unique morphological and electrophysiological characteristics of SGNs.

Although more research is required, it is very likely that both Schwann cells and melanocytes can be easily cultured from hair follicle explants (from the mouse whisker pad), though it is unclear whether they originate from one multipotent stem cell or from two different (stem) cell pools (Chapter 7). In the inner ear, such cells could potentially be put to use in restoring the peripheral glial cells around the SGNs, or to renew melanocytes in the stria vascularis. As etiologic knowledge on many types of deafness is still incomplete, future insights may lead to applicability of these cell types in treating hearing loss.

The onset of human hearing

In the mouse and rat, hearing develops predominantly after birth [32]. In contrast, the development of the cochlea in humans (as well as guinea pigs [33] and chinchillas [34]) occurs during gestation (Chapters 2-4). However, in all mammals, the cascade of developmental events that leads to hearing is largely identical. At which fetal age auditory function starts in the human remains an intriguing question, one that very few studies have investigated or have speculated on.

For simplicity's sake, hearing can be defined as the generation of an action potential in a reaction to sound, which is propageted to the brain (therefore disregarding any 'higher' features such as synchronicity and central processing, which likely continue to develop after birth). Taking this into account, there are two absolute requirements: (1) the right cells should be present at the right location, and (2) there should be a functional electrochemical environment. Unfortunately, there is a lack of knowledge on both aspects in the human fetal cochlea. Do we understand all the key cell types involved in hearing? Much insight has been gained on hair cell function, but is there hearing if interdental cells do not develop, or Claudius'

cells for that matter? Also, we do not know the exact contribution of each cell type to the cochlear ionic homeostasis. For example, do satellite glial cells play a role in potassium regulation (which they likely do)? Or, what are the exact routes of potassium recycling?

Even within these limitations, an educated guess can be made using the following assumptions: hearing is possible (1) when the spiral ganglion neurons are connected to hair cells, and (2) when there is a functional endocochlear potential (see Chapter 4 for an explanation of the term 'endocochlear potential').

As shown in Chapter 2, the first contact between hair cells and SGNs occurs in the basal turn at W12, refining in the weeks thereafter. At W18, a configuration of type-I and type-II SGNs and inner and outer hair cells can be found in the basal turn that by and large mimics the adult situation. However, the question remains whether a positive endocochlear potential is present at 18 weeks of gestation (which is, for ethical reasons, impossible to measure in an experimental setting). Based upon the morphological development of SGNs and hair cells, we have proposed, as have others, (Chapters 2-3) that hearing commences around W18-20. However, this statement has been made without taking the endocochlear potential into account (Chapter 4). There are several studies measuring auditory responses in preterm human neonates. One study measured evoked otoacoustic emissions and observed (very weak) activity in neonates born at 28 weeks of gestation [35]. Unfortunately presence of these responses was not investigated in all neonates of that particular age, and younger subjects (very preterm neonates) were not measured. In a diff erent study measuring automated auditory brainstem responses in preterm neonates, a bilateral pass was first observed at W27-28, steeply increasing to W32 where pass rates included almost all subjects [36]. Both studies suggest that the earliest week at which hearing in humans commences is around W28. However, as the used auditory tests have limitations in their sensitivity, the actual onset of hearing could occur earlier.

In mice and in gerbils, the rise of the endocochlear potential has been studied during embryonic development [37, 38]. These studies concluded concluded that a certain level of maturation of gap junctions and tight junctions is required before the endocochlear potential develops. Data from Chapter 4 studying several key potassium channels and other proteins that are thought to play a role in the generation of the endocochlear potential indicate that this system of potassium-regulating structures is still immature at W18. For example, the intermediate cells do not yet express KCNJ10 and the basal cells have not or are barely formed. A

study investigating the fetal stria vascularis by means of electron microscopy in a few human cochlear samples from stages older than W19 found that basal cells and gap junctions could be clearly observed at the end of W24 [39]. When comparing the limited amount of human immunohistochemical and electron microscopical data from all investigated developmental stages to the timelines of mouse and gerbil cochlear development, a clear pattern emerges. Extrapolating the functional onset of the endocochlear potential in these animals to the human developmental timeline indicates that hearing is unlikely to take place in a human cochlea at W18-W20. We now speculate that human hearing commences somewhere between W26 and W28 (in the 7th month of pregnancy, around the start of the third trimester).

Future research and applications

Both basic research investigating physiology and development of auditory function and more clinically oriented research in genetics and stem cell therapies help in discriminating between normal and pathological conditions and in finding new treatment strategies for patients with hearing loss.

Investigating later gestational stages and even adult human cochlear tissue could extend the developmental insights gained by this work. However, obtaining material of sufficient quality has of course both practical and ethical issues. Other investigations could focus on mapping the expression of all genes known to be involved in SNHL. This would provide more knowledge on the involved cell types and damaged structures, which in turn will provide valuable input to the field on therapeutic interventions. Finally, regardless of whether or when gene or stem cell therapies become clinically available, there is much knowledge to be gained by investigating the causes of SNHL. For a large portion of hereditary SNHL cases, the cause of their hearing loss remains unknown. Further, patients are not yet screened for all known mutations. As knowledge on the genetics of hereditary hearing loss continues to increase and genetic screening methods become more extensive and cheaper, much progress should be expected on this topic within the next decade.

Footnotes:

1: Rhombomeres are developmental segments of the neural tube that later form the rhombencephalon, the hind-brain.

References

1. Yntema CL: **An experimental study of the origin of the cells which constitute the VIIth and VIIIth cranial ganglia and nerves in the embryo of Amblystoma punctatum.** J Exp Zool 1937, 75:75 – 101.
2. D'Amico-Martel A, Noden DM: **Contributions of placodal and neural crest cells to avian cranial peripheral ganglia.** Am J Anat 1983, 166:445 – 68.
3. Wakaoka T, Motohashi T, Hayashi H, Kuze B, Aoki M, Mizuta K, Kunisada T, Ito Y: **Tracing Sox10-expressing cells elucidates the dynamic development of the mouse inner ear.** Hear Res 2013, 302(May):17 – 25.
4. O'Rahilly R: **The Early Development of the Otic Vesicle in Staged Human Embryos.** J Embryol Exp Morphol 1963, 11(December):741 – 55.
5. Freyer L, Aggarwal V, Morrow BE: **Dual embryonic origin of the mammalian otic vesicle forming the inner ear.** Development 2011, 138:5403 – 14.
6. Sandell LL, Butler Tjaden NE, Barlow AJ, Trainor PA: **Cochleovestibular nerve development is integrated with migratory neural crest cells.** Dev Biol 2014, 385:200 – 10.
7. Freter S, Fleenor SJ, Freter R, Liu KJ, Begbie J: **Cranial neural crest cells form corridors prefiguring sensory neuroblast migration.** Development 2013, 140:3595 – 600.
8. Zeng F-G, Kong Y-Y, Michalewski HJ, Starr A: **Perceptual consequences of disrupted auditory nerve activity.** J Neurophysiol 2005, 93:3050 – 63.
9. Bruska M, Woźniak W: **The origin of cells of the cochlear ganglion in early human embryos.** Folia Morphol (Warsz) 2000, 59:233 – 8.
10. Ayer-Le Lievre CS, Le Douarin NM: **The early development of cranial sensory ganglia and the potentialities of their component cells studied in quail-chick chimeras.** Dev Biol 1982, 94:291 – 310.
11. Lumsden A, Sprawson N, Graham A: **Segmental origin and migration of neural crest cells in the hindbrain region of the chick embryo.** Development 1991, 113:1281 – 91.
12. Steel KP, Davidson DR, Jackson IJ: **TRP-2/DT, a new early melanoblast marker, shows that steel growth factor (c-kit ligand) is a survival factor.** Development 1992, 115:1111 – 9.
13. Adameyko I, Lallemend F, Furlan A, Zinin N, Aranda S, Kitambi SS, Blanchart A, Favaro R, Nicolis S, Lübke M, Müller T, Birchmeier C, Suter U, Zaitoun I, Takahashi Y, Ernfors P: **Sox2 and Mitf cross-regulatory interactions consolidate progenitor and melanocyte lineages in the cranial neural crest.** Development 2012, 139:397 – 410.
14. Ladher RK, O'Neill P, Begbie J: **From shared lineage to distinct functions: the**

development of the inner ear and epibranchial placodes. Development 2010, 137:1777 – 85.

15. Spicer SS, Thomopoulos GN, Schulte BA.: **Structural evidence for ion transport and tectorial membrane maintenance in the gerbil limbus.** Hear Res 2000, 143:147 – 161.
16. Eckhard A, Gleiser C, Rask-Andersen H, Arnold H, Liu W, Mack A, Müller M, Löwenheim H, Hirt B: **Co-localisation of K(ir)4.1 and AQP4 in rat and human cochleae reveals a gap in water channel expression at the transduction sites of endocochlear K(+) recycling routes.** Cell Tissue Res 2012, 350:27 – 43.
17. Jiang H, Wang L, Beier KT, Cepko CL, Fekete DM, Brigande JV: **Lineage analysis of the late otocyst stage mouse inner ear by transuterine microinjection of a retroviral vector encoding alkaline phosphatase and an oligonucleotide library.** PLoS One 2013, 8:e69314.
18. Corwin JT, Cotanche DA: **Regeneration of sensory hair cells after acoustic trauma.** Science 1988, 240:1772 – 4.
19. Ryals BM, Rubel EW: **Hair cell regeneration after acoustic trauma in adult Coturnix quail.** Science 1988, 240:1774 – 6.
20. Rubel EW, Furrer SA, Stone JS: **A brief history of hair cell regeneration research and speculations on the future.** Hear Res 2013, 297:42 – 51.
21. Brigande JV, Heller S: **Quo vadis, hair cell regeneration?** Nat Neurosci 2009, 12:679 – 85.
22. Cotanche DA, Kaiser CL: **Hair cell fate decisions in cochlear development and regeneration.** Hear Res 2010, 266:18 – 25.
23. Okano T, Kelley MW: **Stem cell therapy for the inner ear: recent advances and future directions.** Trends Amplif 2012, 16:4 – 18.
24. Yamanaka S: **Induced pluripotent stem cells: past, present, and future.** Cell Stem Cell 2012, 10:678 – 84.
25. Chen W, Jongkamonwiwat N, Abbas L, Eshtan SJ, Johnson SL, Kuhn S, Milo M, Thurlow JK, Andrews PW, Marcotti W, Moore HD, Rivolta MN: **Restoration of auditory evoked responses by human ES-cell-derived otic progenitors.** Nature 2012, 490:278 – 282.
26. Sieber-Blum M, Grim M, Hu YF, Szeder V: **Pluripotent neural crest stem cells in the adult hair follicle.** Dev Dyn 2004, 231:258 – 69.
27. Amoh Y, Li L, Katsuoka K, Penman S, Hoffman RM: **Multipotent nestin-positive, keratin-negative hair-follicle bulge stem cells can form neurons.** Proc Natl Acad Sci U S A 2005, 102:5530 – 4.
28. O'Connell MP, Weeraratna AT: **Hear the Wnt Ror: how melanoma cells adjust to changes in Wnt.** Pigment Cell Melanoma Res 2009, 22:724 – 39.
29. Wong CE, Paratore C, Dours-Zimmermann MT, Rochat A, Pietri T, Suter U, Zimmermann DR, Dufour S, Thiery JP, Meijer D, Beermann F, Barrandon Y,

Sommer L: **Neural crest-derived cells with stem cell features can be traced back to multiple lineages in the adult skin.** J Cell Biol 2006, 175:1005 – 15.

30. Johnston APW, Naska S, Jones K, Jinno H, Kaplan DR, Miller FD: **Sox2-Mediated Regulation of Adult Neural Crest Precursors and Skin Repair.** Stem Cell Reports 2013, 1:38 – 45.
31. Kumar A, Brockes JP: **Nerve dependence in tissue, organ, and appendage regeneration.** Trends Neurosci 2012, 35:691 – 9.
32. Jones SM, Jones TA (Eds): **Genetics, Embryology, and Development of Auditory and Vestibular Systems.** 1st edition. Plural Publishing, Inc; 2011.
33. Rubel EW, Fay RR (Eds): **Development of the Auditory System.** 1st edition. Volume 20. Springer-Verlag New York; 1998.
34. Jones HG, Koka K, Tollin DJ: **Postnatal development of cochlear microphonic and compound action potentials in a precocious species, Chinchilla lanigera.** J Acoust Soc Am 2011, 130:EL38 – L43.
35. Chabert R, Guitton MJ, Amram D, Uziel A, Pujol R, Lallemant J-G, Puel J-L: **Early maturation of evoked otoacoustic emissions and medial olivocochlear reflex in preterm neonates.** Pediatr Res 2006, 59:305 – 8.
36. Van Straaten HL, Tibosch CH, Dorrepaal C, Dekker FW, Kok JH: **Efficacy of automated auditory brainstem response hearing screening in very preterm newborns.** J Pediatr 2001, 138:674 – 8.
37. Steel KP, Barkway C: **Another role for melanocytes: their importance for normal stria vascularis development in the mammalian inner ear.** Development 1989, 107:453 – 63.
38. Souter M, Forge A: **Intercellular junctional maturation in the stria vascularis: possible association with onset and rise of endocochlear potential.** Hear Res 1998, 119:81 – 95.
39. Lavigne-Rebillard M, Bagger-Sjöbäck D: **Development of the human stria vascularis.** Hear Res 1992, 64:39 – 51.

A

APPENDIX

SUMMARY
SAMENVATTING
ABBREVIATIONS
LIST OF PUBLICATIONS
ABOUT THE AUTHOR

Summary

The embryonic development of the human cochlea (the organ of hearing) has been investigated for over one hundred years. Still, little is known about the development on a cellular and protein level, which is important to better understand etiologies and pathologies of various types of sensorineural hearing loss. Knowledge of the normal gene expression patterns and cell fate specification in the human cochlea therefore aids the development of gene and cell-based therapeutic strategies.

For this reason, we acquired a series of human fetal cochlea of different stages of gestation and investigated several aspects of the normal development of the human cochlea in **Chapters 2-4**.

Chapter 2 investigated the development of the hair cells and the spiral ganglion neurons. Cochlear hair cells develop out of an undifferentiated epithelium. We showed that, at the 10th week of gestation (W10), all epithelial cells expressed both SOX9 and SOX10 with the addition of SOX2 expression in the prosensory domain. We found the first developing hair cell at W12, coinciding with downregulation of SOX9 and SOX10 in this cell, to be followed later by downregulation of SOX2. Markedly, outgrowing neurites from spiral ganglion neurons were found penetrating into the cochlear duct epithelium prior to the first hair cell differentiation. These neurites directly targeted the hair cells as they developed. Investigating Peripherin expression (in the mature cochlea only expressed in the type-II spiral ganglion neurons), showed that all spiral ganglion neurons expressed this protein in early stages, and that expression gradually diminished and became restricted to the type-II spiral ganglion neurons by 18 weeks. At 20 weeks, the expression profiles in hair cells and spiral ganglion neurons matched the expression patterns of the adult mammalian cochlea.

Chapter 3 investigated a third cochlear cell type, the peripheral glial cell. The adult human cochlea contains three different types of peripheral glial cells: myelinating and unmyelinating Schwann cells and satellite glial cells. In this chapter, we focused on the developmental distribution of the peripheral glial cells and on the onset of myelination of spiral ganglion neurons, one of the prerequisites of normal hearing. We observed glial cells at our earliest investigated stage (W9) in all three neuronal domains: both near central and peripheral processes and at the location of the SGN cell bodies. Glial cells associated themselves with SGN cell bodies from W12 onwards and these satellite glial cells populated the spiral ganglion in a spatiotemporal gradient. In the cochlear nerve, radial sorting and myelination was observed at W22, prior to myelination of the peripheral processes. We proposed

that the three types of glial cells in the human adult cochlea are all derived from the precursor cells observed at W9, and that the observed developmental patterns support a neural crest origin of these cells in the human.

Chapter 4 investigated the development of the stria vascularis and cochlear potassium regulation, including its relation to syndromic and nonsyndromic sensorineural hearing loss. At W12, melanocytes were found migrating into the cochlea and penetrating the basement membrane of the lateral wall epithelium, forming the intermediate cellular layer of the stria vascularis. In the following weeks, these melanocytes tightly integrated with the developing marginal cells, the epithelial cellular layer. We showed the expression of several melanocytic proteins (MITF, SOX10, KIT), potassium regulating proteins (Na^+/K^+-ATPase, KCNQ1, KCNJ10), and gap junction proteins (GJB2, GJB6, GJA1, GJE1) in this developing structure. All these proteins are known to be involved in different types of hereditary sensorineural hearing loss except GJE1, which could therefore be a potential new associated locus for this disease. Based on the data from Chapters 2-4 and literature on development of hearing in animals we propose that hearing in the human commences between W26 and W28, later than previously suggested.

Chapters 5-7 are related to the neural crest stem cells residing in the hair follicle bulge. These cells, first discovered a decade ago, are of strong interest to stem cell researchers as they could serve as a pool of easy accessible stem cells capable of differentiating into multiple cellular lineages (amongst which are neurons and glial cells). Potentially, they could be used to regenerate various cochlear tissues. However, in Chapter 5 and Chapter 6 we showed that a protein (TUBB3) often used in immunochemistry to detect a neuron is also expressed both in skin and hair follicle melanocytes in humans. This could indicate that cells from the melanocytic lineage mistakenly were identified as neural crest stem cells. This insight was used in Chapter 7, where we cultured mouse hair follicle bulge explants to investigate expression of TUBB3. Strikingly, cultured cells expressing this protein were not of the neural lineage but rather from the melanoglial lineage. Together, this showed that the proposed neural crest stem cell residing in the hair follicle bulge might need revision. However, as both melanocytes and peripheral glial cells are present and have important functions in the cochlea, hair follicle bulge cells remain a suitable candidate when investigating the regeneration of these tissues.

Samenvatting

Al meer dan honderd jaar wordt er onderzoek gedaan naar de embryonale ontwikkeling van de humane cochlea (het gehoororgaan). Er is echter nog steeds weinig bekend over deze ontwikkeling op een cellulair of gen/eiwit-niveau. Deze kennis is van groot belang om de etiologie en pathologie van verschillende typen van sensorineuraal gehoorverlies beter te kunnen begrijpen. Kennis over het normale patroon van genexpressie en celdifferentiatie in de humane cochlea draagt bij aan de ontwikkeling van genetische en op (stam)cel gebaseerde therapieën.

In een serie van humane foetale cochlea's van verschillende stadia van ontwikkeling hebben wij een aantal aspecten van de normale ontwikkeling onderzocht in **Hoofdstukken 2-4.**

Hoofdstuk 2 onderzocht de ontwikkeling van de haarcellen en de spiraal ganglion neuronen (SGN). Cochleaire haarcellen ontwikkeling zich vanuit een ongedifferentieerd epitheel. We toonden aan dat in de 10e week van de zwangerschap (W10) alle epitheliale cellen zowel SOX9 en SOX10 tot expressie brengen met daarnaast ook SOX2 expressie in het 'prosensory domain'. De eerste haarcel zagen we zich ontwikkelen in W12, waarbij dit samenging met downregulatie van SOX9 en SOX10 in deze cel, enige weken later gevold door downregulatie van SOX2. Opvallend genoeg vonden we ingroei in het cochleaire epitheel door de neuriten van de SGN voorafgaand aan de ontwikkeling van de eerste haarcel. Deze neuriten richtten zich gelijk naar de haarcel zodra deze zich ontwikkelde. Het onderzoeken van Peripherin expressie (wat zich in de volwassen cochlea alleen in de type-II SGN bevindt) toonde aan dat eiwit door alle SGN tot expessie werdt gebracht in de vroege embryonale fasen maar dat deze expressie geleidelijk verminderde en selectief werd voor type-II SGN in W18. Het expressieprofiel in de haarcellen en de SGN kwam in W20 overeen met het bekende patroon van de volgroeide cochlea bij zoogdieren.

Hoofdstuk 3 onderzocht een derde cel type in de cochlea, de 'peripheral glial cell'. De volwassen humane cochlea bevat weer drie verschillende typen van deze cel: gemyeliniseerde en ongemyeliniseerde Schwann cellen en 'satellite glial cells'. In dit hoofdstuk richtten we ons op de verspreiding en differentiatie van deze cellen tijdens de ontwikkeling in de cochlea, en op het ontstaan van myeline rondom de spiraal ganglion neuronen: een van de vereisten voor een normale functie van het gehoor. We zagen al gliale cellen in de jongste fase die we onderzochten (W9) in alle drie de neuronale domeinen: zowel rond de centrale en perifere uitlopers als bij de cellichamen van de SGN. Vanaf W12 gingen deze cellen een nauwe relatie

aan met de cellichamen van de SGN en werd het spiraal ganglion middels een spatiotemporele gradient bevolkt. In de nervus cochlearis ontdekte we 'radial sorting' en myelinisatie in W22, voorafgaand aan myelinisatie van de perifere SGN uitlopers. Vanwege deze bevindingen achten we het zeer waarschijnlijk dat deze drie type gliale cellen in de humane cochlea allen afkomstig zijn van de voorlopercel die we zagen in W9, en dat deze observaties ook passen bij een neurale lijst oorsprong van deze cellen in de mens.

Hoofdstuk 4 onderzocht de ontwikkeling van de stria vascularis en de cochleaire kaliumhuishouding, met een verdieping in syndromale en niet-syndromale typen van sensorineuraal gehoorverlies. In W12 zagen we dat melanocyten migreerden in de cochlea en dat ze penetreerden door het basaalmembraan van het epitheel in de laterale wand, hierdoor zo de intermediare cellulaire laag van de stria vascularis vormend. In de hieropvolgende weken integreerde deze melanocyten zich sterk met de zich ontwikkelende marginale cellen. Hiernaast toonden we het expressieprofiel aan van verschillende melanocytaire eiwitten (MITF, SOX10, KIT), kalium regulerende eiwitten (Na^+/K^+-ATPase, KCNQ1, KCNJ10) en gap junction eiwitten (GJB2, GJB6, GJA1, GJE1). Van al deze eiwitten is het bekend dat ze betrokken zijn in verschillende vormen van erfelijke sensorineurale gehoorverliezen behoudens GJE1, wat wellicht mogelijk een nieuw geassocieerde locus voor deze aandoening zou kunnen blijken.

Gebaseerd op alle data van Hoofstukken 2-4 en kennis over de ontwikkeling van het gehoor bij knaagdieren vangt het menselijk gehoor waarschijnlijk pas aan tussen W26 en W28, later dan vooralsnog frequent wordt aangenomen.

Hoofdstukken 5-7 hebben betrekking op de neurale lijst stamcellen die zich bevinden in de haarfollikel bulge regio. Deze cellen, ruim tien jaar geleden ontdekt, zijn zeer interessant voor stamcelonderzoek omdat ze mogelijk kunnen dienen als een zeer toegankelijk bron van stamcellen die zich nog kunnen diff erentieren in verschillende nuttige celtypen (waaronder neuronen en gliale cellen). Potentieel zouden deze cellen dan ook kunnen worden ingezet voor het herstel van verschillende cochleaire weefsels. Echter, in Hoofdstuk 5 en Hoofdstuk 6 lieten we zien dat veelgebruikt eiwit (TUBB3) om neuronen mee aan te tonen middels immunohistochemie ook in expressie komt in melanocyten in de huid of haar bij de mens. Dit heeft als gevolg dat melanocyten wellicht vaker ten onrechte zijn geïdentificeerd als neurale lijst stamcellen. Dit inzicht hebben we vervolgens gebruik in Hoofdstuk 7 om de expressie van TUBB3 te onderzoeken in kweken van de haarfollikel bulge uit de muis. Opvallend genoeg liet dit inderdaad zien dat de gekweekte cellen die TUBB3

tot expressie brachten niet van neurale maar juist van melanogliale oorsprong zijn. Tezamen betekent dit dat het zich bevinden van een neurale lijst stamcel in de haarfolikkel heroverwogen zal moeten worden. Echter, omdat zowel melanocyten als gliale cellen wel afzonderlijk voorkomen in de haarfollikel en deze celtypen belangrijke functies hebben in de cochlea blijft de haarfollikel een interessante kandidaat ten aanzien van onderzoek naar weefselherstel.

Abbreviations

CD	cochlear duct
CN	cochlear nerve
IHC	inner hair cell
KO	Kölliker's organ
NCSC	neural crest stem cell
OC	organ of Corti
OHC	outer hair cell
PGCs	peripheral glial cells
PPs	peripheral processes
SG	spiral ganglion
SGN	spiral ganglion neuron
SNHL	sensorineural hearing loss
ST	scala tympani
SV	scala vestibuli
W#	weeks of gestation

Proteins

aceTUBA	acetylated tubulin
ATP1A1	sodium/potassium-transporting ATPase
COL4	collagen type IV
DCT	dopachrome tautomerase
FN	fibronectin
GJA1	gap junction protein, alpha 1 (connexin 43)
GJB2	gap junction protein, beta 2 (connexin 26)
GJB6	gap junction protein, beta 6 (connexin 30)
GJE1	gap junction protein, epsilon 1 (connexin 23)
KCNJ10	inwardly-rectifying potassium channel subfamily J, member 10
KCNQ10	potassium channel, voltage-gated KQT-like subfamily Q, member 1
LAM	laminin
MBP	myelin basic protein
MITF	microphthalmia-associated transcription factor
MYO7A	myosin VIIa
NGFR	nerve growth factor receptor ($p75^{NTR}$)
PCNA	proliferating cell nuclear antigen
PRPH	peripherin
S100B	s100 calcium binding protein B
SLC2A1	solute carrier family 2 (facilitated glucose transporter), member 1 (also known as GLUT)
SOX	sry-related HMG box
TUBB3	class III β-Tubulin
TYRP1	tyrosine-related protein 1
TYRP2	tyrosine-related protein 2

List of Publications

1. Rodríguez-Contreras A, van Hoeve JSS, Habets RLP, Locher H, Borst JGG: **Dynamic development of the calyx of Held synapse.** Proc Natl Acad Sci U S A 2008, 105:5603 – 8.
2. Bruijn J, Duivenvoorden H, Passchier J, Locher H, Dijkstra N, Arts W-F: **Medium-dose riboflavin as a prophylactic agent in children with migraine: a preliminary placebo-controlled, randomised, double-blind, cross-over trial.** Cephalalgia 2010, 30:1426 – 34.
3. Bruijn J, Locher H, Passchier J, Dijkstra N, Arts W-F: **Psychopathology in children and adolescents with migraine in clinical studies: a systematic review.** Pediatrics 2010, 126:323 – 32.
4. Locher H, de Rooij KE, de Groot JCMJ, Doorn R Van, Gruis NA, Löwik CWGM, Chuva de Sousa Lopes SM, Frijns JHM, Huisman MA: **Class III β-tubulin, a novel biomarker in the human melanocyte lineage.** Differentiation 2013, 85:173 – 181.
5. Locher H, Frijns JHM, van Iperen L, de Groot JCMJ, Huisman MA, Chuva de Sousa Lopes SM: **Neurosensory development and cell fate determination in the human cochlea.** Neural Dev 2013, 8:20.
6. Locher H, de Groot JCMJ, van Iperen L, Huisman MA, Frijns JHM, Chuva de Sousa Lopes SM: **Distribution and development of peripheral glial cells in the human fetal cochlea.** PLoS One 2014, 9:e88066.
7. Locher H, Frijns JHM, Huisman MA, Chuva de Sousa Lopes SM: **TUBB3: Neuronal Marker or Melanocyte Mimic?** Cell Transplant 2014, 23:1471 – 3.
8. Locher H, Saadah N, de Groot S, de Groot JCMJ, Frijns JHM, Huisman MA.: **Hair follicle bulge cultures yield class III β-tubulin-positive melanoglial cells.** Histochem Cell Biol 2015:87 – 91.
9. Locher H, de Groot JCMJ, van Iperen L, Huisman MA., Frijns JHM, Chuva de Sousa Lopes SM: **Development of the stria vascularis and potassium regulation in the human fetal cochlea: Insights into hereditary sensorineural hearing loss.** Dev Neurobiol 2015, 75:1219-40.

About the Author

Heiko Locher was born on September 1, 1982 in Amsterdam, the Netherlands. He studied medicine at the Erasmus University of Rotterdam with a focus on otorhinolaryngology during his rotations *(oudste co-schap)*, and worked on a clinical trial for pediatric migraine with dr. J.K.J. Bruijn. He obtained his medical degree in 2010.

In addition he finished a two-year research master's program in Neuroscience in 2008 at the Erasmus University under supervision of prof.dr. J.G.G. Borst as well as the Exchange Honours Master of Neurosciences from the Free University of Amsterdam and the Erasmus University. During these years he worked on second-harmonic generation imaging of bulk-endocytosis in the calyx of Held and calcium imaging in the calyx of Held collaterals.

He started working as a PhD candidate in 2010 at the Leiden University Medical Center with prof.dr.ir. J.H.M Frijns as promotor. This research was performed both at the department of Otorhinolaryngology with dr. M.A. Huisman and at the department of Anatomy & Embryology with dr. S.M. Chuva de Sousa Lopes.

In 2014 he started his clinical residency in otorhinolaryngology at the LUMC under supervision of prof.dr.ir J.H.M Frijns and dr. A.G.L. van der Mey.


cochlea
cochlea